A NEW APPROACH FOR DETECTING HYDROTHERMAL ALTERATIONS USING REMOTE SENSING DATA: A CASE STUDY FROM LAKE VICTORIA GOLD FIELDS, TANZANIA

Thesis

submitted for fulfillment of a

Doctoral Degree in Natural Sciences (Dr. rer. nat.)

to

Faculty of Natural Sciences (III)

Martin-Luther-University Halle-Wittenberg

by

Elisante Elisaimon Mshiu

Born on 25.09.1978 in Hai, Kilimanjaro, Tanzania

Reviewers: Prof. Dr. Gregor Borg

(Martin-Luther-University Halle-Wittenberg)

Prof. Dr. Cornelia Gläßer

(Martin-Luther-University Halle-Wittenberg)

Prof. Dr. Hartwig Frimmel

(Julius-Maximilians-Universität Würzburg)

Halle (Saale), 14.07.2014

ABSTRACT

Remote sensing hydrothermal alteration mapping has been employed in mineral exploration for decades. Both multispectral and hyperspectral data have been the most used remote sensing data, this is because of their ability in identifying spectrally the individual hydrothermal alteration minerals. Depending on spectral resolution of these data sets, it has been possible to map specific mineral alterations, which are related to base or precious metal mineralization. Different approaches have been applied for the mapping of the hydrothermal alterations, for example, the extraction of the key alteration minerals from the alteration assemblage, band rationing, composite images, and various statistical methods are some of these techniques. However, there has been a challenge in the quality of the results obtained. For example, it is still difficult to differentiate the hydrothermal minerals and minerals of non-hydrothermal origin such as minerals from weathering and metamorphic processes. The best example is the problem to differentiate hydrothermal chloritization from the chloritic metamorphosed basalts. This ambiguity normally leads to misinterpretations of the mapped alterations and can create challenges or problem for the identification of exploration targets.

This study presents an approach for hydrothermal alteration mapping by satellite remote sensing data. The method has shown to improve the quality of alteration mapping and also to simplify the identification of precious metal exploration targets. Geological maps and SRTM data were used as the sources of information to identify tectonic structures, since structural elements such as fractures and shear zones are known as the crustal features or conduits for mineralizing fluids. Landsat ETM+ data were used to map areas, which may have been affected by hydrothermal alterations and the statistical method "Feature Oriented Principal Component Analysis (FOPCA)" was used as the extracting tool of these altered areas. Identification of the lineaments that were potentially involved in carrying hydrothermal fluids was achieved by applying the GIS functions clumping and sieving, which led to particularly interesting results. The analysis has revealed linear alteration patches that coincide with regional and local crustal lineaments. In this study the linear alteration patches are interpreted to have acted as hydrothermal fluid conduits. The linear alteration patches are consistent with both tectonic structures and gold occurrences and locally gold deposits in the study area. ASTER data was used to map the individual alteration minerals and their systematic zoning in the study area. The mapping of alteration zones was achieved through the technique that uses more than one key mineral for each hydrothermal alteration assemblage. In addition, the supervised classification as well as the mathematical rules applied has made it possible to realize the systematic alteration zoning around mineralization zones. Results from ASTER data also have revealed the correlation between alteration zoning and gold deposits, and fit the most accepted Archaean granite-greenstone gold deposit models. Moreover, the size and shape of proximal alterations are consistent with the reported size range for hydrothermal alteration zones in orogenic gold deposits as well as the associated tectonic structures. The mapped alteration zones have shown their differences in the spectra measured by TerraSpec (VNIR-SWIR) spectroscopy instrument in samples taken from each alteration zone. Also samples from the mapped alteration zones have revealed differences in mineralogy through light microscopy thin section studies, Scanning Electron Microscopy (SEM) and X-ray Diffraction Analysis (XRD). The conducted geochemical analyses have revealed Au anomalies in the selected test sites, which also associate with the proximal alteration zones. Furthermore, Au corresponds with its most known pathfinder elements such as Ag, Sb, Hg, Tl, Bi, Mo and B.

TABLE OF CONTENTS

FIGURE CAPTIONS

TABLE CAPTIONS

APPENDIX CAPTIONS

1   INTRODUCTION

The advancement in technology has triggered the high demand of natural resources, for example, the current observed high demand of strategic metals. Unfortunately, the shortage observed also corresponds with the current decrease of deposit discoveries. The disequilibrium observed needs a solution before this shortage reaches its peak. This has caught public attention and prompted discussions so far. Currently, individual countries as well as countries in groups are forming special task forces as efforts to ensure themselves with adequate supply of the required metals. The best example is the formation of the European Innovation Partnership (EIP), the overall objective of EIP is to increase the availability of raw materials for Europe (EIP, 2013). Countries endowed with natural resources on the other hand benefit from the system through exporting the required metals. Most of the developing countries rely on the utilization of their natural resources to sustain their economic development. For example, in Tanzania the mining sector has been a significant component in the backbone of the country's economy since the 1990s (Semkiwa, 2005). Therefore, the overall effect of inadequate raw materials e.g. for strategic metals, together with the decrease of deposit discoveries has been not selective in that it has affected both developed and developing countries alike. The equilibrium between the needs and availability of minerals and metals could be reached through additional efforts and innovations in mineral exploration. Availability of relevant data and new approaches in mineral exploration are amongst the efforts needed to increase the number of discoveries. There are several data sets, which have been used in mineral explorations and satellite remote sensing data is among these data introduced to the industry since the 1970s. It has been included in exploration programs and this utilization has contributed to the discovery of some of the new mineral deposits. This includes for example, the discovery of the Los Menucos gold district in Argentina in 1998 by Arminex, S.A. through regional exploration by employing Landsat Thermatic Mapper (TM) satellite data (Kruse et al., 2002). Another example is the recent discovery of Au and Cu mineralization by Advanced Spaceborne Thermal Emission and Reflection (ASTER) data in Chubko in a prospect owned by Kentor Gold Ltd in the Northern Territory, Australia (Treadgold, 2012; Close and Scrimgeour, 2013). The above examples of the discovered deposits by satellite remote sensing data together with its ability to be used in geological mapping reveals the data is reliable and significant for mineral exploration. This study focused on using integrated remote sensing data, innovatively, to investigate hydrothermal alterations around gold deposits in the Lake Victoria Gold Fields (LVGF).

1.1   Hydrothermal System

A hydrothermal fluid is a major component in any hydrothermal system and the water in these fluids originates from different sources such as meteoritic, sea water, connate water, metamorphic and juvenile/magmatic water. The hydrothermal fluids are mostly from mixed sources, meaning that the solution may have more than one source from the above list (Pirajno, 2009). Apart from water, hydrothermal fluids also contain other components, including elements such as complexing agents (S, Cl) and metals (e.g. Ag, Au, Se, Tl, Cu, Mo, REE, Ti, etc.) that later determine the fluid "fertility" and transport such metals and deposit them at favorable environments to form a mineral deposit. These fluids can also contain various ions and gases (e.g. $-NH_4$, $-OH$, Co_3^{-2}, $CO2$, SO_2, HSO_4^{-2}, H_2S, $-Cl$, Na, ^+K, and Ca^{+2}), which normally cause mineralogical and geochemical changes in the host rock and result to mineral alteration. This is the change of primary minerals in the host rock to secondary stable minerals. The resulted secondary minerals are in equilibrium with the new physical-chemical

environments. The hydrothermal fluids are transported from their sources through channelways, for example, tectonic fractures or shear zones within crust. Moreover, these structures act as traps to hydrothermal fluids and mineralization at large (Groves et al., 2000; Goldfarb et al., 2005; Pirajno, 2009).

Geological processes such as uplift and erosion are responsible for exposing the altered host rock on the surface. Some of the primary alteration minerals may continue to be stable for a long time under the surface environments whereas others change again to different new stable mineral phases during weathering. Atmospheric conditions, low temperature and pressure, water, Eh, pH, are the catalysts to reactions, which lead to the change of some of the hydrothermal minerals on the surface. For example, hydrothermal anhydrite in veins can be hydrated to gypsum and subsequently dissolved in near surface environments. But gypsum can also form as supergene byproduct of sulfide oxidation when sulfuric acid generated in the supergene system reacts with calcium carbonate (Palache et al., 1951). Hypogene hydrothermal minerals, for example sulfides and silicate minerals such as feldspars may be oxidized to Fe-oxides/hydroxides and clay minerals in near surface environments (Klein and Day, 1994; Angelica et al, 1996). However, some of the hydrothermal alteration minerals, as said before, remain stable in the near surface conditions. For example, muscovite/sericite, chlorite, epidote, carbonates, silica, illite are amongst the hydrothermal minerals that remain stable and can be found in near-surface and surface environments. For a hydrothermally altered rock that is overlaid with a weathered profile, at depth a saprolite lies direct in contact with the host rock. On top of the saprolite is a progressive gossans dismantling towards the latosols at the top most part of the profile. Hematite and/or goethites are commonly the dominant Fe-rich phases in latosols after weathering reactions of primary hydrothermal minerals like magnetite and sulfides (Klein and Day, 1994; Angelica et al, 1996). Angelica et al, (1996) reported latosols overlaying lateritic iron crust in an Au mineralized area in Aguas Claras, the latosol exhibit a yellowish-white colour over the sedimentary wall-rocks and a predominantly reddish-brown colour over the gossans. Latosols in this area are mainly composed of kaolinite, Al-goethite, gibbsite, hematite and quartz. Many of these alteration minerals can be detected by remote analytical methods and thus lend themselves to systematic remote sensing alteration mapping, which is the main subject of this PhD-thesis.

1.2   Hydrothermal Alteration Mapping

Overall, hydrothermal systems including the one associated with mineralization and effects of paleo-hydrothermal fluids can be detected indirectly through the recognition of alteration minerals in host rocks and loose sediments. This is because the distribution of these minerals on the surface still reflect the underlying effects of hydrothermal fluids on the rocks (e.g. Klein and Day, 1994; Angelica et al, 1996). The mapping of hydrothermal alteration can be achieved through detection of these minerals, which are directly or indirectly related to hydrothermal systems. Fe-oxides/hydroxides, carbonates, sulphates, sericite, chlorites, and different clays are some of these minerals.

The detection of alteration minerals on the surface can be through mineral spectroscopy (Hunt, 1977; Goetz et al., 1983; Pirajno, 2009; Thompson and Thomson, 1996; Sabins, 1999). Visible to near-infrared (VNIR), shortwave infrared (SWIR) and thermal infrared (TIR) regions of the electromagnetic spectrum, all have shown to be useful in detecting these minerals, but mostly the spectroscopically active minerals. Satellite-borne remote sensing sensors use similar technology. Since their introduction, the data collected have been used in different geological aspects including hydrothermal alteration mapping (Gupta, 2003; Brown et al., 2006; Pirajno, 2009). For example, Crosta et al. (2003) used Advanced Spaceborne Thermal Emission and Reflection (ASTER) data to map

the alteration minerals related to epithermal gold deposits in Patagonia, Argentina. Also Rowan and Mars (2003) used ASTER data for lithological mapping in Mountain Pass, California. The present PhD study has used the integrated satellite remote sensing data to map hydrothermal alteration minerals related to gold mineralizations of the Archaean granite-greenstone models with the specific objectives stated in the following section. The Lake Victoria Gold Field (LVGF) is situated in the Archaean Tanzania Craton and is endowed with a number of major gold deposits and has therefore been selected for this case study.

1.3   Objectives of the study

The overall objective of this study is to improve the quality of hydrothermal alteration mapping by remote sensing satellite data. Hydrothermal alteration mapping have been used as one of the key tools for targets generation. For example, mineral alterations assemblages like carbonate and sericite alteration are mostly found proximal to mineralization zones in Archaean granite-greenstone gold deposits. As one of the proximal alteration minerals, these minerals can be used to locate the potential exploration targets. Therefore, accurate mapping of hydrothermal related minerals by remote sensing data will increase confidence in the selection of exploration targets during the searching for mineral deposits.

1.3.1   Specific objectives

I.   To map the geological structures related to hydrothermal alterations by using Landsat ETM+ and Shuttle Rader Topographical Mission (SRTM) data

II.   To use more than one diagnostic mineral in identifying hydrothermal alterations related with Archaean gold deposit models by using the Advanced Spaceborne Thermal Emission and Reflection (ASTER) data

III.   To map systematically the hydrothermal alteration zoning around Archaean granite-greenstone belt gold deposits by using the hydrothermal alteration patterns extracted from Advanced Spaceborne Thermal Emission and Reflection (ASTER) data

IV.   To test and show spatial relationships between the identified alteration patterns, lineament tectonics and ore deposits or mineralization

1.3.2   Significance of the Study

It is obvious the method will improve and partly simplify the whole process of target identification. Accurate alteration mapping will contribute and hopefully lead to the discovery of additional mineral deposits. It is also known satellite remote sensing data are relatively cheap when compared to other data sets as well as the ground-borne exploration methods. Hence, the achievement of the above objectives will lower exploration costs mostly during the reconnaissance stages, since it can be applied in the early exploration stages as a first data-based desktop approach.

2   METHODOLOGY

This section summarizes the overall approach applied in this study (Fig. 2.1). Spatial and non-spatial data sets have been used in this study, Shuttle Radar Topographical Mission (SRTM) data, Geological Maps, Landuse/Topographical Maps, Landsat ETM+, Advanced Spaceborne Thermal Emission and Reflection (ASTER) data, minerals spectra, and geochemical data during advanced stage of this PhD project . The data were used in different stages of this study depending on the specific objectives mentioned in the introduction section.

3

2.1   Objective I

SRTM data, geological maps, landuse/topographical maps and Landsat ETM+ data were analyzed to accomplish Objective-I. SRTM data were used for the extraction of the surface expressed geological lineaments in the study area. This process was performed with reference to information about tectonic structures of the region. The background geological information was obtained from geological maps of the study area as well as the scientific publications available from the study area. Landuse and topographical maps were used to validate the identified lineaments before digitalization; this was done purposely to avoid anthropogenic linear features such as roads, railways and transmission lines to interfere with the interpretation. Also geological structures were extracted from geological maps for comparison as further proof of the extracted SRTM lineaments. Detailed steps on the approach used to extract these lineaments are described in section 5.

Landsat ETM+ data was used to identify places, which were affected by hydrothermal alterations in the study area. Landsat ETM+ data spectral resolution does not have the ability to identify the individual alteration minerals. But collectively by using spectral characteristic of the two groups of alteration minerals, that is the Fe-oxides/hydroxides and hydroxyls-sulphates-carbonates, it is possible to identify the areas, which were likely to have been affected by hydrothermal alterations. Further steps of analyses (clumping and sieving) were performed on the results from Landsat ETM+ data to identify the geological structures shown to have been involved in the hydrothermal systems and associated alteration processes. This is because of the fact that tectonic structures within crust are the principal channelways of transporting the hydrothermal fluids from their sources towards the traps and thus potential mineralization zones. Results from the two independently analyzed data sets, SRTM and Landsat ETM+ data, were superimposed for interpretation. The detailed steps on the method used for Landsat ETM+ data processing and analysis are described in section 6.

2.2   Objective II

Results from Objective-I were used to select the favorable areas for the alteration mapping of achieving Objective-II. The area selected (the Bulyanhulu Mining District) is highly fractured and shows high intensity of hydrothermal alteration according to the overlay results from Landsat ETM+ and SRTM data. ASTER data was used in the extraction of different alterations related to Archaean granite-greenstone belt gold deposit models, these are lode-Au (vein type) and shear zone-hosted deposits, Au-VMS deposits, and Intrusion related deposits. The ASTER data was selected to be used at this stage because of its ability to map individual alteration minerals. The data has relatively high spectral resolution compared to Landsat ETM+ data. The important thing to note is that the extraction and mapping of the alteration is based on the identification of more than one diagnostic mineral. For example, sericite alteration can be extracted and supported by using the presence of two or more of the associated mineral phases i.e. sericite/muscovite, chlorite, and illite. The hyperspectral data could also be used at this stage but the budget did not allow buying such expensive data. The detailed processing, analysis and interpretation of the ASTER data is described in section 7.

2.3   Objective III

The alterations extracted from ASTER data in Objective-II were used for mapping the alteration zoning for achieving the following Objective-III. One of the characteristics of hydrothermal mineral deposits is that they form alteration zones at or adjacent to, and laterally away from the fluid focal points or upflows, the fluid focal points are also prospective areas for mineralization. Alteration minerals in these zones reflect the pressure-temperature conditions of their formation, fluid

4

chemistry, host rock mineralogy and fluid to rock ratio. For example, distal alteration minerals are formed as a result of low fluid temperature and low fluid to rock ratio. If that is the case, alteration zoning around fluid upflow or mineralized zones can be mapped using alteration mineral assemblages e.g. the extracted alteration types from Objective-II above.

Mapping of alteration zoning was conducted by following the approach that will further allows to identify individual alterations in the end product. This is because the ability to identify these zones will simplify interpretation processes and later identification of exploration targets. The mapping was through combination of alteration zone in a process which resembles the construction of Golomb Rulers in mathematics. The procedures and results for the whole process of creating alteration zoning are found in section 7.

2.4   Result Validation

Two field campaigns were conducted in the three selected test sites of the study area. Both rock and soil covered areas were included in the selected test sites. These sites are those areas that showed alteration zoning similar to gold deposit models in Archaean granite-greenstone belts. Samples collected from the alteration zones in Objective-III were analyzed by different methods for testing and verification. Field observations, colour variations between alteration zones from soil covered areas as well as differences in spectral shapes between alteration zones in both soil and rock covered areas were used at this stage. Detailed verification of alteration zones was performed through mineralogy studies in each alteration zone. Thin sections examination of minerals and ore minerals in samples from soils and rocks using both light microscopy and Scanning Electron Microscopy (SEM) was conducted. XRD analysis was also included in the identification and verification of alteration minerals.

Geochemistry of rocks and soils as another important tool in hydrothermal alteration studies and mineral exploration was conducted to investigate relationships between elements, which typically constitute molecules of alteration minerals. Investigation of gold concentrations and related pathfinder elements in respect to the alteration zones was another method used during validation, also mineral spectroscopy by TerraSpec (VNIR-SWIR) instrument was applied to verify differences between alteration zones.

Interpretations from aerial and ground magnetic data from a publically released exploration technical report by **Tembo Gold Corp. Company** in which the explored area include two of the test sites in this study, were also included for comparison with the alteration zones mapped from the ASTER data.

INPUTS	PROCESSING	RESULTS
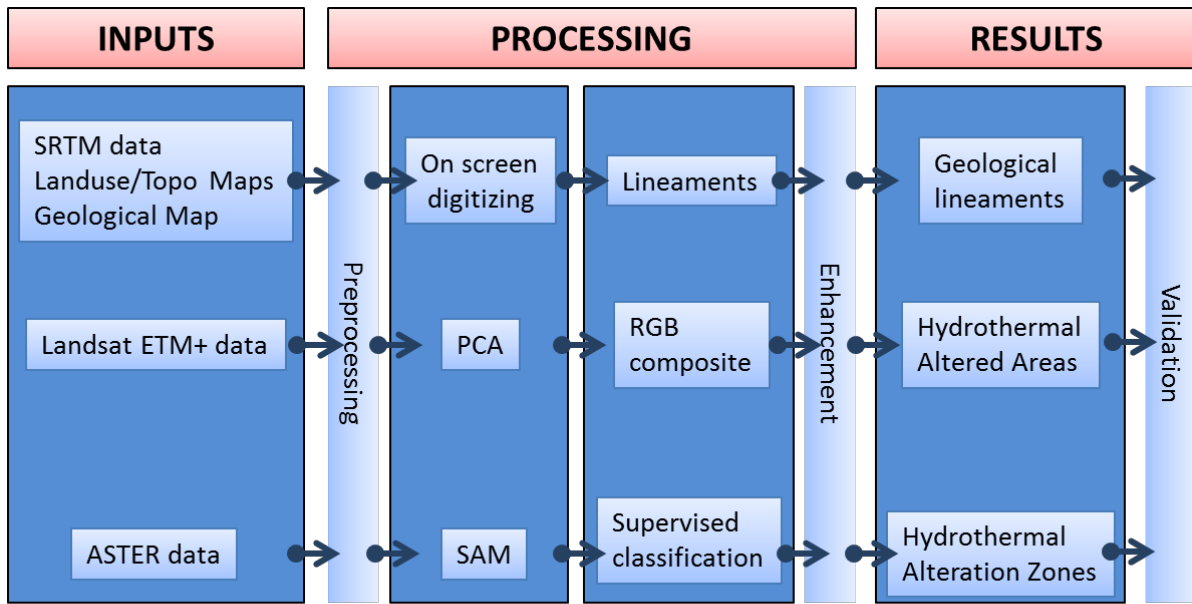
PCA Principal Component Analysis
SAM Spectral Angle Mapper
RGB Red Green Blue

Figure 2.1 The summarized workflow of this study

3   THE GEOLOGY OF THE STUDY AREA

This section gives a general description on the geology of the Archaean Tanzania Craton and Sukumaland Greenstone Belt (SGB) (Fig. 3.2). Most of the descriptions have been referred from old to recent geological reports and different publications, which have described the geology and gold mineralization of the Craton (e.g. Stockley, 1936; Harpum, 1970; Barth, 1990; Borg and Shackleton, 1997; Ikingura et al., 2010). Additionally, several reports from a technical cooperation project from 1988 to 1993 between Germany through the Bundesanstalt für Geowissenshaften und Rohstoffe (BGR) and Tanzania by the Geological Survey of Tanzania (GST) as well as some exploration reports from different companies have described in detail some parts of region and therefore were effectively used in this section. The publications used are mostly from 1990s to recent, for example Borg et al. (1990) and Kabete et al. (2012). The geological map of the whole SGB has been digitized in this study from more than 25 quarter degree sheet (QDS) maps most with scale of 1:100,000, 1:125,000 and 1:250,000.

3.1   The Study Area

3.1.1   Climate, Topography and Vegetation Cover

The Lake Victoria gold field (LVGF) is comprised of seven regions of the Tanzanian mainland, namely, Mara, Mwanza, Shinyanga, Singida, Tabora, Geita and Simiyu. The Sukumaland greenstone belt (SGB) is mainly found in the Geita, Simiyu and Shinyanga regions. Referring to the published climate data (e.g. Tesha, 2003), the region has mainly two seasons, i.e. a rainy and a dry season. The rainy season is confined within a time window from October to May and the remaining months of the year have minimal to no rainfall, characteristically in these months especially June, July and August , the areas

are dry (Fig. 3.1). The two rainy seasons together give the mean annual rainfall of about 1.264 mm. The temperature in the region ranges between 14°C and 30°C whereby September is the warmest month with an average temperature of 29.2°C at noon, and July is coldest with an average temperature of 14.6°C at night. Topographically, the area is hilly for example in the northern SGB, west and south-west of Geita; also the area has gentle slopes and flat lowlands. Pediments which generally are gently sloping towards the drainage depressions are also present. These pediments are vulnerable to erosion, particularly where vegetation cover has been removed as a result of cultivation, small scale mining, or overgrazing. The average elevation in SGB is 1.300 to 1.100 meters above sea level (Tesha, 2003). Some parts of the study area are covered by open forests, mostly to the west of the Geita district. The forest covers mainly open and closed woodlands to the western side of the SGB and is a hindrance to mineral exploration in this area. Other parts of the SGB are covered with bushed grassland and cropland, which mostly dies in the dry season (Survey and Mapping division, Ministry of Natural Resources and Tourism, Tanzania, 1996).
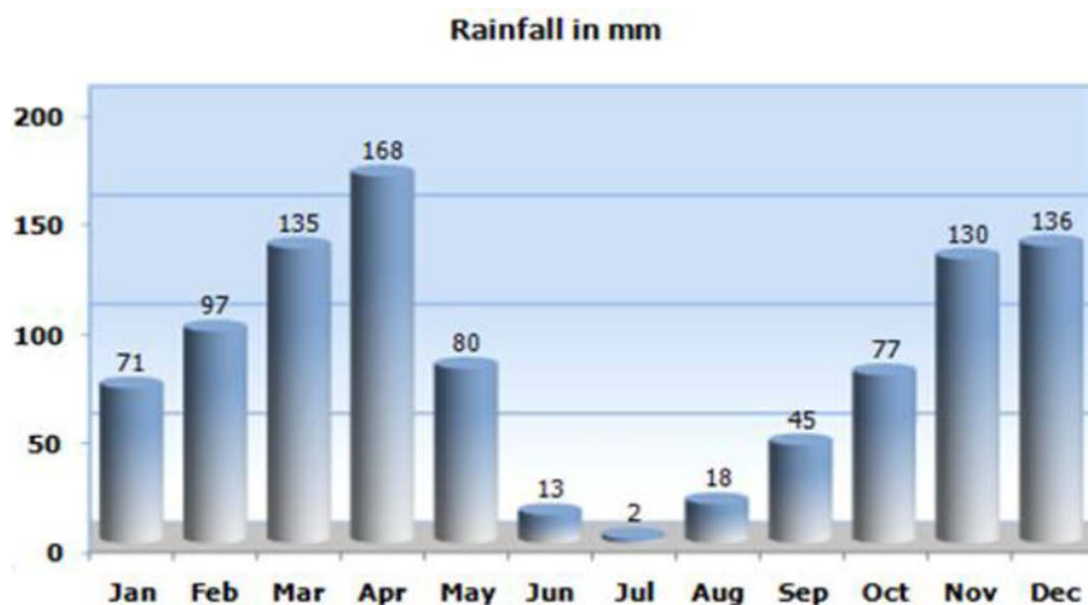
Figure 3.1 Average rainfall in mm for Kahama district, (graph adapted from Pauls and Goldsmith, 2012)

3.1.2   Location and Accessibility

The study area can be accessed by air or motorway from Dar es Salaam, the Tanzania business city. By air it takes approximately 1 hour and 30 minutes from Dar es Salaam to Mwanza, then with small charter planes it takes about 30 or 45 minutes from Mwanza to Geita or Bulyankhulu Gold Mines respectively, these are amongst the major gold mines in the region, which have small airstrips. By using the road from Mwanza to the study area, one has to drive approximately 200 km in a mixed tarmac and dirt roads, the latter becoming impassable easily during the rainy season.

3.2   Geological Background

3.2.1   Geology of the Lake Victoria Gold Field (LVGF)

The Lake Victoria Gold Field (LVGF) (Fig. 3.2) is situated on the stable Archaean Tanzania Craton, the central nucleus of the preserved Archaean continental crust in East Africa. The Craton extends from central Tanzania towards southwestern Kenya and is bordered by the Neoproterozoic Mozambique

Belt rocks towards the east. Further towards southeast Uganda, the Craton is bounded by the 2.0 Ga Proterozoic metamorphic rocks, which locally constitute the Ruwenzori Belt (Clifford, 1970; Borg and Shacklecton, 1997). The western side the Craton is bordered by the newly defined Mesoproterozoic (1.37 Ga) Bukoban rocks, these rocks are comprised of gently folded to flat lying tabular and commonly reddish sedimentary units i.e. shales, siltstones, sandstones, arkoses, ortho-quartzites and dolomitic limestones with cherts, stromatoliths and occasional ooliths. These sediments are typically anorogenic and of continental origin and are partly associated with flood basalts and andesites (Henderson, 1960; Halligan, 1962; Harpum, 1970; Bath, 1990; Pinna et. al., 2004). The southern part of the Archaean Tanzania Craton is bordered by the Paleoproterozoic high grade metamorphic Ubendian Belt, which joins the Mesoproterozoic (ca. 1.37-1.30 Ga) Karagwe-Ankolian metasediments to the far west. The latter is comprised of a variety of high grade metamorphic rocks of both sedimentary and igneous orgin, e.g. biotite-garnet-kyanite schists, quartzose-garnetiferous gneisses, amphibolite and hornblende gneisses, phyllites, crystalline limestones, graphitic schists, and granulites. Structural features of the Ubendian rocks were caused by a strong deformation that gave rise to both cataclastic and crystalloblastic deformation, which also resulted in the presence of mylonites, e.g. in the Livingstone Mountains and also phylonites found everywhere in the belt (McConnell, 1950; Spurr, 1952; Harpum, 1970; Quennell et al., 1986; Boniface, 2009). The eastern part of the Archaean Tanzania Craton is bordered by the Paleoproterozoic Usagaran and Neoproterozoic Mozambique Belts. The belts are extensively migmatized and comprise high-grade metamorphic rocks ranging from schists to gneisses. Granulites and biotite gneisses of pelitic origin occupy a large portion of the total thickness of the Usagaran Belt, which is also considered to be the counterpart of the Ubendian Belt (Quennell et al., 1986; Muhongo et al., 2003; Pinna et al., 2004).

The Archaean Tanzania Craton has been subdivided into two main terranes: the deformed high-grade metamorphic terrane of central Tanzania and the low-grade granite–greenstone terrane of northern Tanzania, southeastern Uganda, and south-western Kenya (Clifford, 1970). Basing on the recent tectonic architecture developed from the syntheses of geochronological studies, which combined new SHRIMP U-Pb data and the interpretation of aero-geophysical data, Kabete et al. (2012) subdivided the country into seven Superterranes. Among the Superterranes, the East Lake Victoria Superterrane, the Lake Victoria-Lake Eyasi Superterrane, and the Lake Nyanza Superterrane are located in the northern part of the Craton. With regard to gold mineralization in the region, the East Lake Victoria Superterrane and the Lake Nyanza Superterrane comprise all major gold deposits discovered so far in the Archaean Tanzania Craton. However, by following the traditional tectonic domains of Barth (1990), the Archaean Tanzania Craton is composed of three lithostratgraphic/tectonic domains, namely the Kavirondian Supergroup, Nyanzian Supergroup and Dodoman Belt.

3.2.1.1 Dodoman Supergroup

The Dodoman Belt as one of the Achaean Tanzanian lithostratigraphic domains is found in the southern part of the Craton in central Tanzania. The belt is comprised of Archaean rocks, similar to other domains, however, with a different metamorphic grade. Contrary to the Nyanzian and Kavirondian, the rocks of the Dodoman have suffered high-grade metamorphism and migmatization (Kröner, 1977). Lithotypes in this belt include hornblende-sericite schist, talc-chlorite schists and highly metamorphosed rocks such as hematite-quartzites, biotite gneisses, amphibolites and garnetiferous hornblende gneisses (Wade and Oates, 1938; Quennell et al., 1956; Barth, 1990; Maboko and Nakamura, 1996). The absence of limestones and pelitic rocks in the Dodoman has been

taken as a diagnostic feature of the Dodoman Belt in comparison to other high-grade metamorphic belts, i.e. the Ubendian and Usagaran. The absence of pelitic rocks has been related to the introduction of a large quantity of granitic materials, which have converted the pelitic rocks to corundum schist, biotite gneisses and migmatites (Hurpum, 1954).

Using strontium isotope dating, the age of lithium-bearing pegmatites from the Dodoman belt were found to be 3.250±325 Ma (Holmes and Cahen, 1955). Furthermore, following the establishment of geological succession, it was suggested that the Dodoman belt represent an event at 2.9 or 3.2 Ga (Barth, 1990; Borg, 1992). Conversely, the dating conducted in both the Nyanzian Supergroup and Dodoman Belt, suggested that the presence of presumably Dodoman rock relicts in Nyanzian is negligible. Migmatitic gneisses, "previously assumed to be the Dodoman basement to the Nyanzian" south of Kahama gave ages of 2.680±3 Ma and 2.570±50 Ma and these results indicates that the migmatitic gneisses are of similar age to the Nyanzian rocks (Rammlmair et al., 1990; Borg and Krogh, 1999). The idea is also well supported by a 2.600 Ma age of Dodoman gneisses in the Iringa area, reported by Maboko and Nakamura (1996), and therefore, it was concluded that the Dodoman and Nyanzian rocks were contemporarily formed following their age similarity (Borg and Krogh, 1999). However, recent studies by Kabete (2008) and Manya (2008) revived the idea from Grantham et al (1945) that the Dodoman Belt constitutes the basement within the Archaean Tanzania Craton and is underlying the Nyanzian rocks. These authors reported 4.013 ± 4 Ma and 3.604 ± 6 Ma U-Pb SHRIMP zircon ages for fuchsite-sericite quartzites from the Dodoman Belt and Sm-Nd > 2.975 Ma for high silica rhyolites from the Nyanzian Supergroup respectively, they have interpreted these ages as the age of an igneous precursor. Whether the Dodoman rocks are the basement to Archaean Tanzania Craton or not, the disagreements above indicate that further studies and particularly far more absolute age dating are required to formulate a correct evolution model that fits with the existence of the Dodoman rocks.

3.2.1.2   Nyanzian Supergroup

The name Nyanzian was proposed by Stockley (1943) for what he was referring to as "Musoma Series" and "Upper Division Basement Complex" as explained in Barth (1990). The Supergroup is comprised of a sequence of basic and acidic metavolcanic rocks, banded iron formations (BIF) and associated clastic metasediments. The latter are reported to accumulate generally in zones of weakness within the Craton (Naylor, 1961, Barth, 1990; Rammlmair et al., 1991; Borg and Shackleton, 1997).

Mafic metavolcanic rocks, which commonly comprise metabasalts and metaandesites, are positioned in the lowest part of the Nyanzian stratigraphy, followed by acid metavolcanics, which are metarhyolitic to metarhyodacitic in composition and locally intercalated with clastic metasediments, e.g. metapelites. Chemical sediments, which are mainly BIF with intercalations of magnetite, chert, quartzite and shale overlie the acid metavolcanics (Stockley, 1936; Grantham et al., 1945; Barth, 1990; Borg, 1992; Borg and Krogh, 1999; Manya and Maboko, 2008; Mtoro et al., 2009). Referring to Borg (1992), the Nyanzian Supergroup is divided into two parts, the Lower and Upper Nyanzian. The Lower Nyanzian comprises ultramafic rocks, mafic to intermediate metavolcanics and graphitic schists, which are pyrite- bearing in places, the Upper Nyanzian comprises BIF, sandstones, siltstones, black shale, lapilli tuffs and felsic metavolcanic flows.

Metavolcanic rocks, converted to greenstones, of both basic and acidic composition are found all over the LVGF. The style of their spatial distribution in the Archaean Tanzania Craton (e.g. in Grantham et al., 1945; Quennell et al., 1956; Harpum, 1970 and Barth, 1990) has defined eight greenstone belts in the region. On the Tanzanian side, there are six greenstone belts, namely Sukumaland (SGB), which is the present study area, Shinyanga-Malita (SMGB), Musoma-Mara (MMGB), Iramba-Sekenke (ISGB), Nzega (NZGB) and Kilimafedha (KGB), on the Kenyan side, there are two greenstone belts, which are Migori-Kendu (MKGB) and Busia-Kakamega (BKGB) (Fig. 3.2, Borg and Shackleton, 1997). The Nyanzian metavolcanics are metamorphosed mostly to greenschist facies grade. Some parts have been affected by contact metamorphism adjacent to later granitic intrusions, which raised the metamorphic grade up to lower and middle amphibolite facies. These rocks are commonly sheared and extensively traversed by quartz veins. Their textures range from fine-grained to medium-grained and the colors vary from black to grey-green and normally the fine-grained rocks are darker colored.

The oldest greenstone rocks in the Nyanzian Supergroup are the > 2.975 Ma (Sm-Nd age) Kibasuka Hills high-silica metarhyolites in MMGB, which have been interpreted to be evidence of older continental crust in Nyanzian rocks (Manya, 2008). Metabasalts in SGB are the second oldest documented rocks, with an age of 2.823±44 Ma (Manya and Maboko, 2003). Various volcanic rocks in the Nyanzian have been dated and, so far the youngest are the MMGB metavolcanics, e.g. tholeiitic basalts, high-Mg metaandesite and metarhyolite rocks, which all gave ages of ca. 2.7 Ga (Manya et al., 2006; 2007). The broad range of ages as well as the described tectonic settings of the Nyanzian greenstone belts (Messo, 2004; Manya, 2004; Wirth et al., 2004; Cloutier et al., 2005; Manya et al., 2006; Mtoro, 2007; Manya and Maboko, 2008) suggest that the greenstones of the Nyanzian Supergroup reflect supracrustal sequences evolved in isolated volcano-sedimentary basins at various geological times as proposed by Manya et al. (2006).

The banded iron formations (BIF) in the Nyanzian Supergroup are fine-grained, laminated and made up of alternating dark material composed of magnetite, hematite and various ferromagnesian minerals, and light bands mainly consisting of fine crystalline quartz or chert (Harris, 1981; Borg, 1992; Maboko, 2001). In places the BIF has been affected by additional silicification and has produced chert. The mode of formation of the BIF is considered to be a chemical precipitation on the seafloor from hydrothermal fluids, which circulated through the underlying mafic volcanic material (Borg, 1994). The age of the BIF was established indirectly through dating of a trachyandesitic unit interbedded with the BIF at Geita Gold Mine. The trachyandesitic unit dates 2.699 ± 9 Ma and apart from being taken as an age of the BIF in the SGB, the age is also considered to represent the youngest age limit for the greenstone sequence in the area (Borg and Krogh, 1999). A similar age within the error range (2.716±11 Ma) has been reported by Chamberlain and Tosdale (2007) for metasandstones interbedded with BIF in the Nzega Greenstone Belt (NZGB). This age difference of BIF from the two greenstone belts i.e. SGB and NZGB suggests that chemical sedimentation in the region occurred in a relatively short specific period approximately within 30 Ma.

The Nyanzian rocks have been intruded by voluminous granitoids (Borg and Shackleton, 1997) and, these granitoids are medium to coarse-grained and are of various colors from light-grey and dark-grey to pink. Some are foliated and contain highly deformed xenoliths and amphibolite rafts of high Mg-andesites, originally caught during the diapiric intrusion of the granites (e.g. in Manya et al., 2006).

The granitoids in the Nyanzian are reported to be of two types, the syn-orogenic granites, which represent the addition of juvenile mantle-derived material into the upper crust, e.g. the 2.668 Ma tonalite-trondjhemite granite (TTG) in the MMGB and the post-orogenic high-K granites (Manya et al., 2007; Mshiu and Maboko, 2012). With reference from previous works (e.g. Mtoro et al., 2009; Manya et al., 2007), the granitoids are described to be younger than the metavolcanics of the Nyanzian Supergroup. The rocks have been emplaced between 2.69 Ga and 2.55 Ga. Rammlmair et al. (1990) and Borg and Krogh (1999) reported the youngest granitoids in the area to be the SGB granodiorites dating at 2.540 ± 70 Ma and 2.530 ± 30 Ma. The average thickness of the Nyanzian rocks estimated from gravity data is reported to be 4 to 6 km, and when Kavirondian rocks are included, the thickness ranges between 5 and 9 km (Borg and Shackleton, 1997).

3.2.1.3   Kavirondian Supergroup

The Kavirondian Supergroup is comprised of rocks, which are similar to sediments of Kavirondo-type in Kenya and hence the type locality name Kavirondian was proposed by Stockley (1943). Kavirondian rocks rest unconformably on top of the Nyanzian Supergroup rocks and their thickness is reported to total approximately 2 km (Stockley, 1943; Gray and McDonald, 1964; Bath, 1990; Borg and Shackleton, 1997).

The Kavirondian Supergroup is made up of non-metamorphosed clastic sedimentary sequences including conglomerates, sandstones and grits, which are interbedded with rare thin horizon of metavolcanics of adakitic composition (Bath, 1990; Manya et al., 2006). These Kavirondian sedimentary rocks are hard compacted pebbly rocks with poor to moderate textural and compositional maturity, these rocks are made up of a great variety of older rocks from the underlying Nyanzian, e.g. banded iron formation (BIF), metavolcanic rocks and granites. The matrix between the pebbles forms a felsitic base with no difference from the groundmass of acid lavas or dacites as described by Stockley (1943) in Quennell et al (1986).

The Kavirondian rocks are widely distributed in the LVGF, they are found in North-Mara and Tarime areas, e.g. in the Majimoto region and Seronera (Gray and McDonald, 1964), but also on small islands in the southern part of Lake Victoria. Kavirondian conglomerates are also well exposed in small outcrop areas on hill tops north of Bulanga-Mirwa (Quennell et al., 1956; Bath, 1990). The occurrence of gold in Kavirondian phyllites, slates, quartzites, sandstone, siltstone and conglomerates at Golden Pride Mine in the Nzega greenstone belt, has revealed the importance of Kavirondian rocks as one of the hosts for gold mineralization in the Craton (Vos et al., 2009; Kwelwa, 2010). In the Sukumaland Greenstone Belt (Borg, 1992; Borg et al., 1992; Borg and Krogh, 1999), the Kavirondian rocks present are mostly conglomerates, grits and quartzites, e.g. in areas around Geita and the Siga Hills.

Kavirondian rocks generally are not different in age to Nyanzian rocks within the data pool of available absolute ages, and these ages range from 2.475 Ma to 2.680 Ma, and currently the age of 2.475 Ma remains to be the youngest age of the Kavirondian rocks in the Tanzania Archaean Craton (Cahen et al., 1984; Borg and Krogh, 1999; Manya et al., 2006; Chamberlain and Tosdale, 2007).

3.2.2   Structures and Geotectonic

The Archaean Tanzania Craton, similar to other stable Archaean Cratons, has been affected by different tectonic forces, and as the outcome, a number of major and minor fault zones, shear zones, folds and dykes characterize the rocks of the Craton. Results from a country-wide aero-geophysical survey indicate a significant number of linear structures (Barth, 1987; 1990) and a number of systems, differing from each other in strike, have been identified. Structural systems with N-S and WSW-ENE directions were identified to be sets of intermediate and mafic dykes, which intruded during different magmatic events. Examples of these dykes are the Proterozoic and Archaean dykes reported in the Sukumaland greenstone belt (Borg, 1990; Borg and Masolla, 1991; Borg and Krogh, 1999). NW-SE and SW-NE systems represent the two dominant sets of Nyanzian (conjugate) shear zones and faults. The other one is a prominent E-W system, which reflects the orientation of Nyanzian rocks striking mostly along the direction of metavolcanics and BIF, for example Nyanzian rocks shown by Vos et al. (2009). Apart from reflecting Nyanzian rocks orientations, the E-W structures also represent some of the major shear zones and faults, for example Bulangamirwa shear zone in the Nzega greenstone belt, which strikes E-W for about 150 km (Kabete, 2008; Kwelwa, 2010).

With reference to Stockley (1948), Grantham et al. (1945) and Borg (1992), two major deformational events, a D_1 and D_2 event, have affected the area. The first deformation, D_1 resulted in the formation of isoclinal folds with steep to vertical axial planes and horizontal fold axes. Strike directions of D_1 followed the general trend of the greenstone rocks. D_2 produced prominent fold shapes with parasitic S- and Z-folds, flexures and kink folds plunging with moderate to relatively steep angles in different directions. These events are reported to be of regionally N-S compressional nature and the best examples are the folds in Sukumaland Greenstone Belt (Borg, 1992).

Cross-folding is a diagnostic characteristic of the Nyanzian deformations and differentiates Nyanzian from later mobile belts, i.e. the Ubendian and Usagaran. Harpum (1970) reported the attitudes of fold axes and axial surfaces of Nyanzian rocks to vary considerably to the extent that they do not correlate even over short distances, this makes the coordinates of various structural planes and vectors in the region to have much dereferences. The seemingly random pattern of fold axes in the Nyanzian has been suggested to be caused probably by the active forces of extensive diapiric granite emplacements. If that is the case, therefore, granitic intrusions are considered to have played an active part in structural attitude and pattern of the Archaean Tanzania Craton.

Structurally the Kavirondian is far simpler than the Nyanzian, e.g. folding is generally open with little tectonic complexity. However, the general trend of Kavirondian folding is similar to that of the adjacent Nyanzian and in most cases Kavirondian appears to have been in-folded within the Nyanzian (Harpum, 1970).
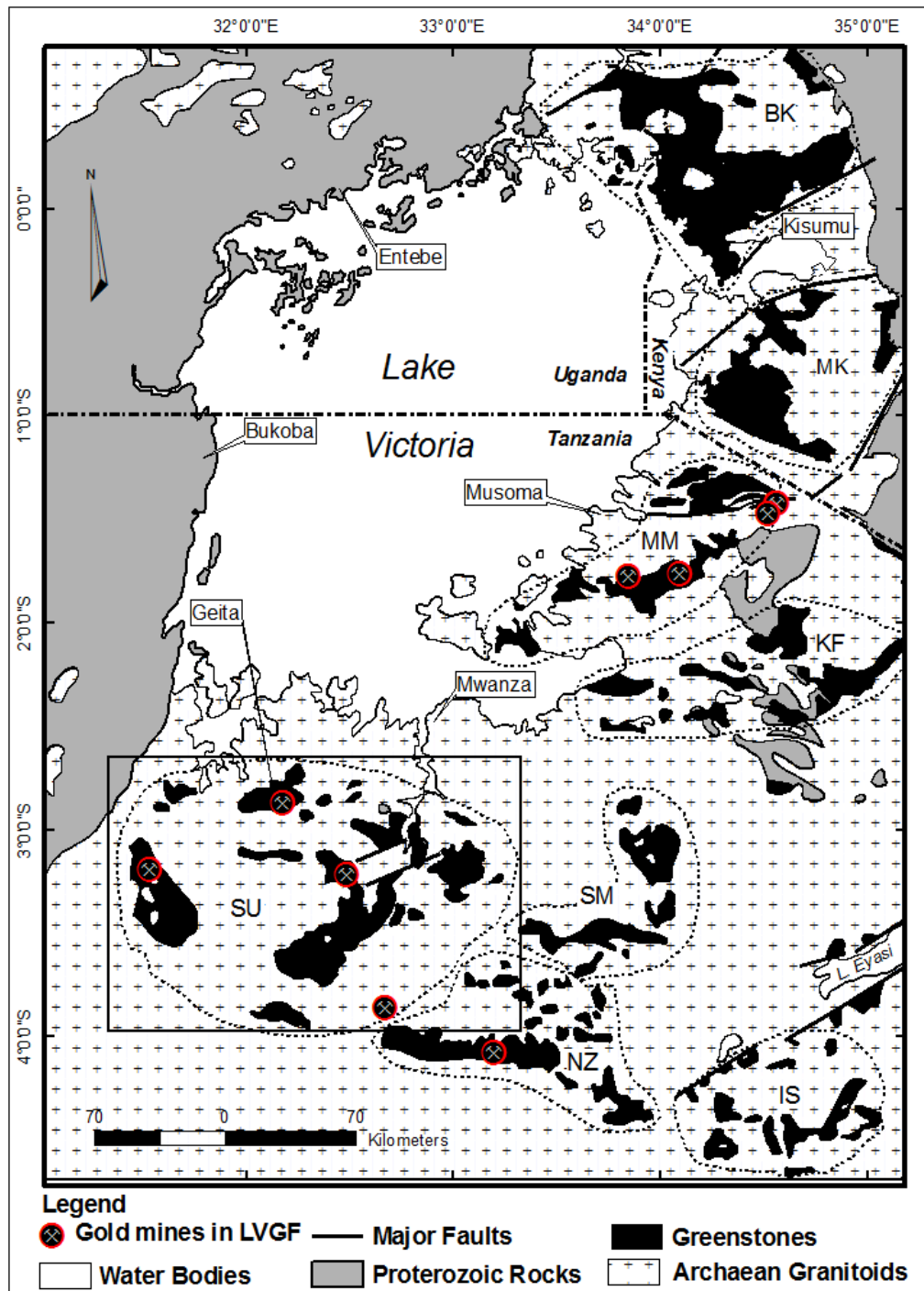
Figure 3.2 Map showing part of Archaean Tanzania Craton and the Lake Victoria Gold Field (LVGF), the greenstone belts and major gold deposits. The greenstone belts are Sukumaland Greenstone Belt (SU) enclosed in the box also the study area, Shinyanga-Malita Greenstone Belt (SM), and Kilimafedha Greenstone Belt (KM), Musoma-Mara Greenstone Belt (MM), Nzega Geenstone Belt (NZ), Iramba-Sekenke Greenstone Belt (IS), Migori-Kendu Greenstone Belt (MK) and Busia-Kakamega Greenstone Belt (BK).The map has been modified from the Geological survey of Tanganyika (1952), Barth (1990), Borg and Shackleton (1997) and Pina et al (2004).

3.2.3   Geology of Sukumaland Greenstone Belt

The Sukumaland Greenstone Belt (SGB) is the largest of all greenstone belts in the Lake Victoria Gold Fields (LVGF). The belt is located in the far west of the Craton and immediately south of Lake Victoria (Fig.3.2). The oval-shaped SGB comprises both basic and acidic metavolcanics, BIF, granites and Kavirondian clastic sediments as major rock types (Naylor, 1961; Manya, 2004; Cloutier et al., 2005; Manya and Maboko, 2008). Mafic volcanics, mostly metabasalts, in some places with pillow structures, occupy the lowest part of the Lower Nyanzian rocks in SGB. The presence of pillow structures in basaltic rocks suggests submarine volcanism. Felsic metavolcanics, mostly rhyollitic flows, overlie mafic metavolcanics in the Lower Nyanzian; they occur in parts locally and hold xenoliths from mafic rocks probably from underlying Lower Nyanzian basalts. Chemical sediments, such as oxide and sulfide-BIF, also occur as minor intercalations within the Lower Nyanzian. Upper Nyanzian is comprised primarily of chemical sediments, mostly BIF, but also felsic metavolcanic rocks, mainly of rhyollitic composition and clastic sediments (Borg, 1992; Mtibilo, 2007). However, regarding the stratigraphy, rocks dating from both the Lower and Upper Nyanzian indicate the two to have formed more or less coevally (Borg and Krogh, 1999; Manya and Maboko, 2003; Manya and Maboko, 2008). Previously, rocks in the Lower Nyanzian, the metavolcanics in the inner arc of SGB were regarded to be relatively older than the Upper Nyanzian rocks, which were mostly metavolcanics in the outer arc. The recent publications indicate that the age relationship of the various units still needs to be unraveled. The BIF in the SGB have been categorized into three types (Borg, 1992), there is magnetite-chert BIF, magnetite-hematite-chert BIF and chert BIF.

Intermediate to mafic dykes and sills are also reported in the SGB and due to a high degree of weathering they can only be detected from underground exposures and aeromagnetic data as has been reported by Eberle (1988) in Borg (1992). The dykes trend N-S and WSW-ENE directions wherein their existence are suggested to be results of mntle derived magmatic activities in the region (Borg, 1994).

SGB is highly endowed with gold mineralization and to date it is the leading greenstone belt for the production of gold. Currently the SGB has four major operating gold mines. The highest grades of gold in the SGB are found mostly in shear zones, as veins and replacements in greenstones and BIF. Mineralization is structural controlled with economic concentrations found in faulted, sheared and highly deformed areas (Borg, 1991; 1994; Mtibilo, 2007). Pb model ages of 2.534 Ma and 2.568 Ma were dated from galena in quartz veins of which these ages are also suggested to date events of gold mineralization in the SGB. The maximum age for gold mineralization in the SGB is reported to be at 2.644 Ma, the age of a lamprophyre dyke that has been mineralized together with BIF in Geita Gold Mine (Borg and Krogh, 1999). Figure 3.3 shows the generalized geological map of the SGB digitized from 25 QDS geological maps.
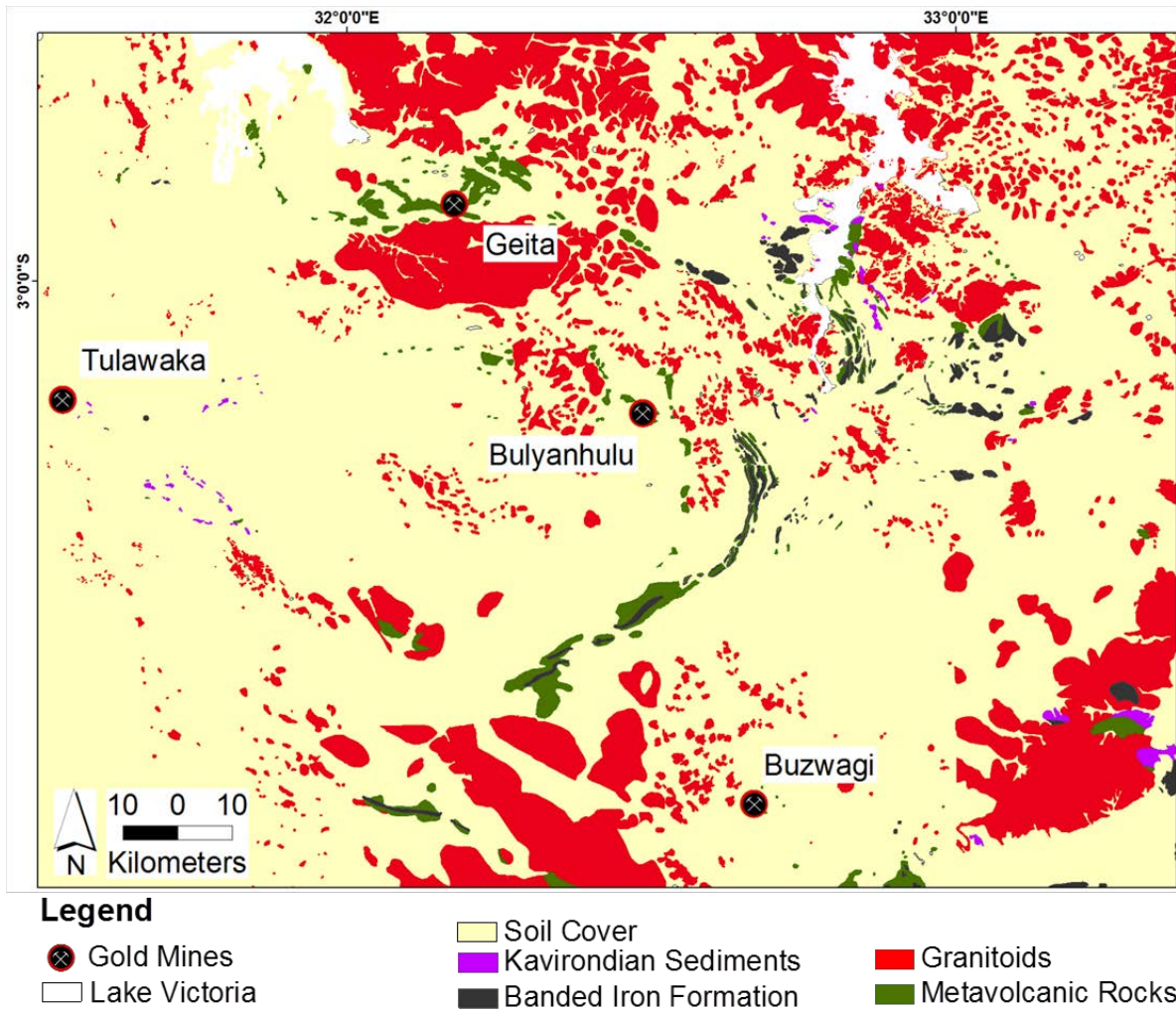
Figure 3.3 Geological map of the SGB compiled from several geological maps of the region

4 MINERALIZATION AND MAJOR GOLD DEPOSIT

The section describes the general mineralization of the LVGF and of the gold deposits in the Sukumaland Greenstone Belt (SGB). The work has been summarized from different scientific papers, reports and geological maps of the study area.

4.1 Mineralization

Most of the gold mineralizations in the Achaean Tanzania Craton are located in Nyanzian Supergroup rocks. The abundant occurrence of gold in this region has led to the name Lake Victoria Goldfield (LVGF); the name represents the gold mining areas around Lake Victoria (Barth, 1990). The history of gold mining in the LVGF started approximately one century ago (Dantz, 1902; Barth, 1990), for example, the discovery of gold in 1898 by Janke, a Germany prospector at Augusta Victoria Reef (nowadays Jubilee Reef) found in the Siga Hills within the now called Sukumaland Greenstone Belt (SGB) (Barth, 1990). Apart from gold mineralization in the region, silver and base metals e.g. copper, lead and zinc, which are mostly associated with gold are also reported in SGB, however, base metals do not occur in economic quantity (Barth, 1990).

Gold mineralization occurs in all Nyanzian rock types (Borg et al., 1990) though economic concentration is commonly found in greenstone rocks and near the edges of Nyanzian greenstones

15

close to the contact with the surrounding granites. To date, there is only one potential major gold mine (Buzwagi Gold Mine) where economic concentration of gold is found predominantly in granites (LaPeare, 2001; Ikingura et al, 2010). Apart from greenstones and granites, other gold-hosting rocks in the LVGF are BIF and more rarely clastic sedimentary units, good examples for such deposits are the Geita Gold Mine in the SGB and the Golden Pride Gold Mine in the NGB (Fig.3.2).

Mineralization in the LVGF is predominantly tectonically controlled whereby major fractures, shear zones, faults and veins were used to channel mineralized hydrothermal fluids from lower crustal sources to the upper crust, causing the formation of gold deposits in the ductile-brittle transition zone and these fractures also appear to have controlled the intrusion of the observed dyke swarms in the region (Barth, 1990; Borg, 1994). Mineralization follows a specific regional tectonic pattern, which can be largely observed through structural elements. It has been reported and is well known that NW-SE and NE-SW are the two dominant regional orientations of gold bearing structures in the region (e.g. in Borg, 1991; Chamberlain, 2003). Areas with intense tectonic deformation, for example areas of tectonic broadening due to the D_2 folding in Geita area (Borg, 1991), appear to have relatively high total abundance of gold. Other favorable locations for mineralization are in areas where greenstones have been intercepted by faults or major shear structures and in areas where intense folding and dykes have deformed the greenstones. From observations made by exploration pioneers, it has been suggested that a greater amount of gold mineralization was possibly driven by late granitic magmatic event(s) (e.g. in Borg, 1991).

Generally, mineral alteration that relates to gold mineralization is typified by carbonatisation and sericitisation, the alteration is reported to post-date the initial deformation that tilted the stratigraphy into its present attitudes (Chamberlain, 2003). However, carbonatisation is a conspicuous feature throughout the Nyanzian sequence (Barth, 1990; Rammlmair, 1991). Other alterations include silicification, chloritisation, ferruginisation, minor tourmalinisation, pyrophyllite, and sulfidation. A general paragenetic sequence of pyrite, pyrrhotite, chalcopyrite, arsenopyrite, galena, sphalerite, magnetite, ilmenite, rutile and hematite has been recorded for a number of sulphides bearing ores in LVGF (Harris, 1961; Gray, 1964; Weiser, 1986).

Harris (1961; 1981) and Borg et al. (1990) described gold occurrences in Lake Victoria Gold Field of which they outlined 5 types of gold mineralization as they are mentioned here below:

- **Impregnated Gold**: Occur as low grade dissemination of auriferous sulfide in metavolcanic rocks, banded ironstones and tuffs. This kind of gold which, locally occurs in the shape of a halo is apparently controlled by the existence of zones of more intense fracturing and brittle deformation.
- **Gold in Mineralized Shear Zones**: Gold with or without sulfides is associated with reefs, lenses and stringers of dark quartz in major zones of shear. These mineralized shear zones occur in country rocks of various kinds but commonly in the greenstones. Shearing has mostly been observed to occur at the contact between two rock types normally granite and greenstones, or between BIF and greenstones (e.g. diorite, as at Geita).
- **Gold in Quartz Reefs**: This is gold with or without sulfides, concentrated in small quartz reefs mostly filling simple fissures.
- **Clastic- Hosted Gold**: This occurs in metasediments of the Kavirondian. Mineralized rocks are commonly conglomerates and quartzite.
- **Gold in Alluvial/Eluvial**: This type of gold is associated with secondary placers and is found associated with all of the above primary gold occurrences. This type of gold occurrence is the one mostly mined by local artisanal miners in the LVGF.

The discovery of gold occurrences in Tanzania has recently extended from greenschist facies rocks to high grade metamorphic rocks, which previously were regarded as barren. Numerous gold occurrences have been reported in high-grade metamorphic rocks of Dodoman and Usagaran-Ubendian Belt and currently in different places of the high-grade metamorphic rocks of Pan-African Orogeny. A good representative example for the Pan-African Orogeny gold is the recent discovered gold deposit in Magambazi, a small town in the Handeni district, northeastern Tanzania (Kabete, 2008). By referring the Superterranes of Kabete (2012), the Magambazi gold deposit is located in the Kilindi-Handeni Superterrane. However, observation of several datasets, combined with geochronology, also similarity in orientation between the NW-SE Lake Nyanza Superterrane and Kilindi-Handeni Superterrane (Kabete et al., 2012), has influenced the author to suggest the amphibolite belt in Handeni is representing the relicts of Archaean greenstone terranes, which were overprinted by Proterozoic high-grade metamorphism of the Pan-African event (s).

Gold in high grade metamorphic rocks is also reported in the Paleoproterozoic Ubendian belts, in areas locally named Mpanda Mineral Field (MMF) and Lupa Gold Field (LGF), as well as in the Usagaran belt (Ikingura et al. 2010). As the consequence of the thriving gold occurrence in high grade metamorphic rocks, exploration companies has been inspired to expand exploration activities towards Proterozoic high grade metamorphic rocks in Tanzania. Currently, senior and junior exploration companies are busy working in these terranes including the Archaean high grade metamorphic rocks of the Dodoman Belt.

Back to the LVGF, there are five major operating mines, these are, Geita, Bulyanhulu, Buzwagi , North-Mara and Tulawaka Gold Mines , the Golden Pride Mine has recently been closed. Most of these major gold deposits are found in the Sukumaland greenstone belt (SGB) except Golden Pride and North-Mara gold mines, which are found in Nzega (NGB) and Musoma-Mara Greenstone Belts (MMGB) respectively. The large number of major gold mines in the SGB helped with the decision on choosing the study area for the project. Therefore, the selection of the study area is based on the number of deposits since it is easier to test and compare the results of this study with gold occurrences in the SGB due to the larger number of deposits and occurrences.

4.2   Major Gold Deposits in Sukumaland Greenstone Belt

4.2.1   Geita Gold Mine

Geita Gold Mine is located in the northern greenstones of the outer arc of the two concentric eye-shaped greenstone sequences in the Sukumaland Greenstone Belt (SGB) (Fig. 3.2). The mine is within E-W trending ca. 60 km long and 15 km wide exposed metavolcanic rocks, immediately to the south of Lake Victoria (Borg, 1994, Fig. 3.2). The rock types surrounding the deposit are chemical sediments, cherts and banded iron formation (BIF), felsic volcanic flows, tholeiitic basalts, massive and laminated tuffs, lapilli tuffs, dioritic intrusives, and clastic sediments like sandstones and black shales (Barth, 1990; Ikingura et al., 2010). The western part of the belt, including the Geita area, is cut by regional scale, NE-trending quartz-gabbro dykes of Proterozoic age and to a lesser extent by NNW-trending Karoo dolerite dykes. The entire belt has undergone greenschist facies metamorphism. Host rocks in Geita are BIF and greenstone units, the overlaying felsic to intermediate tuffs and relatively low grade gold in diorite intrusives (Borg, 1990; 1994).

Structurally, Geita has been affected to a large extent with a D_2 folding; D_2 was deduced on the orientation of spaced cleavage observed within weathered sediments of which measurements of the foliations suggests a NNE-SSW compression direction. The folding is isoclinal, reclined anticline with

axis plunging ca. 45° towards 350°. Its axial plane strikes approx. 40° and dips 60° towards NW, but also shows variations and bends due to refolding (Kuhn and Germann, 1991; Borg 1994). The main zone of mineralization is situated in the major D_2 fold closure (Borg, 1993), within zones of intensive shearing and mylonisation. Ore minerals related to gold occurrence include pyrite, auriferous pyrite and minor pyrrhotite. Abundant magnetite and minor chalcopyrite are also present. High grade ore is reported to follow breccias zones, shear zones especially where more than one shear zones meet and closely spaced ductile-brittle fracture systems (Borg, 1990; Borg and Rittenauer, 2000; Ikingura et al., 2010). Other mineralized zones occur at the sheared contacts between lamprophyre dykes and BIF and within dykes parallel to quartz veins (Borg 1994).

Mineral alterations in Geita reveals zonation, proximal to mineralization is silica-pyrite alteration in BIF and pervasive and patchy silica-pyrite ± sericite ±ankerite and +/- calcite alteration in diorites but epidote is also common. Borg (1994) also added actinolite, biotites and subordinate stilpnomelane, minnesotaite to relate with gold mineralization in Geita. In some areas green hornblende together with the intergrowth actinolite/tremolite were observed. Distal to mineralization, alteration is dominated by calcite ± chlorite ± biotite minerals. Hematite alteration also has been identified and has been suggested to occur as the result of late oxidizing fluids reacting with the Fe-rich carbonate alteration formed during mineralization. Evidence of the above suggested mechanism are calcite veins found within late fractures which are hematite stained as reported by Ryan and Speers (2002). However, the presence of hematite has been suggested by Borg (1994) to be the attribute of meteoritic water and/or supergene processes. Presence of the mineral assemblage actinolite/tremolite-biotite-stilpnomelane-pyrite-pyrrhotite gives an estimated temperature range from 350°C to 480 °C for the hydrothermal alteration and associated environment of gold mineralization in Geita (Borg, 1994).

4.2.2 Bulyanhulu Gold Mine

Bulyanhulu Gold Mine is one of the giant gold deposits in Sukumaland Greenstone Belt (SGB) with a proven reserve of > 20 million ounces of gold at an average ore grade of 15 g/t (Ikingura et al., 2010). Bulyanhulu has been studied in detail by Chamberlain (2003) from where most of the descriptions in this part have been extracted. The mine is located in the inner arc of the two concentric eye-shaped greenstone rocks in Sukumaland Greenstone Belt (SGB) (Fig 2). Geologically, the host rocks of the mine are comprised of Archaean mafic units starting from basaltic lavas which are light-green to grey-green in colour and are reported to have been deposited in a subaqueous setting due to the observed sharp and highly regular characteristics of the boundary between it and the underlying sedimentary rocks (Chamberlain, 2003). These basalts are massive, brecciated, foliated and locally show well-preserved pillow structures. Ikingura et al. (2010) described these basalts as mostly tholeiitic and are a continuation of the Rwamagaza metabasalts that yielded a Sm-Nd isochron age of 2823 ± 44 Ma reported by Manya and Maboko (2003). Apart from basaltic lavas, other basic rocks in Bulyanhulu are metandesites and gabbro intrusions. Felsic metavolcanic rocks have also been reported in Bulyanhulu, locally, they have been categorized into ash, lapilli and agglomerates. Clastic metasedimentary rocks, locally the Kisii shales (25 m thick and 6 km long) are hosting the principal mineralized quartz veins, Reef-1, in Bulyanhulu. Felsic intrusive, granitic in composition, intrudes the above mentioned metavolcanic rocks on the SW side of the mine as shown in Fig. 4.1 from Chamberlain, (2003).

Similar to other gold deposits in the SGB e.g. Geita gold mine (Kühn and Germann, 1992; Borg, 1993, 1994; Borg and Rittenauer, 2000), mineralization in Bulyanhulu is structurally controlled. However, for the case of the Bulyanhulu deposit, shear zones are the main ore-controlling structures that follow a metapelitic unit. For example the principal quartz vein, the Reef-1, has been formed as an extensional vein within an active high-angle reverse shear zone during an inferred D_2 shortening event. Numerous shear zones with NW-SE trending orientations have been identified in the deposit; they are also observed to orient sub-parallel to lithological contacts. The principal shear, the host of the principal mineralized quartz vein, coincides with the Kisii shales. Apart from shear zones, other structures such as a NE-trending series of faults, running perpendicular to shear zones and barren, have been reported (Chamberlain, 2003). Mineralization is found in quartz veins, mostly in Reef-1 which is sub-vertical, dipping approx. 80° to 85° degrees. There is also Reef-2, which is also sub-vertical and contains high-grade gold, however, it has no continuity. Low grade gold of subeconomic value has been reported in veins running sub-parallel to the main veins, and the same grade has also been found in porphyry in some places. Thiboutot (1991) in Chermbalain (2003) described Bulyanhulu as a VMS-style deposit, however, Chamberlain (2003) reported the same deposit to be Archaean lode-Au deposit, and if it was a VMS gold, then the gold has been remobilized into structures by the later events. However, the model by Charmbalain (2003) is also supported by Ikingura et al. (2010), they have reported Bulyanhulu gold to be epigenetic through observed gold association with hydrothermal alterations and sulfides as well as by replacement textures. The principal ore minerals related to gold mineralization are pyrite, chalcopyrite and pyrrhotite; others are sphalerite and bismuthotelluride (Bi-Te), which are commonly found as inclusions in chalcopyrite. Arsenopyrite, galena, hessite and gersdorffite occur as minor ore minerals. The association between chalcopyrite and gold (± bismuth and telluride) is reported to account for the highest grade of gold in the deposit. Silver and copper appear to be the elements with direct association to gold, most of the examined gold indicates to occur as native gold or as electrum.

The volcanic rocks have been affected by seafloor spilitisation and have been converted by regional metamorphism to greenschist facies grade; these effects led to the characteristic development of extensive (also regional) chlorite-calcite alteration. However, Chamberlain (2003) reported overprinting of the above regional alteration by gold-related hydrothermal alteration at the Bulyanhulu deposit. Moreover, the late alteration mineral zoning around mineralized structures is composed differently from minerals that are the product of regional metamorphism. Evidence of hydrothermal alteration includes physical gain alignment texture mostly proximal to mineralized zones, and destruction of original mineralogy and growth of hydrothermal minerals. Proximal to mineralized zones, principal alterations are silicification, carbonatisation, sericitisation (white mica) and chloritization, this zone extents up to 60 m and in other places 70 m (Chamberlain, 2003; Ikingura el al., 2010). Upon examination of ore specimens, it has been suggested that carbonate and sericite constitute the significant hydrothermal alteration assemblage. They are pervasive and form micro-veins that cross-cut primary quartz with calcite observed to replace feldspars (Ikingura et al., 2010).
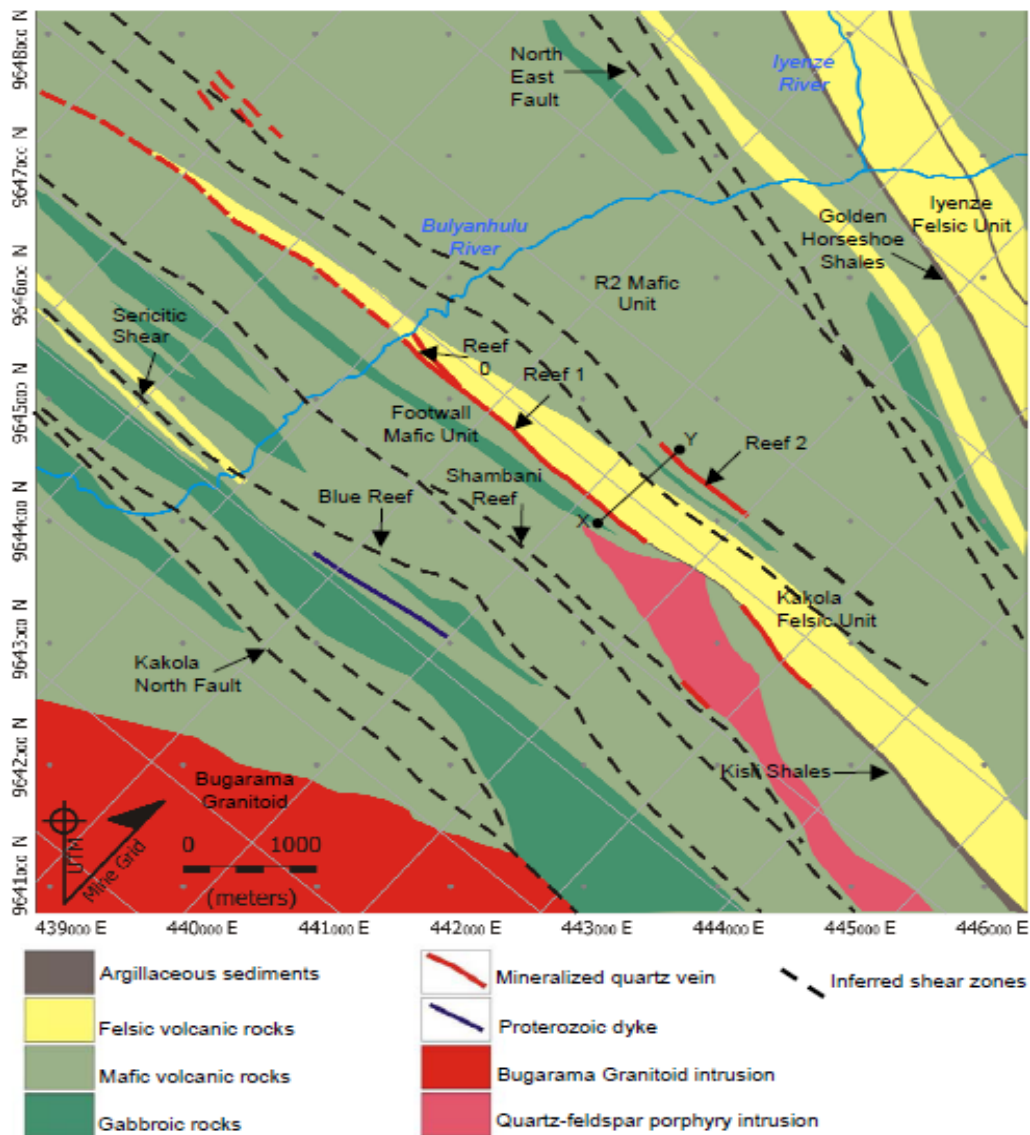
Figure 4.1 Detailed geological map of Bulyanhulu gold mine deposit from Chamberlain (2003)

4.2.3 Tulawaka Gold Mine

Tulawaka deposit is a low-tonnage, high grade (15g/t) deposit, which have approx. 1.71 million ounces (Ikingura et al., 2010).The mine is situated approximately 160 km SW of Mwanza and far west within the SGB (Fig. 2). The deposit is located between the two "eye"–shaped concentric greenstone sequences, previous known as Lower and Upper Nyanzian. The stratigraphy of Tulawaka is comprised of Archaean, Proterozoic and Phanerozoic rocks. Such mixed geological eons together with the tectonic forces that have affected the different rocks in the region, makes the geology of Tulawaka more complicated. The area is covered with a pile of loose sediments (silty sand) with a thickness ranging from 0.5 to 4 meters. The sandy soils are believed to have been transported from north to south and eroded from their source, which are Bukoban sedimentary rocks (Sanfo, 2002). This sand covers a discontinuous layer up to 4 m thick of lateritic duricrust that includes pisolitic material and lateritic gravels. They commonly contain angular fragments of white quartz that are more abundant at the base of the duricrust and have been described as a quartz rubble zone. There are very few outcrops in the region and few emerging banded iron formation (BIF) and granite hills

20 km in the vicinity of Tulawaka mine. The underlying geology at Tulawaka is made by metavolcanics and metasedimentary rocks, which have been metamorphosed to the grade of upper greenschist to amphibolite facies (Thompson, 2002; Kabete al., 2012). The source of metamorphism at Tulawaka is generally related to granitic intrusions. Metavolcanics are tholeiitic metabasalts to metaandesite and metarhyodacites. Trace elements and Nd isotope compositions suggest the metasedimentary rocks at Tulawaka represents a mixture between juvenile detrital component (metavolcanic rocks) and an older differentiated detrital component, which their source is argued to be probably the Dodoman (Cloutier et al., 2005). The rock units above are intruded by 2.544 Ma leucogranites and aplitic dykes; the age of which was suggested to mark the upper limit of gold mineralization at Tulawaka. Mafic volcanism took place at 2.823±44 Ma (Cloutier et al., 2005), which is reported to correlate with the Rwamagaza metabasalt isochron of Manya and Maboko (2003), tens of kilometers east of Tulawaka.

Structurally, the E-SE trending Tulawaka-Nzega Shear is the regional structure suggested to have possibly influenced gold mineralization in Tulawaka (personal communication with V. John). By using the magnetic susceptibility technique, it was shown that major units were folded into relatively tight folds, reclined to the WSW with a reclined axial plane dipping approximately 50 degrees to the ESE (personal communication with V. John). The amplitude of these folds appears to be on the order of hundreds of meters, and wavelengths are of at least one to two hundred meters. Folding in Tulawaka is reported to have occurred most likely syn-metamorphic to late-peak metamorphism, and, after a certain amount of buckling, the west overturned limb of the large anticlinal fold was breached by a westerly-verging fault. Syn- to late-tectonic magmatism produced porphyries which were injected along this thrust fault. Deformation along the thrust fault created several flexures and jogs that became the site of dilation where quartz veining was focused. Flexure and auriferous veins are defining the high grade Au-bodies at Tulawaka gold mine. The above mentioned thrust fault represents the foundation of the Tulawaka East deposit which is the main deposit in the area (Bardoux, 2002 in Rocca and Reid, 2004).

Gold mineralization is hosted in quartz veins, which cross-cut mafic amphibolite and metavolcanic sedimentary rocks, but is also hosted in stockwork quartz within the porphyries (Ikingura et al., 2010; Kabete et al, 2012). Gold occurs in native form within veins or disseminated within quartz grains. Some saprolites, which are mineralized, show no direct spatial relationship with the mineralized quartz veins and this observation suggests that chemical remobilization of gold by a fluctuating water table probably resulted in the accumulation of supergene gold after weathering of the disseminated auriferous sulfides (Rocca and Reid, 2004). The most important primary ore mineral is pyrite, which occurs in all rock units as euhedral grains or smeared out along foliation planes. Pyrrhotite and chalcopyrite are predominantly confined to quartz veins in the dolerite dykes and generally associated with chlorite. Apart from pyrite and pyrrhotite, other sulfides are arsenopyrites and chalcopyrites. The common accessory minerals are biotite, sericite, muscovite, chlorite, epidote and talc-serpentine, all found normally within or adjacent to quartz veins (Ikingura et al., 2010).

Fractures filled with chlorite are very common and breccias made of angular fragments of variable sizes from country rocks are found within a matrix made of "milled" country rocks and a matrix, which generally consists of chlorite and calcite. Apart from the abundance of chlorite and calcite, other types of alterations reported from Tulawaka are sulfidation, carbonatisation, and sericitisation (Ikingura et al., 2010).

4.2.4   Buzwagi Gold Mine

Buzwagi Gold Mine is among the four major gold mines in the region, the mine is located to the southeastern SGB in the area between the SGB and northwestern edge of the Nzega Greenstone Belt (NGB) (Fig.3.3). Buzwagi is underlain by Nyanzian rocks, the dominant lithotypes being orthoclase-rich granites (porphyritic granites), which have intruded Lower Nyanzian metabasalts and intermediate metavolcanic rocks. The granites are inturn crosscut by several narrow, fine-grained, K-feldspar-rich aplitic dykes. The orthoclase-rich granites are the one hosting the principal mineralization zone in Buzwagi and also underlie the majority of the area proximal to the mineralization. Other rock types are metavolcanic rocks, which are reported to be less abundant in the deposit; these are mafic to intermediate in composition with well-developed shear banding on an mm to cm scale (LaPeare, 2001). The metavolcanic rocks contain mineralization as well, however, in smaller amounts and mostly in areas where quartz veins and sulfides dominate (Ikingura et al., 2010). Both granites and metavolcanic rocks have been subjected to shearing, which resulted in a curvilinear N-S trending shear system, which is dipping at 60° to 75° in an easterly direction along a strike length of approx. 900 m - 1000 m and varying width from 5 m to 20 m (LaPeare, 2001). The above fracture shear is considered as a third-order structure of the main E-W Bulagamirwa shear zone, which also controls the mineralization at the Golden Pride and Tulawaka Gold Mines (Ikingura et al., 2010; Kabete et al., 2012). The N-S shear is characterized by intense quartz veining and stockworks which are continuous along the entire outlined structure. The veins are associated with quartz-fluorite-pyrite +/- chalcopyrite, and it is in these veins where gold is dominantly concentrated. Another shear zone runs within the mafic unit at the south end of the main zone and the shear branches-off to the west from the main granite-hosted shear along the contact between granites and mafic volcanics. Gold in this shear zone is associated with secondary, banded-magnetite and pyrite. Disseminated fine grained-magnetite is also reported to be common throughout the mafic unit (LaPeare, 2001). Thus, in Buzwagi the main ore minerals are pyrite and chalcopyrite, which are mostly found associated with gold in quartz veins. The granites are the rock unit which hosts the majority of the deposit, approximately 70%, whereas mafic metavolcanic and ultramafic rocks host approx. 10% and 3-4% of the gold mineralization respectively. Shear zone-hosted and intrusive porphyry-hosted models are the two deposit models, which have been suggested for the Buzwagi gold deposit. The latter is supported by several observed features such as distal carbonate alteration, proximal silicification and quartz-sericite alteration, as well as potassic alteration and disseminated magnetite in the ore zones. Enrichment of fluorine in the form of fluorite, barium, and depletion of CO_2 are other characteristic features observed in Buzwagi Au deposit (LaPeare, 2001). Quartz-sericite alteration is reported to be very common in Buzwagi, the alteration suggested to have been caused by intensive shearing and veining which occur throughout the granite. Other reported alteration minerals are chlorite, hematite, biotite, and serpentines, which are found in an ultramafic unit intercalated with the mafic metavolcanics to the south of the deposit (LaPeare, 2001)

5   LINEAMENT EXTRACTION FROM SRTM DATA

This part describes in detail the processes involved in the analysis of SRTM data as well as the discussion on the geological lineaments obtained from interpretation of the data set used in this study.

5.1   Introduction

Geological structures (e.g. shear zones, faults, folds, fractures and joints etc.) are very important physical components in hydrothermal fluid systems. These structures are typically used as pathways or rather, conduits of the hydrothermal fluids from their deeper sources to upper levels in the crust. Furthermore, most of the hydrothermal ore deposits have a direct spatial relationship to geological structures (e.g. fold hinges, jogs, fracture triple junctions etc.). Structures act as pathways and traps of the hydrothermal fluids during magmatism and therefore play a significant role in the hydrothermal fluid systems and at large in mineralization process. As a consequence, geological and tectonic structures constitute key features and should be one of the first data sets to be gathered during early stages of mineral exploration programs.

Remote sensing technology is nowadays extensively applied in structural geological studies. Data from remote sensing, both aerial and space-acquired, provide a completely new dimension in terms of synoptic view (Gupta, 2003). Different types of remote sensing data are nowadays used as sources to identify geological structures. For example, aero-geophysical data, mostly aeromagnetic, has been a popular data set in mineral exploration for a long time; the data set is purposely used for identifying underground geological units and cross-cutting or dividing structures during regional exploration. It is still a major tool in regional exploration because of this method has a significant depth-penetrating power, which identifies the surface-obscured tectonic structures within the first kilometer of the earth's crust. Despite the technical availability of aero-geophysical data, their cost is still high, and as a consequence, they constitute a significant portion of the overall exploration costs.

Shuttle Radar Topographical Mission data (SRTM) is another type of remote sensing data that have been introduced to users since 2000 (Rodriguez et al., 2006).It is important to note that this data is for free and is available as downloads from different websites (e.g. http://glcf.umd.edu/). Recently, SRTM data has been shown to be a useful tool in the extraction of geological structures and different approaches of analysis can be applied to the analysis of SRTM data to enhance the structures (Ghoneim and El-Baz, 2007; Kinabo et al., 2008; Youssef, 2009; Kusky et al., 2011; Masoud and Koike, 2011). The most important thing is that SRTM data is available for free and also allows the mapping of a large area, similar to other commercially available remote sensing data (e.g. in Kinabo et al., 2008; Masoud and Koike, 2011). Geological characteristics, such as the displacement of lithological beds, truncation of beds, drag effects, scarps triangular facets, alignment of topography including saddles and knobs, streams and straight segment of stream, etc. (Gupta, 2003), allow tectonic structures to be identified in SRTM data. Geological structures or better lineaments in SRTM data are normally mapped after processing/enhancing these images. Different digital techniques for enhancing linear features are nowadays available; for example shading has been mostly used to enhance lineaments by both automatic and manual extraction (e.g. Saha et al., 2006; Masoud and Koike, 2011). From SRTM images, lineaments can be identified using features like sharp tone or colour change, texture, pattern and association (Gupta, 2003). However, care must be taken to avoid mixing of results with artificial linear features during interpretation. The objective of this part of the study was to map the tectonic structures, the significant vectors towards any hydrothermal mineralization, in the Sukumaland Greenstone Belt (SGB) by using the inexpensive data sets, in this case SRTM data.

5.2   Methodology

SRTM data was collected through a radar system on board of the Space Shuttle Endeavour on 11th to 22nd February 2000. The System used two synthetic aperture radars, a C-band system (5.6 cm; C-RADAR) and an X-band system (3.1 cm; X-RADAR) (Farr and Kobrick, 2000). Calculated errors for SRTM data for Africa are as mentioned in the Table 5.1 below:

Table 5.1 Errors associate with SRTM data (Rodriguez et al., 2006)

ERRORS	METERS
Absolute Geolocalion Error	11.9 m
Absolute Height Error	5.6 m
Relative Height Error	9.8 m
Long Wavelength Error	3.1 m

The 1 arc data (SRTM-1, 30 m X-Y resolution) and 3 arc data (SRTM-3, 90 m X-Y resolution and ±30 m root mean square error z accuracy) are the two types of SRTM data available. The latter is available for the areas outside United States and this study has used it for the extraction of geological lineaments in the SGB. The SRTM image used in this study is a sub-scene within the coordinates 2° 0´ 2˝- 3° 59´ 53˝ S latitudes and 30° 59´ 51˝- 33° 59´ 32˝ E longitudes.

The techniques for the identification of linear features from spatial data sets such as satellite and SRTM images are diverse. However, automatic and manual lineament extractions create two major categories of results. For example, the use of algorithms for the automatic identification and extraction of geological lineaments from SRTM is currently common (e.g. Morris, 1991; Tripathi et al., 2000; Masoud and Koike, 2011). In principle, the technique behind the method is edge-detection whereby spatial and morphological filters are the basic tools used to detect lineaments. In this study manual identification of lineaments was used since it allows incorporating geological information obtained from the study area and hence makes the process to be knowledge-based. The SGB has two major regional sets of lineaments, a NE-SW and a NW-SE trending set (Fig.5.3A). These two sets of tectonic structures are important in the region since they also control the regional position of gold mineralization in most of the deposits.

Before extraction, enhancement techniques relevant for visual analysis were applied. Enhancement methods such as stretching and histogram equalization as well as sharp colour ramps were applied during the display of the SRTM image (Fig. 5.1A). Shading is another technique, which has played a great role in the enhancement of lineaments. During shading, directional sun illumination was applied with respect to the two dominant sets of tectonic structures in the region. Sun illumination at 315° NW azimuth and 45° altitude was applied to enhance the NE-SW trending tectonic lineaments whereas 045° NE azimuth and 45° altitude was applied to enhance the NW-SE lineaments (Fig. 5.1B, Fig. 5.1C). Identification and extraction was done on both colour ramp and shaded images, the process relied on abrupt change in colour (tonal patterns), topographical scarps, and linear drainage patterns. On-screen digitization was used to extract the identified lineaments, in which amongst the criteria used was to pick the visually recognizable linear features with a length of at least ≥ 2 km.
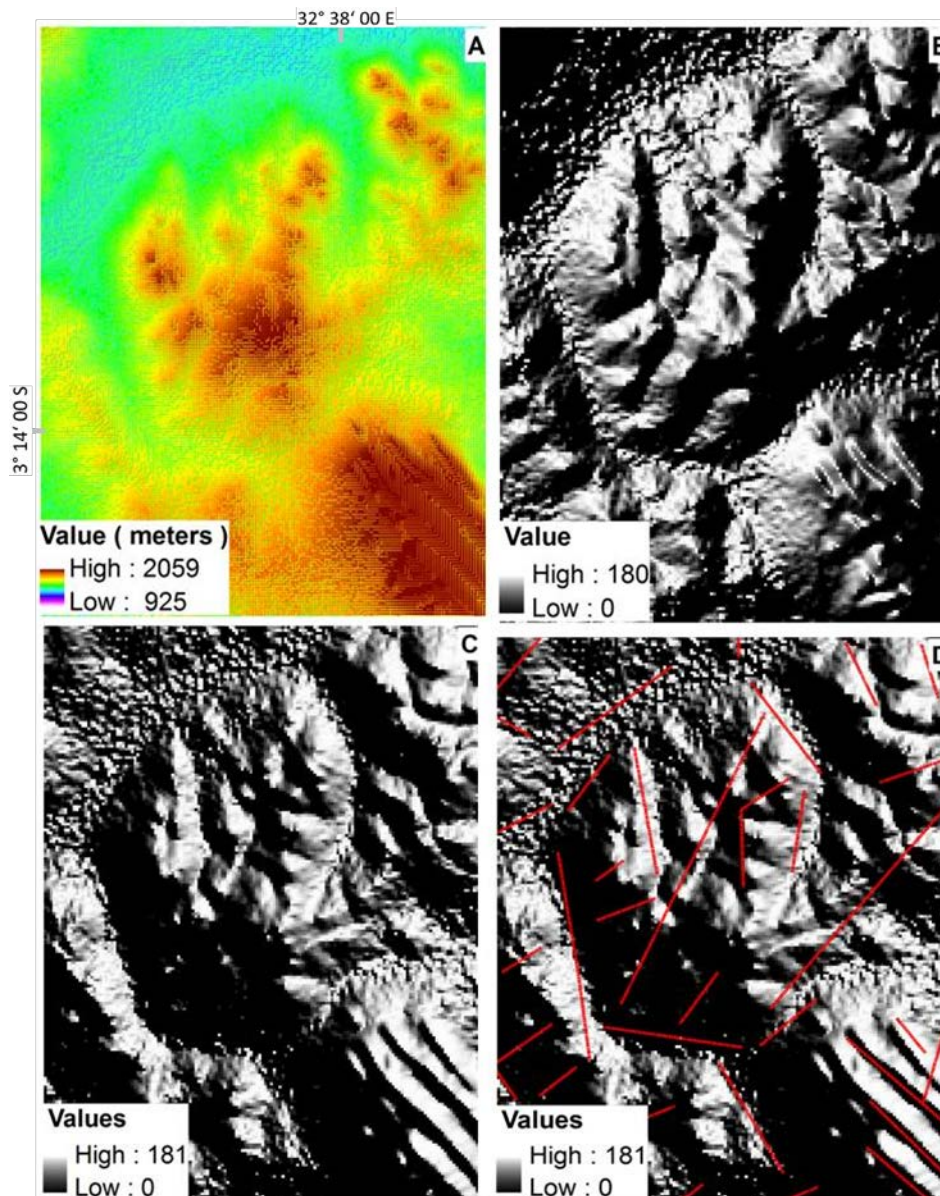
Figure 5.1 Images from SRTM data, the area shown measures 18 km by 14 km **A**: Stretching in histogram equalization **B**: Hill shading at 315° NW and 45° altitude **C**: Hill shading at 45° NE and 45° altitude **D**: Image **C** overlain by lineaments extracted from SRTM data

Validation of the extracted lineaments was done by examining the correlation between the identified lineament and manmade lineaments in the landuse maps. Lineaments which showed spatial correlation with manmade lineaments were removed from the database. This process was performed to make sure that there is no mix from anthropogenic linear features such as roads, railways, and electrical transmission lines, which are also found in the study area. Accuracy of the SRTM lineaments was calculated through overlaying of the extracted SRTM lineaments with known tectonic fractures (e.g. faults, shear zones, joints) from geological maps. The results revealed that 70% of lineaments from geological maps spatially coincide with the SRTM lineaments. The processes involved in the analysis and interpretation of SRTM data are summarized in the workflow diagram of Fig. 5.2 below.

INPUTS

SRTM data

Geological map

Landuse map

Georeferencing

LINEAMENTS ENHENCEMENT

- Histogram equilization
- Streching & sharp colour ramps
- Shading in
  (NW-SE, NE-SW sun direction)

Digitization

VALIDATION

comparison of extracted lineaments with structures from geological maps

removal of artificial lineaments

RESULTS
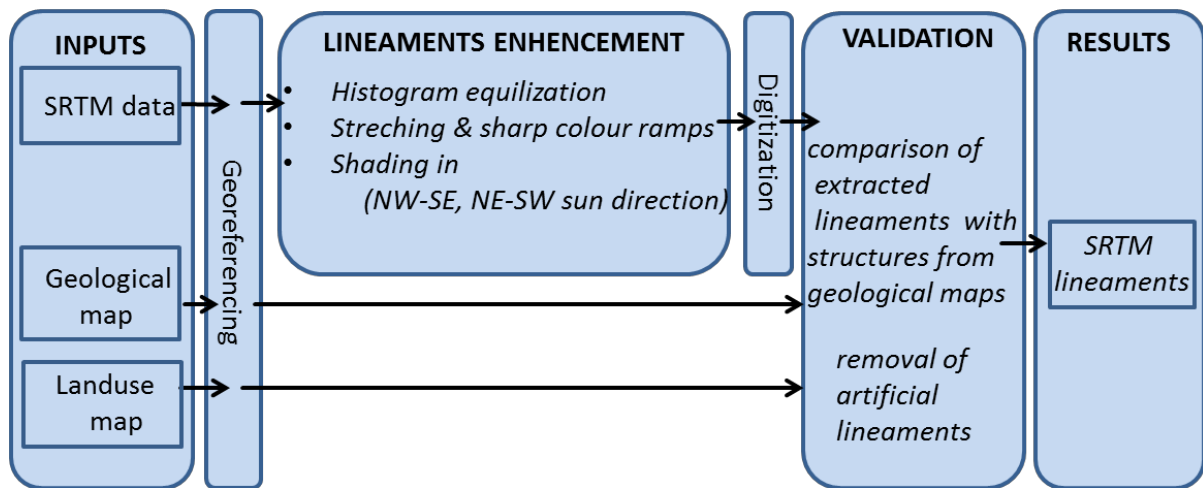
SRTM lineaments

Figure 5.2 Workflow for the analysis of SRTM data

5.3 Results and Discussion

Lineaments extracted from SRTM data have unveiled the significance of the data set in structural mapping by remote sensing technique. The 90 m resolution SRTM data, which is the only spatial resolution available for areas outside United States, has proved suitable even in the detection of relatively small lineaments up to < 1 km long (appendix 2).

The knowledge-based interpretation has led to a surprisingly large number of lineaments extracted from SRTM data. Prior to the present study the region had relatively few known structures shown in geological maps (Fig. 5.3A). For example, particularly the western side of the SGB is mostly covered with thick soils and/or forests and to date had very few geological structures documented (Fig. 5.3A, appendix 1). SRTM results have revealed that the SGB has been intensively sheared and/or fractured (Fig. 5.3B, appendix 3). The large number of structures obtained suggested to have been contributed by characteristics of the radar system. It is generally difficult to identify a geological structure underneath a thick forest through aerial photo interpretation or conventional field geological mapping, but the properties exhibited by radar rays seem to have overcome these obstacles. Characteristically, radar systems collect information on objects' surfaces, for example object heights. This means that radar data, such as SRTM, represent elevations of the reflective object surfaces like tree canopies, building roofs and bare grounds. However, SRTM data are not reduced to bare Earth (Slater et al., 2006). The ability of the radar system to detect surface elevations indirectly allows for the possibility of detecting linear features on the Earth's surface. Features like subtle linear topographical scarps or vertical offsets made by tectonic structures, e.g. faults offsetting different rocks units are identified through an abrupt and geometrically systematic change of elevation in SRTM data.

Results from the present study have also revealed that forest characteristics have contributed to a great extent in the identification of geological structures. Generally, a forest is dominated by types of trees with similar characteristics. For example, a forest has a typical range of tree heights (e.g. Neumann et al., 2010). Based on the height factor, when these trees grow on a certain geological structure e.g. fault, the concealed fault location or even fault dislocation will have a chance to be projected onto the forest canopy as heights difference and therefore can be detected by the radar sensor as a change in elevation. Hence, the detection of a large number of newly detected geological structures mostly in the western part of the area which is the densely forest covered part of the

Sukumaland Greenstone Belt is suggested to have been successful due to both radar and forest characteristics (Fig. 5.3).
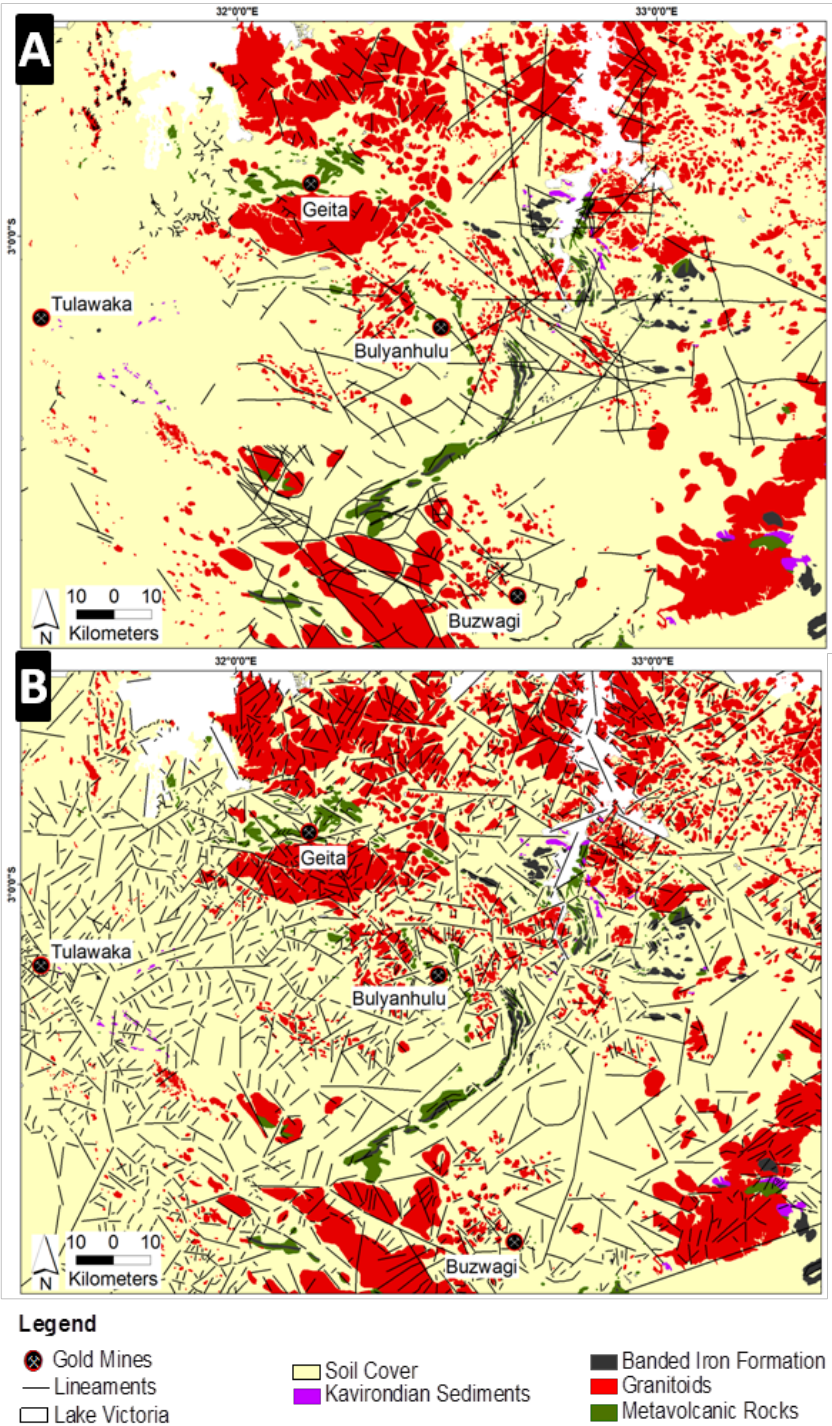
Figure 5.3 Geological maps of the SGB, **A:** SGB geological map and its tectonic structures **B:** SGB geological map and lineaments extracted from SRTM Data.

The NE-SW and NW-SE trending lineaments are the dominant sets of lineaments extracted from the SRTM data of this region (Fig. 5.4, Fig. 5.5). There is an additional set of structures, which trends E-W but is relatively less significant compared to the number of lineaments that make up the other two sets. Observations have also revealed that the SRTM lineaments overall show a strong similarity with the known tectonic patterns of the region (e.g. in Borg and Shackleton, 1997). In addition, the SRTM

data set has revealed a far greater number of lineaments than was previously known from geological maps (Fig.5.4). The consistency shown between SRTM lineaments, tectonic structures from geological maps, and the interpreted regional tectonic stress regimes together with the large number of lineaments extracted, has proven the robustness of SRTM data in structure mapping. The data set has positively identified the dominant tectonic structures of the region and has also identified tectonic structures in areas where few or no geological structures were documented before.

The presence of discrepant lineaments, which differ from faults shown in geological maps, might be due to several factors. The source data for lineament, i.e. the one used to extract geological structures found in geological maps may also include human errors, which may be one of the contributing factors. Geological maps of the study area indicate some structures were also extracted from interpretation of aeromagnetic data. Characteristically, aeromagnetic data is capable of detecting lineaments located several meters to hundreds of meters beneath the Earth's surface, e.g. mafic dykes. Such deep-seated lineaments cannot be detected by radar systems and thus they cannot be identified in SRTM data. Other structures were extracted using different data sets and different techniques such as aerial photos and conventional field geological mapping. Hence, the presence of different sources of tectonic structures in the SGB geological maps supports the argument that there can be some lineaments from the two overlain lineament sets, which do not show any spatial correlation, and this makes up the remaining 30% of uncorrelated lineaments from the SGB geological maps.
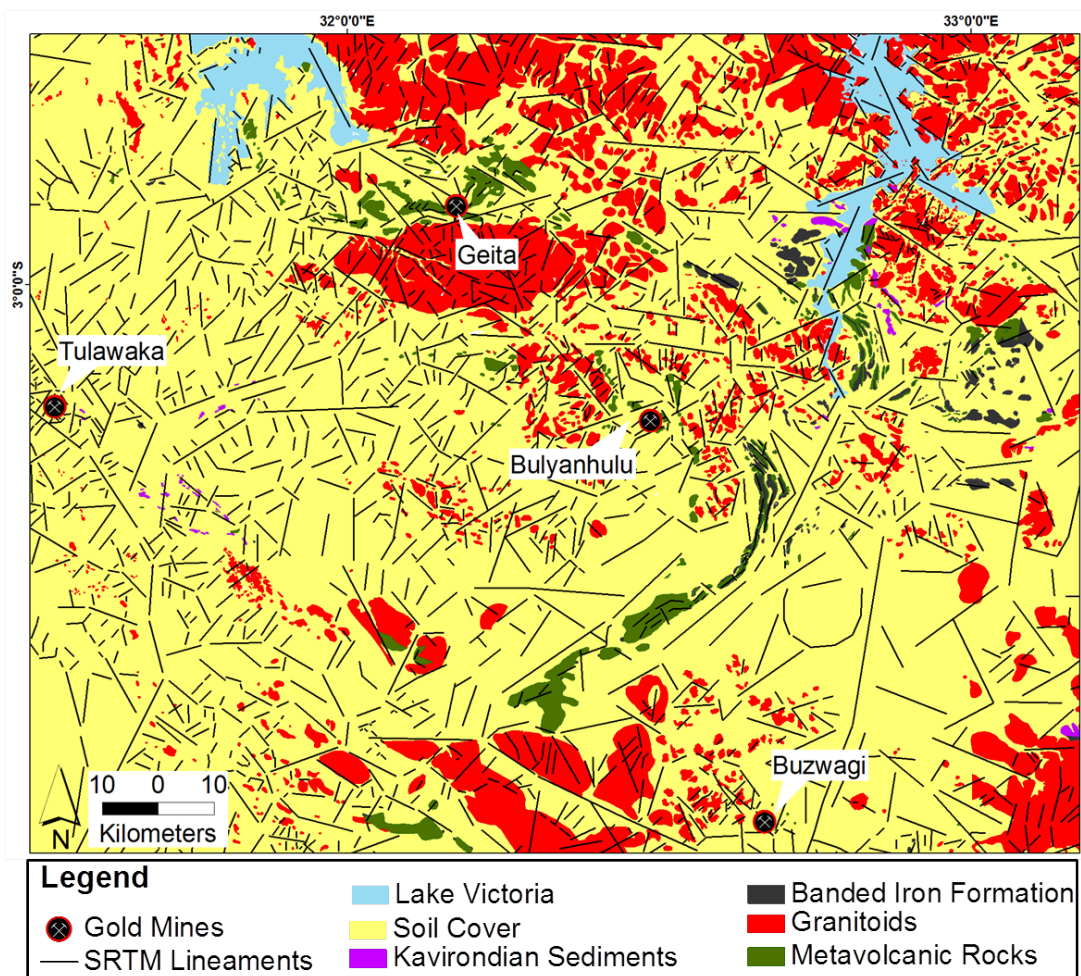
Figure 5.4 The SGB geological map superimposed with lineaments extracted from SRTM Data.

28
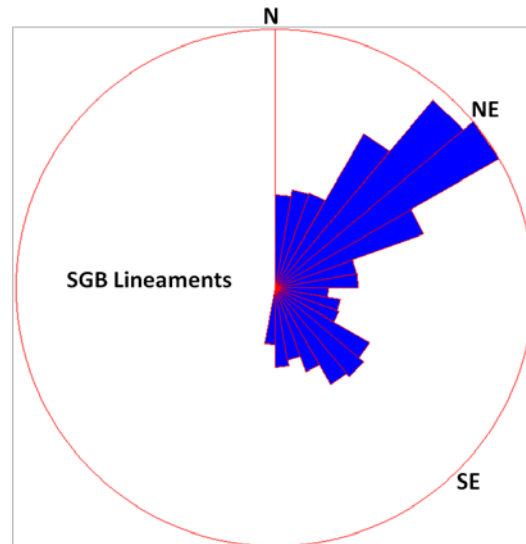
Figure 5.5 The rose diagram of the strike of SRTM lineaments in the SGB indicating two sets of lineaments (NE-SW and NW-SE), the NE-SW lineaments are relatively large in number compared to NW-SE ones as it is revealed by the frequencies (size) in this rose diagram.

5.4   Conclusion

In spite of the low spatial resolution (90 m), SRTM data has proven to be a useful tool in geological mapping. The process of lineament identification was comparatively easy and is highly accurate due to the knowledge-based method used, which has allowed to incorporate the regional tectonic characteristics of the study area. Artificial linear features were avoided by cross-checking the results with landuse maps during interpretation, this has increased confidence to the results obtained. The data has positively revealed the two dominant sets of tectonic structures in the SGB. Moreover, a large number of lineaments or better tectonic structures were extracted from the SRTM data additional to the relatively few previously mapped geological structures shown in geological maps. The western, densely forested-part of the study area revealed to have a substantial number of lineaments, which strike in a similar pattern corresponding to the regional tectonic stress regime. By considering the two major NW-SE and NE-SW striking sets of lineaments are interpreted as a set of conjugate shears (e.g. Borg and Shackleton, 1997), the overall stress regime can be assumed with the direction of σ1 trending N-S and the direction of σ3 oriented E-W. The resulted large number lineament will further stimulate mineral exploration activities for structural controlled gold deposits in the western part of the SGB, which until now had only a limited number of geological features (e.g. linear tectonic structures) documented.

6   HYDROTHERMAL ALTERATION MAPPING BY LANDSAT ETM+

6.1   Introduction

Hydrothermal wall rock alteration that has occurred as a result of the effects of hydrothermal fluids interacting with wall rocks is one of the geological phenomena that can be mapped by use of multispectral remote sensing data. By definition, hydrothermal alteration refers to any modification or change of rocks or minerals caused by the reaction of a hydrothermal fluid with pre-existing solid phases. The process causes mineralogical and geochemical modifications and thus changes the rocks

adjacent to permeable fractures and hydrothermal veins. Source of hydrothermal fluids may be magmatism (juvenile), metamorphism, sea water, meteoritic water or connate water. Most of the hydrothermal fluids are of mixed origin in which more than one of the above sources can dominate. Characteristically, the fluids are hot (approx. 50°C to > 500°C) aqueous solutions with variable amounts of ligands (e.g. CO_2, H_2S, SO_2, CH_4, N_2), compounds (e.g. HCL and NaCl) and metals and metal complexes such as Au and Au $(HS)^{2-}$ respectively (Pirajno, 2009).

Rock porosity, permeability and reactivity are amongst the rock properties with significant roles in the migration and diffusion of hydrothermal fluids in host rocks. Porosity and permeability can control infiltration of fluids from veins laterally into the wall rocks. However, far more voluminous transportation of these fluids is through tectonic fractures, e.g. fractures, faults and joints as well as shear and breccia zones (Goldfarb et al., 2005; Pirajno, 2009). These crustal fractures act as conduits and locally as funnels to large volume of fluids in hydrothermal systems. The above described role of tectonic fractures reveals a significant interdependence between fractures, hydrothermal fluids and hydrothermal alteration processes. As a consequence, tectonic lineaments, which are common remotely visible expressions of fault and shear zones, are very important traces of hydrothermal systems.

Fluid components within the hydrothermal fluid pathways (tectonic fractures), under changing of physical and chemical conditions (e.g. pressure, temperature, pH, Eh), react with the primary wall rock forming minerals and the process results in the formation of secondary (alteration) minerals, which have equilibrated with and are stable in this new environment. Contemporaneous with the alteration process, the changes in physical and chemical conditions as well as the ongoing alteration reactions trigger the precipitation of other fluid contents such as precious and base metals to create mineral deposits. Hydrothermal alteration minerals commonly create specific zones of secondary minerals within the host rocks due to varied specific stability conditions for these minerals. Normally, the alteration halos created spatially exceed the mineralized zone *sensu stricto*. The zoned secondary minerals thus created, are normally visible as alteration halos around veins and mineral deposits. The wider spatial extent of the alteration halos makes it easier for them to be recognized than the mineralization itself, and the alteration minerals have thus been used in both historical and modern geological/mineralogical exploration techniques for the search of mineral deposits (Groves et al., 2000; Pirajno,2009). For example, Lowell (1991) reported the importance of the spatial distribution of hydrothermal alteration minerals in locating the main outflow zones of hydrothermal systems, which indirectly lead to the recognition of mineral deposits, for his case porphyry copper deposit.

A special characteristic of the alteration minerals is that, when exposed to radiations such as natural sunlight, they reflect distinctive spectra with diagnostic characteristic features capable of being detected by satellite sensors (Hunt, 1979; Clark et al., 1993). Landsat TM is amongst the most commonly used satellite multispectral remote sensing data in mineral exploration. It has been used to locate target areas during reconnaissance stages of exploration (e.g. Spatz, 1997; Carranza and Halle, 2002). Landsat TM comprises spectral data from three bands (bands 1, 2, and 3) in the visible to near infrared region (VNIR) and three bands (bands 4, 5, and 7) in the shortwave infrared (SWIR) region of the electromagnetic spectrum (http://glcf.umd.edu/). Such spectral resolution is capable of discriminating areas rich in Fe-oxide/hydroxide and clay - sulphate-carbonate mineral groups (Fraser and Green, 1987; Crósta and Rabelo, 1993). As an outcome of Landsat spectral characteristics, the data set is restricted to the identification of areas affected by alteration processes but they are not capable of identifying individual hydrothermal minerals (Carranza and Halle, 2002). Landsat

Enhanced Thematic Mapper (ETM+) is presently the latest sensor in the series of Landsat satellites. Modifications made in ETM+ over the TM sensor include new features such as the addition of a panchromatic band with 15m spatial resolution, an on-board full aperture solar calibrator, 5% absolute radiometric calibration, and a thermal IR channel with a four-fold improvement in spatial resolution over the TM sensor. All bands in Landsat ETM+ have 30 m spatial resolution, except for the panchromatic band, which has a 15 m resolution. The size of a standard Landsat ETM+ image is 183 km × 170 km for all bands provided (http://glcf.umd.edu/).

There are several techniques which are used for the processing and enhancement of Landsat data, most of the techniques aim to minimize error and magnify the contrast between hydrothermal minerals from other objects in the image. For example, dark object subtraction has been reported to be simple and a common method for minimizing atmospheric errors in Landsat images (e.g. Carranza and Halle, 2002). Band rationing, statistical methods such as feature-oriented principal component analysis (FPCS) and software defoliant (DPC), and the mineral imaging method, are amongst the techniques which have been used for the identification of hydrothermally altered rocks on Landsat TM images (Segel, 1983; Fraser and Green, 1987; Crósta and Moore, 1989; Crósta and Rabelo 1993; Carranza and Halle, 2002, Liu et al., 2011). For example, Carranza and Halle (2002) reported good results for the mapping of hydrothermal alteration minerals in densely vegetated areas. The other PCA methods have been reported to be successful in arid and semi-arid regions (e.g. Crósta et al., 2003; Moore et al., 2008; Liu et al., 2011).

6.2   Methodology

6.2.1   Landsat ETM+
The Landsat scenes path 171 Row 062 and path 171 Row 063 used in this study were acquired on 07th August, 2001 by the Landsat ETM+ sensor. The selection of scenes was purposely taken in August to obtain images taken in the dry, commonly cloudless season in Tanzania. As a consequence, the dry season images have relatively little interference from vegetation, water and cloud cover (Carranza and Hale, 2002). Prior to analysis, the images were geo-referenced and an appropriate projection for the study area was applied.

In order to carry out the analysis of Landsat ETM+ data, bands from visible-near-infrared (VNIR) and shortwave- infrared (SWIR) regions were used to extract a specific group of hydrothermal alteration minerals. In general, signal enhancement in mapping hydrothermally alteration minerals by Landsat data, aims to identify clay minerals and iron oxide/hydroxide minerals (Fraser and Green, 1987; Crósta and Moore, 1989; Loughlin, 1991; Crósta and Rabelo, 1993; Carranza and Hale, 2002).
Fe-minerals can be better identified using band 1 and 2 in Landsat data and clay minerals in band 5 and 7. However, spectral characteristics of the above two groups of minerals are also expressed by vegetation and can thus cause interference during analysis. Alternatively, the remaining part of the spectrum shows opposing characteristics between minerals and vegetation, the two mineral groups behaving opposite to vegetation in spectral band 3 and 4. Hydrothermal minerals give high reflection in band 3 and absorption in band 4 whereas vegetation can exhibit strong absorption in band 3 and high reflection in band 4. Therefore, the spectral characteristics above reveals that band 3 and 4 can be used together with bands 1, 5, and 7 during analysis to differentiate spectra of hydrothermal alteration minerals from spectra belonging to vegetation (Loughlin, 1991; Carranza and Halle, 2002).

6.2.2 Principal Component Analysis (PCA)

Principal component analysis is often used as method of data compression. It allows redundant data to be compacted into fewer bands. The dimensionality of data is reduced and collected into PCA bands known as principal components (PCs). The resulting PCs are uncorrelated, independent and more interpretable (Faust, 1989; Jensen, 1996; Cheng, 2002; Davis 2002; Cheng, 2006). By definition PCA is a mathematical procedure that uses orthogonal matrix to convert a set of observations of possibly correlated variables into a set of values of linearly uncorrelated variables called principal components. The technique suppresses irradiant effects and enhances signals from target materials such as alteration minerals (e.g. Crósta et al., 2003).

The process can be easily explained by the two bands graphically in Fig. 6.1 below. In an *n*-dimension histogram, an ellipse (2D), ellipsoid (3D) or hyperellipsoid (more than 3D) is formed if the distributions of each input band are normal or near normal. To perform PCA, the axes (original bands) are rotated in such a way that the coordinates of each pixel in spectral spaces are changed as well as the data file values. The resulting new axes, which are then the PCs, appear parallel to the axes of the ellipse. The first principal component (PC1) is the measure of the highest variation within the data, and the second principal component (PC2) is the widest transect (the major or longest axis) of the ellipse that is orthogonal i.e. perpendicular to the first PC (PC1). To sum-up, each successive PC is the widest transecting of the ellipse that is orthogonal to the previous components in the *n*-dimensional space of the scatter plot (Taylor, 1977). Something important to note is that the first few bands account for a high proportion of the variance in the data, however, in other cases useful information are gathered from the PCs with the least variance (Faust, 1989). PCA has become the standard statistical approach for image processing because it can reduce the number of correlated image bands to form a small number of independent PCs that represent variability carried by multiple images.   It also increases the interpretability of the components as combination of previous/original multiple bands (Sigh and Harrison, 1985).
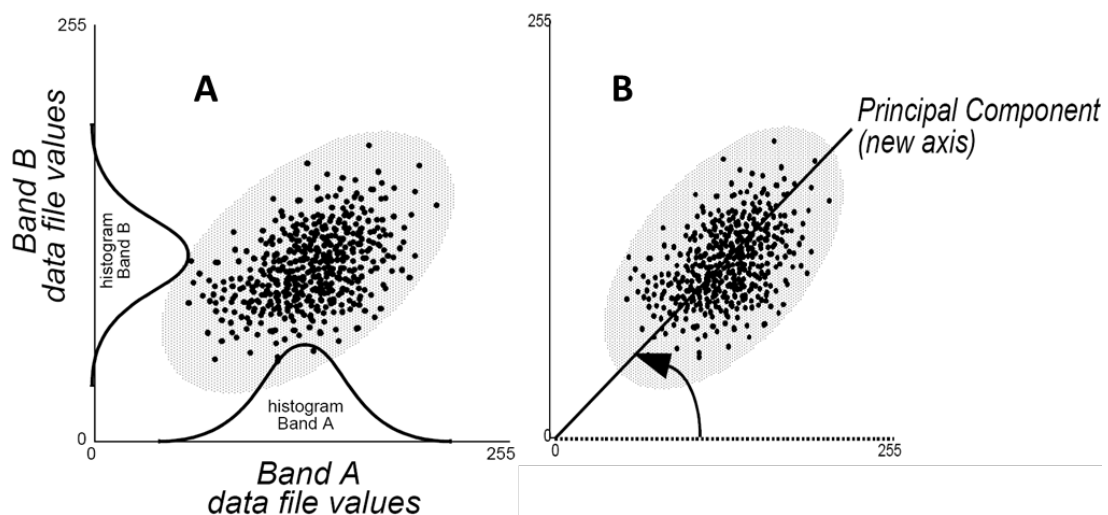
Figure 6.1 Scatter Plots showing bands as variables (A), and resulting principal component after PCA analysis (B) (Taylor, 1977)

6.2.2.1   PCA in Alteration Minerals Mapping

There are several PCA techniques, which have been proposed for the mapping of hydrothermal alteration minerals. Selective-PCA is one of them and this technique uses 2 bands amongst the seven bands of Landsat TM in enhancing and identifying signals from alteration minerals. The two bands used are the one believed to carry the characteristic spectra for the alteration minerals (Chavez and Kwarteng, 1989). Software defoliant technique or directed principal components analysis (DPCA) of two band ratios is also another type of PCA, which has been used in image enhancement (Fraser and Green, 1987). The technique uses two band ratios each created using two bands selected in respect to signals representing vegetation and alteration minerals. The PCA has been reported to be simple and relevant for alteration mapping and has proven positive in reducing the effects of vegetation (Fraser and Green, 1987; Wilford and Creasey, 2002; Crósta et al., 2003). A popular PCA in alteration mapping is the Crósta technique (Crósta and Moore, 1989; Loughlin, 1991; Crósta and Rabelo, 1993); the technique also known as feature-oriented principal component analysis (FPCS). It employs 5 bands (band 1,3,4,5 and 7) out of 7 bands in Landsat TM for the enhancement of the signals from hydrothermal alteration minerals (Fig. 6.2). The bands used are grouped into two groups (each group with 4 bands) in respect to the reflectance signals from Fe-oxide/hydroxide and clay minerals and each group is separately PCA-processed to get the enhanced signals from the mentioned two mineral groups above. The technique is able to predict whether the target material is represented by bright or dark pixels in the resulting PC images according to the magnitude and sign (+/-) of the eigenvectors (Carranza and Hale, 2002).
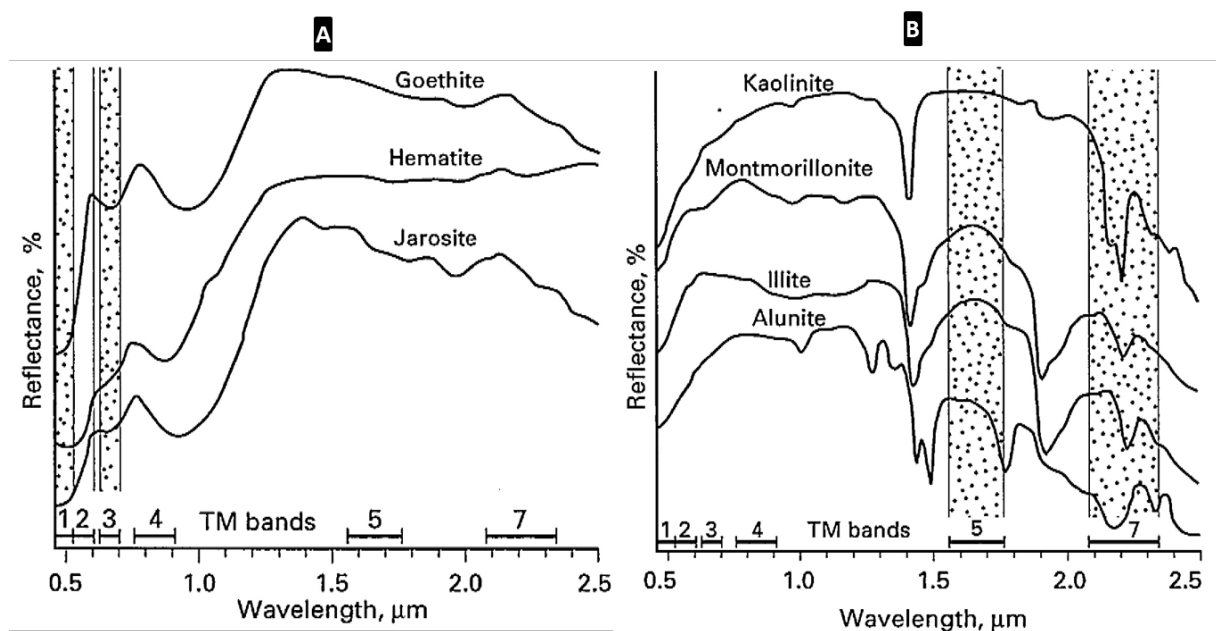
Figure 6.2 Generalized reflectance spectra of Fe-oxide/hydroxides **(A)** and clays minerals **(B)**, and Landsat TM bands spectral windows 1 to 7 indicated (Sabins, 1996; 1999).

6.2.2.2   Feature-Oriented Principal Component Analysis (Crósta Technique)

In this study, the feature-oriented principal component selection (FPCS) (Crósta and Moore, 1989; Loughlin, 1991; Crósta and Rabelo, 1993) was used to map the areas affected by hydrothermal alteration in the SGB. The choice of the method is based on a larger number of bands that it utilizes in comparison to other PCAs. With the five bands used, it means spectral information over a wide spectrum is used to delineate alteration minerals. In that sense, alteration mineral signals will be extracted by involving more spectral features than other PCAs and will hence be relatively more distinctive.

The technique ensures that unwanted signals from materials such as vegetation are separated from geological/mineralogical target materials and are collected in a different principal component (PC). For this reason, the use of the Crósta technique does not require pretreatment of data for the suppression of vegetation signals since they will be collected in one of the resulting PCs separate from the one containing target minerals. Loughlin (1991) used the Crósta technique on bands 1, 3, 4 and 5 for the extraction of spectral signatures related to Fe-oxide/hydroxide and bands 1, 4, 5 and 7 to extract spectra from clay and mica minerals, as well as carbonates and sulphates. Spectra from these minerals will be mapped separately into either PC3 or PC4 whereas PC1 and PC2 collect signals from albedo and/or topographic information and contrast between VNIR and SWIR regions respectively. The PCs, which carry target spectra, will have high eigenvector loadings in their respective diagnostic bands but with opposite signs (+ or -).

In this study the vegetation signals were carried in PC3 with a high eigenvector from band 4 in both mineral groups. They have high positive loadings (0.8978) in the Fe-oxide/hydroxide group and high negative loadings (-0.7271) in the clay minerals group (Table 6.1 and 6.2). Signals from Fe-oxide/hydroxide minerals are carried in PC4. The PC has a moderate positive loading (0.4410) from band 1 and high negative loading (-0.7777) from band 3 (Table 6.1). The above observation indicates that signals from the target minerals are represented by low (dark) DN values. Thus, PC4 had to be negated by multiplying it by -1 to make pixels with Fe-oxide/hydroxide minerals displayed as bright (Fig. 6.4B). Signals from clay minerals are similarly carried in PC4 (Table 6.2), the PC has high negative loading (-0.5838) from band 5 and high positive loading (0.5235) from band 7. Also PC4 had to be negated by multiplying it with -1 for signals from hydroxyl minerals to appear as bright pixels (Fig. 6.4C).

The resulting two images (Fig. 6.4B and 6.4C) were used to create a composite image in R: G: B (Red, Green, and Blue) combination of which a third image in the composite is the sum of the two resulting mineral images. Generally, an RGB image displays mixed colors depending on the proportions contributed from each image. For the hydrothermally altered area, the pixels need to have high values from all mineral images. The hydrothermal alteration minerals are identified by pixels with high values from the two mineral images. Therefore, pixels representing hydrothermally affected areas will appear white in the RGB image (Fig. 6.4D).

Table 6.1 PCA results showing eigenvector statistics from bands 1, 3, 4 and 5 of Landsat ETM+. The bands were selected to depict spectral responses from Fe-oxide/hydroxide minerals.

	PC1	PC2	PC3	PC4
Band1	0.4161	-0.7943	0.0383	**0.4410**
Band3	0.4345	-0.2232	-0.3958	**-0.7777**
Band4	0.3273	0.5401	0.8978	-0.2896
Band5	0.7287	-0.5624	-0.1892	0.3410

Table 6.2 PCA results showing eigenvector statistics from bands 1, 4, 5 and 7 of Landsat ETM+. The bands were selected to identify spectral responses from clay minerals.

	PC1	PC2	PC3	PC4
Band1	0.3808	-0.9056	0.1416	-0.1216
Band4	0.3110	0.0646	-0.7271	0.6086
Band5	0.7042	0.3405	-0.2176	**-0.5838**
Band7	0.5122	0.2444	0.6356	**0.5235**

6.2.3   Extraction of Hydrothermal Alteration Areas

Supervised classification was applied to the RGB image (Fig. 6.4D) so as to select and cluster the hydrothermal alteration pixels in one class. In this process the light colored pixels representing the hydrothermally altered areas were grouped together. The process was followed by changing pixel values using the GIS recode function, this resulted in the suppression of the unwanted pixels that were given a value of 0 and the value of 1 was attributed to the remaining target pixels (Fig. 6.5B).

The resulting image from supervised classification was then taken further to GIS processing with the purpose of reducing some errors which might be contributed by other objects, which gave similar spectra as alteration minerals (e.g. man-made objects) and similar minerals that are of non-hydrothermal origin. GIS function clumping was applied to the resulting image to polygonize the adjacent contiguous hydrothermal alteration pixels. The process resulted in different shapes of the hydrothermally altered polygonized pixels. Then sieving was applied to the clumped image so as to remove the singly isolated and scattered pixels, those appearing unattached in relation to the relatively larger polygons. The concept behind is that the area that have been affected by alteration will have always several (many) pixels clumped together when compared to those from other sources. This is due to the nature of the process in which the fluids normally tend to accumulate in traps with enough spaces. Sieving was performed repeatedly to the clumped image by varying the minimum number of clumped pixels to determine the optimum and minimum number of clumped pixels that can be removed to leave the altered and relatively larger polygons in clearer shapes. 50 and 100 clumped pixels were the sieved pixels, which gave significant changes to the alteration image and stands here as the best examples for this technique (Fig. 6.5B and 6.5C). In regard to Landsat ETM+ spatial resolution (30 m), the areas represented by 50 and 100 sieved pixels are equivalent to 0.045 km^2 and 0.09 km^2 respectively. Finally, the resulting "clean" image was overlaid with the extracted SRTM lineaments for further interpretation (Fig. 6.5D).
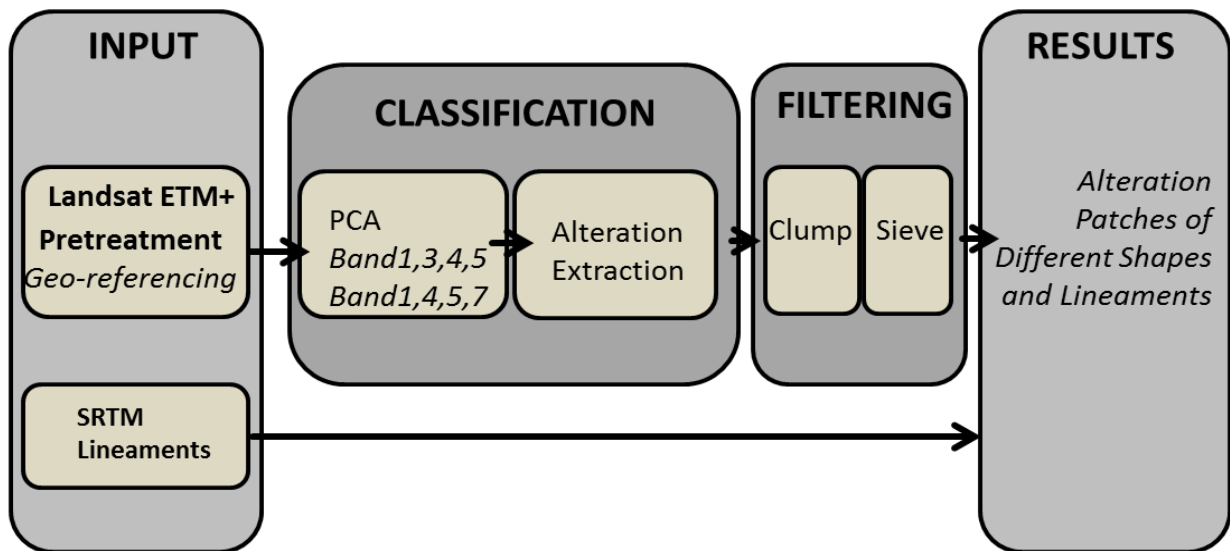
Figure 6.3 Workflow for the analysis of Landsat ETM+ data
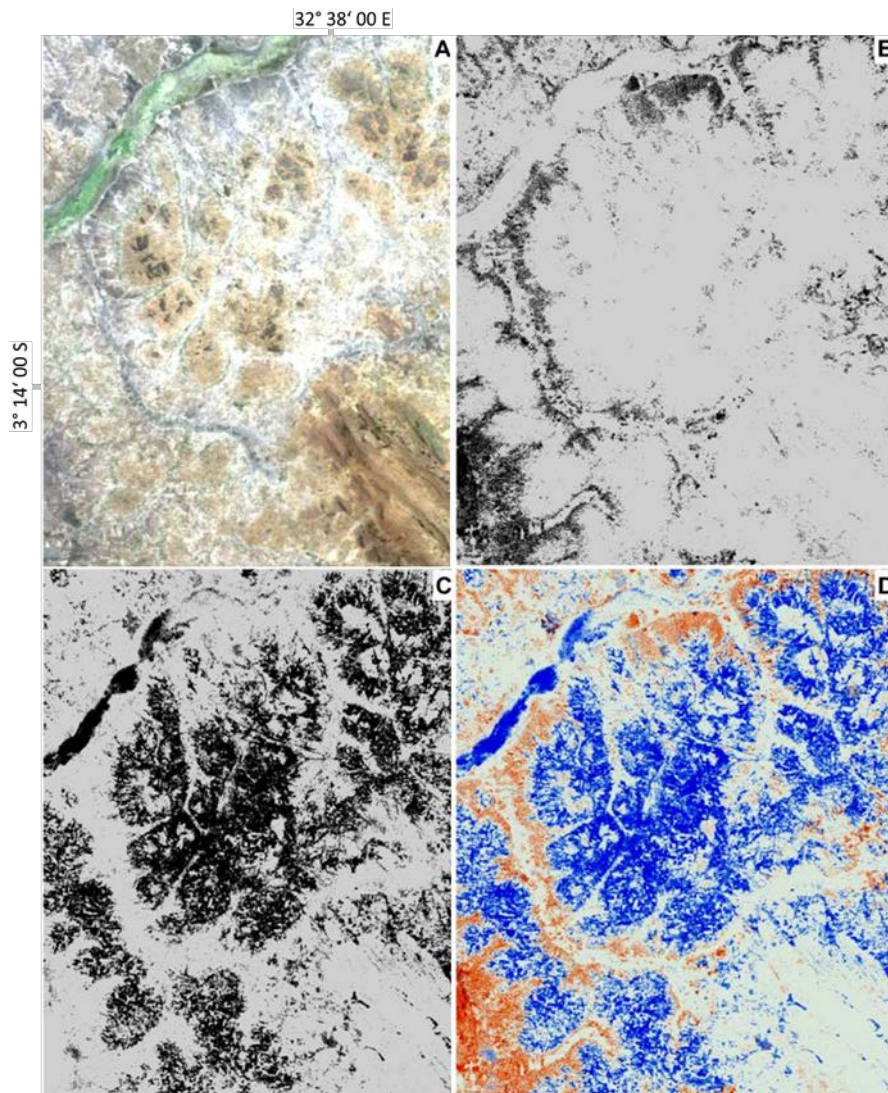
Figure 6.4 Landsat ETM+ images covering the part of the Kahama mining district, the area is 18 km by 14 km. **A**: Composite image in true colour RGB bands 3:2:1 **B**: PC4 for the Fe-oxide/hydroxide minerals **C**: PC4 for the Hydroxyl minerals **D**: RGB composite image.

36

6.2.4   Identification of Potential Hydrothermal Fluid Conduits

The applied GIS functions of clumping and sieving gave the possibility to realize different polygon shapes made from the contiguous pixels of the hydrothermally affected areas. The observation shows that most of these polygons are geometrically linear. They are made of compacted pixels characterized by a high intensity white colour, which are organized as linear patches (Fig. 6.5B and 6.5C). The question thus arose if the linear patches represent some of the tectonic fractures (shear zones/faults) involved in the hydrothermal systems within the SGB? To test whether the linear patches represent tectonic fractures, SRTM lineaments, which were independently extracted in this study, section 5, were overlain over the extracted hydrothermal alteration patches (Fig. 6.5D).
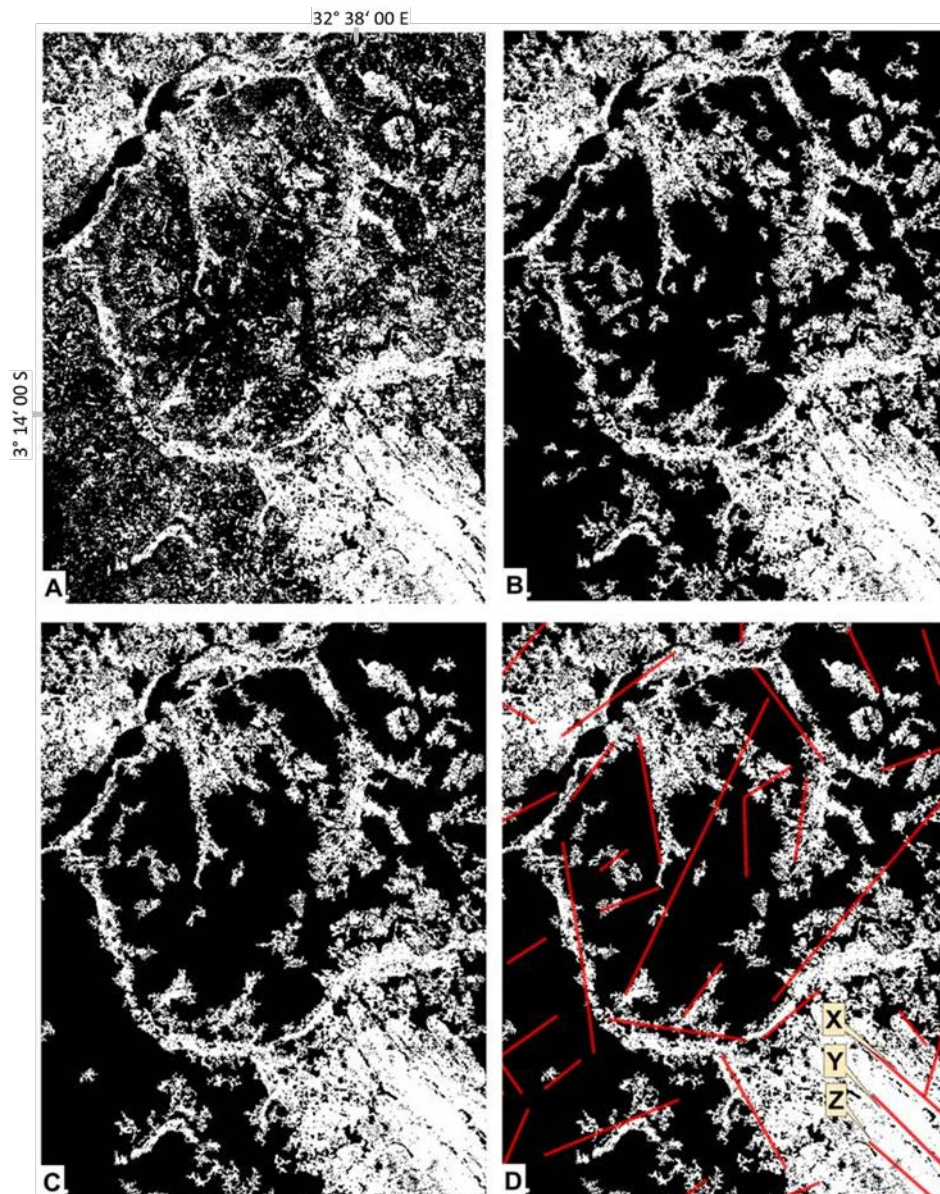
Figure 6.5 Hydrothermal alteration images covering the part of the Kahama mining district, the area is 18 km by 14 km. t **A**: Clumped image, not sieved **B**: Sieved image with ≤ 50 clumped pixels removed **C**: Sieved image with ≤ 100 clumped pixels removed **D**: Image **C** overlain by extracted SRTM lineaments.

6.3   Results and Discussion

6.3.1   Hydrothermally Alteration in SGB

Results from Landsat ETM+ showed that the Sukumaland Greenstone Belt (SGB) has been intensively affected by hydrothermal alteration and that the spatial distribution of the alteration largely follows the known SGB structural pattern (Fig. 6.6; Appendix 4). The extent of the alteration suggests that the area has been strongly injected with hydrothermal fluids. Additional observations indicate that all rock types in the SGB have been affected locally by hydrothermal alteration although some specific rock types such as metavolcanic rocks, banded ironstones, and clastic metasedimentary rocks have been subjected to particularly intensive alteration (Fig. 6.6). It is interesting to note that all presently known major gold deposits in the SGB (Bulyanhulu, Geita, Buzwagi and Tulawaka Mines) as well as major gold occurrences are located within and in the vicinity of the areas affected by hydrothermal alterations (Fig. 6.6). For example, Bulyanhulu Gold Mine to the east of the SGB is located within a linear alteration patch that trends in a NW-SE direction (Fig. 6.8). A similar observation is true for artisanal mining sites at Nyakagwe village and other gold occurrences within the mining district.
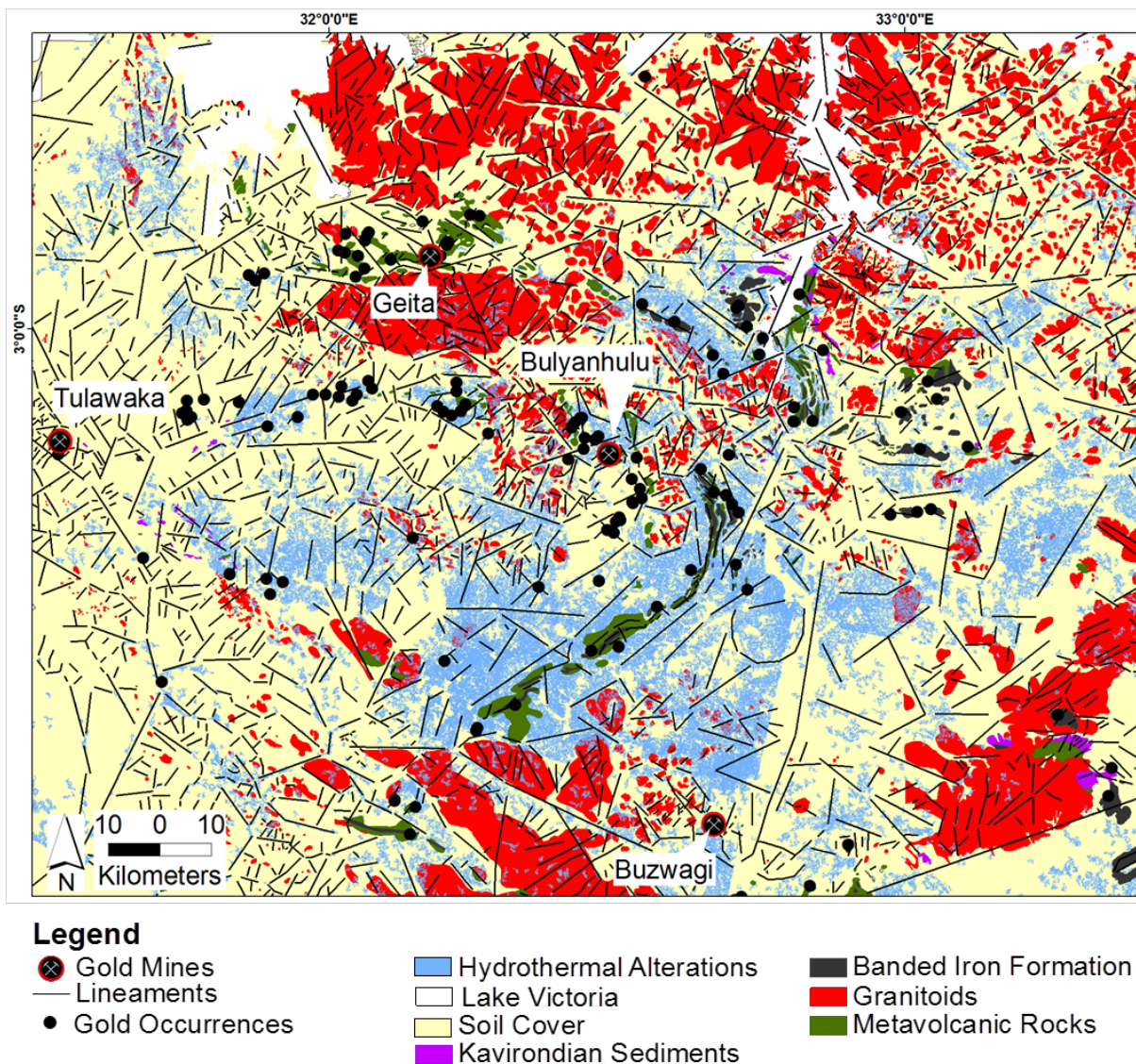
Figure 6.6 The SGB geological map and SRTM lineaments overlain by hydrothermal alteration as well as gold deposits and gold occurrences

The alteration results have also been compared with SRTM elevation data to investigate the possible interferences from soil accumulations; result has eliminated the doubt of the possibility of soil interference (preferential clay mineral accumulation) in areas of low elevation that could have caused the linear patterns (Fig. 6.7). The result indicates that no direct correlation between hydrothermal alteration patches and low land areas but that hydrothermal alteration patterns occur distributed throughout the topographic elevation range. The effects of such interference would have been even more challenging if the distribution i.e. the spatial shapes and extent of alteration areas were comparable to the distribution pattern of lowland areas; the results however show no such coincidence.
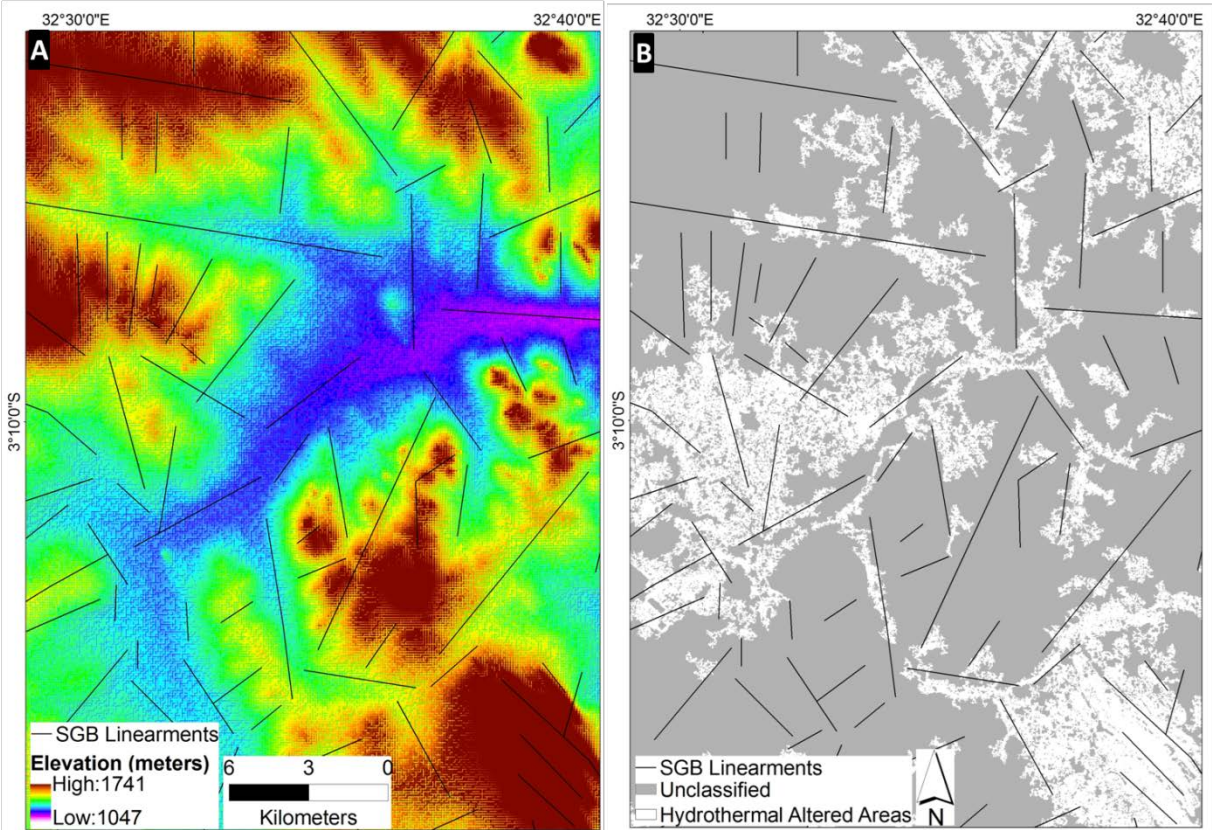
Figure 6.7 Images from the part of Bulyanhulu mining district showing comparisons between elevation in meters and hydrothermal alteration areas, **(A)** Elevation image from SRTM data with lineaments **(B)** hydrothermal alteration image overlain with lineaments extracted from SRTM data

6.3.2 The Potential Channelways for Hydrothermal Fluids

SRTM lineaments and hydrothermal alteration areas have been extracted independently from two different data sources as already described in section 5. The data sets had also markedly different spatial resolutions with SRTM data having 90 m and Landsat ETM+ 30 m resolution. Despite their differences, the results showed to be useful and of great relevance to mineral exploration. An overlay of the two sets of results has revealed the positive correlation between some of the SRTM lineaments and linear alteration patches from Landsat ETM+. The detailed observation of the overlaid layers (Fig. 6.8) suggests that the linear alteration patches represent the former pathways for hydrothermal and potentially metalliferous fluids during major geological events. The alteration patches are linear, straight and have similar patterns in comparison to both SRTM lineaments and mapped tectonic fault and shear zone structures within the SGB.

The observations indicate the linear alteration patches to have widths ranging from approximately 300 m to 10 km. The variations observed in this study are suggested to relate to specific types of geological structures utilized by hydrothermal systems. Tectonic structures have different dimensions, for example shear zones tend to be wider compared to faults. In the above case, alteration patches related to shear zones will commonly have wider dimensions compared to the patches associated with faults.

The present results also indicate that, in the case of two parallel lineaments adjacent to each other that have both been affected by hydrothermal fluids, only one broad linear alteration patch is formed. Patches of this kind show a strong intensity near the lineament edges and in the center area between them. A particularly instructive example for this is the area between lineaments Y and Z (Fig. 6.5D). Strong alteration intensity in the center area between the two lineaments is suggested to be a focal point of the effects of the hydrothermal fluids.

In the case of parallel and closely spaced lineaments, the alteration intensity is strong and uniform throughout the entire area between the two lineaments. However, outside areas and in areas away from lineaments, the alteration intensity is gradually decreasing, for example in areas outside X and Z (Fig. 6.5D). Observations also indicate that some SRTM lineaments have no spatial correlation with the alteration patches (Fig. 6.8). The presence of such lineaments implies that not all lineaments were involved in and affected by the hydrothermal system. This observation can assist to distinguish the metallogenically potentially "fertile" structures from barren ones. Likewise there are linear alteration patches, which do not match any recognizable SRTM lineaments. Factors such as failure to identify these lineaments from SRTM data is suggested to contribute to the observed discrepancy. This could be due to a lack of a topographical expression by the lineament itself, possibly due to its location far deep within the Earth's crust or a widespread surficial cover and weathering of the rocks cut by faults, in a way that has been proposed by Kinabo et al. (2008). Lineaments of such character might not carry a surface expression and thus can be still difficult to identify in SRTM data.
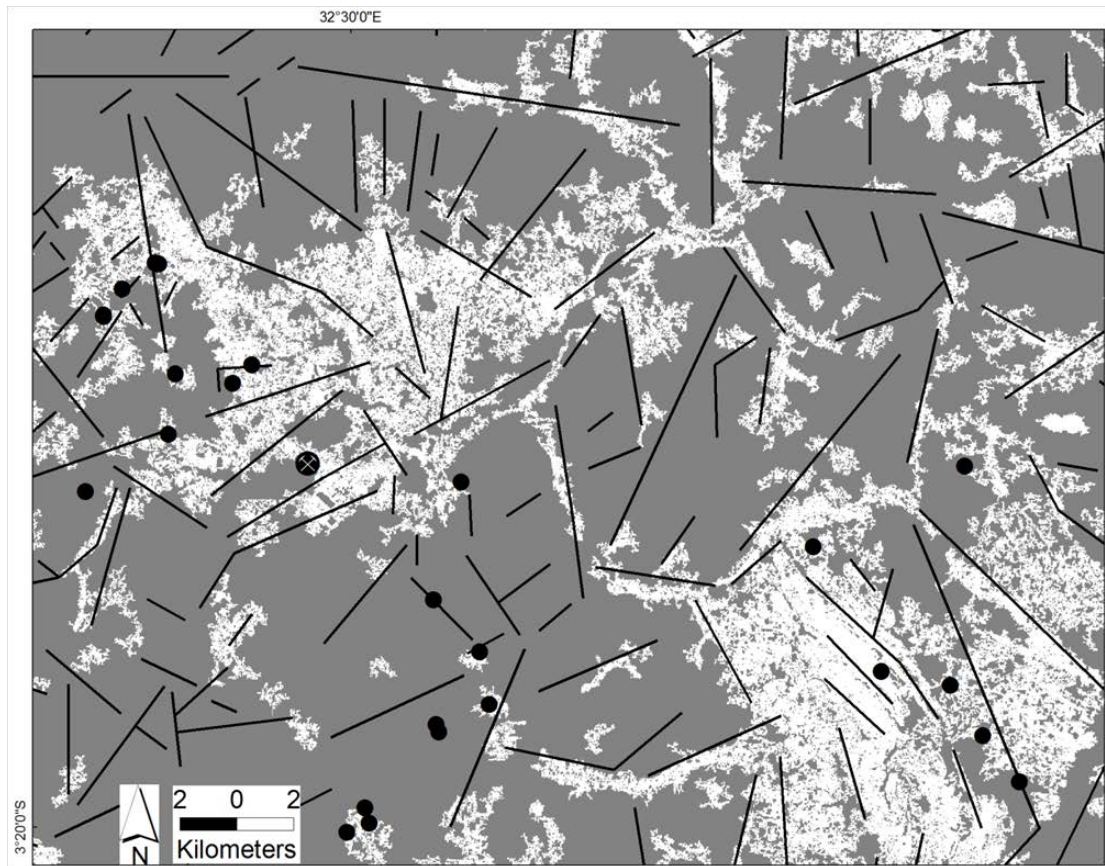
Figure 6.8 The hydrothermal alteration map showing the linear alteration patches overlaid with SRTM lineaments. The alteration map used is a sieved image with ≤ 50 clumped pixels removed.

6.4   Conclusion

Supervised classification together with the selected GIS functions has revealed to be competent in identifying hydrothermally altered areas in the SGB. The technique has identified the areas which have been affected by hydrothermal alteration, and the correlation shown between linear alteration patches and SRTM lineaments as well as fault structures from geological maps is a positive proof to this concept. The linear alteration patches, which are interpreted to represent former fluid pathways, coincide spatially with major gold mines and major gold occurrences in the region. Hence, the ability of the method to use Landsat ETM+ data to identify hydrothermal fluid pathways provides another tool for the exploration of new mineral deposits. The observed spatial relationship between hydrothermally altered areas, tectonic lineaments and gold occurrences in the region have shown that when SRTM and Landsat ETM+ data are used jointly, they give significant confidence in choosing target areas for mineral exploration. Thus, in searching for precious and base metal deposits which are related to hydrothermal systems, SRTM and Landsat ETM+ data can be suitable tools for target generation during reconnaissance exploration.

41

7   HYDROTHERMAL ALTERATION MAPPING BY ASTER DATA

This part describes the ASTER data analysis in the aspect of hydrothermal alteration mapping. ASTER data has relatively high spectral resolution when compared to Landsat ETM+ data and thus can map the individual alteration minerals. The new approach in mapping hydrothermal alterations as well as the technique to manifest alteration zoning around the hydrothermal upflows areas will be described in this chapter. The mapping area was selected following the results from Landsat ETM+ data and particularly for an area indicated as being highly fractured and altered.

7.1   Introduction

Advanced Spaceborne Thermal Emission and Reflection Radiometer (ASTER) data is a geological successor of Landsat TM data (Gozzard, 2006). ASTER has been relatively improved compared to Landsat TM both in spatial and spectral resolution. While Landsat TM data is only capable of depicting areas which have been affected with hydrothermal alterations, the relatively high spectral resolution ASTER data is capable of identifying individual alteration minerals originated from hydrothermal processes (e.g. in Rowan and Mars, 2003; Crósta et al., 2003; Tangestani et al., 2008). Both Landsat and ASTER data have been used intensively in the mapping of hydrothermal alteration minerals during mineral exploration programs. Detailed definition about hydrothermal alteration is in section 6, but the hydrothermal alteration itself is usually recognized by the presence of characteristic mineral associations, which coexist under similar physical-chemical conditions in hydrothermal systems (Guilbert and Park, 1986). However, it is not only hydrothermal alteration process that results in the formation of alteration minerals, there are other types of processes that can result in similar minerals as in hydrothermal alteration. For example, low temperature supergene alteration and deuteritic alteration can result in some secondary minerals similar to those produced from hydrothermal alterations. Supergene alteration is caused by weathering and oxidation of minerals when exposed to atmospheric conditions, the process normally results in palagonitic soils nearly devoid of phyllosilicates but which contain nanocrystaline ferric oxide and hematite (Morris et al, 2001). The deuteritic alteration process is related to degassing of the host lavas or by interaction of lavas with meteoritic water or the atmosphere during emplacement. The process also results in the formation of palagonite and various iron minerals. Contrary, a hydrothermal alteration process is caused by a hot fluid that migrates along fractures and other conduits. Both supergene and deuteritic alterations takes place at the earth's surface and in near surface environments, the same environment where we expect to detect hydrothermal alteration minerals by remote sensing satellite data. Thus, there is a possibility of mixing of minerals from all processes mentioned above. Apart from processes, which result in analogous alteration minerals, most of the hydrothermal alteration minerals are also rock forming minerals of different rock types. Chlorite, the key mineral in hydrothermal chloritization and propylitization, is also the principal mineral of the metavolcanic greenstone rocks related to low grade metamorphism. More recently, several cases with similar problems have been reported in different places, for example Brown et al. (2006) reported the difficulty of distinguishing the hydrothermally formed chlorite from chloritic metamorphosed basalts. In addition, alteration minerals, which are associated with structures, have two optional sources; they could possibly indicate tectonic control of the hydrothermal fluids or can represent zones of intense weathering controlled by percolating groundwater in fracture systems. Therefore, although there is a large pool of multispectral remote sensing data for the mapping of the hydrothermal alteration minerals, for example Landsat TM and ASTER data, there is also a challenge of

interferences from minerals originated from non-hydrothermal processes. Most researchers (e.g. Pirajno, 2009) have pointed out the interference problem, however, they are still suggest to study regional alteration patterns by spectral remote sensing for the better understanding of hydrothermal alteration patterns and mineralization.

Hydrothermal alterations near to mineralization zones characteristically form mineral zones with specific mineral assemblages. These minerals are normally the result of similarity in physical-chemical conditions in the hydrothermal systems. The alteration zones formed extend spatially from veinlets, vein systems, single ore shoots and up to regional scale. The alteration mineral zoning exhibited systematically around hydrothermal systems cannot be created by other non-hydrothermal alteration systems e.g. supergene and deuteritic alteration processes (Klein and Day, 1994). This is because of the major reason that the hydrothermal alteration sequence reflects temperature variation and a temperature gradient from the hydrothermal fluid upflows. For example, proximal alterations, which normally are located along fractures in the fluid trap areas, reflect high temperature environments as opposed to more distal (cooler) alteration zones. The above characteristic of hydrothermal alterations cannot be displayed by the other alteration processes since the later occur in low temperature environments by involving meteoritic water, which normally results only in low temperature minerals throughout the system.   Under the aspect of exploration, the alteration zones or better the alteration halos are much easier to locate than the ore bodies possibly contained within them. Apart from extending wider than the deposit itself, hydrothermal alterations around mineral deposits differ laterally and vertically depending on the type or model of the mineral deposit. But on the other hand, there are alteration types, which feature in more than one type of mineral deposits. Furthermore, the lithology is also reported to control the type of alteration (Groves et al., 2000; Goldfarb et al., 2005).

7.2   Mineral Alterations in Orogenic Lode Gold Deposits

The Lake Victoria Gold Field (LVGF) is located in the Archaean Tanzania Craton. Apart from the greenstones and granites, the terrain hosts ultramafic rocks, chemical sedimentary and clastic sedimentary rocks also of Archaean age, as described in section 3 in more details. The region comprises all major gold deposits in Tanzania and by referring to the mineralization models, the (orogenic) shear zone hosted lode gold deposit model fits these deposits (this study). For example, the detailed study on the geology and genesis of the Bulyanhulu gold mine by Chamberlain (2003) has reported the deposit to relate to Archaean lode gold deposits in many aspects. The deposit is structurally controlled and mineralization is hosted in quartz veins (locally Reef 1 and Reef 2), in the two main steeply-dipping reverse-oblique shear systems. The deposit exhibits a syn-volcanic hydrothermal system, or which a fluid inclusion study indicates that the pre-ore quartz has composition of magmatic origin (Chamberlain, 2003). The ore stage fluids were carbonic with temperature ranges between 300° to 450°C with an elevated CH_4 content. Basalts in this deposit are characterized by carbonate alteration and the rhyodacites are dominated by sericitisation, carbonate alteration and silicification. Hydrothermal alteration along mineralization zones has been divided into patterns. According to Chamberlain (2003),there is proximal alteration, which extends between 2 and 20 meters, and is dominated by carbonate alteration (calcite and dolomite), quartz, sericite but chlorite, quartz, pyrite ± arsenopyrite occur as minor mineral phases as well. The intermediate alteration zone is between 5 and 10 meters wide, of which is characterized by carbonate (calcite), sericite, chlorite, and quartz ± pyrite ± rutile ± ilmenite, titanite being the minor minerals. The distal alteration zone, according to the same author, extends up to 50 meters beyond the strongly sheared

zone and is mostly dominated by chlorite and calcite minerals. At the Bulyanhulu mine, it has been noted that the pre-ore alteration assemblages differ from gold-related hydrothermal alteration by the lack of mineral zoning around mineralized structures (Chamberlain, 2003).

In regard to general characteristics of Archaean lode gold deposits, the deposits are structurally controlled and mostly found within or adjacent to first order structures, around rigid granitoid bodies or in specific "locked-up" fold-thrust structures. They display mineral zonal patterns that reflect effects of hydrothermal fluids from the ore zone to the least altered host rocks (Lobato and Vieira, 1998; Walton and Jambor, 1998; Groves et al., 2000). Carbonate alteration dominates both the visible and chemical hydrothermal alteration and has been pointed as the best example for carbonate alterations formed as the result of reaction between CO_2-rich fluids and wall rocks. In these deposits, alterations vary, mostly reflecting on the fluid composition and wall rock chemistry. However, the assemblages are consistent in deposits of all ages and can occur worldwide (Clark et al., 1989). Mineralogical complexity within the inner alteration zones is a commonly observed feature. This has been related to factors such as narrow shear zone width and an episodic nature of deformation and fluid infiltration, which normally result in alteration zones with complex cross-cutting relationships. The effect can result in the overprint of distal alterations over proximal alteration zones (Groves et al., 2000).

Within a single host rock there is little variation in alteration for hundreds of meters parallel to the structures that have been used to carry the hydrothermal fluids. Distal alterations are found all over the hydrothermal system contrary to inner alteration zones which are normally restricted to fault-fault or fault-lithological contacts, dilatational flexures and other areas with extremely high fluid flux (Groves et al., 2000). Quartz is the dominant mineral in veins together with Fe- and As-bearing sulfides (pyrite or arsenopyrite) and carbonates (ankerite, dolomite, and calcite). Pyrite and pyrrhotite are common in metamorphosed igneous rocks whereas arsenopyrite is found to be more dominant in metasedimentary host rocks. In felsic igneous and clastic sedimentary host rocks, calcite is the dominant carbonate and sericite is the most common phyllosilicate (Klein and Day, 1994). Albite, white mica or fuchsite, chlorite, scheelite, siderite and tourmaline have been reported to be the common gangue minerals in veins within greenschist facies host rocks (Clark et al., 1989; Mueller and Groves, 1990; Mikucki and Ridley, 1993; Yeats and Vanderhor, 1998; Groves et al., 2000; Goldfarb et al., 2005; Kreuzer, 2006). Table 7.1 is a summary of the proximal alteration minerals with respect to host rock types, physical conditions and crustal level for Archaean lode gold deposits, the table has been summarized from different sources by Chamberlain (2003). For some deposits, a zone occurring immediate between mineralization and distal alteration is characterized by minerals including montimorillonite, illite, chlorite, and epidote (Kreuzer, 2006). The outermost zone is dominated by chlorite and carbonates (calcite), which wrap around inner zones (Phillips and Groves, 1984; Klein and Day, 1994). Inner alteration zones can be up to 2 or 3 times the width of the vein they are enclosing but can reach as wide as 100 m where they surround multiple or structurally complex veins (Peters and Golding, 1989). Yeats and Vanderhor (1998) reported that alteration can also reach up to 200 m wide into the wall rocks. In this range carbonate minerals may form a restricted zone from few meters to tens of meters away from small-scale veins within shear zones. Sometimes hydrothermal fluids may alter the host rocks within a regional shear zone in a range of up to a kilometer or more in width (Klein and Day, 1994). Geochemical data has revealed that hydrothermal fluids in lode gold deposits introduce Na_2O, Rb, Li, and Ba which are more localized, immobile elements (e.g. Al, Ti, V, Y and Zr), and mobile elements (e.g. Fe, Mg, Cr, Ni, and Sc) (Groves and Foster, 1993). Other components are K_2O, H_2O, S and As, also with introduction or destruction of SiO_2. Characteristically, they have high Au: Ag ratios and low base metal as well as low Sn content.

These deposits exhibit variable enrichment of Ag, As, B, Bi, Mo, Hg, Sb, Te, and W, Cu, Pb and Zn are generally slightly elevated above the regional background. However, it has been noted that Pb may be anomalous in some deposits (Yeats and Vanderhor, 1998; Groves et al., 2000; Dubé and Gosselin, 2007). Yeats and Vanderhor (1998) reported Au, As, Bi, Sb, Pb, W and Mo are counted as the main pathfinder elements for this deposit model.

Table 7.1 Summary of proximal hydrothermal alteration minerals for the four dominant host lithotypes of Archaean lode gold deposits in the Yilgarn Craton, which can serve as an analogue to the SGB in Tanzania (Chamberlain, 2003)

Deposit class	Mafic	Ultramafic	Granitoid	BIF	Sulphide/Oxide
Epizonal 250º-400ºC <1-2 kbar (<5 to 8 km)	ALBITE ANKERITE Dolomite Muscovite Chlorite Biotite Tourmaline	FUCHSITE DOLOMITE Mg-CHLORITE Mg-biotite Muscovite Tremolite Talc	WHITE MICA ALBITE Ankerite/calcite Chlorite Biotite Tourmaline	ANKERITE CHLORITE Muscovite Albite Biotite	PYRITE Arsenopyrite Rutile Hematite Magnetite
Mesozonal 375º-550ºC <2-3 kbar (<7 to 12 km)	AMPHIBOLE BIOTITE PLAGIOCLASE Calcite/ankerite Clinozoisite Chlorite K feldspar Titanite	TREMOLITE PHLOGOPITE Mg-CHLORITE Calcite/dolomite Ca amphibole Talc	BIOTITE AMPHIBOLE K FELDSPAR Calcite Ca plagioclase Titanite Muscovite Epidote	AMPHIBOLE ANKERITE Chlorite Feldspar Muscovite Biotite	PYRITE Arsenopyrite Ilmenite Magnetite Chalcopyrite
Hypozonal 525º-650ºC <3-4 kbar (<10 to 15 km)	DIOPSIDE GARNET Ca amphibole Biotite Calcite Ca plagioclase K feldspar Cordierite Clinozoisite	DIOPSIDE OLIVINE Tremolite Phlogopite Calcite Mg chlorite Garnet Anthophyllite Spinel	DIOPSIDE K FELDSPAR Hornblende Biotite Ca plagioclase Titanite Calcite Garnet	AMPHIBOLE Hedenbergite Fe garnet Olivine Biotite Calcite/siderite	PYRRHOTITE Arsenopyrite Loellingite Pyrite Ilmenite Magnetite Chalcopyrite

Orogenic lode Au deposits represent the main component of the greenstone deposit clan (Poulsen et al., 2000), however, in greenstone terranes the Au-rich volcanogenic massive sulfide (VMS) and intrusion-related gold deposits are also reported as being associated with Archaean terranes (Poulsen et al., 2000; Dubé and Gosselin, 2007; Robert et al., 2007). The latter two deposit types can be juxtaposed against greenstone lode-Au deposits during strains that characterize Archaean greenstone belts. It is reported that their primary characteristics may be overprinted by deformation contrary to the lode-Au ones, which are normally formed during the syn- to late main phase of deformation, the later time of origin favors the characteristic features of lode-Au deposits to remain preserved (Groves et al., 2000; Poulsen et al., 2000).

 Au-VMS deposits occur in greenstone belts of various ages; they are commonly underlain by subvolcanic intrusions and sill-dyke complexes and are typically metamorphosed to greenschist and lower amphibolite facies (Dubé and Gosselin, 2007). More about the characteristics of Au-VMS can be found from different sources (e.g. Hannington et al., 1999; Poulsen et al., 2000; Dubé and Gosselin, 2007), but most important to this study are the alteration minerals associated with Au-VMS deposits. Proximal to mineralization the dominant alterations are reported to be sericitic to

silic/advanced argillic (aluminous) and carbonate ± anhydrite, presence of advanced argillic alteration is reported to indicate low pH conditions similar to conditions found in epithermal environments (Dubé and Gosselin, 2007). Mn-rich garnet-biotite assemblage or manganiferous garnet-Zn-rich staurolite-chloritoid-biotite-muscovite-chlorite assemblage might also be present (Hannington et al., 1999; Dubé et al., 2007). The distal alteration pattern is dominated by a chloritic (Mg-rich Chlorite)/propylitic with sericite or clay-sericite (argillic) halo (Hannington et al., 1999).

Intrusion-related gold deposits are also structure controlled within and at varied distances around intrusions (Sillitoe, 1991; Sillitoe and Thompson, 1998; Lang and Baker, 2001). Contrary to other deposits, in the intrusion-related deposits mineral and metal zoning is poorly developed or absent over both vertical and lateral distances (Sillitoe and Thompson, 1998; Robert et al., 2007). However, alteration within intrusions is mostly confined to narrow alteration envelopes around individual veins of which it has been reported that carbonate alteration, which is accompanying Au mineralization, is locally well developed (Belven, 2005). Generally, the deposits are typically restricted to a narrow sericite-carbonate-feldspar alteration on quartz veinlets (Robert et al., 2007). Feldspar alteration in these deposits is dominated by albite and/or K-feldspar minerals (Lang and Baker, 2001). In some deposits, especially in the subvolcanic ones, advanced argillic alteration has been recognized (Sillitoe et al, 1998; Lang and Baker, 2001). Other alteration that may be associated with intrusion-related gold deposits are silicic and greisen (Lang and Baker, 2001). Below is a summary table of common hydrothermal alteration minerals around gold deposits in the Archaean greenstone belts, together with alteration minerals associated with major gold mines found in the Sukumaland Greenstone Belt in Tanzania (Table 7.2)

Table 7.2 Summary of hydrothermal alteration minerals around gold deposit types in Archaean greenstone belts, some of these minerals were used to map hydrothermal alteration zones in this study

Deposit Type	Proximal Mineral Alteration	Intermediate Mineral Alteration	Distal Mineral Alteration
Orogenic(Lode)-Au	carbonate(ankerite,dolomite,calcite,siderite)sericite,albite,fuchsite,chlorite, tourmaline	Kaolinite, montimorillonite, illite, chlorite, epidote	chlorite, carbonate(calcite)
Au-VMS	silicic,sericitic, carbonate±anhydrite, advanced argillic(pyrophyllite), Mn-rich garnet,biotite,staurolite,chloritoid, chlorite,muscovite	Not clear	chloritic(Mg-rich chlorite), clay-sericite(argillic),
Intrusion Related Gold	carbonate,sericite,feldspar (albite±K-feldspar),advanced argillic, silicic, greisen, skarn	Not clear	Not clear
Geita Gold Mine	silicic,sericite, ankerite±calcite,epidote, actinolite,biotite	Not clear	chlorite, calcite, hematite
Bulyanhulu Gold Mine	silicic, carbonate,sericite,chlorite,	Not clear	chlorite, calcite
Tulawaka Gold Mine	muscovite,chlorite,epidote,biotite, carbonate, sericite,talc,serpentine	Not clear	chlorite, calcite
Buzwagi Gold Mine	sericite, potassic(K-feldspar),chlorite,biotite,florite, serpentine	Not clear	Carbonate

7.3   ASTER Data Alteration Mapping

ASTER data have shown the ability to identify different hydrothermal minerals. This is mainly because of the relatively high spectral resolution of the ASTER data, the characteristics of spectra from alteration minerals as well as the characteristic alteration zones, which are commonly found to be associated with mineral deposits. The remote sensing satellite data have been used in identifying hydrothermal alterations and indirectly to locate new target areas during early stages of exploration (e.g. Crósta et al., 2003; Rowan and Mars, 2003; Brown et al., 2006; Tangestani et al., 2008; Mars and Rowan,2010). Several studies have been conducted so far on remote sensing alteration mapping, of which most studies were focused on the identification of different alteration minerals and ASTER data have also been used in these studies (e.g. Crósta et al., 2003; Tangestani et al., 2008). In addition, different techniques are currently known and have been intensively used for image analysis (e.g. Fraser and Green, 1987; Crósta and Moore, 1989; Kruse et al 1993; Boardman and Kruse, 1994). By referring to the previous studies on hydrothermal alteration mapping, most of the analytical methods used one diagnostic mineral from an alteration mineral assemblage as the representative mineral to identify a particular alteration. The logic behind this concept is that the diagnostic mineral selected is a spectrally dominant contributor to that mineral assemblage (e.g. Thompson and Thompson, 1996; Crósta et al., 2003; Rowan and Mars, 2003; Brown et al., 2006; Tangestani et al., 2008). However, with the obstacles shown by the possible interference of minerals from non-hydrothermal sources as described earlier, the use of only one principal mineral to represent all minerals in an alteration assemblage still poses the possibility of unintentional mixing of non-hydrothermal minerals during mapping of hydrothermal alterations. This part of the study is aimed to minimize the interference of non-hydrothermal minerals by designing a technique that will involve more than one diagnostic mineral from a hydrothermal alteration assemblage to extract the hydrothermal alteration patterns. The technique is further aimed to increase the accuracy in identifying target areas through a method, which will manifest the zoning of hydrothermal alterations with respect to common mineral deposit models. In this study, hydrothermal alterations from Archaean greenstone gold deposit models as well as hydrothermal alterations reported in major gold deposits in the Sukumaland Greenstone Belt were used (Table 7.2).

Sukumaland Greenstone Belt (SGB) as described in section 3 and 4 is the leading greenstone belt for gold production in the LVGF. Gold deposits in the SGB are epigenetic in origin with mineralization at all major gold mines being structurally controlled (refer section 4). Different types of alteration zones have been identified in deposits from SGB and have revealed to correlate with hydrothermal alterations of Archaean lode gold deposits in other terrains of similar geological setting, for example in the Archaean Yilgarn Craton in Western Australia, the Abitibi Belt in the Superior Province in Canada and the Barberton greenstone belts in the Kaapvaal Craton, South Africa (Goldfarb et al., 2005).

7.4   Methodology

7.4.1   Selection of the Key Minerals from Alteration Assemblages

The principal minerals from each alteration assemblage were selected from Thompson and Thompson (1996), from deposit models in the Archaean greenstone belts as well as alteration minerals documented from major gold deposits in the SGB (Table 7.2). In this study, more than one key mineral from alteration assemblages were used for the mapping of alteration zones (Table. 7.3). Advanced argillic (pyrophyllite), and argillic alterations have also been reported in some of the

greenstone belt gold deposits (Table 7.2). For example, in lode-Au, Au-VMS and Intrusion related Au deposits (Peters, 1987; Peters and Golding, 1989; Sillitoe et al., 1998; Hannington et al., 1999; Lang and Baker, 2001; Dubé et al., 2007). These two alteration types were also included in the analysis and they can also be found in the vicinity of gold mineralization in Archaean greenstone belt deposits, mostly in Au-VMS and in Intrusion-related gold deposits. Silicification was not included in the mapping of the present study due to difficulties in identifying quartz minerals with ASTER data. Additionally, their bulk and sometimes predominant presence in the background as major rock forming minerals can intensify the interference problem. Silica is a common mineral in most of the host rocks, for example, in granitoids quartz constitutes a large percentage of the total rock-forming minerals and therefore is expected to cause a significant interference. More important to note is that for the ASTER data the thermal infrared (TIR) bands, which contain characteristic spectral features for silica, has a low spatial resolution (90 m) and as a result, its spectrum cannot be uniquely distinguished. Hence, few alteration minerals, which are commonly found around the deposits in Archaean greenstone belts, particularly those minerals, which are spectroscopically active, were chosen for alteration mapping in this study (Table 7.3).

Table 7.3 The list of diagnostic alteration minerals used for the mapping of alterations in the SGB

DIAGNOSTIC ALTERATION MINERALS	POSITION IN THE PATTERN
Calcite, Dolomite, Ankerite, Siderite	Proximal
Pyrophyllite, Sericite, Diaspore	Proximal
Montimorillonite-Illite, Kaolinite/Dickite, Chlorite	Proximal, Intermediate
Sericite(muscovite)-Illite, Chlorite	Proximal, Intermediate
Chlorite, Epidote, Calcite	Distal

7.4.2   ASTER Data Analysis

ASTER is one of the five instrument sensor systems on-board of the satellite Terra, which was launched on December, 1999. It has a unique combination of a wide spectral coverage from visible near-infrared (VNIR) through shortwave infrared (SWIR) to the thermal infrared (TIR) regions of the electromagnetic spectrum (Table 7.4). The spatial resolution of ASTER bands varies, VNIR bands have 15 m resolution and SWIR and TIR have 30 m and 90 m resolutions respectively. ASTER data has 14 bands including 6 bands from the SWIR region; this means it has 4 more bands in the SWIR region compared to the 2 bands in Landsat 7 ETM+. The presence of more bands in the SWIR region as well as 6 bands in the thermal infrared (TIR) region makes ASTER data relatively spectrally powerful and can thus identify the individual hydrothermal alteration minerals. ASTER images are available at relatively cheap prices depending on the processing level requested by the user. The data is obtained from different sources e.g. United States Geological Survey (USGS) and Earth Remote Sensing Data Analysis Center (ERSDAC) in Japan. For reference, the detailed information about ASTER data has been well summarized in Rowan and Mars (2003) and Gozzard (2006). The ASTER data used in this study are Level 1A Visible-Near Infrared (VNIR)/Shortwave-Infrared (SWIR) and Thermal Infrared (TIR) data, collected at 08:34 AM on July 03, 2000, the data were bought from the Earth Remote Sensing Data Analysis Center (ERSDAC) in Tokyo, Japan.

Satellite	Sensor	Number	Spectral Range	Scene Size	Pixel Resolution

		of Bands			
ASTER	VNIR	1 to 3	0.52 - 0.86 µm	120 X 150 km	15 meter
	SWIR	4 to 9	1.600 - 2.430 µm		30 meter
	TIR	10 to 14	8.125 - 11.65 µm		90 meter

7.4.2.1 Preprocessing

Processing of multispectral data to derive accurate surface compositional information requires a chain of steps significantly different to 'standard' image-processing techniques (Gozzard, 2006). This is because before pre-processing ASTER data is not reliable as a source of geological information. Therefore, important processing steps are required to convert ASTER images into a usable and meaningful form. Image registration was important to make sure images fit to the study area. The projection used for the SGB images was UTM, zone 36 south and WGS-84 datum. Image-to-map registration by using landuse map of Kahama district was applied to correctly fit the image, objects such as roads and river triple junctions were helpful in the process. The ASTER Level 1A data used in this study were also corrected to remove sensor and atmospheric errors. The atmospheric correction tool the Fast Line-of-sight Atmospheric Analysis of Spectral Hypercubes (FLAASH) embedded in ENVI software was used in this process. FLAASH is the first atmospheric correction tool developed by Spectral Sciences under the sponsorship of the U.S. Air Force Research Laboratory. It incorporates MODTRAN atmosphere models and aerosol types to be applied on the scene. For the ENVI (the Environment for Visualizing Images) software, the embedded FLAASH contains MODTRAN4 (Matthew et al., 2000). FLAASH includes other features such as correction for the adjacency effect (pixel mixing due to scattering of surface-reflected radiance) and option to compute a scene-average visibility (aerosol/haze amount). It has the advanced techniques for handling stressing atmospheric conditions, such as the presence of clouds and adjustable spectral polishing for artifact suppression. Apart from ASTER data, FLAASH also supports the hyperspectral sensors and other multispectral sensors such as IRS, Landsat, RapidEye and SPOT. The resulting image from FLAASH, are the pixels with the surface reflectance values that can be compared to typical library spectra. Results from FLAASH are ready for the extraction of useful surface (geological) information provided that the corrections were properly applied (ENVI, 2009).

7.4.2.2 Normalized Difference Vegetation Index (NDVI)

Amongst the major obstacles in the mapping of hydrothermal alteration minerals by both hyperspectral and multispectral remote sensing images is vegetation (Crippen and Blom, 2001; Yu et al., 2011; van der Meer et al., 2012). In heavily vegetation covered areas, it is difficult for the satellite sensors to detect signals from the underlying soils and rocks. This means, with multispectral images, minerals and rocks under the thick cover of vegetation are difficult to be mapped. Moreover, interference between mineral and vegetation spectra is another problem. Mixing of these spectra makes it difficult to distinguish most minerals from vegetation, which causes a great chance of mixing the vegetation signals into spectra of extracted minerals during analysis. However, various techniques have been proposed to minimize this problem (e.g. in Yu et al., 2011), and masking of the pixels which are mostly covered with vegetation is one of the alternatives.

The vegetation covered areas can be easily identified by the vegetation indices (VI). They are one of the primary sources of information for operational monitoring of the Earth's vegetative cover. The indices combine reflectance measurements from different portions of the electromagnetic spectrum

to provide information about vegetation cover on the ground (Campbell, 1996). They are radiometric measures of the spatial and temporal patterns of vegetation photosynthetic activity related to canopy biophysical variables such as leaf area index (LAI) and normalized difference vegetation index (NDVI) (Rouse et al., 1974; Elvidge and Lyon, 1985; Asrar et al., 1985). Vegetation indices can also be applied to multispectral remote sensing images (e.g. Pearson and Miller, 1972). Calculation of indices by multispectral images is simply by combining reflectance through different bands carrying vegetation spectral features, the main purpose is to contrast the high infrared and low red reflectance that characterizes photosynthetic vegetation. For example, Pearson and Miller (1972) reported the (near infrared/red) ratio for separating green vegetation from soil background, the VI was named simple vegetation index (SVI). NDVI is another type of vegetation index which has been widely used in many applications including regional and continental-scale monitoring of vegetation cover (e.g. Wessels et al., 2004). NDVI have also been used in different geological studies, for example, during mapping of the hydrothermal alteration minerals (e.g. Elvidge and Lyon, 1985; Carranza and Halle, 2002).In this study, NDVI (equation I below) was used to identify those pixels with a high percentage of vegetation signals, thus indirectly it was applied for mapping the highly vegetated areas in the study area.

NDVI = (B3-B2/B2+B3)……………………………………………………………………equation I

As it has been described before, spectra from vegetation normally interfere with mineral spectra during analysis. And by masking these pixels it will to a large extent reduce errors from vegetation interference. For the case of this study, pixels with more than 60% NDVI were masked during extraction of the hydrothermal alteration minerals. 60% NDVI was chosen as an optimal percentage by considering the fact that the image was collected in a dry season under the assumption that during this time window the study area will be less and scarcely vegetated. This is also supported by the regional climate of the study area as described in section 3. The ASTER images chosen were from July, 2000, since in Tanzania this month falls in a dry season. Therefore, > 60% NDVI will represent the highly vegetated pixels in the dry season and these were masked during the analysis of ASTER data so as to reduce vegetation interference.

7.4.3   Extracting Alteration Zones

As stated above, hydrothermal alteration is a result of characteristic mineral associations, specifically mineral assemblages, which are formed during the hydrothermal process depending on the chemistry and temperature of the fluids as well as the composition of the host rock. A hydrothermal alteration assemblage/zone therefore is formed by more than one alteration mineral. Apart from the fact that alteration zones are comprised by more than one mineral, there are key distinctive minerals in each alteration assemblage. These are the diagnostic minerals, which are most significantly used to recognize hydrothermal alterations. An important point to note is that these key minerals differ depending on the deposit type or models. Just for better understanding, a good example is the high-sulfidation epithermal deposit, for which the key minerals representing propylitic alteration are calcite, chlorite and epidote and the associated minerals are sericite and clays. In low-sulfidation systems, for the same propylitic alteration, wairakite replaces chlorite in the list of key minerals whereas chlorite is present only as an associate mineral and not a key mineral as in high sulfidation deposits (Thompson and Thompson, 1996; Thompson et al., 1999; Hedenquist et al., 2000). In the present study, key minerals from each alteration (e.g. calcite-dolomite-siderite-ankerite, pyrophyllite-

sericite-diaspore, muscovite-illite-chlorite and chlorite-calcite-epidote) were used to extract alteration zones. For an alteration zone with less than 3 key minerals, the associated alteration minerals were added to reach a total of 3 minerals (Table 7.3).

7.4.3.1 Spectral Angle Mapper (SAM)

SAM is amongst the techniques used to extract information from remote sensing images both multispectral and hyperspectral data e.g. ASTER and AVIRIS respectively. It is the endmember extraction method that looks for exact pixel matches through similarity in spectral shapes between image spectra and reference spectra (Kruse et al., 1993). The algorithm determines the similarity by calculating the angle between the two spectra and treats them as vectors in a space with dimensionality equal to the number of bands. Smaller angles represent closer matches to the reference spectrum (Fig 7.1, Eguation II). The reference spectra used in SAM can be obtained from spectral libraries such as Unites States Geological Survey (USGS) and Jet Propulsion Laboratory (JPL) and they can also be extracted directly from the image as region of interest (ROI) average or Z-profile spectra.
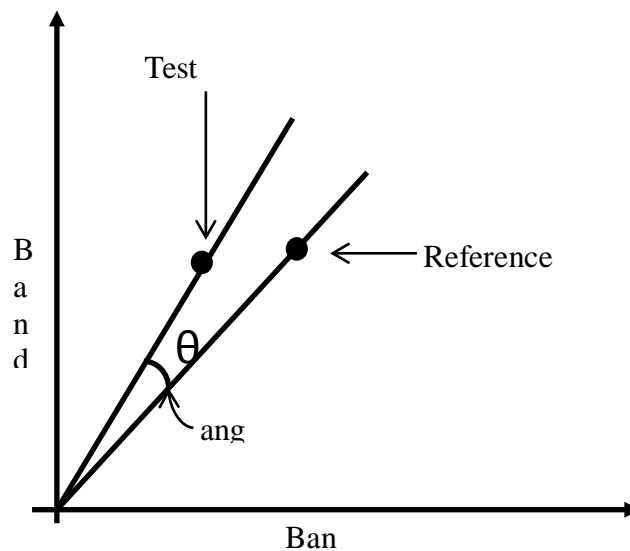
Figure 7.1 Sketch describing SAM analysis (see text for explanation)

By measuring the angle θ between two vectors, one determines the relationship between the vectors. If the angle between the vectors is 90°, then they are orthogonal and there is no correlation between the vectors. If the spectral angle is greater than 90°, the cosine has negative values. For example, the cosine is -1, when the angle is 180°. Correlation between vectors increases as the angle between them is reduced. At 0°, the vectors have a correlation coefficient of 1 which means the two spectra are indistinguishable (Fig. 7.1). The important thing to note is that cosine is independent of the brightness values to be compared (Kruse et al., 1993).

$$\theta = \cos^{-1}\left(\frac{\sum_{i=1}^{n} t_i r_i}{\sqrt{\sum_{i=1}^{n} t_i^2 \sum_{i=1}^{n} r_i^2}} \right)$$ ………………………………………………………….equation II

From equation above:

n = number of spectral bands

t = the reflectance of the actual spectrum or test spectrum

r = the reflectance of the reference spectrum

The SAM angle values obtained are in radians, they are calculated for each channel between image and reference spectrum and assigned to the corresponding pixel in the output SAM image. The derived spectral angle maps form a new data cube with the number of bands equal to the number of reference spectra used in the mapping process. In other words, one output image is obtained for one reference spectrum. The resulting images are called rule images or endmember images with values being spectral radian angles. In these images the smaller angles will be represented by darker pixels, the endmember images need to be classified to get the final results. This is done by referring the chosen threshold angle; it is already known that smaller angles represent closer matches to the reference spectrum. In SAM results of this study, the smallest angle classes of generally less than 0.23 radians were chosen as the endmembers or better as the alteration minerals extracted from ASTER images. SAM algorithms have been applied to both hyperspectral and multispectral data for the mapping of the hydrothermal alterations in different places and is therefore common in geological studies (e.g. Crósta et al., 1998; Ranjbar and Honarmand, 2007; Tangestani et al. 2008; Ranjbar et al., 2011).

7.4.3.2   Alteration Zone

Supervised classification was applied to the minerals which constitute an alteration zone. During classification, the classes containing all three minerals or two minerals were selected to represent the referred alteration zone. In this process, pixels representing only one mineral were neglected by suppressing them to zero. The process was followed by recording the selected pixels with new unique numeric value play part as identity (ID) of that particular alteration zone.

7.5   Realizing the Alteration Zoning

7.5.1   The Golomb Ruler

The new unique values given to each alteration during recording process were technically chosen to avoid interferences after combination. The technique used to select these values correlate very close to the construction of Golomb Ruler in mathematics. The integer numbers given to pixels of each alteration zone were selected objectively to be distinctive so that later they can be used as indicator to the referred alteration (Table.7.5). By definition, a Golomb Ruler is a series of integer numbers called marks along an imaginary ruler such that no two pairs of marks will have the same distance apart (Gardner, 1972). In other words, the distance between any two marks in a Golomb Ruler is

unique in that ruler (Fig.7.2). However, a perfect Golomb Ruler has a maximum of four marks (Golomb, 1972). Rulers with more than four marks are known as Optimum Golomb Rulers. They are defined as the shortest length for a given number of marks. More details about the Golomb Ruler can be found in Dollas et al. (1998). The Golomb Ruler has different applications in various fields including radio communication, X-ray crystallography, coding theory and radio astronomy (Babcock, 1953; Santoro et al., 1986; Dollas et al., 1998).

Figure 7.2 A sketch showing the example of a Golomb Ruler

In this study six distinctive integers were used (Table 7.5), the integers are distinctive to pixels of each alteration zone. When all alteration zones are added together arithmetically, the resulting sum of all the integers or better the values representing each alteration zone will be unique with no any sort of duplicate or reproduction of the original integers. The unique values which were used to represent alteration zones have made it easy to identify the alteration types especially in areas where there is complex mixed alteration.

Table 7.4 Alteration types and their indicator values

ALTERATION	INDICATOR VALUES
Unclassified	0
Chlorite-calcite-epidote	1
Sericite/muscovite-illite-chlorite	2
Kaolinite/dickite-illite	4
Montimorillonite-illite-chlorite	8
Calcite-dolomite	40
Pyrophyllite-sericite-diaspore	100
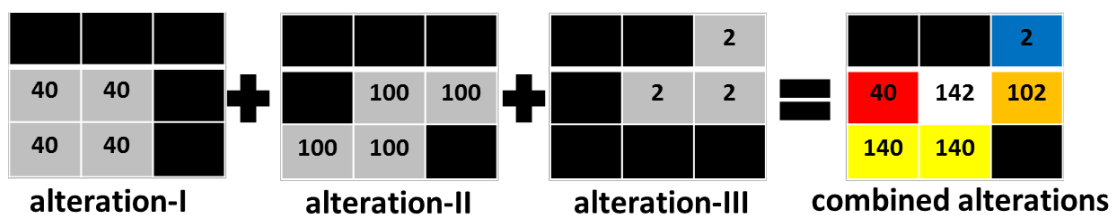
Figure 7.3 Example of the hydrothermal alteration combination by using Golomb Ruler marks

By referring to Figure 7.3 above, it was possible to identify the individual hydrothermal alterations in the resulted image after the combination of individual alterations. For instance, in the overall image of the combined alterations (Figure 7.3, right), a light colored pixel with value 142 indicates a mixture of all three alterations. Blue pixel with the value 2 indicates presence of alteration-III only, indirectly, it indicates that there is no mixed alteration in that pixel. Figure 7.4 are alteration images south of

Bulyanhulu Gold Mine and a resulting overall alteration image from the combination of individual alterations of the same area. The whole analysis of ASTER data in this study is summarized in the workflow and decision tree diagrams in Fig. 7.5 and Fig. 7.6.

A: carbonate
B: montimorillonite+illite-kaolinite-chlorite
C: muscovite-illite-chlorite
D: chlorite-calcite-epidote
E: combined alterations
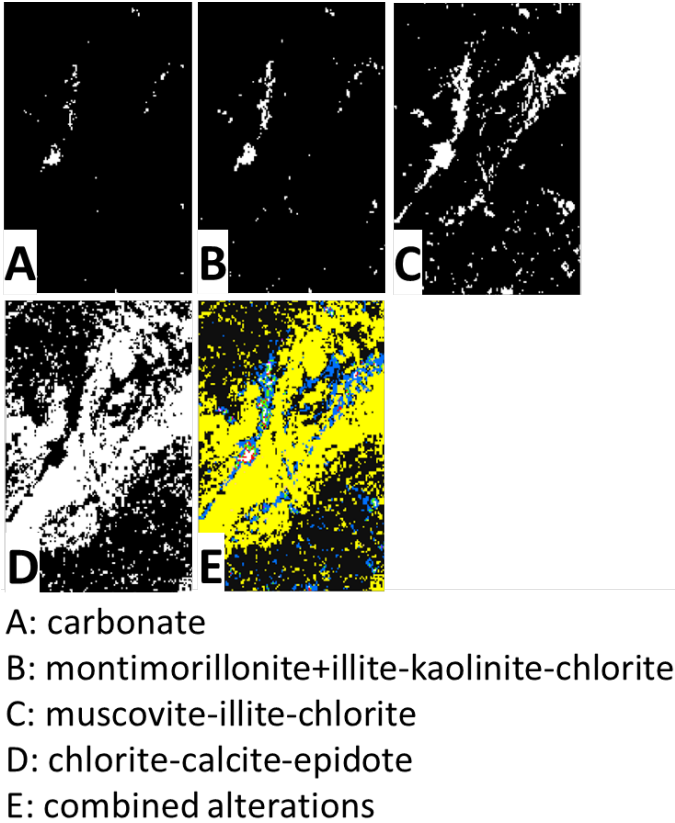
Figure 7.4 The image from Kahama mining district showing the mapped individual alteration types (**A-D**) used to create hydrothermal alteration zoning and the overall composite alteration map (**E**).
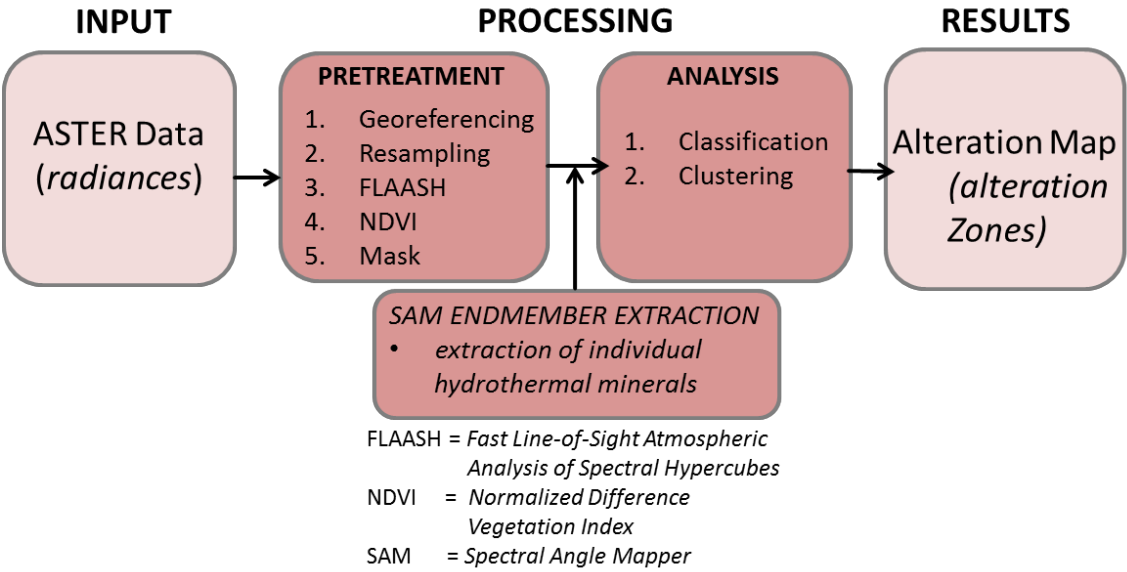
Figure 7.5 Workflow for the analysis of ASTER data
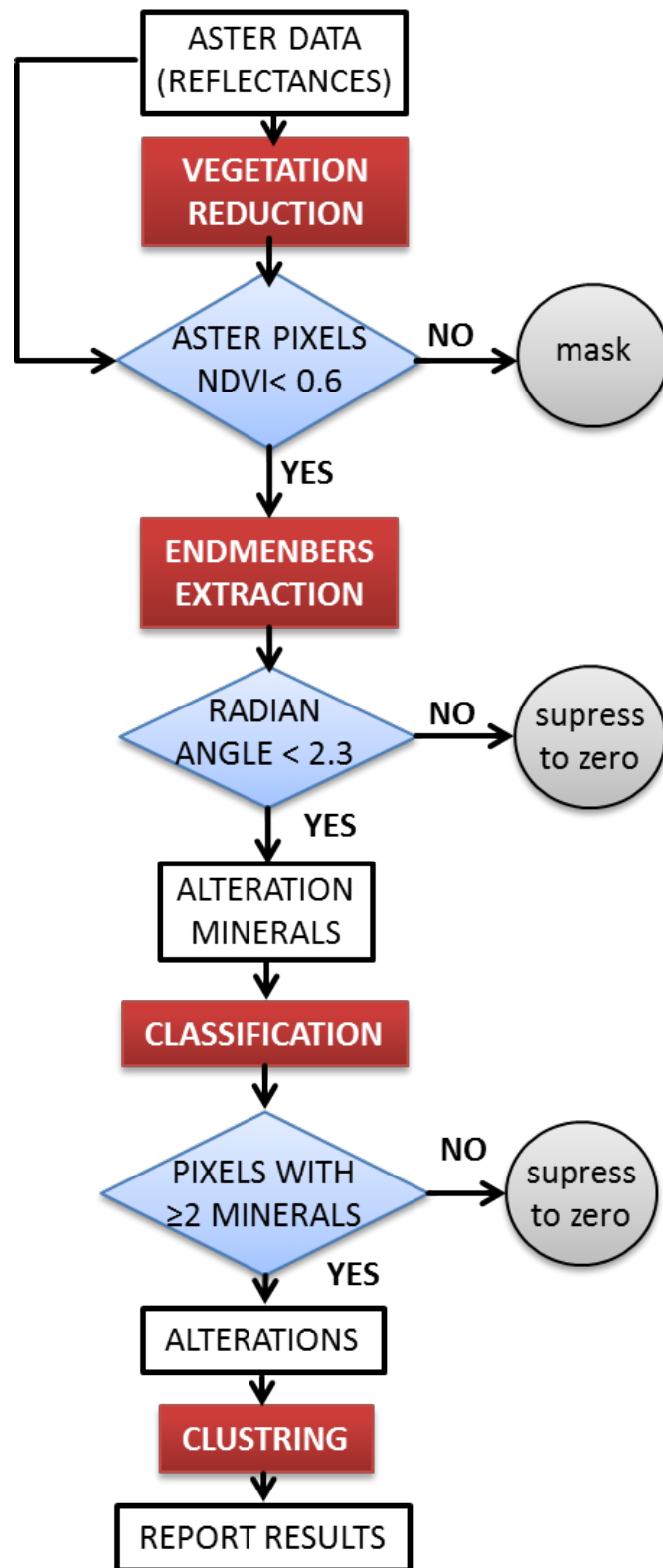
Figure 7.6 Decision tree for the analysis of ASTER data

7.6   Results and Discussion

7.6.1   The Identified Alteration Zoning versus Archaean Greenstone Belt Deposit Models

The overall image obtained has revealed alteration zoning in different places of the study area (Fig.7.7). The question was to whether the resulting zoned sequences are in agreement with the typical alteration zones of the referred gold deposit models (Table 7.2). By referring to major gold deposits in the SGB, carbonatisation, sericitization and silicification were the common alterations proximal to mineralization whereas chlorite-calcite alteration is reported to be distal alteration around mineralization zone (Ikingura et al., 2010). The alteration zones mapped from ASTER data have generally revealed the same pattern. Proximal alterations are located in the innermost areas of the sequence, near to the mineralization, whereas chlorite-calcite-epidote alteration occurs as the outermost zone. In between proximal alterations and distal ones there is an intermediate zone of which its constituent minerals are sericite/muscovite-chlorite-illite in Table 7.3, the zone is always located next to the distal (chlorite-calcite-epidote) alteration and enclose the inner alteration zones in the sequence (Fig. 7.7).
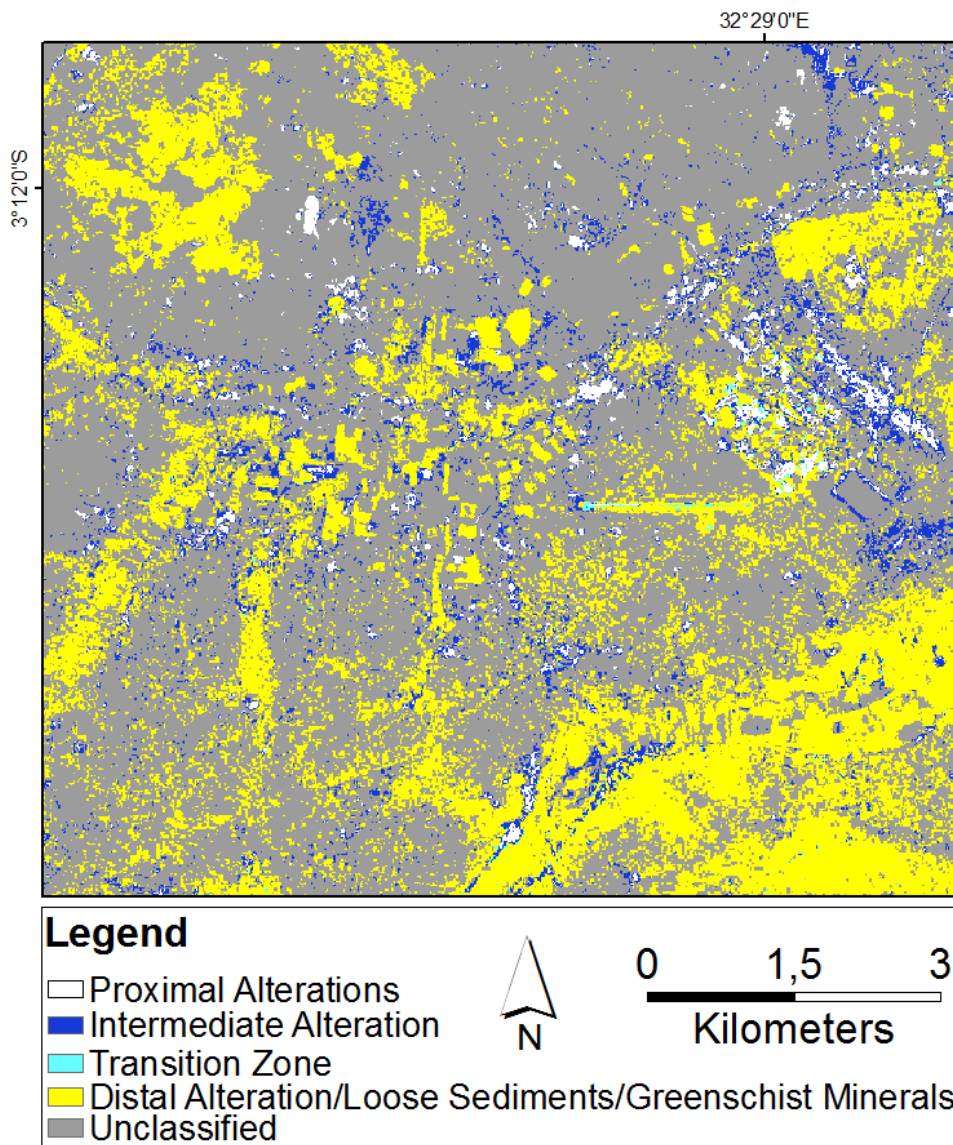
Figure 7.7 Overall alteration map of the Bulyanhulu mining district

The observations of this study indicate that the resulting alteration zones are not restricted by the type of surface geological materials. Alteration zoning is observed on both loose sediments/soils and in areas with exposed bed rock. For example, field observations indicate that alteration zones in Block KHA and Block KH (Fig. 7.8) are located in areas, which are covered with soils and rocks respectively. The two areas show similarity with regard to alteration sequences and both areas lithologically are located in the mafic to intermediate metavolcanic rocks reported to have been intensively silicified and carbonatized. In these areas brown mica-alteration is reported to be intensive and extends up to tens of meters along quartz veins (Pauls and Goldsmith, 2012).

Block KHE is situated to the SW of Bulyanhulu Gold Mine (Fig. 7.8). Although the detailed geological map of Bulyanhulu mine does not cover the area under this alteration pattern, it is possible that the area is underlain by granitoids. The Bugarama granitoid intrusion (Fig. 4.1 in section 4) covers the area SW of the Bulyanhulu Mine, of which, with reference to the spatial overlay of the maps, the granitoid intrusion is inferred to host the Block KHE alteration pattern. However, the possibility that the alteration zoning is situated at the boundary between granitoids and greenstones should not be excluded.
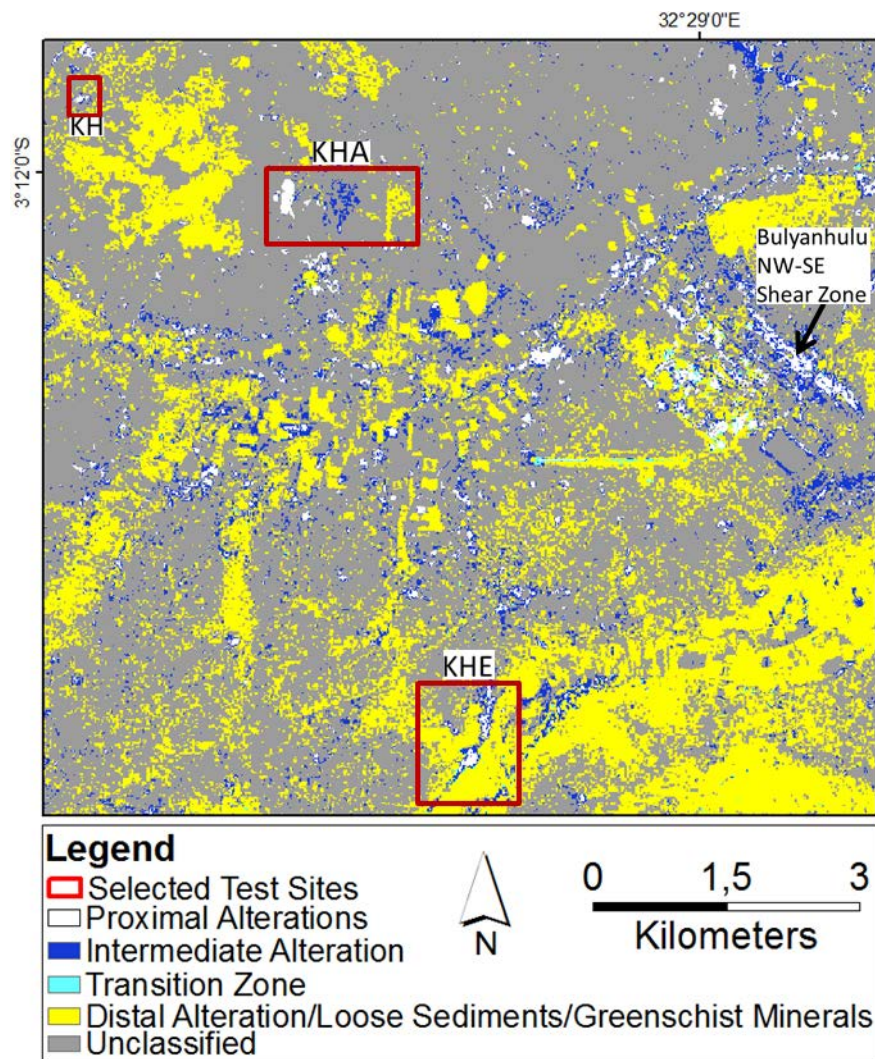
Figure 7.8 Overall alteration map of the Bulyanhulu mining district showing Bulyanhulu Gold Mine and three selected test sites (red squares).

From the alteration zoning observed it has also been possible to depict the geological structures related to hydrothermal alteration. Areas indicated as proximal alteration zones follow the pattern of tectonic structures i.e. faults and shears zones. Most of these proximal alteration zones are located within the tectonic fractures, this observation also agrees with the proximal alterations which characterize the greenstone belt gold deposits (e.g. Groves et al., 2000). For example, Block KHE (Fig.7.11) is located within a NE-SW trending shear zone SW of the Bulyanhulu Gold Mine (Fig. 7.8). Proximal alterations at this site shows to be located along the margins of the shear zone, which are interpreted to have locally formed either a "pull-apart" structure or a parasitic fold or an intersection between two intersecting shear zones of faults. The structure is suggested to have provided a potential favorable trap for the accumulation of hydrothermal fluids during magmatism. The NW-SE proximal alteration to the east of the area coincides with the NW-SE oriented Bulyanhulu shear zone, which hosts the mineralized quartz veins of the Bulyanhulu deposit. The shear zone trend is reported to be around 310° degree NW (Pauls and Goldsmith, 2012); this is similar to the observed trend of the proximal alterations observed in this study.
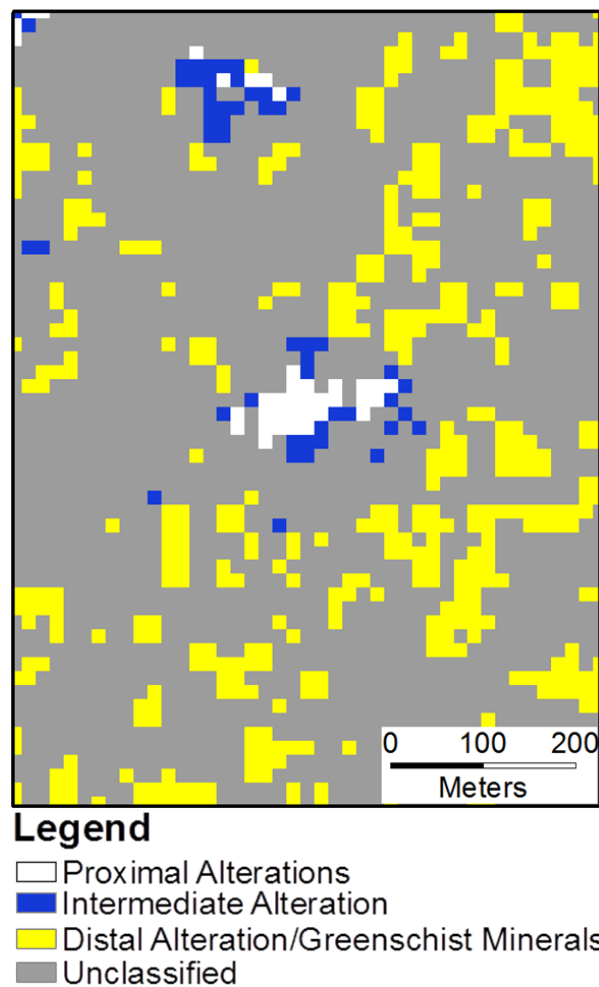
Figure 7.9 Block KH, the rock covered area (rhyolitic metabasalts) showing symmetrical alteration zoning, the zoning is located along a small shear striking at ca. 50° (NE-SW).
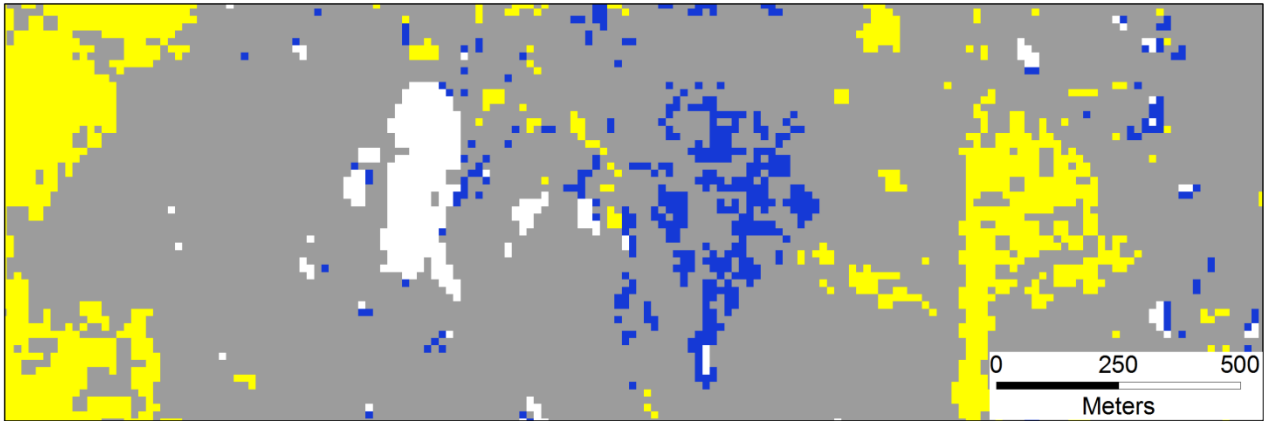
Legend
- Proximal Alteration
- Intermediate Alteration
- Distal Alteration /Supergene /Greenschist Minerals
- Unclassified

Figure 7.10 Block KHA, the soil covered area showing asymmetrical alteration zoning
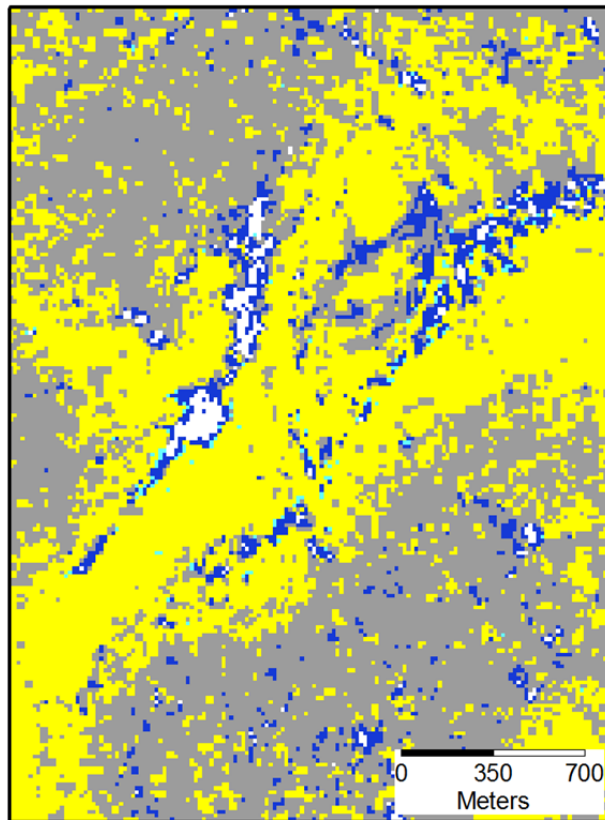
Legend
- Proximal Alterations
- Intermediate Alteration
- Transition Zone
- Distal Alteration/Supergene/Greenschist Minerals
- Unclassified

Figure 7.11 Block KHE alterations showing the symmetrical alteration zoning along the left margin of the NE-SW shear zone to the south of Bulyanhulu Gold Mine.

7.6.2 Features Observed from Alteration Zoning

The boundaries between alteration zones can be relatively clearly seen, for example there is a clear boundary between distal alteration zone (chlorite-calcite-epidote) and intermediate alteration zone. In some places the boundary is marked by a transition zone, pixels with mixed distal and intermediate alterations (KHE, Fig.7.11, and Fig.7.12). Similarly, the boundary between the intermediate zone and proximal alteration zones are relatively sharp. The boundary between the intermediate zone and distal alteration is suggested in this study to serve as the margins for the prospective areas as it separates the proximal alterations from the far more extensive distal alteration. The same boundary can be used to predict the shape and dimensions of the mineralization zones as it corresponds to the geometry of most of the Archaean granite-greenstone gold deposit models. Observation indicate that most of the alteration sequences starting from an intermediate zone have a length of less than 1 km and are a few tens to hundreds of meters in width. Proximal alteration zones in this study all are less than 500 m in length and less than 250 m in width. The described dimensions are also in agreement with the dimensions of alteration haloes related to greenstone belt gold deposits reported from different places (e.g. Peters and Golding, 1989; Klein and Day, 1994; Eilu and Mikucki, 1998; Yeats and Vanderhor, 1998; Chamberlain, 2003; Goldfarb et al., 2005; Dubé and Gosselin, 2007).

Legend
☐ Proximal Alterations
■ Intermediate Alteration
■ Transition Zone
■ Distal Alteration/Supergene/Greenschist Minerals
■ Unclassified
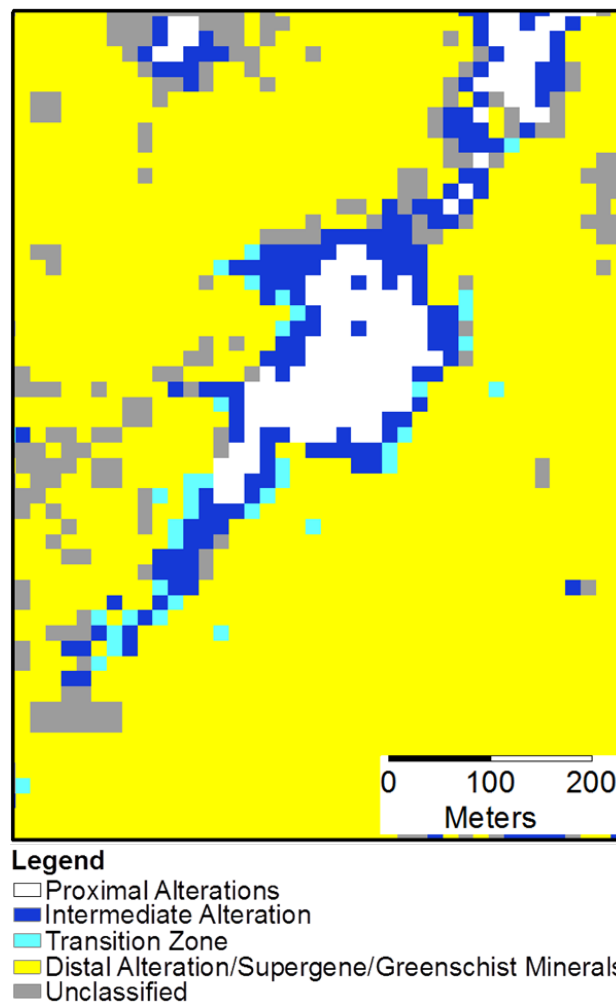
Figure 7.12 Block KHE showing the symmetrical alteration zoning with relatively clear boundaries between alteration zones as well as the transition zone between distal and intermediate zone.

60

For the wide spread of distal alteration (chlorite-calcite-epidote) is obvious that it can also be attributed to another origin apart from hydrothermal alterations. The study area is geologically located in a granite-greenstone belt terrane, therefore, it must be assumed that the distal alteration zone is a mixed product from hydrothermal alteration and pervasively occurring greenschist facies metamorphic minerals. However, with respect to greenstone belt gold deposit models, chlorite-calcite-epidote alteration is the outermost alteration in the sequence (e.g. in Chamberlain, 2003). As far as the exploration for these deposits is concerned the mixing of greenschist facies minerals in the distal zone will cause no difficulty during identification of exploration targets, since this will focus primarily on the proximal and intermediate alteration signatures; particularly where these occur in a systematic zoned fashion. Moreover, the systematic alteration zonation revealed from this study provides a suitable technique to avoid the interference of non-hydrothermal minerals during the selection of exploration targets. Additionally it is not possible for the non-hydrothermal alteration sources such as weathering to exhibit such systematic and particularly symmetrical alteration sequence. Overprinting of the greenschist facies metamorphism by hydrothermal alteration minerals in these orogenic terranes is a characteristic feature caused by the late injection of mineralizing fluids, which normally occur during syn- to post peak metamorphism (e.g. in Mueller and Groves, 1990; Groves et al., 2000; Chamberlain, 2003). This geological phenomena increases confidence to the mapped alteration zones since it shows the hydrothermal alterations always overprint the greenschist facies metamorphism (also in Groves et al., 2000). This means the mapped minerals reflects the hydrothermal alteration, which is the late event. For weathering processes where clays and other minerals are also weathering products, which sometimes accumulate in lowland areas, these minerals will not form a systematic mineral zonation in a sequence similar to that of hydrothermal alteration. This has also reported by Klein and Day (1994) as they were describing the gold deposit models in the Archaean terranes.

The alteration zoning patterns observed in the study area locally exhibit both symmetric and asymmetric geometries, for example, Block KHE and Block KH (Fig.7.9, Fig. 7.12) show symmetrical alteration zoning whereas Block KHA indicate an asymmetric zoning (Fig.7.10). The geometries and symmetries shown may have been caused mostly by the physical properties of the host rocks whereby rock reactivity and tectonically induced permeability e.g. from shearing or fracturing may be the controlling factors (Hedenquist et al., 2000; Pirajno, 2009).

7.7   Validation

Systematic sampling was done by following and traversing the alteration zones during two fieldwork campaigns (Fig. 7.13). Rock and soil samples were collected from each alteration zone of the three selected test sites which are Block KHA, Block KHE and Block KH (Fig.7.8). These samples were analyzed by different mineralogical and geochemical methods to investigate the difference between the mapped alteration zones.

Legend
- ▢ Proximal Alteration
- ▮ Intermediate Alteration
- ▮ Distal Alteration /Supergene /Greenschist Minerals
- ▮ Unclassified
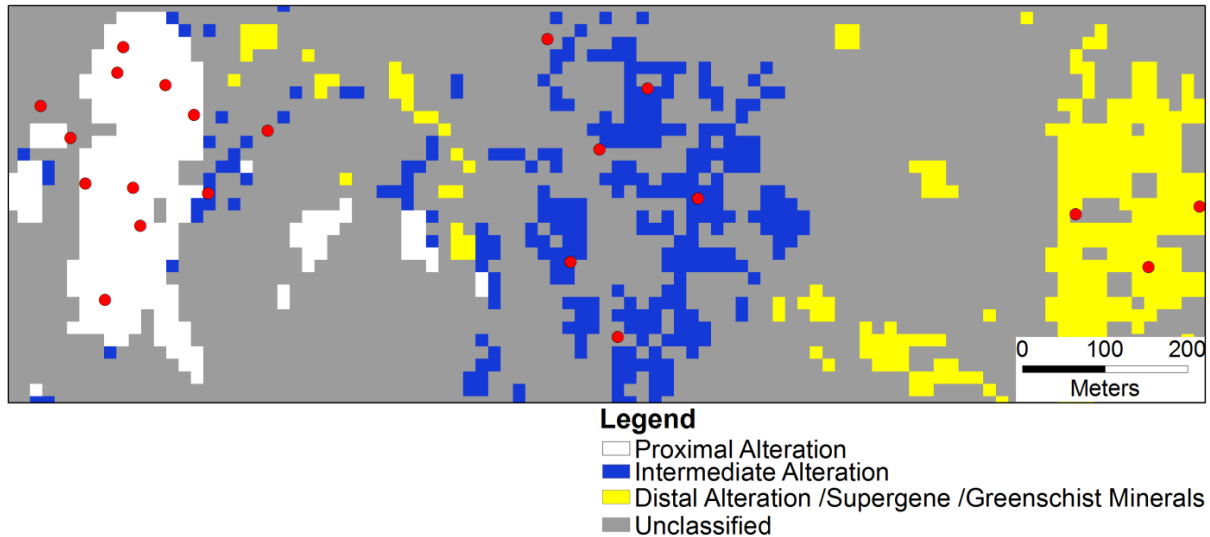
Figure 7.13 Block KHA Hydrothermal alteration zones and sampling points (red dots)

7.7.1   Visual Observations

Visual observation for the collected samples and comparing them with the mapped alterations was the first step taken during the process of validation. The observed systematic change of sample colour (soil) between different alteration zones is a striking feature that indicates the mineralogical differences in the various alteration zones. The soil samples collected from the field area shows a change in colour that corresponds to the alteration pattern identified from ASTER data analysis, the best example is alteration zoning of Block KHA (Fig.7.14). It is obvious that colour changes indicate variations in mineral compositions. Therefore, the observation is supporting the idea and indirectly indicates that the mineralogical variation is the cause of different alteration zones in the area. Proximal alteration correlates to light orange-brownish colored soil samples (e.g. sample KHA 25) whereas intermediate and distal alteration are characterized by dark brown (e.g. sample KHA 28) and dark greyish brown soils respectively (e.g. sample KHA 32) (Fig. 7.14).
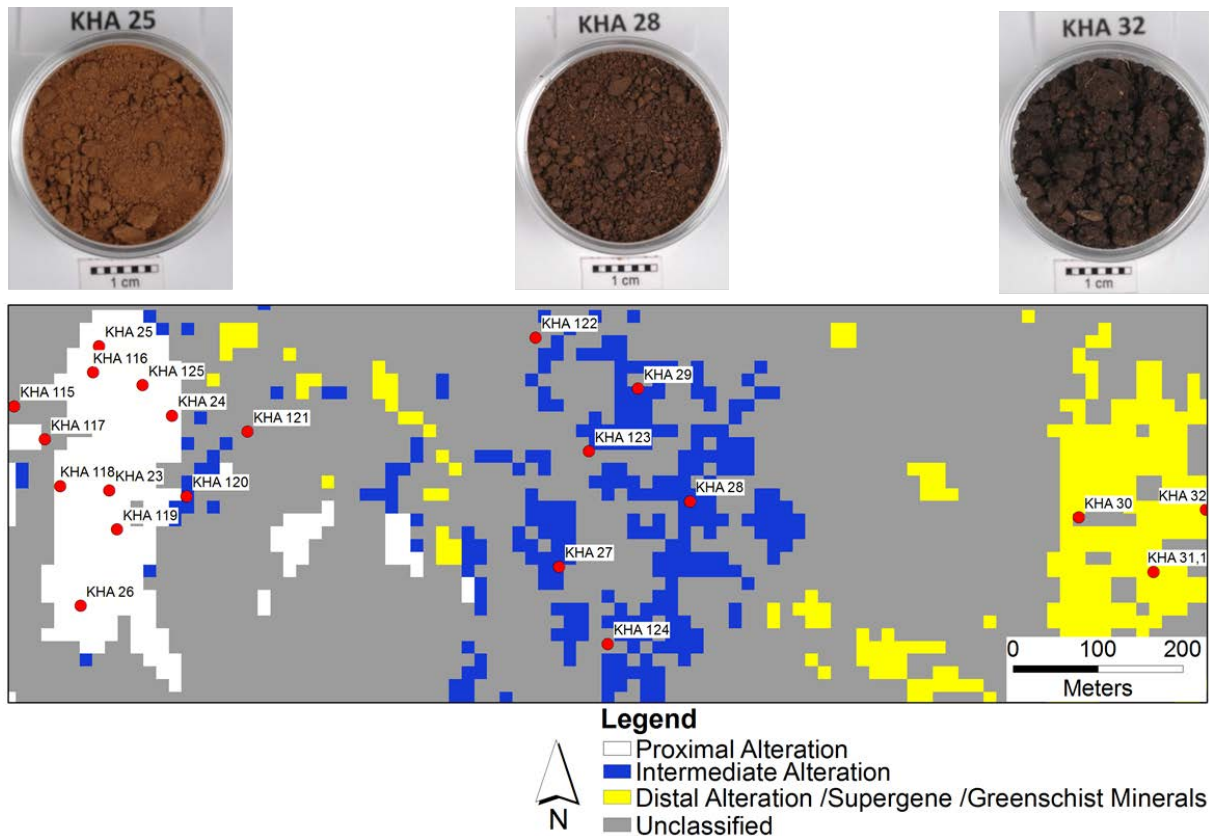
Figure 7.14 Colour variations between samples from different hydrothermal alteration zones in Block KHA

7.7.2 Laboratory VNIR-SWIR Reflectance Spectroscopy

Laboratory visible to near infrared (VNIR)-short wave infrared (SWIR) reflectance spectroscopy was also used for further validation of the alteration zones. This is a tool used to identify materials based on the properties of the chemical bonds and crystal lattice in compounds such minerals. The technique is sensitive to small changes in the chemistry and/or structure of the material (Clark, 1999). Variation in mineral composition normally causes changes to wavelength position and the shape of the absorption band in the spectrum. The causes of absorptions shown in spectra are electronic processes and molecular bonds vibration of the chemical compounds. This means that certain spectral features in the spectrum are indicative of specific chemical bonds in the mineral. Therefore, spectroscopic measurements can be used to detect different minerals by using the spectral features in the electromagnetic spectrum as effects of specific chemical bonds in minerals (e.g. Al-OH, Mg-OH, Fe-O, -CO_3, H_2O, etc.). Apart from mineral identification, spectral analysis can give an indication to the determination of the abundance and physical state of the detected minerals (Clark, 1999; Thompson et al., 1999; Hauff, 2005). More details about VNIR-SWIR reflectance spectroscopy of minerals can be obtained from Burns (1973), Farmer (1974), Hunt (1977) and Clark (1999).

VNIR-SWIR spectral measurements for samples in this study were taken with a TerraSpec[TM] instrument after all samples were oven-dried at 40°C for 72 hours, also the homogeneity of the soil samples was ensured by maintaining the sample grain size to an average of below 2 mm by sieving.

TerraSpec[TM] is a portable machine manufactured by Analytical Spectral Devices (ASD). It is a compact and field portable precision instrument with a full spectral range (350-2500 nm) and a 5 nm spectral resolution. Processing of the collected data was performed by using ViewspecPro software, of which important corrections and conversions were done as preprocessing steps to prepare the spectra for interpretation. Apart from visual interpretation under the guide of diagnostic absorption features for different minerals, the Specmin 3.1 software was also used to compare the measured spectra with reference library spectra for the identification of individual minerals. More details on preprocessing and interpretation including the use of the software can be obtained from Hauff (2005).

7.7.2.1   Block KHA

The VNIR-SWIR spectra obtained from the three alteration zones in Block KHA samples have shown significant differences, this is strongly revealed at the wavelength positions 1400 nm and 2200 nm as well as 2350-2400 nm (Fig.7.15). The absorption features observed around these regions are caused by different minerals e.g. clays, carbonates, micas etc. (Hauff, 2005; Thompson et al., 1999). Changes of mineralogical compositions in the alteration zones can be tracked through spectral absorption features of spectra from the three extracted alteration zones. For example, the clearly seen kaolinite doublets at 1400 nm and 2200 nm changes their shape from a doublet in the proximal alteration zone to a single absorption features in the distal alteration zone. The same is observed for the wavelength position at 2350-2400 nm whereby the features, which are normally shown by kaolinite and illite are smoothed out from proximal to distal alteration zones. Spectra from samples in the distal alteration zone indicate the dominance of smectite minerals, as the 2350-2400 nm features has been relatively smoothed when compared with those from proximal and intermediate alteration zone. The mineralogical differences observed can also be used to interpret the spatial temperature variation between alteration zones, proximal alteration has been affected by higher temperature compared to the outer zones. Spectra from this zone indicate the dominance of kaolinite mineral for which the temperature stability is reported to range from 100 to 220 °C (Hedenquist et al., 2000). Towards the outer zones, kaolinite is decreasing and gradually replaced by a mixture of kaolinite and illite-smectite. As described in the above section, distal alteration is dominated by smectite group minerals. Smectite minerals are characteristically formed in the distal and low temperature region of hydrothermal systems. They are normally stable at temperature below 150°C (Hedenquist et al., 2000).

Apart from absorption features, the reflectance of the spectra from these samples also decreases away from the proximal zones in a sequence corresponding to the alteration zones. Although reflectance can also be influenced by other factors apart from mineralogical differences (e.g. water content, grain size), these factors were reduced by drying the samples and by sieving to maintain a homogenous grain size for all samples. Spectra from proximal alterations show a higher reflectance compared to the outer zones (Fig.7.15). High reflectance correlates to the light brownish orange colored soil samples sampled from proximal zones whereas low reflectance correlates to the darker samples from distal alteration zones. The brighter the sample the higher the reflectance and this indirectly reflects the change in mineralogical compositions in these samples.
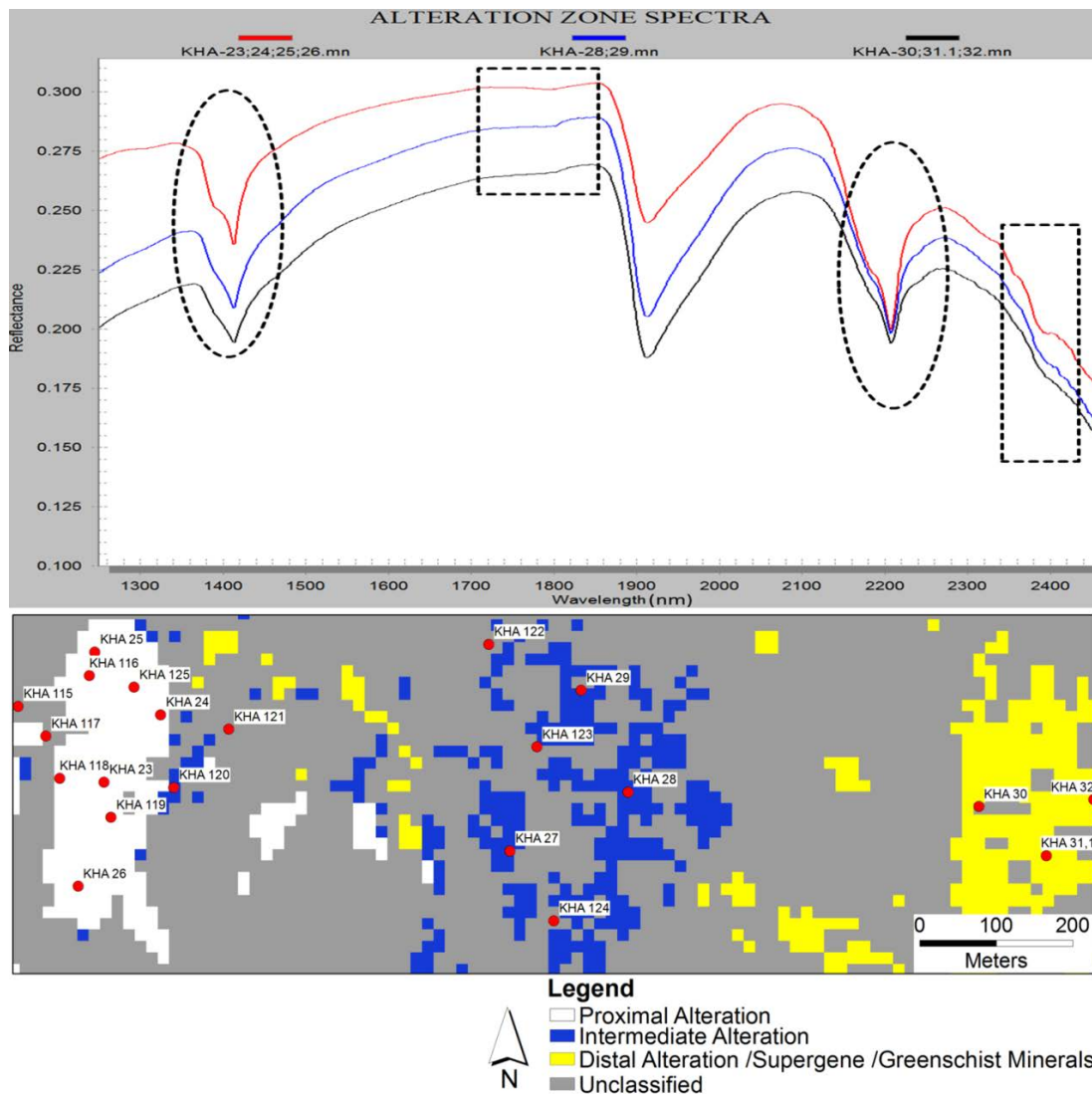
Figure 7.15 Average spectra from alteration zones in Bock KHA, red spectrum = proximal alterations, blue =intermediate alteration and black = distal alteration.

7.7.2.2   Block KHE

Spectral differences such as in Block KHA are also observed in Block KHE (Fig.7.16), however, in this area the absorption features are relatively difficult to distinguish. There are very diminutive differences, which are less obvious to recognize. The differences are mostly found in the dimensions of the absorption features. The absorption feature at 1400 nm shows differences in both shapes and dimensions, absorption at around 2200nm reveals no notable difference. At around 1800 nm there is a broad but shallow absorption feature, for which differences in the alteration zones can be recognized.   The interesting observation is that spectra reflectance values are in a sequence that follows the alteration zoning. The outer zones are having relatively higher reflectance when compared to proximal zones; this is contrary to the reflectance in Block KHA. The distal and intermediate alterations are reflecting at around 0.36 and 0.34 respectively whereas proximal ones are reflecting at around 0.26. As it was described in the above sections, mineralogical variation is one of the factors causing reflectance differences.
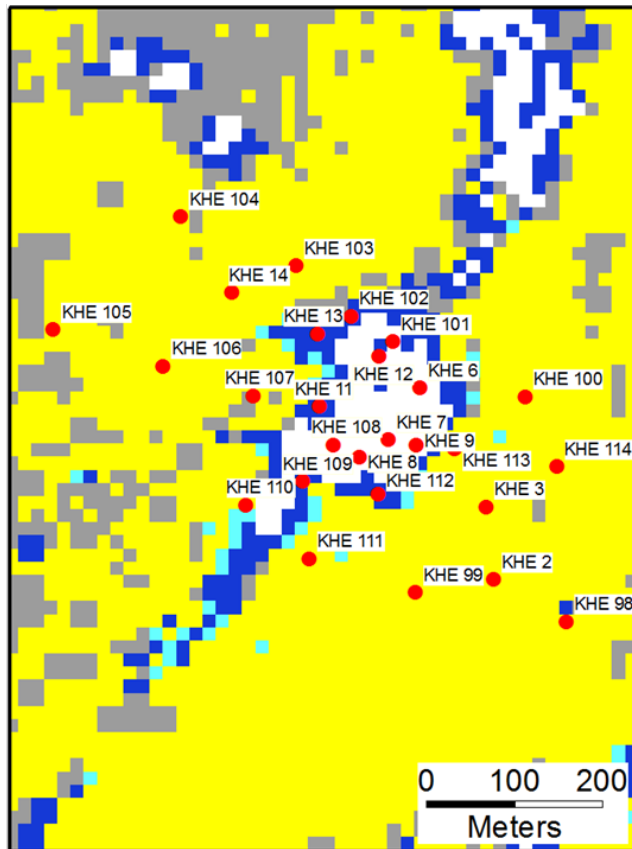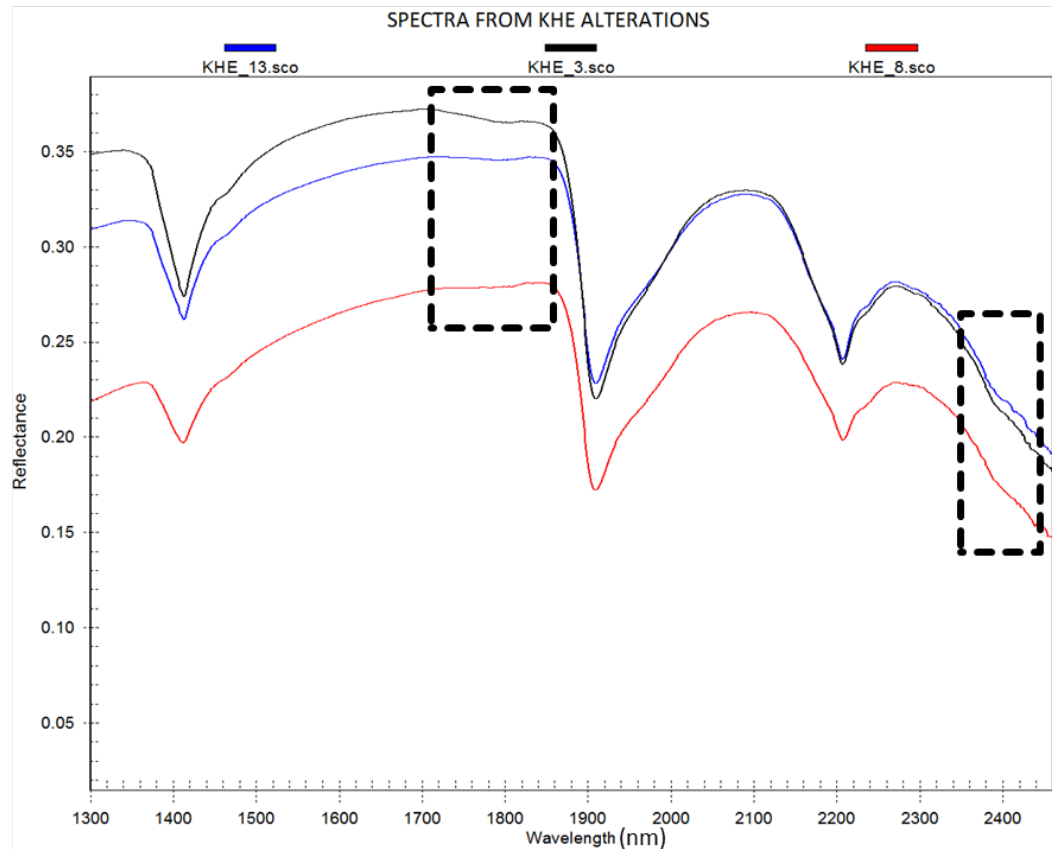
Figure 7.16 Spectra from alteration zones in Bock KHE, red = proximal alteration, blue = intermediate alteration, black = distal alteration.

The systematic increase of reflectance from proximal alterations towards the distal zones may also reflect mineralogical variation in these zones. But the observed opposing reflectance trend in Block KHE contrary to spectra from other test sites might also indicate high organic carbon in this area. The dominance of organic carbon means reducing the brightness of the soils and the consequence is the low reflectance in the proximal alteration zone. This observation need further work in future to investigate the other possible causes and explanations for such opposing trend of reflectance value.

7.7.2.3   Block KH

Spectral measurements were taken in different parts of the rock samples collected since they had different surfaces i.e. fresh surfaces, weathered surfaces and with inhomogeneous mineral distribution. With regard to the spectral measurements taken from these rock samples, treating all spectra in one pool will not be meaningful. Hence, in this study, only the spectra from the relatively homogeneous fresh surfaces were used for comparing the mapped hydrothermal alteration zones (Fig.7.17).

Figure 7.17 Pictures of KH 87 and KH 95.1 rock samples taken from intermediate and proximal alteration zones respectively

Samples from alteration zones have also revealed spectral differences from different alterations zones (Fig.7.18). All spectra indicate to be dominated by amphibole minerals, which the interpretation of these spectra has revealed the mineral to be dominantly hornblende. Despite the dominance of amphibole minerals, the effect of hydrothermal alteration can be seen. The spectral differences shown between distal (sample KH 134), intermediate (sample KH 87) and proximal alteration zones (sample KH 95.1) are suggested to have been influenced by hydrothermal alteration minerals (Fig. 7.18). Spectra from proximal alterations can be differentiated from the intermediate alteration zone by having significant absorption features at around 1400 nm and 2200 nm. The 1400 nm and 2200 nm features are mostly indicative for clays, micas carbonates, and possibly sulphates. The shapes of the absorption features at the region around 2330 nm indicate a similarity between

proximal and the intermediate zone but the two zones show a difference to the distal alteration zone. The distal alteration has a broad and smooth absorption feature in this spectral region (Fig.7.18, region under the box); the difference could indicate the presence of more carbonate minerals in the intermediate and proximal zones compared to the distal zone. Some of these minerals are clearly seen on rock samples. The absorption features at around 1400 nm and 2200 nm apart from other minerals confirm the presence of a significant amount of clay minerals in the proximal alteration zones when compared to the outer zones. The slope between 1500 nm and 2100 nm indicates a higher amount of iron-rich minerals in the proximal and intermediate alteration zones but not in the distal alteration zone. Therefore, the spectra from the three alteration zones have revealed the differences between the ASTER data -mapped alteration zones and have further confirmed the presence of minerals that signify a proximal alteration zone. There are also differences in reflectance between alteration zones. Proximal alterations have high reflectance maximum at approx. 0.30 whereas the intermediate zone reflects maximum at 0.135. Distal alteration has the lowest reflectance when compared to inner alterations maximum at around 0.12 (Fig.7.18). The different reflectance between the alteration zones gives further evidence that there is a systematic mineralogical variation between the different alteration zones. The region marked by a box at Fig. 7.18 shows most of the differences between Block KH spectra.
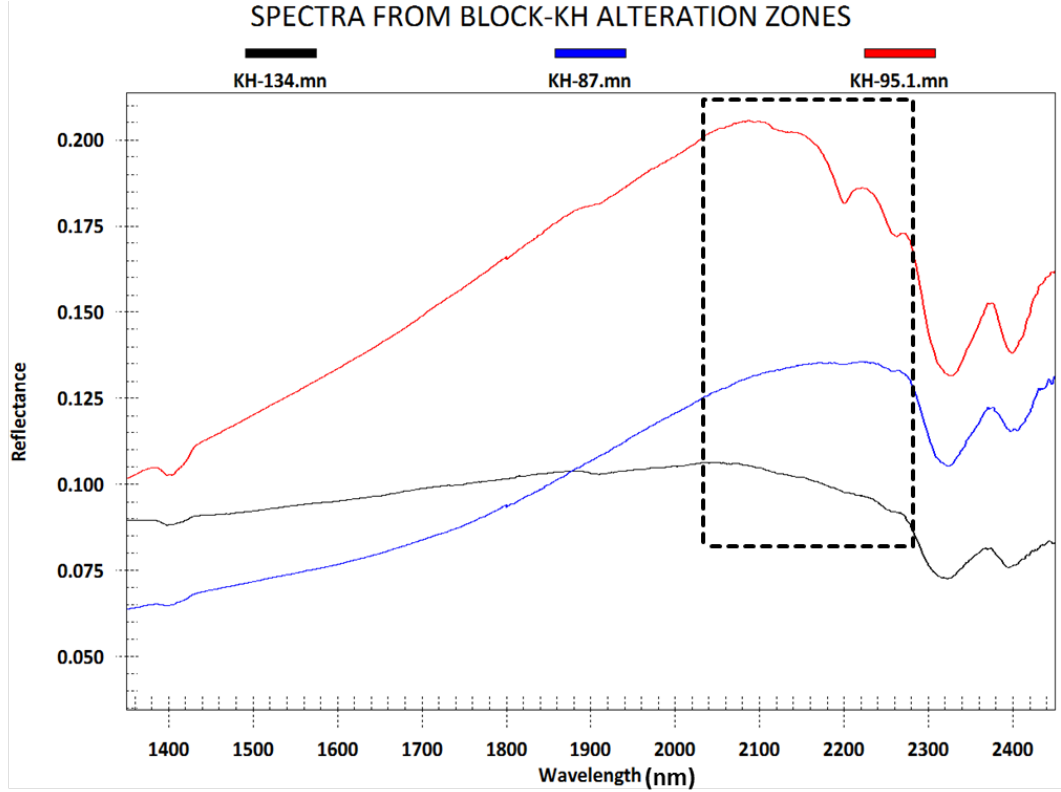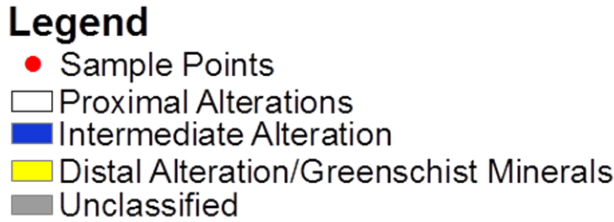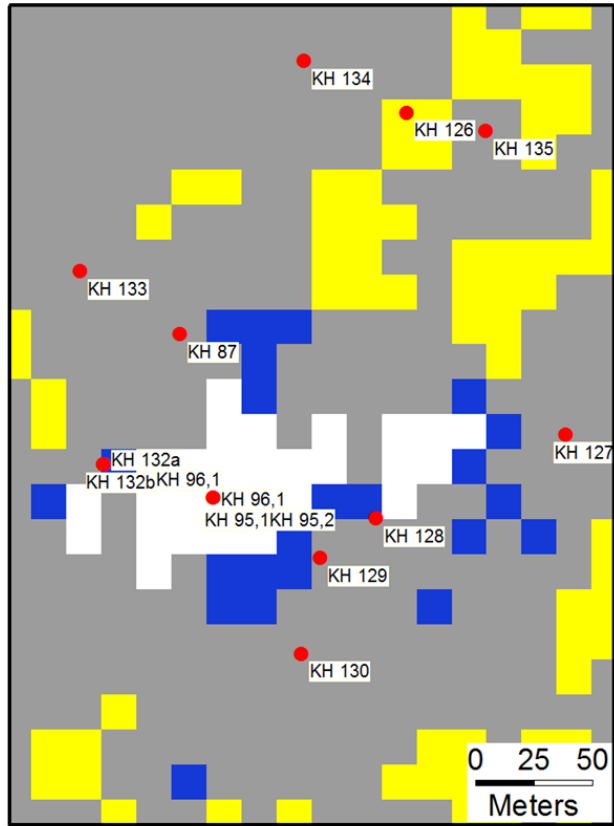
Figure 7.18 Showing spectral variation between alteration zones in Bock KH, red = proximal alteration, blue = intermediate

7.7.3 Mineralogical Differences between the Alteration Zones

Light microscopic analysis of the thin sections as well as scanning electron microscopy (SEM) revealed the presence of minerals, which directly or indirectly characterize the alteration patterns ,this will be shown in the below sections. A detailed XRD study of the various samples taken in the field was beyond the timeframe of this PhD-project, which is mainly focused on the remote sensing identification of alteration zones. However, a comparison of the data from remote sensing and from VNIR-SWIR-spectroscopy was attempted and thus a limited number of XRD analyses were performed on Block KHA samples for the identification of clay minerals, generously by staff of the Petrology and Economic Geology as well as by staff of the Mineralogy and Geochemistry groups at the Institute of Geology and Geography. XRD results have revealed the presence of illite, nacrite, kaolinite and montimorillonite (Appendix 5-10), which most of these minerals were also identified in VNIR-SWIR TerraSpec analysis. The results of these analyses or rather the identified minerals are also summarized in the following paragraphs and in Table 7.6.

7.7.3.1 Block KHA

Block KHA is a soil covered area whereby a total of 21 soil samples were collected from this site.

Proximal Alteration Zone: Clay minerals, kaolinite-dickite, kaolinite, montimorillonite, illite, pyrophyllite, nacrite, and montimorillonite were identified; other minerals are carbonates, barite, serpentine, ilmenite, pyrochlore, sulfides (sphalerite, galena), and Cu oxides (Table 7.6; Appendix 11-19).

Intermediate Alteration Zone: Illite, Illite-smectites/montimorillonite, kaolinite, barite, gypsum were the minerals identified in the intermediate alteration zone (Table. 7.6). This alteration zone is differentiated from proximal alteration zone by the abundance decrease of kaolinite and increase of smectite family minerals.

Distal Alteration Zone: Samples from this zone have revealed the presence of chlorite, epidotes, and clay minerals i.e. illite-montimorillonite, haloysite, smectites and kaolinite, other minerals are hematite/limonite. In this zone the trend shows kaolinite minerals have significantly decreased and smectite family appears to be the dominating phases (Table 7.6).

7.7.3.2 Block KHE

Block KHE is a soil covered area, a total of 27 soil samples were collected from this site.

Proximal Alteration Zone: Samples from this alteration zone have revealed a variety of minerals. The zone has illite-smectite, barite, sulfide minerals (pyrite, chalcopyrite, sphalerite, and galena), kaolinite, muscovite, other minerals are wolframite, Cu oxides, fluorocarbonate, and edgarbaileyite ($Hg_6Si_2O_7$) (Table 7.6; Appendix 20-28).

Intermediate Alteration Zone: The zone has montimorillonite, illite-smectites and muscovite, which were identified from VNIR-SWIR spectra (Table.7.6).

Distal alteration Zone: The zone is dominated by clay minerals i.e. kaolinite-smectite, smectites, and chlorite (Table.7.6).

Proximal alteration zone has shown to be different from other alteration zones by the presence of the varied sulfide minerals, also minerals like Cu-oxides and edgarbaileyite. The latter minerals are not found in the intermediate and distal alteration zones. There is no clear difference in clay minerals between the three alteration zones. The observation could have been caused by the farming activities in the test site; this might have resulted to the dislocation or mixing of the clay minerals.

Table 7.5 Minerals identified in alteration zones in the test sites

METHOD	Block KHA (soil samples)		
	Proximal	Intermediate	Distal
VNIR-SWIR Spectroscopy	kaolinite-dickite, pyrophyllite,diaspore	kaolinite,illite, illite-smectite, montimorillonite	smectite/montimorillonite,chlorite, epidote,
Light Microscopy	hematite, mixed clays,	clays	clays
SEM	Ilmenite, serpentinite, clays, kaolinite, galena, carbonates, barite, sphalerite, hematite, mixed clays	gypsum/anhydrite barite,	hematite/limonite epidote,clays chlorite,quartz
X-Ray Difraction (XRD)	Nakrite , Kaolinite, Illite	kaolinite,illite,nacrite montimorillonite	kaolinite,nacrite illite, montimorillonite

Table 7.6 continue

METHOD	Block KHE (soil samples)		
	Proximal	Intermediate	Distal
VNIR-SWIR Spectroscopy	illite,smectite, muscovite kaolinite,	montimorillonite, muscovite, illite-smectite,	kaolinite-smectite, Fe-chlorite, illite-chlorite
SEM	barite, pyrite,chalcopyrite galena, sphalerite, epidote mixed clays	mixed clays	mixed clays

Table 7.6 continue

METHOD	Block KH (rock samples)		
	Proximal	**Intermediate**	**Distal**
VNIR-SWIR Spectroscopy	carbonates,	amphiboles,	amphiboles,
	clays, sericites,	hematite, gypsum,chlorite,	chlorite/ epidote
	chlorites,	calcite,	hematite,
	amphiboles		carbonate
Light Microscopy	chlorite, epidote,	chlorite, epidote,	
	silicified quartz, pyrites,	sericite, clays,	
	chalcopyrite, sericites, clays,	magnetite,	chlorite, epidotes
	pyrrhotite, carbonates,	hematite,	silica,pyrite,
	magnetite,	carbonates,	carbonates,
	hematite	silica, pyrite, chalcopyrites	
SEM	plagioclases, pyrite, pyrrhotite,	epidote, chlorite,	chlorite, epidote,
	sphalerite, apatite ,chalcopyrite, chlorite, hematite/goethite		quartz,

7.7.3.3 Block KH

Block KH is the area with a hill of andesitic metavolcanic rocks, a total of 14 rock samples were collected from this site.

Proximal Alteration Zone: Fine grained carbonates, sulfide minerals (pyrite, chalcopyrite, pyrrhotite, and sphalerite) and silica definitely from silicification runs parallel to shear fabrics in the proximal alteration zone (Fig.7.19). Sericite, chlorite, epidote, amphiboles, plagioclases, hematite/goethite and clay minerals are other minerals that are also present in the Block KH proximal alteration zone (Table 7.6; Appendix 29-31).
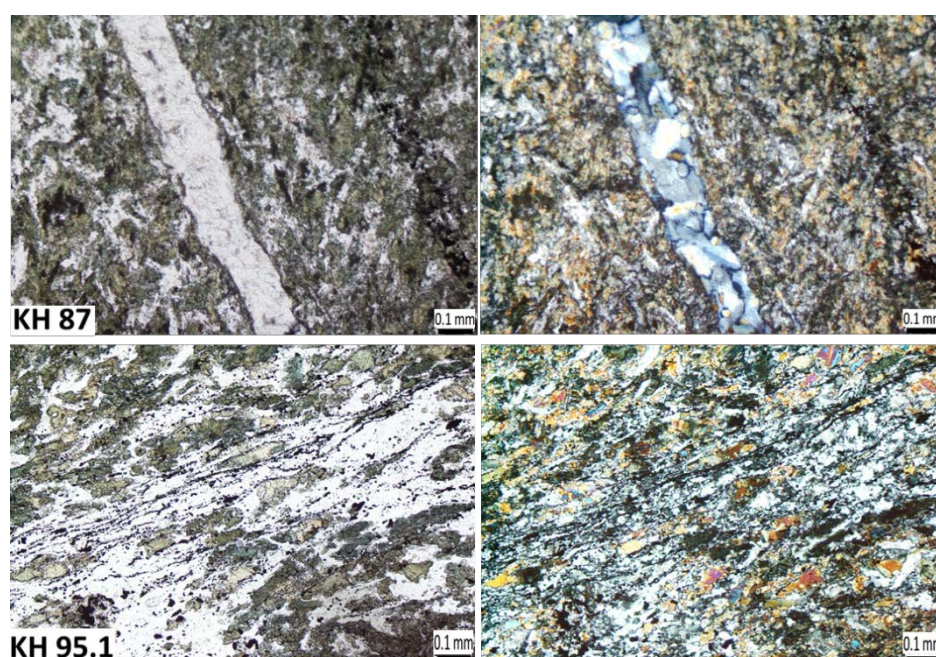
Figure 7.19 Thin section pictures under plane polarize light (left) and crossed polar (right); the fine linear opaque minerals in sample KH 95.1 are sulfides.

The proximal alteration zone in Block KH is located in a highly sheared area as was observed during the field campaign. The area is characterized by intensive fracturing and foliation; the direction of the shear zone is also confirmed by the orientation of minerals in the thin sections as well as by shear fabrics. The shear zone in the area strikes ca. 050° NE direction, the best example of the shear fracturing can be seen in the photos below (Fig. 7.20). The micro-fractures along shear zone are filled with quartz, which lack well defined crystal shapes but show silicification (KH.95.1, Fig.7.21).
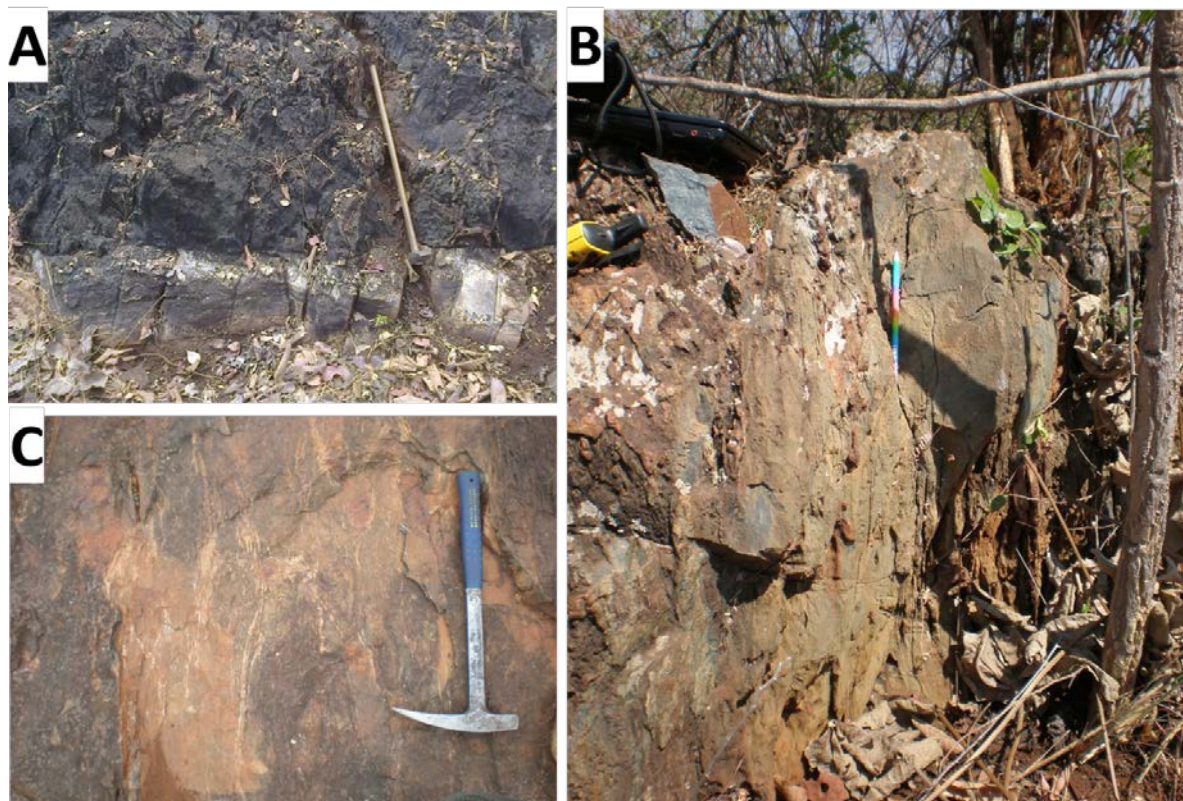
Figure 7.20 The outcrop pictures from rock exposures in Block KH. **A**: shearing has affected both metavolcanic rocks (dark color) and a pegmatite (light color), **B**: showing a typical, vertically dipping shear zone **C**: showing sheared veinlets (light strips) parallel to the direction of the handle of the laid geological hammer.

Intermediate Alteration Zone: The conspicuous minerals in this zone are chlorite, calcite, hematite, epidote, sericite, clays, and sulfides (pyrite, chalcopyrite). The intermediate zone is located in a relatively less sheared area as revealed by the less foliated and more randomly orientated minerals (e.g. KH 87) when compared to minerals in the proximal alteration zone (e.g. KH 95.1) (Fig.7.19).This is also an indication that the proximal alteration zone coincides with a tectonic zone of shearing. Mineralogically, the difference between proximal and intermediate alteration zones is revealed by a zonation in the sulfide minerals in the thin sections whereby pyrite and chalcopyrite are the sulfides found in the intermediate zone as opposed to samples from the proximal zone, which contain pyrite, chalcopyrite plus pyrrhotite and sphalerite.

Distal Alteration Zone: In this zone the rock samples collected contain chlorite, epidote and carbonates (calcite). Other minerals are quartz with silicification, hematite, amphiboles (hornblende) and pyrites.
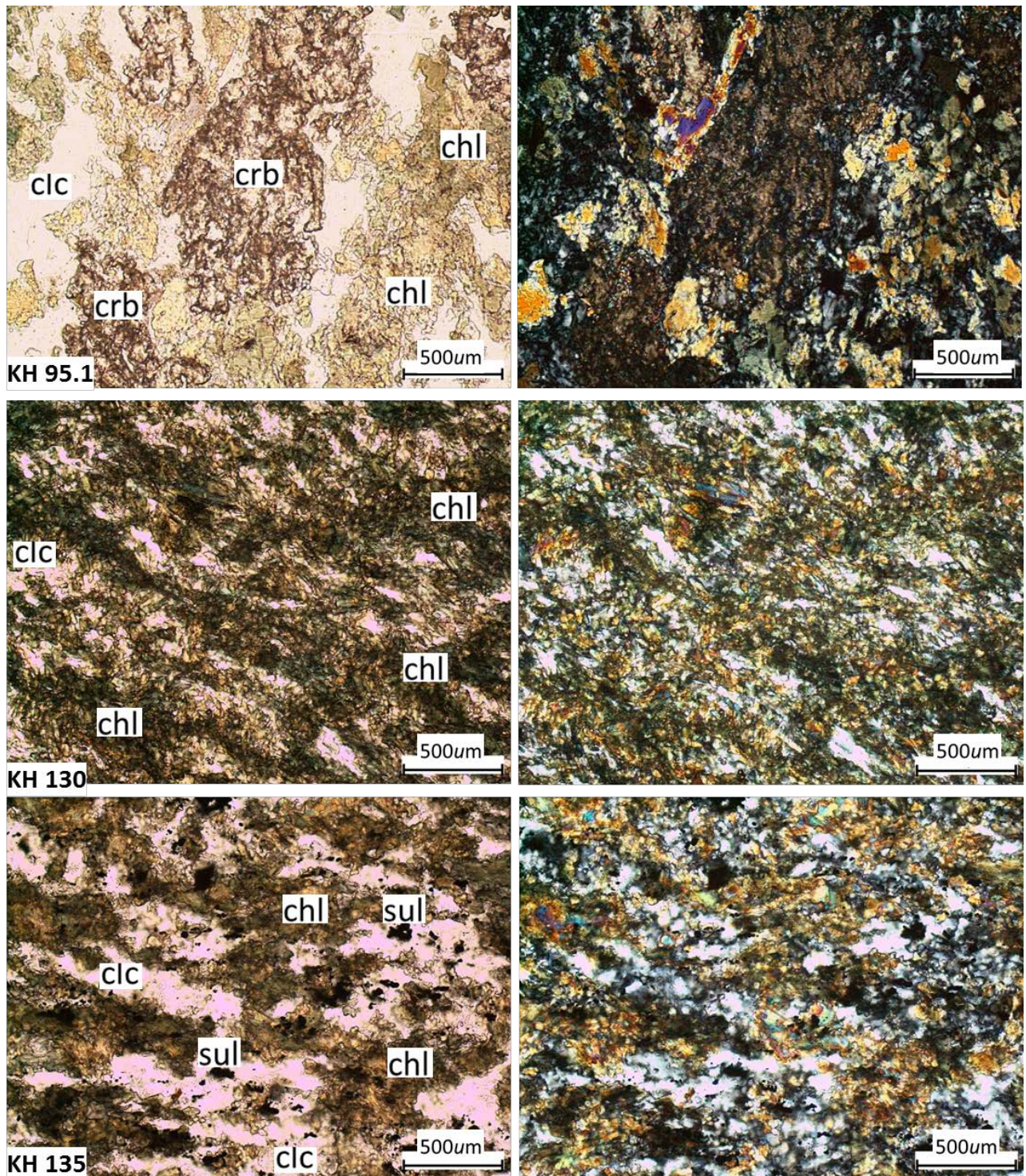
Figure 7.21 Thin section pictures showing alteration minerals in alteration zones from Block KH, pictures under plane polarized light (left) and crossed polar (right). **crb** = carbonate , **chl** = chlorite, **sul** = sulfides (opaque grains), **clc** = silicification.
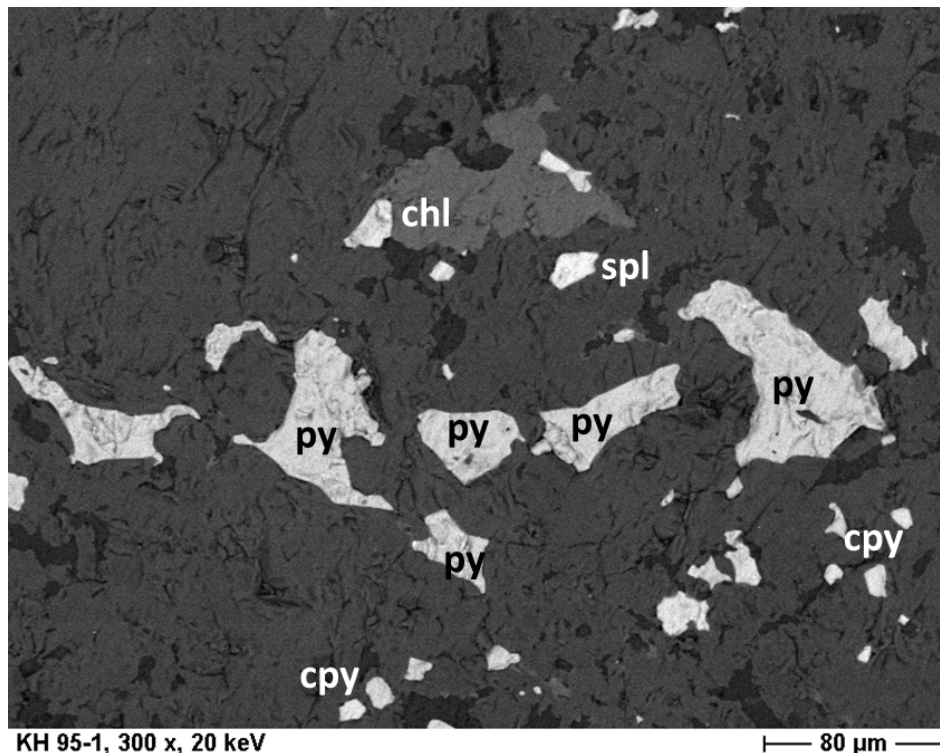
Figure 7.22 Scanning electron microscope (SEM) image sample KH 95.1, showing sulfide minerals in the proximal alteration zone, py = pyrite, cpy=chalcopyrite, spl= sphalerite, chl = chlorite

7.8   Conclusion

Alteration mapping by ASTER data has revealed the extent and effects of hydrothermal alterations in the SGB. The mapped alteration zones correlate with the reported hydrothermal alteration patterns of the major gold deposits of the region and also correspond to alteration models exhibited by Archaean gold deposits in general (e.g. Ikingura et al.,2010). Proximal, intermediate and distal alteration zones are the alterations extracted from ASTER data of which the proximal alteration zone is expected to be nearest to the mineralization zone, which typically is also a feature of crustal weakness, such as a shear zone.

The method used gave confidence to the identified alteration results since the alteration zones were extracted by using more than one diagnostic mineral from each hydrothermal alteration assemblage. The technique is suggested to reduce the problem of interference of similar minerals those originating from non-hydrothermal sources. The method will also help in the identification of potential exploration targets that are spatially associated with the resulting proximal alteration zone. The result from remote sensing alteration mapping in the SGB indicate the size, geometrical shape and orientation of proximal alteration zones and these in general agree with the Archaean gold deposit models. Most of the linear proximal alteration zones are associated with tectonic structures such as shear zones and their size ranges from few hundred meters to few kilometers in length and tens of meters in width. The outcome of the validation has revealed that the method has added potential values to satellite remote sensing data in mineral exploration since it has increased the relative accuracy in mapping hydrothermal alteration zones.

8   GEOCHEMISTRY

The interpretation of geochemical data is a very important tool in the investigation of most geological activities, and particularly, in mineral exploration these data are used to study the trend of element concentrations or better to identify anomalous concentrations of specific elements which are related to mineralization. Moreover, both major and trace elements can be used in various methods to study mineral alterations. For example, various alteration indices are known and the Ishikawa alteration index (AI) and chlorite-carbonate-pyrite index (CCPI) are amongst the indices used for tracking the geochemical and mineralogical changes associated with hydrothermal alteration (Ishikawa et al., 1976). Due to the significance of geochemical data sets in mineral exploration, it has been suggested to focus on geochemical characteristics of mineral deposits (Carranza, 2012). Geochemical anomalies are normally caused by the effects of hydrothermal fluids on primary rock-forming minerals of the host rocks. Interaction of hot hydrothermal fluids with host rocks result in element-/metal-enrichment or -depletion and in mineral alteration (Safron, 1936; Goldberg et al., 2003; Hanningston et al., 2003; Pirajno, 2009; Carranza, 2012). For example, enrichment of K and depletion of Na could indicate destruction of plagioclases (albite) during alteration processes whereby K replaces Na in the zones near to mineralization by forming sericite minerals. Replacement of plagioclase by sericite also accounts for the loss of Sr, which is an abundant element in igneous feldspars (e.g. Kreuzer, 2006). Pb and Zn could reflect the occurrence of galena and sphalerites respectively. High arsenic (As) concentration is related to pyrite minerals in the ore zones due to the bonding behavior of As into pyrite (Kreuzer, 2006). There is also a genetic link between hydrothermal alteration and mineralization, for example, Kishida and Kerrich (1987) reported a positive correlation between gold and muscovite-albite alteration, also the highest gold anomalies correspond to a transition zone between carbonate-muscovite and carbonate-albite alteration at Kerr-Addison mine in Canada. Therefore, the correlation between Au mineralization and mineral alteration, as well as geochemical anomalies, reveals the importance of the latter in mineral exploration. Eilu and Mikucki (1998) reported the chemical behavior of various elements across the Bulletin lode-gold deposit in Wiluna, Western Australia. Similar geochemical behavior has been reported in other deposits and is sometimes of different styles. For example, Large et al. (2001) have reported high concentrations of Thallium (Tl), Antimony (Sb) and Mercury (Hg) proximal to the ore zone and depletion of Na, Ca and Sr in the Rosebery deposit, Eastern Australia. Apart from individual elements, pioneers in mineral exploration have also reported the significance of some element ratios such as Ba/Sr and Rb/Sr in the relation to ore zones. For example, the Ba/Sr ratio reaches its peak in the ore zone due to the fact that Ba can substitute K in the white mica structure and Sr is depleted due to destruction of albite as was reported earlier. Similar effects are expected to apply to the Rb/Sr ratio although it has been cautioned that the ratio might show relatively weak anomalies (Large et al., 2001). The revealed significance of geochemical alteration elements has made them to be used effectively in mineral exploration. Hedenquist (2000) listed almost similar elements but specifically Au, Ag, As, Hg, Se, Sb and Tl which he suggested the elements to be used more commonly during epithermal deposits exploration. In addition, Zn, Pb, Sn, Mo, Te, Bi, Ba, Cu can also be included for the exploration of high sulfidation deposits. Ag, As, B, Bi, Hg, Mo, Sb, Te and W are reported to be significantly enriched in gold-bearing veins of orogenic gold deposits, Cu, Pb, and Zn in these deposits are generally slightly elevated above regional background with a note that Pb may be anomalous in some deposits (Yeats and Vanderhor, 1998; Groves et al., 2000; Goldfarb et al., 2005). In this study, immobile elements, low field strength cations or Large Ion Lithophile Elements (LILE), individual major and trace elements, gold as well as the pathfinder elements for gold were studied to investigate their distribution and behavior across the mapped alteration zones in the study area.

Element mobility refers to the chemical changes which take place in rock after its formation, usually through interaction with fluids (Rollinson, 1993). Processes which influence mobility of elements are weathering, diagenesis, metamorphism and through interaction with hydrothermal fluids. Element mobility can be detected from mineralogical phases and compositional changes that took place in a rock as a result of any process mentioned above and from mineral assemblages. The apparent trends of elements resulting from these processes, e.g. hydrothermal activities, may be used to indicate volume changes, which arise from the removal or addition of a single component of the rock (Rollinson, 1993). For example, immobile elements (Al, Zr, Ti and Y) are normally concentrated during alteration processes such as decarbonatisation and dehydration and result in the decrease of the total rock volume; also immobile elements are diluted during volume gain by processes such as silicification (Rollinson, 1993 in Chambelein, 2003). Therefore, upon hydrothermal activities, the immobile elements will apparently increase or decrease in concentration, without being added or removed, in areas affected by hydrothermal alteration depending on the alteration reactions responsible and these results can be used to deduce the overall volume change of the host rock.

Lithophile elements (K, Ba, Rb, Sr) are elements which are unsuitable in size and/or charge to cation sites of the minerals during fractional crystallization of magma, and they normally concentrate in the melt phase of magma. Their distribution or trends are governed by their partition coefficients between crystals, silicate melts and aqueous phases (Kerrich and Fryer, 1988; Rollinson, 1993). Ratios such as K/Ba, Rb/Ba, Rb/Sr and Ba/Sr increases and K/Rb observed to decrease during progressive fractional crystallization. Mineral deposits, which are regarded to have a magmatic input are also reported to show the same partitioning trend, the process is consistent with the derivation of hydrothermal fluids from late-stage magmas as is also stated in Chamberlain (2003). Large ion Lithophile elements (LILE) have been used to study the fluid source processes in mesothermal gold quartz vein deposits that are spatially associated with granitoid intrusion, for example shown by Kerrich and Fryer (1988) and Borg (1994), and also by Chamberlain (2003) for the Bulyanhulu gold mine. For example, K/Ba, Rb/Ba, Rb/Sr and Ba/Sr ratios increase from least altered to altered lithologies at the Bulyanhulu Mine. This trend was reported to indicate a magmatic input to the hydrothermal fluids involved in mineralization at Bulyanhulu gold mine (Chamberlain, 2003).

Individual major and trace elements can be used to check the destruction of primary rock forming minerals as well as the formation of secondary minerals as a product of hydrothermal alteration processes. During hydrothermal fluid infiltration the chemistry of hydrothermal fluids and change in P-T conditions normally destabilize the equilibrium of the primary minerals in host rocks. As a result they force minerals to alter into another mineral phase that will be stable under the newly created environment. These changes can be traced by using major and trace elements variations in geochemical data.

8.1   Sampling for Mineral Exploration
In the early days of modern mineral exploration, most geochemical exploration was based on outcropping rock samples and samples from bedrocks obtained by drilling (Mazzucchelli, 1989). This is because during that time it was believed that surface soils were not reliable as a geochemical sampling medium. However, the dispersion patterns in bedrocks are more restricted laterally than in soils, in addition, the dispersion in bedrock is complicated due to the development of zones of depletion and enrichment, which also has been reported by Mazzucchelli (1989). Since the 1990s it

has increasingly been reported that the anomalies related to gold mineralization are spatially better developed in near surface soils than in deeper bedrock samples. For example, Mazzucchelli (1996) reported gold mineralization detected by soil geochemistry in soils over a laterite profile in the Mystery zone, Eastern Australia. The mineralization was reflecting the underlying ferricrete horizon, although at low lever concentration. From his investigation, he came to conclude that soil geochemistry is a robust and cost effective tool for gold exploration. Several gold deposits have been discovered through soil geochemistry so far, for example, Junction and Challenge-Swordman as reported by Bonwick (1995) in Mazzucchelli (1996) are some of these deposits. From the facts described above, samples from the three sites in this study, which showed alteration zoning in ASTER data, two of the sites have being soil covered (Blobk KHA, Block KHE) and one rock covered (Block KH) (Fig. 8.1), and these three sites have been geochemically analyzed for further validation of the mapped alteration zones.
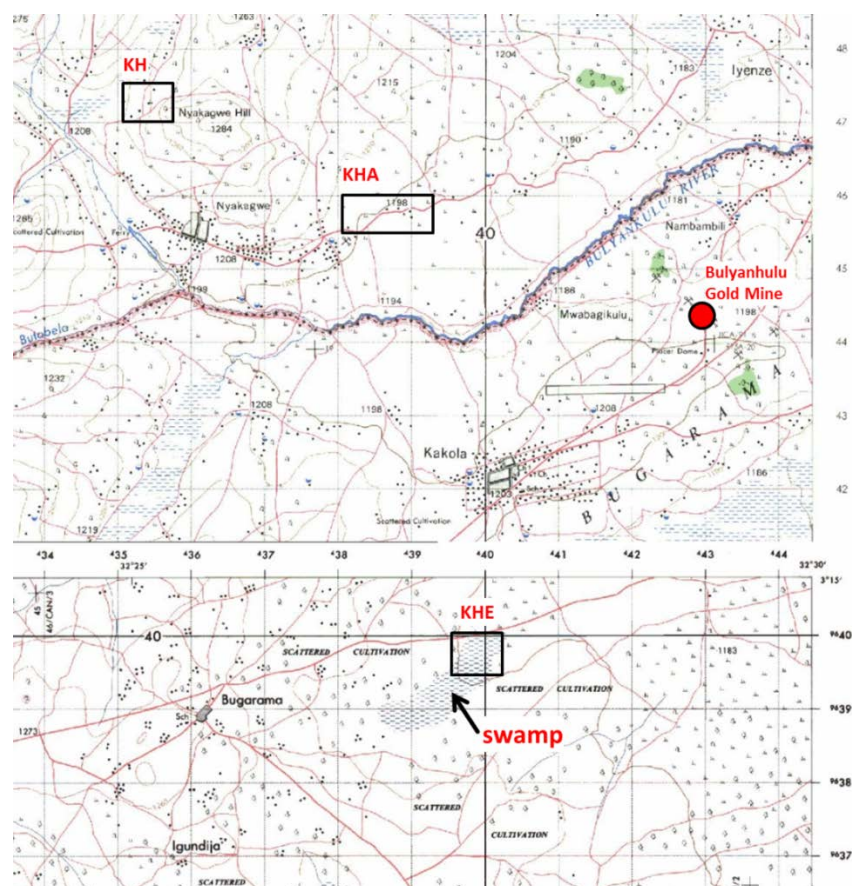
Figure 8.1 Show location of the three test sites (boxes) and Bulyanhulu gold mine a red dot, overlaid on to topographical maps of the Bulyanhulu mining district.

8.2   Geochemical Analyses

Both rock and soils samples were analyzed by the internationally certified ACME Analytical Laboratories in Vancouer, Canada. 30 g of pulverized sample was used for analysis, which is a standardized sample size to give a representative sample for analysis of elements which tend to be subjected to nugget effects, for example Au. Inductively Coupled Plasma Mass Spectrometry (ICP-MS) was the technique used and a total of 53 elements were analyzed after ultra-trace aqua regia digestion was applied to the samples.

8.3   Results and Discussion

8.3.1   Block KHA

Block KHA is one of the three selected test sites, selected after a thorough interpretation of the mapped alterations from ASTER data. The geochemical data from the samples collected were analyzed with respect to these alteration zones, i.e. proximal, intermediate and distal alteration zones and in comparison to the Archaean granite-greenstone gold model, which is the mineralization type expected in this region(Borg and Shckleton,1997). Geochemical results have revealed the presence of a Au anomaly in the Block KHA proximal alteration zone. In reference to the work of other pioneers, it is reported that the background Au content for autochthonous soils resting on most igneous rocks is ranging from 2 to 5 ppb (Kishida and Kerrich, 1987; Eilu and Mikucki, 1998). In this study the minimum Au content in the proximal alteration at Block KHA is 26.2 ppb and maximum is 63.5 ppb (Table 8.2). Therefore, with regard to the above background values, the identified high Au concentration in the proximal zone, meets the criteria for the area to be marked as a significant Au anomaly.

Another observed feature was on the spatial relationship between gold (Au) and pathfinder elements within alteration zones. An overlay of alteration zones and Au as well as its pathfinder elements indicates a perfect spatial correlation in Block KHA. Ag, Hg, Sb, Mo, Bi, B, Tl, are some of the elements, which show a good positive correlation with Au and also a systematic variation in respect to different alteration zones. Concentrations of these elements increase consistently from distal to proximal alteration zones (Fig. 8.2). High concentrations of immobile elements, specifically Al-Ti-Y, coincide with proximal alteration and follow the trend similar to pathfinder elements. Statistical analysis through Pearson correlation coefficients have revealed results similar to the above observation in which Au has shown a high degree of positive correlation with some elements such as Ag, Mo and Y, as well as Ag ,Mo, Ti, Zr and Bi. Other positive correlations are shown by elements such as Cu, Co, Zn, Pb and Ba, but also Mo, Sb and Ti, Y and Tl (Table 8.3, Table 8.4). Statistical analyses further revealed some of the likely alteration processes that have taken place in the area. For example, a high degree of positive correlation between Ca, Mg, Mn, and Fe may reflect carbonate alteration, whereas the correlation between Zn, Pb, Cd, and S may indicate base metal sulfidation (Table 8.4). Correlation between K, Ba and P could be the indicator of presence of apatite minerals and sericitic alteration. Na does not show correlation with any of the elements and by referring from geochemical data, most samples measured Na below the detection limit (Table 8.4). The geochemical behavior shown by Na may indicate that albite alteration was not an important process in the hydrothermal system at Block KHA and possibly albite were replaced by sericite minerals. There are correlations also between trace elements such as Cr, Co, and V and carbonate alteration indicator elements, the correlation observed might indicate association between alteration and trace elements, the observed trace elements may have been added during influx of hydrothermal fluids.
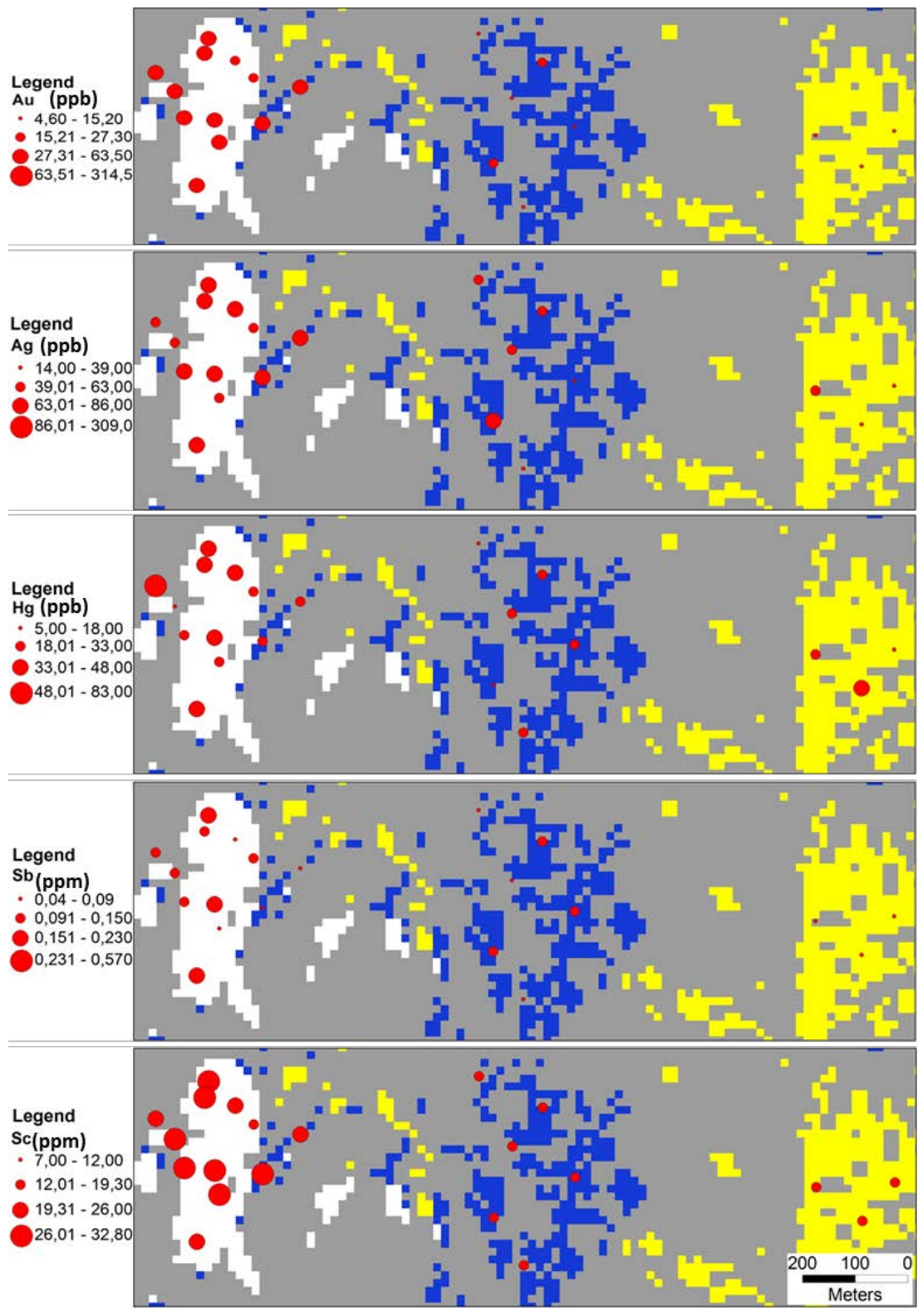
Figure 8.2 Alteration map of Block KHA overlain with concentrations for Au and some of the pathfinder elements, the size of the red dots corresponds to the concentration of the elements.

Table 8.1 Pearson correlation coefficient table showing the coefficient of correlations between different elements from Block KHA samples, □ indicate coefficients ≥ 0.7 both positive and negative

	Au	Ag	Hg	Sb	As	Ni	Co	Ba	Mo	Cu	Pb	Zn	Ti	B	Bi	Al	W	Tl	Se	Te	Zr	Y
Au	1,0																					
Ag	0,7	1,0																				
Hg			1,0																			
Sb				1,0																		
As					1,0																	
Ni						1,0																
Co				-0,6		0,5	1,0															
Ba	-0,6			-0,5		0,5	0,7	1,0														
Mo	0,7	0,5	0,5	0,8			-0,7	-0,6	1,0													
Cu						0,6	0,9	0,6	-0,6	1,0												
Pb								0,6	-0,5	0,7	1,0											
Zn	-0,5					0,6	0,7	0,6			0,6	1,0										
Ti	0,6	0,5	0,5	0,8			-0,5		0,9				1,0									
B														1,0								
Bi	0,5	0,5									0,6				1,0							
Al						0,9	0,5		0,6							1,0						
W																	1,0					
Tl							0,5		0,6					0,5				1,0				
Se																			1,0			
Te																				1,0		
Zr		0,5										-0,5									1,0	
Y	0,7	0,7						0,6						0,7		0,7		0,5				1,0

Table 8.2 Pearson correlation coefficient table showing the coefficient of correlations between different elements from Block KHA samples, □ indicate coefficients ≥ 0.7 both positive and negative

	Ag	Pb	Zn	Cu	Co	Mn	Fe	Mg	Ca	P	Cr	Ba	Ti	Al	Na	K	Sc	S	Sr	Cd	V
Ag	1,0																				
Pb		1,0																			
Zn			1,0																		
Cu		0,7	0,6	1,0																	
Co		0,6	0,7	0,9	1,0																
Mn	-0,5		0,8	0,7	0,9	1,0															
Fe		0,5		0,8	0,7	0,6	1,0														
Mg			0,8	0,7	0,9	0,9	0,6	1,0													
Ca			0,8	0,7	0,9	0,9	0,5	1,0	1,0												
P										1,0											
Cr				0,6	0,9	0,7	0,7	0,8	0,6	0,6	1,0										
Ba			0,6	0,6	0,7	0,8	0,5	0,8	0,8		0,5	1,0									
Ti	0,5				-0,5	-0,5		-0,6	-0,6	0,5			1,0								
Al				0,6	0,5		0,5				0,6			1,0							
Na															1,0						
K								0,7								1,0					
Sc	0,7				-0,5		-0,5	-0,5					0,8	0,5			1,0				
S				0,6		0,6	0,6	0,6	0,7	0,6	0,5	0,6				0,5		1,0			
Sr													0,7			0,7			1,0		
Cd			0,6							0,5										1,0	
V		0,6		0,8	0,8	0,7	0,9	0,7	0,7		0,7	0,6	-0,6				-0,5				1,0

With the scanning electron microscope (SEM), ore minerals such as, galena, pyrite, and sphalerite have been identified in samples from Block KHA, also together with Cu and Au in native forms. Some of the analyzed elements from samples in the proximal alteration zone show the associations

between themselves that indicate the possibility of other ore minerals in the area. For example, the observed correlation between Au, Ag and Sb possibly indicate the occurrence of gold as electrum (Au, Ag) or in fahlore minerals (of the tetrahedrite-tennantite solid solution series).

Graphical presentations of the elements Al-Ti-Y shows these elements to be immobile since they exhibit positive correlation to each other (Fig. 8.3). Further, the plots separate samples from proximal alteration zone from the intermediate and distal zones. The boundary between intermediate and distal alteration is not clear but rather gradational in the same diagrams. The relatively high concentration of the immobile elements in the proximal alteration zone could indirectly indicate element contractions of the host rock probably caused by hydrothermal alteration processes. The trend shown by the large ion lithofile elements i.e. their ratios K/Ba, Rb/Ba, Rb/Sr and K/Rb indicate the possibility of magmatic contributions in the hydrothermal fluids. Ratios K/Ba, Rb/Ba, Rb/Sr, all have a positive correlation to each other and also to Au, their values increase from the distal towards the proximal zone. As it is revealed in the K/Ba,Rb/Ba and Rb/Sr plots Fig. 8.3, most samples from the proximal alteration zone have high LILE ratios compared to the outer alteration zones. The K/Rb ratio tends to decrease towards the proximal alteration zone; this observation also supports the overall alteration concept. Therefore, the relatively high concentrations of large ion lithofile elements have revealed the magmatic input on Block KHA. Moreover, results shown by LILE indirectly endorse the presence of a proximal alteration zone, which normally is consistent with magmatic systems and located in or adjacent to the hydrothermal fluid upflow centers. Hence, the correlation between high Au concentrations and high LILE ratios as well as the proximal alteration zone, prove positively the identification of alteration zones by remote sensing technique, i.e. the ASTER-mapped alteration zones in Block KHA.
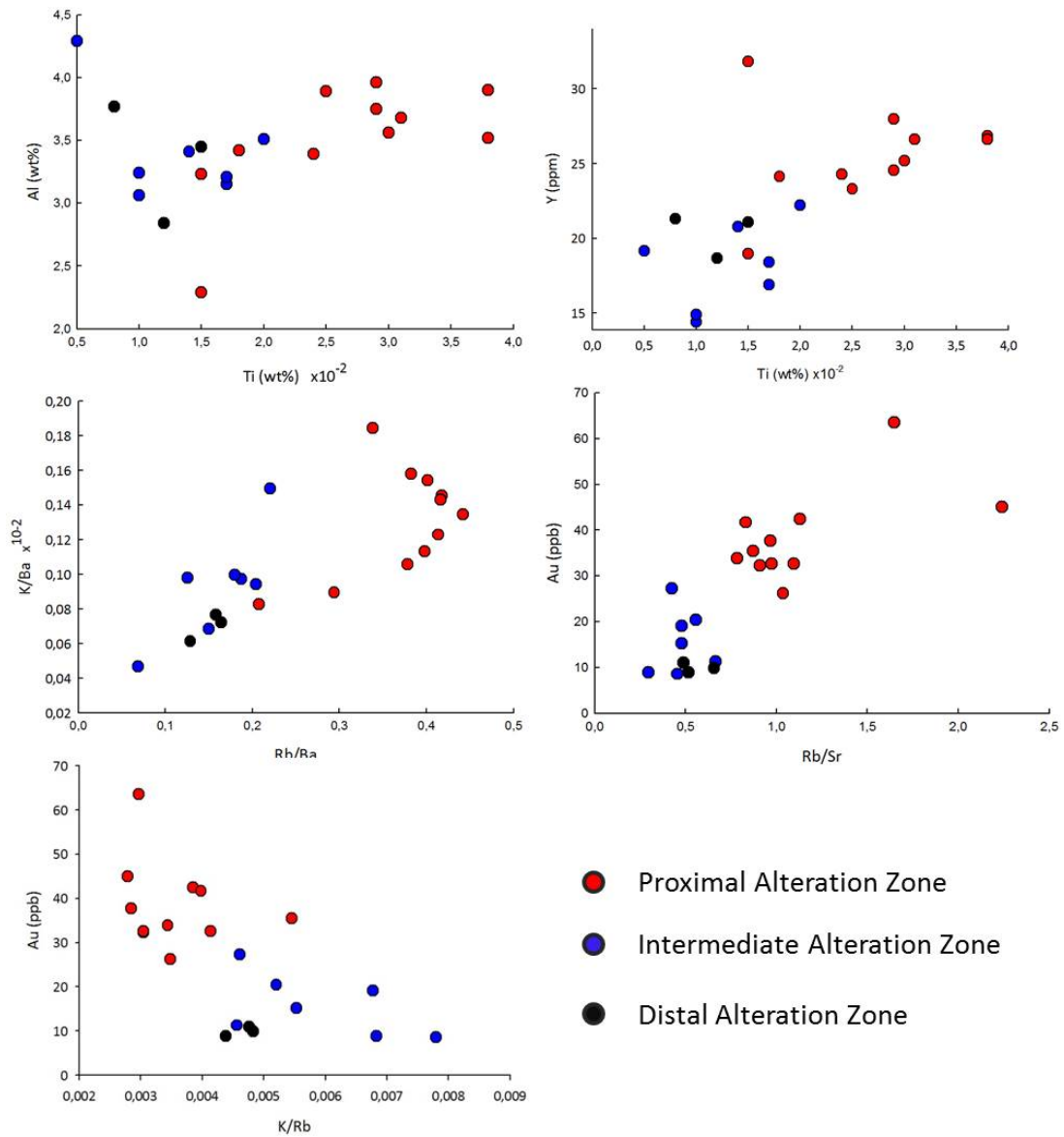
Figure 8.3 Correlation plots of immobile and LIL elements from geochemical data from Block KHA.

Table 8.3 Geochemical results for some of the analyzed soil samples from Block KHA area, DL=below detection limit.

SAMPLE	Mo	Cu	Pb	Zn	Ag	Ni	Co	Mn	Fe	As	U	Au	Th	Sr	Cd	Sb	Bi	V	Ca	P	La	Cr	Mg	Ba	Ti	B	Al
	ppm	ppm	ppm	ppm	ppb	ppm	ppm	ppm	%	ppm	ppm	ppb	ppm	ppm	ppm	ppm	ppm	ppm	%	%	ppm	ppm	%	ppm	%	ppm	%
KHA 23	1.59	46.3	10.2	14.3	73	41.4	12.5	371	4.42	2.3	0.9	37.7	8.6	40.1	0.07	0.23	0.19	122	0.06	0.03	36.6	62.5	0.07	97	0.04	1	3.52
KHA 24	1.04	33.6	8.1	9.9	60	25.4	10.8	244	3.31	1.6	0.6	26.2	5.9	22.2	0.04	0.13	0.11	98	0.04	0.02	26.9	42.4	0.05	55	0.02	1	2.29
KHA 25	1.33	51.0	10.0	16.1	80	45.6	15.2	382	4.64	3.2	0.8	32.3	7.9	43.4	0.04	0.2	0.22	129	0.07	0.03	36.7	62.3	0.08	89	0.04	1	3.9
KHA 26	1.33	45.5	9.1	30.9	67	43.4	15.1	500	4.18	2.4	0.8	33.9	7.3	40.9	0.07	0.18	0.14	117	0.11	0.03	37.2	62.7	0.09	77	0.03	2	3.68
KHA 27	0.93	48.4	10.2	16.1	67	33.4	16.3	541	5.07	2.4	0.8	19.1	5.8	40.2	0.02	0.12	0.23	164	0.4	0.02	26.6	60.5	0.18	87	0.02	1	3.15
KHA 28	0.62	47.6	10.0	18.2	30	35.4	17.6	676	4.84	2.3	0.9	11.3	5.9	36.2	0.04	0.1	0.11	152	0.26	0.02	34.1	57.8	0.19	161	0.01	1	3.41
KHA 29	0.6	53.8	9.4	19	49	35.2	16.9	497	4.93	2.5	0.5	20.4	5	31	0.01	0.1	0.09	153	0.34	0.02	24	73.8	0.23	93	0.01	2	3.24
KHA 30	0.31	46.3	10.6	26	43	36.2	19.1	894	3.86	2.6	0.9	11	6.3	60.2	0.02	0.07	0.08	105	0.58	0.02	42.6	59.3	0.32	228	0.02	1	3.45
KHA31,1	0.58	33.0	9.4	50.1	29	27.9	16.5	827	2.88	1.2	1	9.9	6.1	53.6	0.08	0.05	0.1	71	0.39	0.03	38.6	41.7	0.22	222	0.01	2	2.84
KHA 32	0.44	47.3	9.9	26.9	31	39.1	17.2	566	4.24	1.3	0.9	8.9	6.3	57.5	0.05	0.05	0.08	111	0.46	0.02	38	58.4	0.32	181	0.01	3	3.77
KHA 115	1.35	49.1	8.8	18.5	57	38.4	15.8	570	4.47	2.1	0.8	35.5	6	42.1	0.05	0.13	0.28	130	0.3	0.04	36.1	65.7	0.09	109	0.03	7	3.56
KHA 116	1.35	45.9	8.8	11.6	77	35.9	14.5	350	4.62	2.3	0.9	63.5	7.3	18.4	0.02	0.12	0.23	138	0.03	0.03	34.8	59	0.06	73	0.02	6	3.39
KHA 117	1.26	47.4	8.8	11.4	56	40	15.7	382	4.46	1.9	1	45	8.4	9.6	0.01	0.15	0.2	128	0.04	0.02	36.2	61.6	0.05	57	0.03	4	3.96
KHA 118	1.24	49.0	8.8	12.7	78	40.7	18.3	548	4.55	1.8	1	32.6	7.6	33.8	0.04	0.1	0.2	131	0.07	0.03	41.8	63.4	0.08	112	0.03	5	3.75
KHA 119	1.08	49.4	10.1	12.2	63	40.3	14.9	366	4.74	1.6	0.9	32.6	8.3	22.1	0.02	0.08	0.17	138	0.04	0.03	32.9	61.8	0.06	63	0.03	4	3.89
KHA 120	0.87	46.8	10.6	10.9	74	34.5	15.3	268	4.29	1.8	0.8	42.4	8.9	23	0.03	0.09	0.15	132	0.06	0.02	36.6	56	0.08	65	0.02	4	3.42
KHA 121	0.67	56.4	14.1	13.2	86	37.3	20.6	526	4.72	1.8	0.9	41.7	8.7	21.2	0.02	0.08	0.59	153	0.15	0.02	51.1	62.7	0.14	85	0.02	4	3.23
KHA 122	0.27	63.5	11.7	38.3	50	51.1	29.6	1115	5.21	2.4	0.5	8.9	5.2	54.4	0.06	0.04	0.11	172	1.46	0.03	35.4	78	0.78	235	0.01	6	4.29
KHA 123	0.48	54.0	10.5	18.5	45	34	19.5	612	4.88	2.9	0.8	8.6	5.2	30.9	0.03	0.07	0.11	161	0.33	0.02	26.3	70.4	0.21	112	0.01	3	3.06
KHA 124	0.87	46.2	9.8	16.4	39	33.3	16	575	4.63	2.1	0.9	15.2	6.4	52.7	0.03	0.06	0.12	147	0.33	0.03	32.2	58.9	0.14	141	0.02	3	3.21
KHA 125	0.95	48.8	9.6	12.1	86	40	14.8	351	4.47	1.7	0.7	27.3	7.1	71.7	0.02	0.07	0.13	135	0.08	0.02	32.9	57	0.08	149	0.02	3	3.51

Table 8.4 Geochemical results for some of the analyzed soil samples from Block KHA area, DL=below detection limit.

SAMPLE	Na %	K %	W ppm	Sc ppm	Tl ppm	S %	Hg ppb	Se ppm	Te ppm	Ga ppm	Cs ppm	Ge ppm	Hf ppm	Nb ppm	Rb ppm	Sn ppm	Ta ppm	Zr ppm	Y ppm	Ce ppm	In ppm	Re ppm	Be ppm	Li ppm	Pd ppb	Pt ppb
KHA 23	0.001	0.11	0.1	26.9	0.1	0.02	39	0.1	0.02	15.1	2.34	0.1	0.58	2.08	38.7	1.9	0.05	29.3	26.9	32.4	0.08	1	1.7	23.6	43	2
KHA 24	0.001	0.08	0.1	19.1	0.1	0.02	28	0.1	0.02	10.6	1.45	0.1	0.25	1.12	23	1.2	0.05	18.4	19.0	28.6	0.08	1	1.8	15.7	11	2
KHA 25	0.001	0.12	0.1	27.6	0.12	0.02	41	0.1	0.02	15.9	2.34	0.3	0.51	2.32	39.4	1.5	0.05	30.3	26.6	33	0.12	1	1.9	27.1	33	6
KHA 26	0.001	0.11	0.1	25.2	0.09	0.02	35	0.1	0.02	14.2	1.76	0.1	0.37	1.81	32	1.6	0.05	21.6	26.6	29.8	0.08	1	2.3	24.7	10	7
KHA 27	0.001	0.13	0.1	17.4	0.07	0.02	5	0.1	0.15	11.7	1.01	0.1	0.36	1.27	19.2	1.2	0.05	22.7	16.9	39.6	0.07	1	2.3	20	12	2
KHA 28	0.001	0.11	0.1	18.1	0.1	0.02	26	0.1	0.03	12.5	1.06	0.1	0.42	1.37	24.1	1.2	0.05	21.7	20.8	44.5	0.08	1	0.7	20.6	22	2
KHA 29	0.001	0.09	0.1	17.5	0.09	0.02	23	0.3	0.04	11.9	0.92	0.1	0.34	1.21	17.3	0.9	0.05	21	14.4	39.5	0.05	1	1.7	17	16	2
KHA 30	0.001	0.14	0.1	16.9	0.13	0.02	30	0.1	0.03	10.9	1.35	0.1	0.53	1.25	29.4	1	0.05	26.7	21.1	56.8	0.1	1	1	14.3	34	2
KHA31,1	0.001	0.17	0.1	14.2	0.15	0.03	42	0.1	0.04	9.6	1.17	0.1	0.23	1.86	35.2	1	0.05	14.4	18.7	49.8	0.05	1	1.1	13.4	10	2
KHA 32	0.001	0.13	0.1	18.6	0.15	0.02	15	0.6	0.06	12.1	1.36	0.1	0.51	1.16	29.7	1.3	0.05	23.6	21.3	51.2	0.07	1	1	15.3	10	2
KHA 115	DL	0.2	DL	25.8	0.1	0.03	83	0.1	0.04	13.8	1.5	DL	0.29	2.75	36.7	1.7	DL	17.7	25.2	31.2	0.11	3	1.6	21.3	38	DL
KHA 116	DL	0.09	DL	27.2	0.13	0.02	40	DL	0.04	13.7	1.57	DL	0.39	1.59	30.3	1.8	DL	22.9	24.3	33.2	0.09	3	1.3	21.4	11	5
KHA 117	DL	0.06	DL	29.5	0.12	DL	17	DL	0.03	15.5	1.88	DL	0.55	1.12	21.5	2	DL	27.3	24.5	34.3	0.09	DL	2	22.8	41	5
KHA 118	DL	0.1	DL	28	0.13	DL	23	DL	0.03	14.8	1.6	DL	0.35	1.48	32.9	2	DL	19.9	28.0	33.3	0.07	4	1.7	27.3	29	3
KHA 119	DL	0.1	DL	27.8	0.11	DL	33	DL	DL	15.4	1.42	DL	0.55	1.36	24.2	1.9	DL	29.6	23.3	32.6	0.08	DL	1.4	22.6	29	3
KHA 120	DL	0.1	DL	27.2	0.15	0.02	30	DL	0.03	14.1	1.48	DL	0.58	1.3	26	1.9	DL	30.9	24.1	37.7	0.1	DL	1.3	20.2	DL	DL
KHA 121	DL	0.07	DL	26	0.16	DL	31	DL	0.03	13.5	1.43	DL	0.43	1.14	17.6	1.7	DL	26.9	31.8	53	0.08	DL	1.9	16.9	DL	4
KHA 122	DL	0.11	DL	18.8	0.15	0.03	14	DL	0.06	12.1	0.93	DL	0.33	0.86	16.1	1.4	DL	18.1	19.2	58.5	0.07	DL	2	16.4	DL	5
KHA 123	DL	0.11	DL	16.7	0.11	DL	20	DL	0.02	11.9	0.73	0.1	0.35	1.16	14.1	1.3	DL	20.8	14.9	42.6	0.06	DL	1.6	15.6	DL	DL
KHA 124	DL	0.14	DL	19.3	0.11	DL	26	DL	DL	13.3	0.93	DL	0.36	1.67	25.3	1.8	DL	21.6	18.4	42.9	0.08	1	1.6	17	DL	DL
KHA 125	DL	0.14	DL	24.8	0.13	DL	48	DL	DL	14.4	1.35	DL	0.47	1.49	30.4	1.6	DL	25.5	22.2	32.3	0.1	DL	1.5	20.5	DL	DL

8.3.2   Block KHE

Block KHE samples also show different geochemical features in their relationship between alteration zones and ore elements. With reference to the generally reported Au background values for igneous rocks, i.e. between 2 to 5 ppb (Kishida and Kerrich, 1987; Eilu and Mikucki, 1998), the geochemical data from this area have also revealed a significant Au anomaly. Block KHE Au concentrations range from 3.8 ppb to 119.7 ppb and most samples measure above 8 ppb of Au (Table 8.7).

The spatial distribution of Au values in respect to the ASTER-mapped alteration zones does not show any significant spatial relationship as in Block KHA (Fig. 8.4). However, high concentrations from ore elements (e.g. Au, Ag, and Hg) are mapped perpendicular to the zonation from proximal towards distal alteration zones. The observed trend would probably mean an asymmetrical geochemical halo. However, the detected NW-SE trend corresponds to the locally known strike direction of the lithotypes. Other elements, for example Sb and Se show enrichment in the central area with correlating trends to Au, Ag and Hg. Generally, there is a significant relationship between Au and these pathfinder elements. For example, Au, Ag, and Hg spatially correlate to each other and reveal similarity in the trend of enrichment as well as the geometrical shapes of the mapped concentrations (Fig. 8.4). The element combination of Au, Ag, Hg, Se and particularly Sb may even indicate a primary ore mineral assemblage of tetrahedrite-tennantite at depth since it appears unlikely that this element association should have moved together if the soil anomaly would have been on transported soil or sediment.

Topographical maps of the mining district indicate that the Block KHE area is located in the area that contain as a swamp (Fig. 8.1). However, during fieldwork the swamp shown on the topographic map was not found. In this area there is farming activity during the rainy season. Could the high Hg content in some samples (e.g. KHE 3) be anthropogenic? The presence of the indicated swamp could possibly be the influence of high Hg content to sample KHE 3 by taking into consideration that there are artisanal mining activities some few kilometers away, for example, Nyakagwe artisanal mining are at around 7 km NW and Bulyanhulu was ca. 6 km NE before the mine was opened (Fig. 8.1). However, further investigation is required on the source of Hg as well as other elements including Au. One possibility is that organic materials could have acted together with water as traps and transporting agents for Au and other associated elements, from their sources to the Block KHE area.

Statistical analysis by Pearson correlation coefficient also has revealed a correlation between different elements, however, the more important ones were those related to Au and hydrothermal mineral alterations. A positive correlation is revealed between Au, Ag, Bi, and Te, also Ag with Bi, Mo, Hg, Cu, As and Sb (Table 8.5), which are all elements might occur jointly in fahlore mineral assemblages. The high degree of correlation shown between Ca, Mg, Mn and Fe indicate the possibility of carbonate alteration as one of the hydrothermal alterations in this area, which is otherwise underlain by mafic metavolcanic rocks and locally granitoids. Also, the observed association between Au and K could indicate sericite alteration, which is amongst the alteration types with direct relationship with Au mineralization (Table 8.6).
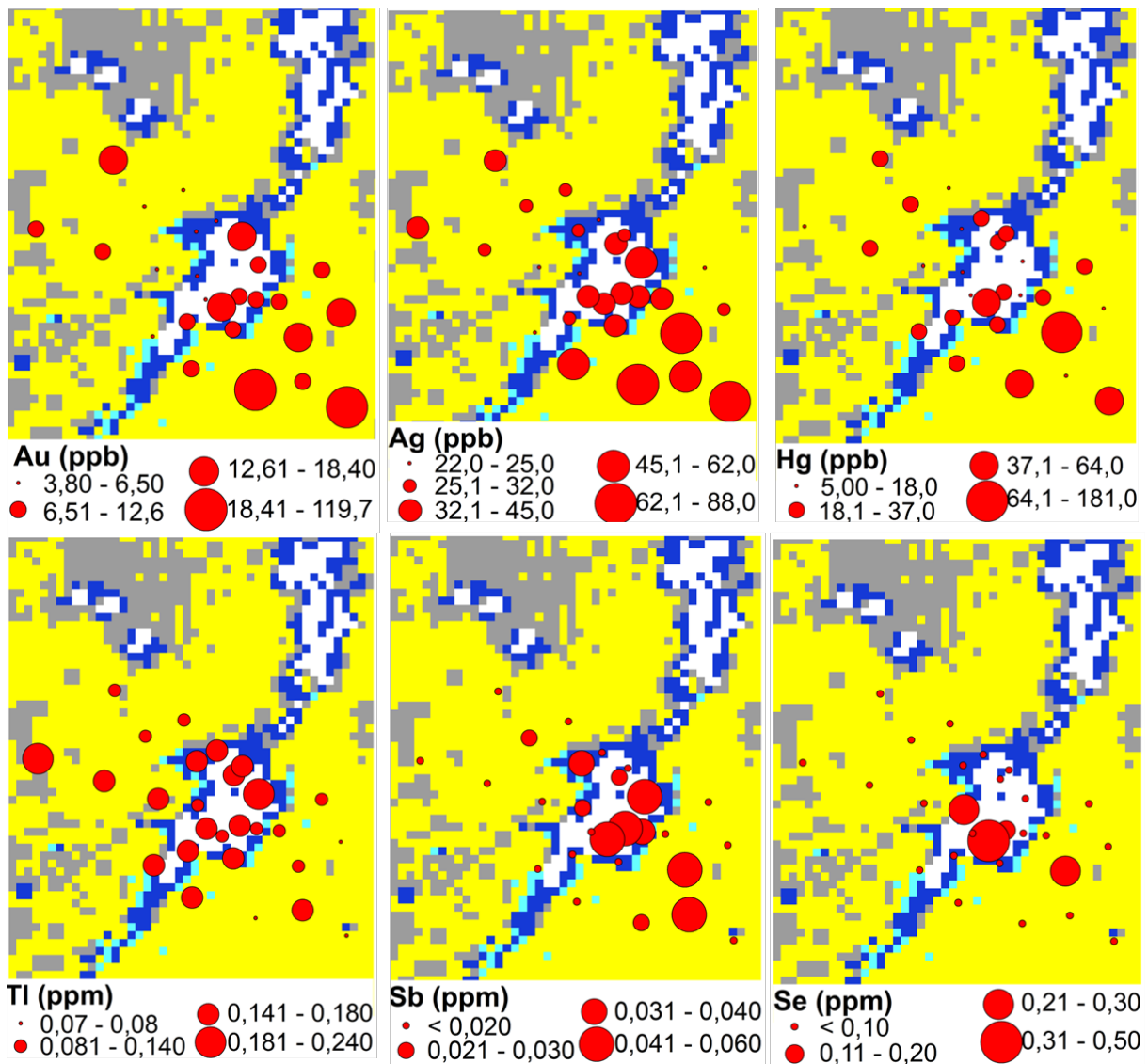
Figure 8.4 An alteration map showing Block KHE test site overlain with Au and some pathfinder elements. The size of the red dots corresponds to the concentration of the respective element. **White**: Proximal Alteration zone, **Blue**: Intermediate Alteration zone, **Cyan**: Boundary between intermediate and distal alteration zones **Yellow**: Distal alteration zone.

Ore minerals such as pyrite, sphalerite, and chalcopyrite have been identified by SEM, also together with Ag and Hg minerals. In Table 8.7 and 8.8, some elements are showing associations indicative of specific ore minerals, this increases the chances to find other ore minerals in the area. For example, the presence of Bi and Te in Block KHE which correlate to each other and to Pb, Fe, S, and Au, might indicate bismuthotelluride minerals. Bismuthotellurides are also reported from Bulyanhulu Gold mine, ca. 1.5 km NE of Block KHE (Chamberlain, 2003). The presence of a positive relationship between Cu, Fe, Sb and S plus the associated elements like Ag, Zn, Pb, Bi, Hg, also does not exclude the possibility of tetrahedrite ($(Cu,Fe)_{12}Sb_4S_{13}$)and/or tennantite ($Cu_{12}As_4S_{13}$) minerals to be found in the area.

Table 8.5 Pearson correlation coefficient table showing the coefficient of correlations between different elements from Block KHE samples, □ indicate coefficients ≥ 0.7 both positive and negative

	Au	Ag	As	Sb	Mo	Cu	Pb	Zn	Ni	Bi	Ba	B	Al	Na	K	Tl	Hg	Se	Te	Zr	Y	Ce	Ti
Au	1,0																						
Ag	0,6	1,0																					
As		0,6	1,0																				
Sb			0,5	1,0																			
Mo					1,0																		
Cu		0,5				1,0																	
Pb	-0,6						1,0																
Zn						0,5		1,0															
Ni					-0,6	0,6	0,8	0,6	1,0														
Bi	0,9	0,6					-0,6		-0,5	1,0													
Ba					-0,7	0,6	0,6	0,5	0,9		1,0												
B												1,0											
Al	-0,6					0,5	0,7	0,5	0,8	-0,6	0,6		1,0										
Na													0,5	1,0									
K	0,6	0,5					-0,5								1,0								
Tl	-0,5					0,5	0,8	0,5	0,8	-0,5	0,6		0,9			1,0							
Hg		0,7			0,5					0,6							1,0						
Se			0,5															1,0					
Te	0,6	0,5								0,5									1,0				
Zr	-0,5		0,5				0,5	0,5		-0,6			0,7	0,6		0,6				1,0			
Y	-0,5					0,5	0,9		0,7	-0,5	0,6		0,6		-0,5	0,6					1,0		
Ce	-0,5					0,6	0,9		0,8	-0,5	0,6		0,7			0,7					0,8	1,0	
Ti			0,5			0,5														0,7			1,0

Table 8.6 Pearson correlation coefficient table showing the coefficient of correlations between different elements from Block KHE samples, □ indicate coefficients ≥ 0.7 both positive and negative

	Ag	Pb	Zn	Co	Mn	Fe	Sr	Cd	V	Ca	P	Cr	Mg	Ba	Ti	Al	Na	K	Sc	Cs	Ce
Ag	1,0																				
Pb		1,0																			
Zn			1,0																		
Co		0,7		1,0																	
Mn				0,8	1,0																
Fe		0,7				1,0															
Sr		0,5	0,6	0,7	0,6		1,0														
Cd					0,6			1,0													
V		0,7		0,5		0,8	0,5		1,0												
Ca				0,7	0,9		0,7	0,6		1,0											
P		-0,5				-0,5			-0,6		1,0										
Cr		0,7	0,5			1,0			0,8		-0,5	1,0									
Mg		0,6	0,6	0,7	0,6	0,5	0,9		0,6	0,7			1,0								
Ba		0,6	0,5	0,8	0,7		0,9			0,6		0,5	0,9	1,0							
Ti			0,5												1,0						
Al		0,7	0,5	0,5		0,9	0,6		0,8			-0,5	0,7	0,6		1,0					
Na						0,5		-0,5		-0,5	0,5					0,5	1,0				
K	0,5	-0,5							0,9									1,0			
Sc		0,8				0,9			0,8			-0,6	0,9	0,5		0,9	0,5		1,0		
Cs						0,8			0,7			0,7		0,5		0,7	0,5		0,7	1,0	
Ce		0,9		0,8	0,5	0,6	0,6		0,7	0,5	-0,5	0,6	0,7	0,6		0,7			0,6		1,0

Immobile elements in Block KHE did not show a good correlation except for Al and Zr which have a positive linear-like trend (Fig. 8.5). Moreover, these elements do not group Block KHE samples by zoned alteration zones. Large ion lithofile elements ratios, for example K/Ba, Rb/Ba and Rb/Sr from this site, have shown a positive correlation (Fig. 8.5). However, similar to the immobile elements, there is no clustering in respect to alteration zones except for the observed feature that samples from proximal alteration plot in regions of low LILE ratios. An interpretation based on LILE ratios suggests the possibility of little or no magmatic contribution. The irregular distribution of Au and other ore elements, which have shown to be irrespective of alteration zones is also supported by Mazzucchelli (1996) and Pwa et al (1998), who reported the behavior of some of the elements that their geochemical haloes are relatively extensive and more indiscriminate compared to the ore zones. The importance of geochemical haloes in exploration has been reported by Carranza (2012) where he insisted on the regional-scale effective use of geochemistry in exploration of mineral deposits in the same sense that the geochemical haloes are wider compared to the mineralized zones. However, factors controlling the infiltration of hydrothermal fluids such as the distance from fluid up-flow zones, fluid-to-rock ratio and porosity also could be some of the contributing causes of irregular geochemical dispersion.

Figure 8.5 Plots showing the relationship of Block KHE immobile and LIL elements with respect to the alteration zones, ● = proximal alteration zone, ●= intermediate alteration zone, ●= distal alteration zone.
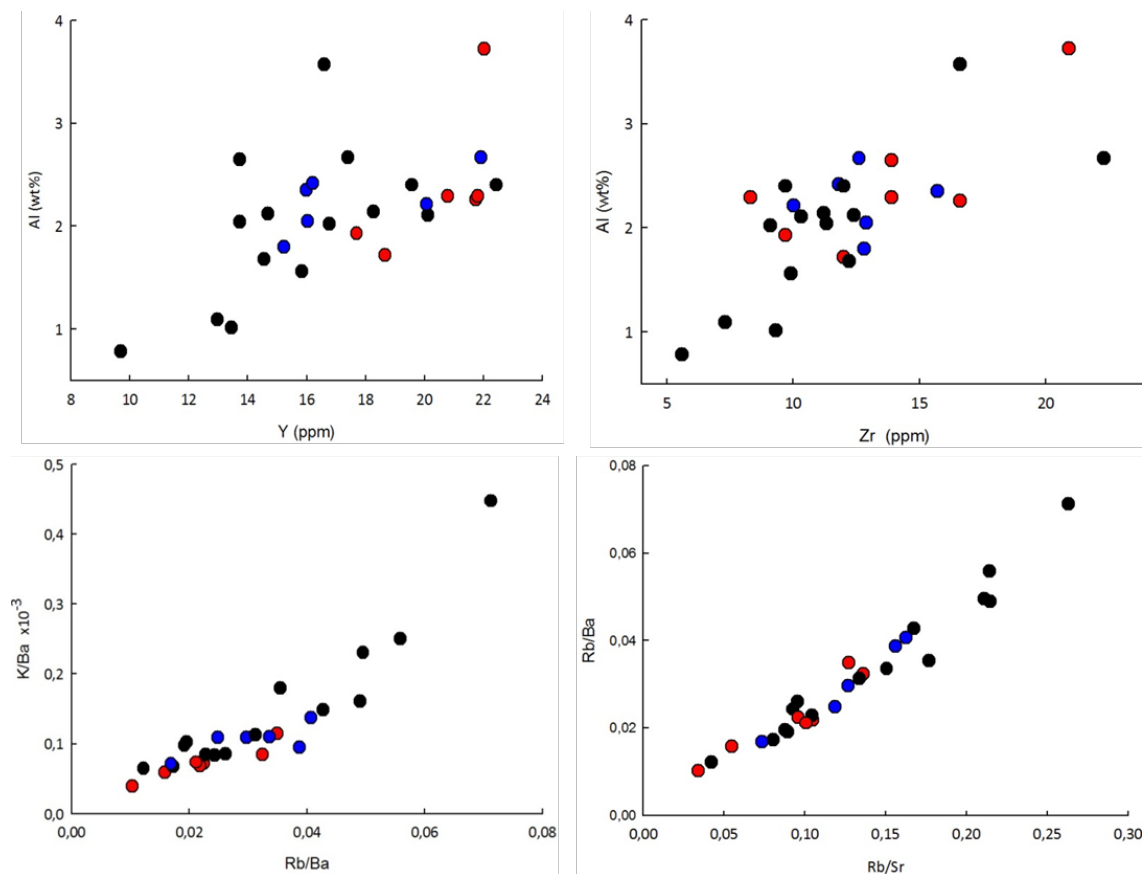
Table 8.7 Geochemical results for some of the analyzed soil samples from Block KHE area, DL=below detection limit.

	Mo	Cu	Pb	Zn	Ag	Ni	Co	Mn	Fe	As	U	Au	Th	Sr	Cd	Sb	Bi	V	Ca	P	La	Cr	Mg	Ba	Ti	B	Al
SAMPLE	ppm	ppm	ppm	ppm	ppb	ppm	ppm	ppm	%	ppm	ppm	ppb	ppm	ppm	ppm	ppm	ppm	ppm	%	%	ppm	ppm	%	ppm	%	ppm	%
KHE 2	0.07	15.8	15.3	29.8	55	13	9.1	347	1.73	2.6	1.6	9	6.9	125	0.01	0.06	0.02	32	0.68	0.01	57.1	25.2	0.33	477	0.005	1	2.67
KHE 3	0.32	18.5	13.8	17.7	88	8.5	5.5	93	1.6	2.2	1.1	16	6.8	57	0.01	0.05	0.23	32	0.32	0.01	56.5	21.2	0.18	249	0.002	1	2.02
KHE 6	0.14	20.6	21.9	34	62	15.3	12.5	359	2.32	1.4	2.5	11	9	120	0.01	0.05	0.02	37	0.8	0.01	66.9	31	0.36	436	0.005	1	3.72
KHE 7	0.15	13.7	16.8	21	35	10.7	9.7	479	1.35	0.7	1.9	12	8.3	97	0.02	0.05	0.15	27	0.66	0.01	53.6	18.4	0.24	414	0.001	2	1.93
KHE 8	0.23	13.8	17.6	18.8	36	11.6	11	553	1.25	0.1	1.9	14	8.2	91	0.02	0.05	0.15	27	0.64	0.02	58.3	17.7	0.23	436	0.002	3	1.72
KHE 9	0.13	18.6	17.1	26.8	37	12.8	9.1	474	1.53	1.1	2.2	11	8.2	146	0.01	0.04	0.06	28	0.83	0.02	67.8	22.1	0.35	506	0.002	1	2.29
KHE 11	0.17	11.8	14.4	15.2	25	7.7	7.3	226	1.41	0.7	1.8	5	7.9	55	0.02	0.03	0.05	29	0.28	0.01	50.2	17.8	0.15	219	0.003	1	1.8
KHE 12	0.24	16.1	20.9	22.3	40	12.1	12.3	584	1.73	1	2.2	6	11.4	84	0.02	0.03	0.05	34	0.52	0.01	73.9	23	0.21	355	0.003	1	2.26
KHE 13	0.29	14.1	17.7	20	31	10	9.2	308	1.75	1.3	2.4	6	10	78	0.01	0.04	0.06	34	0.36	0.01	56.5	22.2	0.2	315	0.003	1	2.35
KHE 14	0.29	11.6	13.6	18.4	27	9.6	6.4	219	1.49	1.2	1.8	4	7.4	63	0.01	0.03	0.06	29	0.34	0.02	46.6	19.7	0.17	240	0.002	1	2.04
KHE 98	0.24	15.7	10.1	31.2	80	6.9	7.4	493	0.72	1.2	0.4	117	2.5	73	0.02	0.02	0.26	15	0.44	0.06	33.5	11.2	0.11	268	0.003	4	0.78
KHE 99	0.26	17.2	10.9	13.3	71	7	7.2	320	1.01	2.5	0.7	120	4.4	41	0.01	0.03	0.47	23	0.31	0.02	43.1	13.4	0.12	174	0.002	2	1.09
KHE 100	0.16	12.8	14.3	19.9	25	12.6	10	605	1.42	0.9	1.2	12	6.3	109	0.02	0.02	0.1	28	0.92	0.02	50.8	20.1	0.29	487	0.002	3	2.12
KHE 101	0.19	13.9	17.1	18.3	32	9.2	7.7	275	1.51	0.9	2	17	9.5	61	DL	0.02	0.08	31	0.39	0.01	56.9	21	0.17	274	0.002	3	2.05
KHE 102	0.26	14.3	17.2	18.3	25	11.1	11.1	368	1.68	0.6	2.4	6	9.3	86	DL	0.02	0.08	32	0.44	0.01	60.9	22.5	0.22	367	0.002	2	2.42
KHE 103	0.18	11.3	14.9	14.5	28	7.3	7.9	242	1.3	0.7	1.8	6	8.9	62	DL	0.02	0.08	28	0.32	0.01	53	17.4	0.14	265	0.002	2	1.68
KHE 105	0.07	18.3	18.2	25.5	45	17.3	13.3	510	2.04	0.6	1	9	9	159	DL	0.02	0.09	37	1.14	0.01	65.3	29.8	0.36	582	0.003	2	3.57
KHE 104	0.17	15.4	15.2	16.9	38	9.6	9.2	540	1.1	1	1.4	17	6.6	96	0.02	0.02	0.11	23	0.64	0.01	54	15.3	0.2	447	0.002	2	1.56
KHE 106	0.16	15.7	18.6	18.2	27	11.5	10.8	463	1.47	0.8	1.7	10	10.3	78	DL	0.02	0.09	30	0.56	0.01	68.9	20.1	0.21	355	0.002	2	2.11
KHE 107	0.22	14.4	16.9	19.3	22	10.2	7.2	202	1.79	0.6	2.6	6	11	69	DL	0.02	0.07	32	0.38	0.01	48.3	24.5	0.18	269	0.002	2	2.65
KHE 108	0.09	18.3	18.7	20.9	39	13	10.9	506	1.42	0.9	1.7	6	9.7	153	DL	0.02	0.08	28	0.78	0.01	75.1	19.8	0.32	505	0.001	2	2.29
KHE 109	0.17	17.2	19.9	22.2	28	13.4	12.7	634	1.43	1	2.4	9	9.6	97	DL	0.02	0.07	28	0.73	0.01	68	21.2	0.26	421	0.001	0	2.21
KHE 110	0.2	17.0	21.5	22.4	23	13.4	14.2	707	1.69	1.1	2	7	11.7	86	DL	0.02	0.08	31	0.65	0.01	74.8	23.9	0.24	407	0.002	1	2.4
KHE 111	0.1	23.4	19.0	23	52	16.7	18.4	1470	1.32	0.7	1	10	7.2	178	0.03	0.02	0.06	39	4.79	0.02	69.8	18.7	0.45	615	0.002	1	2.4
KHE 112	0.15	15.1	19.2	25.9	36	16.2	12.7	688	1.65	0.9	1.3	13	8.7	96	0.02	0.02	0.08	31	1.12	0.01	74.5	24.5	0.33	459	0.001	1	2.67
KHE 113	0.24	13.7	17.4	22	35	11.9	13	556	1.45	1	1.2	12	7.5	87	0.01	0.02	0.08	29	0.77	0.02	61.3	21.7	0.25	407	0.002	2	2.14
KHE 114	0.17	10.4	12.4	11.8	29	7.4	8.6	530	0.86	0.7	0.9	18	5.4	45	DL	0.02	0.11	22	0.32	0.01	46.1	12.3	0.12	223	0.002	0	1.01

Table 8.8 Geochemical results for some of the analyzed soil samples from Block KHE area, DL=below detection limit.

SAMPLE	Na %	K %	W ppm	Sc ppm	Tl ppm	S %	Hg ppb	Se ppm	Te ppm	Ga ppm	Cs ppm	Ge ppm	Hf ppm	Nb ppm	Rb ppm	Sn ppm	Ta ppm	Zr ppm	Y ppm	Ce ppm	In ppm	Re ppm	Be ppm	Li ppm	Pd ppb	Pt ppb
KHE 2	0.04	0.04	0.1	4.1	0.15	0.02	9	0.1	0.02	8.1	0.74	0.1	0.33	0.4	11.6	0.7	0.05	22	17.4	99	0.05	1	2.4	12	10	2
KHE 3	0.02	0.04	0.1	3.6	0.12	0.02	181	0.3	0.04	6.5	0.71	0.2	0.17	0.3	12.2	0.7	0.05	9	16.8	109	0.02	1	1.6	9.3	10	2
KHE 6	0.02	0.05	0.1	5.4	0.23	0.02	5	0.1	0.02	11.5	1.14	0.1	0.35	0.3	15.2	1	0.05	21	22.0	136	0.07	1	4	16	57	2
KHE 7	0.01	0.03	0.1	3.9	0.15	0.02	24	0.2	0.05	6.7	0.67	0.1	0.13	0.2	9.3	0.7	0.05	10	17.7	92	0.04	1	2	9.4	26	2
KHE 8	0.01	0.03	0.1	3.6	0.14	0.02	45	0.5	0.02	5.9	0.81	0.1	0.14	0.3	9.5	0.6	0.05	12	18.7	102	0.04	1	2.1	9.4	20	2
KHE 9	0.01	0.03	0.1	4.1	0.14	0.02	11	0.1	0.06	7.2	0.47	0.1	0.28	0.3	8	0.7	0.05	14	20.8	119	0.02	1	2	11	10	2
KHE 11	0.01	0.03	0.1	3.5	0.11	0.02	6	0.3	0.02	5.1	0.7	0.1	0.23	0.4	8.9	0.5	0.05	13	15.2	99	0.03	1	1.1	8.7	15	2
KHE 12	0.02	0.03	0.1	4.6	0.16	0.02	26	0.1	0.02	7.6	0.88	0.1	0.29	0.4	11.5	0.7	0.05	17	21.8	143	0.04	1	2.2	14	19	2
KHE 13	0.01	0.03	0.1	4.2	0.18	0.02	15	0.1	0.02	7.5	1.05	0.1	0.28	0.5	12.2	0.7	0.05	16	16.0	114	0.04	1	1.9	15	10	2
KHE 14	0.02	0.06	0.1	3.8	0.12	0.02	24	0.1	0.02	6.4	0.82	0.1	0.17	0.6	13.4	0.6	0.05	11	13.7	90	0.03	1	1.8	10	20	2
KHE 98	0.00	0.12	DL	1.8	0.07	0.02	64	0.1	0.06	2.3	0.36	DL	0.11	0.6	19.1	0.4	DL	6	9.7	74	DL	DL	0.7	3.7	DL	DL
KHE 99	0.01	0.04	0.1	2.4	0.08	DL	60	0.1	0.04	3.3	0.39	DL	0.09	0.5	8.6	0.4	DL	7	13.0	78	DL	DL	1.1	4.7	DL	DL
KHE 100	0.01	0.05	DL	3.3	0.12	0.02	29	0.1	DL	6	0.46	DL	0.23	0.5	9.5	0.7	DL	12	14.7	97	0.04	DL	1.9	9.8	DL	DL
KHE 101	0.01	0.03	DL	4.3	0.15	DL	37	DL	DL	6.7	0.61	DL	0.21	0.4	9.2	0.8	DL	13	16.0	113	0.03	DL	1.8	9.7	DL	DL
KHE 102	0.02	0.04	DL	4.5	0.18	DL	22	0.1	DL	7.2	0.91	DL	0.22	0.4	10.9	0.8	DL	12	16.2	125	0.03	4	2.6	13	DL	DL
KHE 103	0.01	0.03	DL	3.6	0.13	DL	12	0.1	DL	5.2	0.63	DL	0.21	0.3	8.3	0.5	DL	12	14.6	108	0.02	1	1.7	8.4	DL	DL
KHE 105	0.02	0.05	DL	5.1	0.24	DL	15	0.1	DL	10.3	1.26	DL	0.22	0.3	15.2	1	DL	17	16.6	141	0.05	DL	2.6	17	DL	DL
KHE 104	0.02	0.03	DL	2.9	0.11	DL	28	0.1	DL	4.6	0.45	DL	0.17	0.3	7.7	0.6	DL	10	15.8	108	0.02	1	2	8.2	DL	DL
KHE 106	0.01	0.03	DL	4	0.16	DL	26	0.1	DL	7	0.68	DL	0.2	0.4	8.1	0.6	DL	10	20.1	131	0.04	DL	2.2	11	DL	DL
KHE 107	0.02	0.04	DL	4.8	0.18	DL	17	0.1	DL	8.3	0.92	DL	0.21	0.4	11.5	0.9	DL	14	13.7	103	0.05	DL	1.6	13	DL	3
KHE 108	0.03	0.02	DL	4	0.16	DL	18	0.1	DL	6.1	0.51	DL	0.13	0.2	5.2	0.7	DL	8	21.8	136	0.04	1	2.6	12	DL	DL
KHE 109	0.01	0.03	DL	4	0.15	DL	19	0.1	0.03	6.9	0.48	DL	0.19	0.2	7.1	0.9	DL	10	20.1	140	0.05	DL	2.5	10	DL	DL
KHE 110	0.01	0.03	DL	4.7	0.15	DL	24	0.1	0.02	7.6	0.54	DL	0.21	0.3	8.6	0.9	DL	12	22.4	150	0.04	DL	2.4	11	DL	DL
KHE 111	0.00	0.04	DL	3.1	0.18	DL	24	0.1	DL	5.9	0.54	DL	0.14	0.1	7.5	0.8	DL	10	19.6	151	0.03	DL	2.2	14	DL	DL
KHE 112	0.01	0.05	DL	4.4	0.18	DL	28	0.1	DL	7.5	0.58	DL	0.25	0.3	11.4	1.3	DL	13	21.9	138	0.03	DL	2.4	14	DL	DL
KHE 113	0.02	0.04	DL	3.7	0.13	DL	19	0.1	0.03	6.3	0.33	DL	0.16	0.3	7.8	0.9	DL	11	18.3	111	0.04	DL	2.3	9.5	DL	DL
KHE 114	0.01	0.04	DL	2.2	0.07	DL	5	0.1	DL	3	0.32	DL	0.15	0.4	7.9	0.5	DL	9	13.4	90	DL	1	1.5	4.2	DL	DL

8.3.3   Block KH

Block KH is the site in the rock-covered area, of which the rocks are Archaean metavolcanic rocks of andesitic to dacitic composition (Paul and Goldsmith, 2012). Geochemical results from the rock samples also have expressed useful characteristics. With reference to background values for Au in igneous rocks, some Block KH samples have indicated an Au anomaly. The amount of gold in these rock samples ranges between 0.2 ppb and 17 ppb (Table 8.11).

In general, there is no spatial correlation between Au and alteration zones. In this area, samples from the distal alteration zone, which is around 100 meters away from proximal alteration zone, have also high gold concentration (Fig. 8.6).

Spatial correlations between elements have been revealed by some of the elements. For instance, Au shows a spatial correlation with Sb Bi, Tl and to some of alteration index elements such as Ca, S, Pb, and Cd (Fig. 8.6). From Fig. 8.6, samples with a high amount of Au (KH 126, KH 133, and KH 136) are showing a strong association with the above mentioned pathfinder elements. Surprisingly, samples taken from proximal alteration zones have relatively low Au concentration i.e. bellow the general background, which is 6 ppb. The observed feature can better described by factors, which define favorable conditions for gold deposition. From field observation, rocks in the proximal alteration zone are intensively sheared relative to those in the distal alteration zone. It is possible that areas adjacent to intensively sheared zone, at the boundaries of the intensive sheared area were more favorable for Au deposition.

High Ca concentration in the proximal zone could possibly indicate carbonate (calcite) alteration. Also, high concentration of Cd have been observed in the same zone, the observed behavior suggests both carbonate and Cd may be indicating the fluid focal point of the hydrothermal system. High concentrations in the proximal zone have been observed for other elements such as Be, Ga, B, Re, Li and Nb, and might point towards a highly fractionated magmatic source rock. The association shown between Au, Pb and S (Fig. 8.6) suggests sulfidation was one of the alterations related with gold mineralization. Correlations between elements are well shown and are described in details in Pearson correlation coefficient results in the following paragraph.
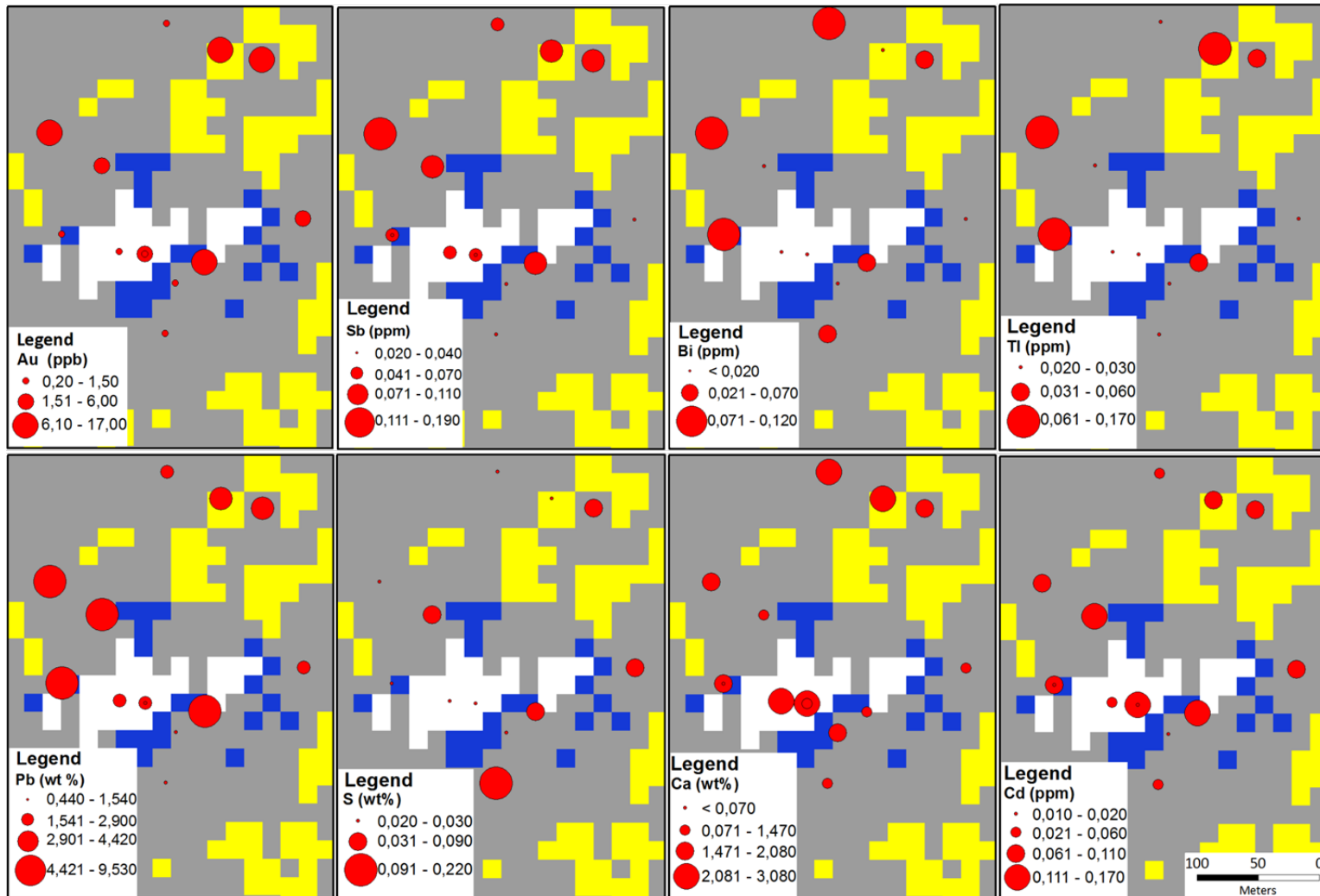
Figure 8.6 Alteration maps showing Block KH overlain with Au and some pathfinder elements, the size of the red dots corresponds to the amount of element in concentration. The colors, White: Proximal Alteration, Blue: Intermediate Alteration, Yellow: Distal alteration.

The Pearson correlation coefficient has revealed relationships between different elements (Table 8.9) and that the association between Au and pathfinder elements is significant. Au has shown a high degree of correlation with As, Sb, Pb, Ba, Tl, Bi, and Ni and also a positive correlation of these elements with Ag, B, Zn and immobile elements such as Zr, Ti and Y (Table 8.9). Cu, Cd and S are also showing correlations in the same trend.

The positive correlation shown between Ag, Cu, Pb, Cd, Zn and S may possibly indicate sulfidation since the mentioned elements are major constituents to some of the sulfide ore minerals. Moderate positive correlation between K and Ba as well as the absence of a significant relationship between the two elements and Na might indicate the presence of sericite alteration (Table 8.9 and 8.10). The observed high degree of correlation between Fe and Mn also with Mg might indicate carbonates or chlorite alterations. Moreover, there is a correlation between Ca, Al, Na and Sr; the association which may possibly indicate plagioclase minerals from the host rock and/or albite alterations.

Table 8.9 Pearson correlation coefficient table showing the coefficient of correlations between different elements from Block KH samples, □ indicate coefficients ≥ 0.7 both positive and negative

	Au	Ag	As	Sb	Mo	Cu	Pb	Zn	Ni	Bi	Ba	B	Al	W	Tl	S	Se	Te	Zr	Y	Ti
Au	1,0																				
Ag		1,0																			
As	0,8		1,0																		
Sb	0,9		0,8	1,0																	
Mo					1,0																
Cu		0,9				1,0															
Pb	0,8	0,7		0,8		0,6	1,0														
Zn				0,5		0,5		1,0													
Ni	0,5			0,5		0,5		0,7	1,0												
Bi	0,5		0,6	0,5						1,0											
Ba	0,8		0,6	0,7			0,7		0,5		1,0										
B							0,7					1,0									
Al													1,0								
W										0,5				1,0							
Tl	0,7		0,5	0,6				0,7			0,7				1,0						
S						0,5							-0,5			1,0					
Se						0,6										0,9	1,0				
Te																0,9	0,8	1,0			
Zr		0,5				0,5	0,5			0,5	0,5								1,0		
Y									0,5				-0,5	-0,5					0,8	1,0	
Ti						0,6							-0,6				0,5		0,8	0,9	1,0

Table 8.10 Pearson correlation coefficient table showing the coefficient of correlations between different elements from Block KH samples, □ indicate coefficients ≥ 0.7 both positive and negative

	Ag	Pb	Zn	Co	Cu	Ba	S	Mn	Fe	Ca	P	Cr	Mg	Ti	Al	Na	K	Sc	Sr	Cd	V
Ag	1,0																				
Pb	0,7	1,0																			
Zn		0,5	1,0																		
Co				1,0																	
Cu	0,9	0,6			1,0																
Ba		0,7				1,0															
S					0,5		1,0														
Mn	-0,5			0,6	-0,5			1,0													
Fe			0,9					0,7	1,0												
Ca							-0,5			1,0											
P	-0,5				-0,6						1,0										
Cr			0,6	0,6		0,5		0,7	0,7			1,0									
Mg									0,6				1,0								
Ti					0,6						-0,5			1,0							
Al							-0,5		0,9					-0,6	1,0						
Na	-0,6				-0,6		-0,5		0,8		0,6			-0,7	0,9	1,0					
K				0,6		0,5		0,7	0,7			0,7					1,0				
Sc			0,7					0,9	0,8			0,8						0,7	1,0		
Sr									0,8						-0,5	0,9	0,8		1,0		
Cd	0,6	0,7	0,7		0,5															1,0	
V			0,5	0,8				0,8	0,9			0,9					0,8	0,9			1,0

Pyrite, sphalerite, pyrrhotite and chalcopyrites are some of the ore minerals identified in thin sections from the rock samples from this area (Table 7.6). But the observed positive correlation of elements from Pearson correlation coefficient supports the presence of other ore minerals. For example, Au, Ag, S, Sb, Tl are the essential elements for criddleite ($TlAg_2Au_3Sb_{10}S_{10}$) minerals, this mineral, however, has not been observed in this study and further work might be required to clarify the exact mineralogical siting of these elements.

The elements Zr-Ti-Y show to be immobile; the immobile character is perfectly expressed by the element combination Ti-Y whereby all samples plotted on a clearly correlating positive line on the graph (Fig. 8.7). However, there is no clustering in respect to the various alteration zones. Therefore, the geochemical values obtained were not convincing to be used in assuming the volume change of the host rock as the result of hydrothermal alteration. However, some samples from the proximal alteration zones plot in the relatively higher value region of the graph compared to samples from intermediate and distal alteration zones (Fig. 8.7).

There is a correlation between LILE ratios Rb/Sr and Ba/Sr, but similar to the character observed for the immobile elements, samples from Block KH are not spatially clustered with respect to the alteration zones (Fig. 8.7). Observed geochemical features in both immobile and LIL elements are suggested to be probably caused by the effect of fluid-to-rock ratio as well as the factors, which controlled the infiltration of fluids into the host rock, for example, the host rock permeability.
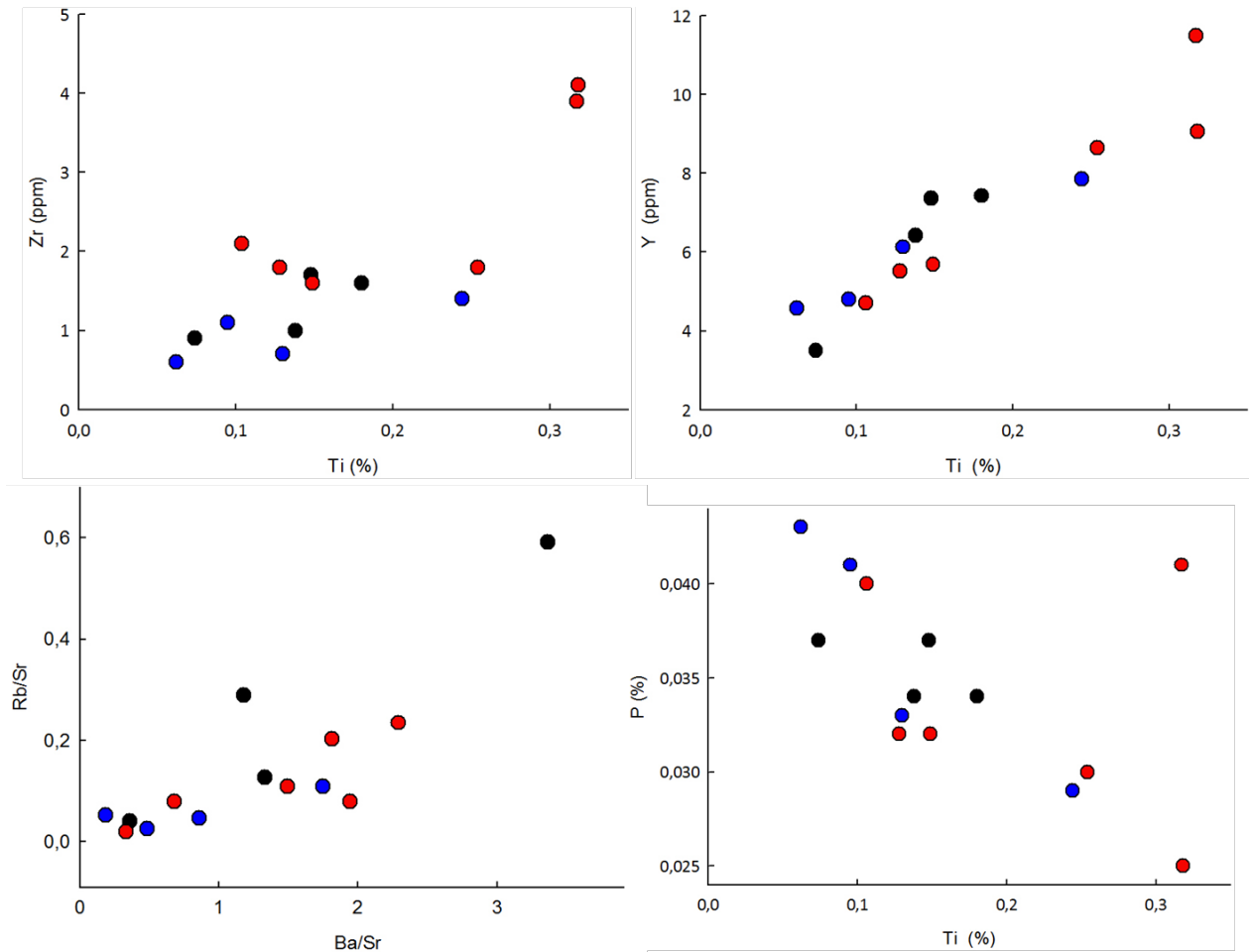
Figure 8.7 Correlartion plots showing the relationship of Block KH immobile and LIL elements with respect to alteration zones. ● = proximal alteration zone, ●= intermediate alteration zone, ●= distal alteration zone.

Table 8.11 Major and trace element geochemical results for some of the analyzed rock samples from Block KH area, DL=below detection limit

SAMPLE	Mo ppm	Cu ppm	Pb ppm	Zn ppm	Ag ppb	Ni ppm	Co ppm	Mn ppm	Fe %	As ppm	U ppm	Au ppb	Th ppm	Sr ppm	Cd ppm	Sb ppm	Bi ppm	V ppm	Ca %	P %	La ppm	Cr ppm	Mg %	Ba ppm	Ti %	B ppm	Al %
KH 87	0.2	32	6.91	36.1	131	33.9	12.9	318	1.85	1.6	0.1	3.6	0.1	15.1	0.17	0.09	DL	77	1.27	0.04	2.7	38.4	0.37	13	0.10	3	1.23
KH 95,1	0.33	30	2.84	43.7	43	25.3	10.9	261	1.4	1.6	0.1	2.2	DL	39.2	0.17	0.07	DL	59	2.28	0.03	1.3	38.9	0.37	26.7	0.13	2	2.61
KH 95,2	0.09	4	0.44	26.5	12	15.3	8.3	296	1.66	1	0.1	0.2	DL	6.9	0.02	0.03	DL	64	1.2	0.03	1.5	35	0.48	12.5	0.15	DL	0.76
KH 96,1	0.04	7	2.7	21.2	18	14.4	8	258	1.45	1.7	0.1	1.5	DL	51.5	0.04	0.05	DL	60	3.08	0.04	2	37.9	0.35	21.8	0.10	2	3.74
KH 126	0.37	28	4.34	38.6	54	53.5	17.4	408	2.76	1.5	DL	7.5	0.3	53.7	0.07	0.09	0.02	112	2.95	0.03	3.1	61.8	0.67	63.3	0.14	2	4.34
KH 127	0.15	126	2.11	40.1	134	32.9	16	197	2.4	0.4	DL	2.5	0.2	37.7	0.09	0.03	DL	76	1.47	0.03	2.9	36.3	0.95	7.1	0.13	DL	2.32
KH 128	0.23	284	9.53	38.5	333	32	10.6	141	1.44	2.1	DL	11.3	0.1	38	0.16	0.11	0.06	58	1.43	0.03	1.6	33.4	0.15	73.9	0.32	3	0.94
KH 129	0.3	10	1.52	21.7	29	14.9	8.5	265	1.66	0.7	DL	1.1	0.3	49.3	DL	DL	DL	51	2.08	0.04	2.1	25.5	0.58	24	0.06	DL	2.75
KH 130	0.23	104	1.54	23.7	61	26	17.6	292	2.28	0.4	DL	0.6	0.2	9.2	0.04	0.04	0.07	70	1.26	0.03	1.9	28.5	0.43	16.1	0.24	DL	0.85
KH 131	0.14	16	2.9	33.4	32	22	11.4	373	2.13	1.5	DL	0.6	0.2	12	0.06	0.08	0.02	79	1.58	0.03	2.2	40.8	0.47	17.9	0.25	1	1.15
KH 132	0.23	48	3.61	40.7	49	42.4	16.6	494	2.48	1.7	0.2	1.1	0.2	19.6	0.07	0.06	0.07	102	1.8	0.04	2.3	57.6	0.74	44.9	0.32	2	1.41
KH 133	0.18	19	6.52	35.6	35	34.6	21.4	500	2.58	17.6	DL	17	0.2	21.8	0.08	0.19	0.11	96	1.65	0.04	2.5	46	0.52	73.4	0.15	2	1.77
KH 134	0.22	2	2.69	30.8	29	17.1	9.2	284	1.63	1.2	DL	DL	0.2	60.7	0.05	0.05	0.1	45	2.26	0.04	1.6	29.5	0.56	21.8	0.07	1	3.02
KH 135	0.07	74	4.42	40.9	89	43.7	16.7	406	2.47	1.6	DL	8.1	0.2	12.6	0.11	0.11	0.07	94	1.84	0.03	2.1	40.8	0.49	16.8	0.18	DL	1.59

SAMPLE	Na %	K %	W ppm	Sc ppm	Tl ppm	S %	Hg ppb	Se ppm	Te ppm	Ga ppm	Cs ppm	Ge ppm	Hf ppm	Nb ppm	Rb ppm	Sn ppm	Ta ppm	Zr ppm	Y ppm	Ce ppm	In ppm	Re ppm	Be ppm	Li ppm	Pd ppb	Pt ppb
KH 87	0.23	0.1	0.3	9.6	0	0.08	DL	0.1	0.02	4	0.45	DL	0.06	0.06	0.7	0.1	DL	1.1	4.8	6.9	DL	2	DL	14.7	DL	DL
KH 95,1	0.32	0.1	0.2	6.7	0	0.03	DL	DL	DL	6.4	1.09	DL	0.06	0.07	3.1	0.1	DL	1.8	5.52	3.1	DL	2	0.2	14	DL	DL
KH 95,2	0.15	0.1	0.1	7.7	0	DL	DL	DL	DL	2.6	0.24	DL	0.12	0.13	1.4	0.1	DL	1.6	5.69	3.7	DL	DL	DL	7.3	DL	DL
KH 96,1	0.48	0.1	0.2	7.1	0	DL	DL	DL	DL	8.6	0.44	DL	0.06	0.05	1.1	0.1	DL	2.1	4.68	5	DL	1	0.2	15.6	DL	DL
KH 126	0.53	0.2	DL	11.1	0.2	DL	6	DL	DL	8.9	9.94	0.1	0.05	0.06	15.5	0.2	DL	1	6.43	7.1	0.03	DL	0.1	18.8	DL	DL
KH 127	0.32	0	DL	6.7	0	0.05	DL	DL	0.04	5.2	2.2	DL	0.04	0.04	2	0.2	DL	0.7	6.13	6.8	DL	1	DL	17.8	DL	DL
KH 128	0.03	0	DL	4.6	0.1	0.09	DL	DL	0.05	3.3	0.47	0.1	0.21	0.26	3	0.3	DL	4.1	9.06	3.8	DL	2	0.3	2.9	DL	DL
KH 129	0.45	0	0.2	6.8	DL	DL	DL	DL	DL	5.4	0.49	DL	0.02	0.03	1.3	DL	DL	0.6	4.58	5	DL	DL	0.1	5.6	DL	DL
KH 130	0.16	0	DL	7.8	DL	0.22	DL	0.3	0.27	2.7	0.22	DL	0.08	0.25	1	0.4	DL	1.4	7.85	4.4	0.03	DL	DL	3.8	DL	DL
KH 131	0.23	0.1	0.1	8.6	DL	DL	DL	DL	DL	3.5	0.21	DL	0.11	0.16	1.3	0.2	DL	1.8	8.64	5.4	0.03	DL	DL	12.6	DL	DL
KH 132	0.22	0.1	0.1	12.2	DL	0.02	DL	DL	0.02	4.3	0.49	0.2	0.21	0.24	4.6	0.5	DL	3.9	11.5	5.7	0.03	DL	0.3	23.7	DL	DL
KH 133	0.30	0.1	0.5	10.6	0.1	DL	DL	DL	0.04	5.3	6.13	DL	0.08	0.08	12.9	0.2	DL	1.7	7.36	5.6	DL	DL	0.2	14.8	DL	DL
KH 134	0.52	0	3.3	6.6	DL	DL	DL	DL	DL	5.9	1.61	DL	0.04	0.06	2.5	DL	DL	0.9	3.5	2.9	DL	DL	0.2	9.3	DL	DL
KH 135	0.27	0.1	0.3	11.1	0.1	0.05	DL	0.2	0.02	4.3	0.59	0.1	0.07	0.09	1.6	0.2	DL	1.6	7.43	4.8	DL	DL	DL	12.8	DL	DL

8.4   Conclusion

The three test sites, which were sampled for geochemical analysis of rock and soil samples respectively, were the ones identified from the results of alteration mapping by ASTER data. All three selected test sites (Block KHA, Block KHE and Block KH) have been found to contain Au anomalies i.e. > 6 ppb Au also to different extents. Also the geochemical data have revealed the correlation between Au and typical pathfinder elements. The geochemical correlation between Au, pathfinder elements and alteration zones has been perfectly demonstrated for Block KHA; in the other two blocks this relationship was not as clear. Clustering of samples with respect to alteration zones has been observed for the immobile and LIL elements for Block KHA and to some extent Block KHE. The failure of clustering in respect to alteration zones in some of the test sites is suggested to be possibly caused by the dispersion behavior of geochemical elements in soils, in which their geochemical haloes are reported to be relatively extensive when compared to the mineralization zones, and in similar manner the alteration zones. High concentrations of the immobile elements Al-Y-Ti in Block KHA indirectly confirm alteration processes in the area since they reflect the contraction effect, for example, dehydration, which may result to reduced volume of the host rocks, and consequently the increased concentration of the immobile elements in host rocks. Similarly, the relatively high ratios of LIL elements (K/Ba, Rb/Ba, Rb/Sr) and low K/Rb infer a magmatic involvement in alteration process in the area. Block KHE and Block KH have also revealed same element and alteration correlation, however, it was not possible in these two blocks to predict the processes involved since there was no clear clustering of samples from proximal alteration zones. This was suggested to have been caused possibly by factors which controlled the infiltration of hydrothermal fluids, such as distance from fluid up-flow, fluid-to-rock ratio and permeability. The presence of proximal alteration zones has been inferred through the correlation between elements, which constitute the assumed alteration minerals. Carbonate, sericite and sulfide are some of these alteration minerals inferred from the analyzed results in Pearson correlation coefficient analysis. Similar to the alteration minerals, the correlation between these elements has predicted some of the ore minerals which were found in proximal zones in the three test sites. Some of the predicted alteration minerals by geochemical data were also identified by other methods i.e. petrographic analysis by both normal light microscope and SEM, also XRD and mineral spectroscopy for clays and carbonates minerals as described in the previous sections.

9 COMPARISON WITH A NEIGHBORING CASE STUDY AREA

In the study area there were and are ongoing exploration activities by different exploration companies since the 1990s and several exploration techniques have been applied during this period. A good example of classical exploration is the prospecting license owned currently by **Tembo Gold Corp.,** an area where the two test sites in this study i.e. Block KHA and KH are located. By referring to a technical company report, which was publically released on August, 2012 (Pauls and Goldsmith, 2012), the area has been explored by various methods. This includes grid soil sampling, laser imaging, an airborne geophysical survey, and ground magnetic survey. Moreover, drilling both by reverse circulation (producing rock chips) and diamond drilling (producing drill core) have been conducted to some of the selected targets, following the interpretation results of the geophysical data as well as soil and rock samples geochemical data. The mapped geology of the area indicates the area to be underlain by mafic to intermediate metavolcanic rocks and mineralization has been reported to be hosted by intermediate metavolcanic rocks of andesitic to dacitic composition. Also minor mafic extrusive rocks and corse-crystalline gabbro have been reported e.g. at the Nyakagwe East prospect (Pauls and Goldsmith, 2012). Finally , the interpretation results including the analyzed geochemical data from drill cores were used to delineate areas with high gold content as well as the geological features, which may be associated with the identified Au anomalies. The above classical exploration techniques have all been applied to this area and are currently the standard exploration procedures.

As a further test for the remote sensing approach to exploration applied in this study, results from the ASTER data analysis were overlain on the geophysical data images and exploration results obtained from the Tembo Gold Corp. The overlay has revealed a significant and striking correlation between the identified proximal alteration zone and Tembo's aeromagnetic anomalies. Fig. 9.1 is the airborne and ground magnetic images from the Tembo Gold Corp. prospect in the Bulyanhulu gold mining district. In the southern part of the area, the linear NW-SE patterns of the magnetic anomalies coincide with the hydrothermal alteration zones that trend in the same direction and display a similar shape to the anomalies (Fig. 9.1). Block KHA test site is located in this prospect and its proximal alteration zone is located on the western edge of a circular anomaly in the aeromagnetic image (Fig. 9.1). Similar observations were revealed by the ground magnetic data of the same area. Proximal alteration and the NW- SE trending magnetic low anomaly north of Block KHA also show a positive correlation (Fig. 9.1). To the NW of the area there are two sub-circular magnetic anomalies (a high and a low), the anomalies coincide very well with the proximal alteration patches and they fall at the center area of these anomalies. Both magnetic anomalies and the proximal alteration patches in the same area also disclose a linear feature, which together with the adjacent linear alteration patch form two parallel trend lines, which strike NE-SW. It could thus be assumed that the observed parallel alteration patches represent the margins of a shear zone, which might have been favorable fluid conduits during fluid injection and during mineralization.
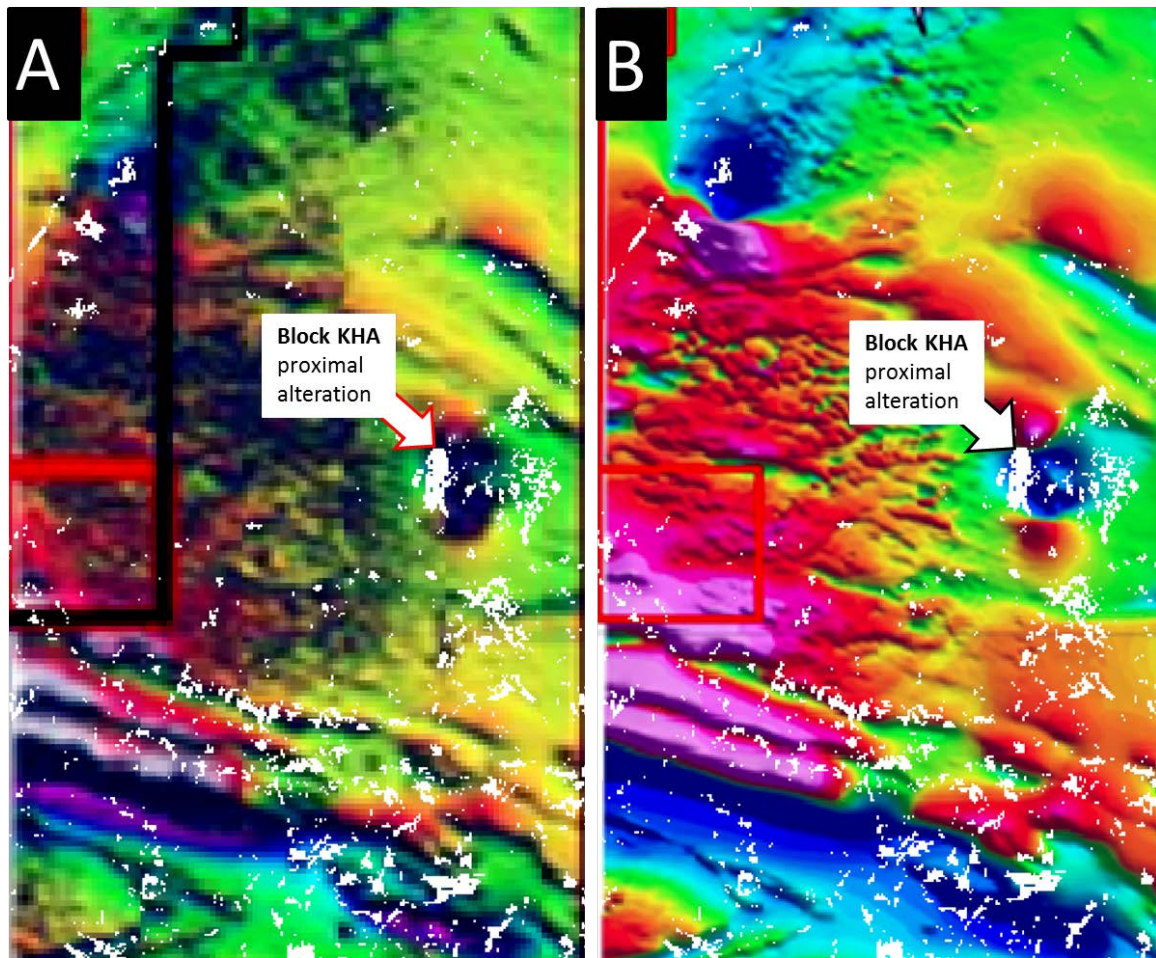
Figure 9.1 Airborne and ground magnetic images from the Tembo Gold Corp. prospecting license found in the Bulyanhulu gold mining district (Pauls and Goldsmith, 2012). **A:** Airborne magnetic image (Tembo data) overlain by hydrothermal alterations from this study (white patches), **B:** Ground magnetic image (Tembo data) overlain by hydrothermal alterations from this study (white patches). The magnetic anomalies in both images indicate a positive correlation with zones of hydrothermal alteration from ASTER data analysis.

From the interpretation by Tembo's staff, the above magnetic data resulted in 14 layers of geological features, such as dykes, intrusive rocks, magnetic domains, and magnetic lithology, and structures such as faults and shear zones, other features also include the identified target areas for drilling programs (Fig. 9.2). The overlay between the interpretations by Tembo's staff and the proximal alteration zones from this study has revealed a significant positive correlation (Fig. 9.3).

**Ground Magnetic Data,
TEMBO GOLD CORP.**

Interpretation, TEMBO GOLD CORP.

**Interpretations from TEMBO GOLD and
hydrothermal alteration from this study**
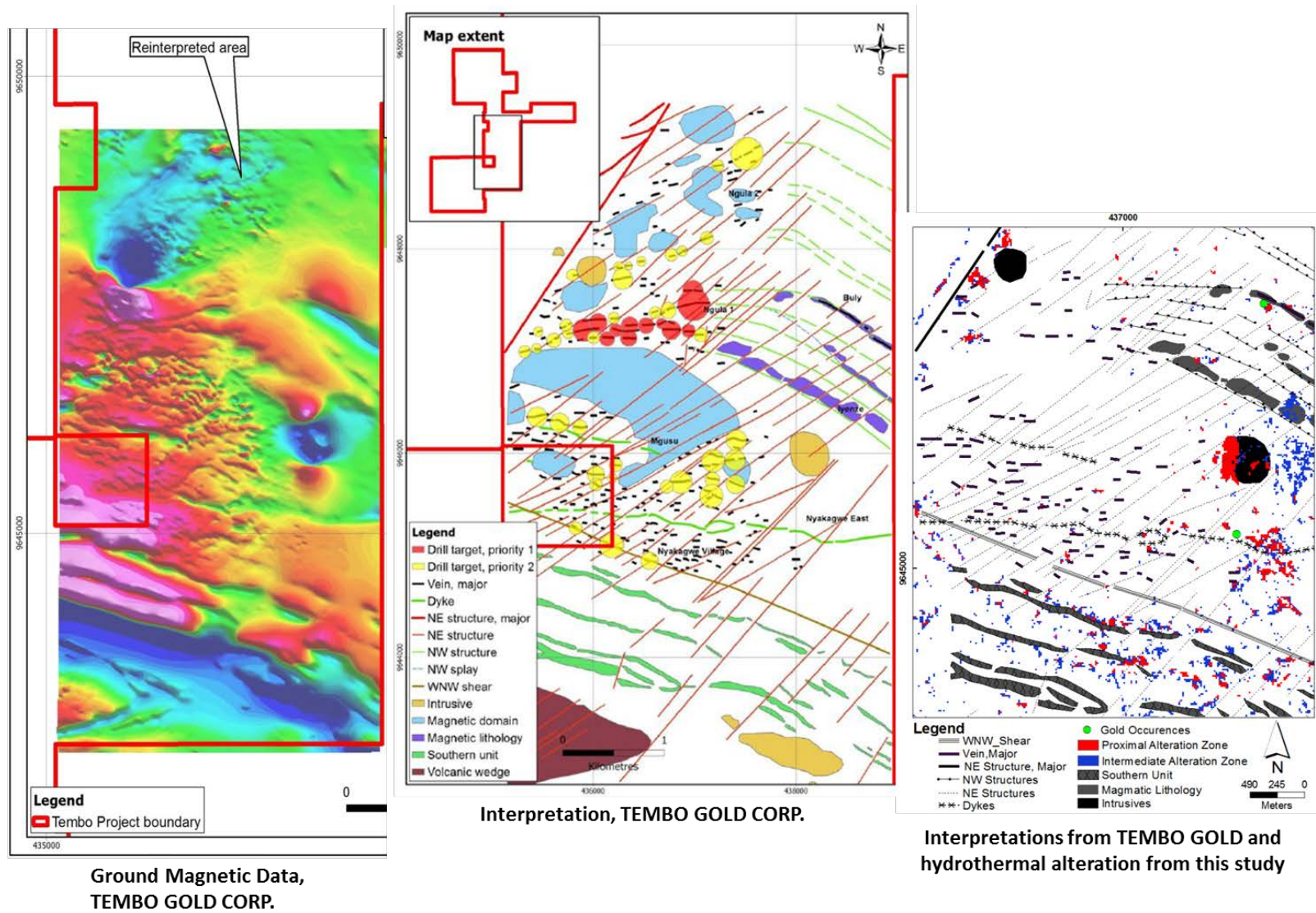
Figure 9.2 Ground magnetic image (left), magnetic data interpretations (middle) and hydrothermal alterations from ASTER data analysis (right).

The proximal alteration zone coincides spatially with circular features, which were interpreted as magmatic intrusions, the alterations are located on the edges of the intrusion e.g. Block KHA (Fig. 9.3). If an underlying intrusion is assumed as the source of mineralizing fluid, it would make sense that the fluid would have been carried more at the edges compared to the central parts of the intrusion. There is also a positive correlation between proximal alteration zones and the interpreted magnetic lithotypes, for example, the magnetic lithotype and southern units, both in some places they coincide with proximal alteration zones. Detailed observations indicate that the alteration follows the shape and trends of some units, e.g. the southern units. The dykes, for example, the E-W –trending in the map, also coincide with proximal alteration zones on the eastern side of the map (Fig. 9.3). These clustered alteration patches, which are located in Nyakagwe, also coincide with the two intersecting NE-SW-trending structures together with the above described dyke.

Interpretations from magnetic data also show that the area has been diagonally cross-cut by extensive NE-SW-trending structures. Some of these structures also coincide with proximal alteration zones, Block KH alteration zoning in the NW part of the area is the best example for this (Fig. 9.3). To the NW of the area there is a major NE-SW structure, which runs parallel to linear alteration patches found on both sides of the structure. It is suggested that the linear alteration patches represent the margins of the shear zone as it has been described in the above section. Generally, the NW-SE-trending structures indicate no significant correlation except for places where they are cross-cut by the NE-SW-trending structures. Major veins mapped from the area have also shown positive correlation with the proximal alteration zones, for example, the vein to the NE of the area, which occurs together with a gold occurrence. This vein is reported to be the continuation of the major vein, which hosts gold mineralization at the Bulyanhulu Gold Mine. The vein is also cross-cut by a NE-SW structure; in this study the structure is suggested to have increased the space for fluid accumulation and thus for mineralization. In the same area the proximal alteration zone coincide with a magmatic lithotype running parallel to this major vein. There are several other veins, which coincide with proximal alteration zones as it is seen from the map (Fig. 9.3). Proximal alteration zones also spatially coincide with the artisanal mining sites, e.g. areas marked with gold occurrence. At Nyakagwe area artisanal mining is still active and has resulted in a large open pit with diameter and depth of around 100 m and 70 m respectively (Fig. 9.3).

Tembo's geochemical results from grid sampling as well as from reverse circulation and diamond drilling core samples were used to delineate areas with anomalous Au concentration during exploration as indicated in the report by **Tembo Gold Corp.** (Pauls and Goldsmith, 2012). An overlay with the alteration results from this study has revealed that Block KHA proximal alteration zones coincide with the areas delineated to have high Au concentration (Fig. 9.4).
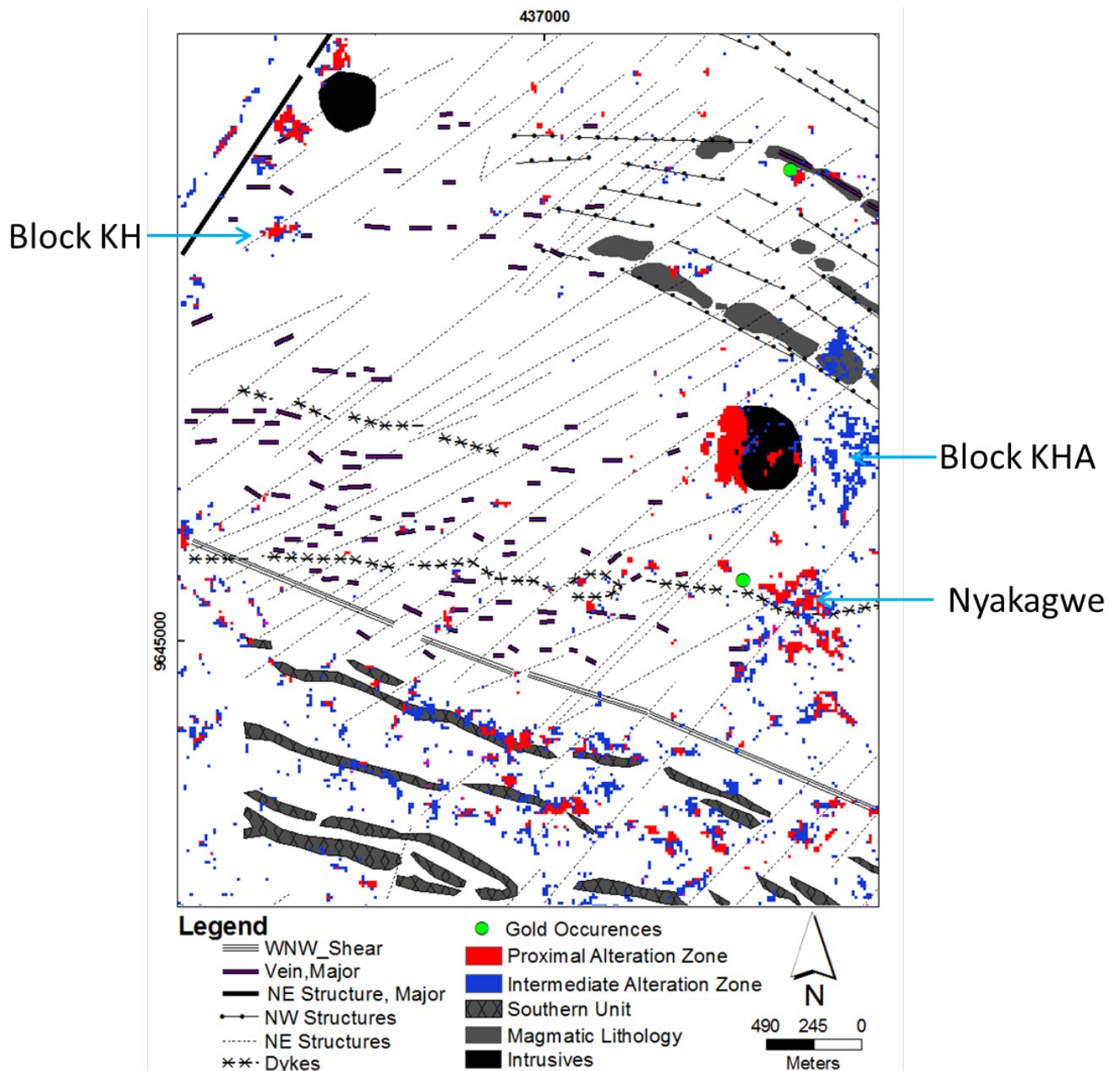
Figure 9.3 Map showing hydrothermal alteration zones compared to geological structures and lithotypes interpreted from magnetic surveyed data by Tembo Gold Corp.

Therefore, the results reported by Tembo Gold Corp. (Pauls and Goldsmith, 2012), both geophysical and geochemical correlate positively with the independently mapped proximal alteration zones of this study. This positive match can be regarded as an independent "proof of concept". In other words, the relationship shown between the Tembo results and the result from this study indicates that the technique used to map hydrothermal alterations can be used to identify the gold prospective areas.
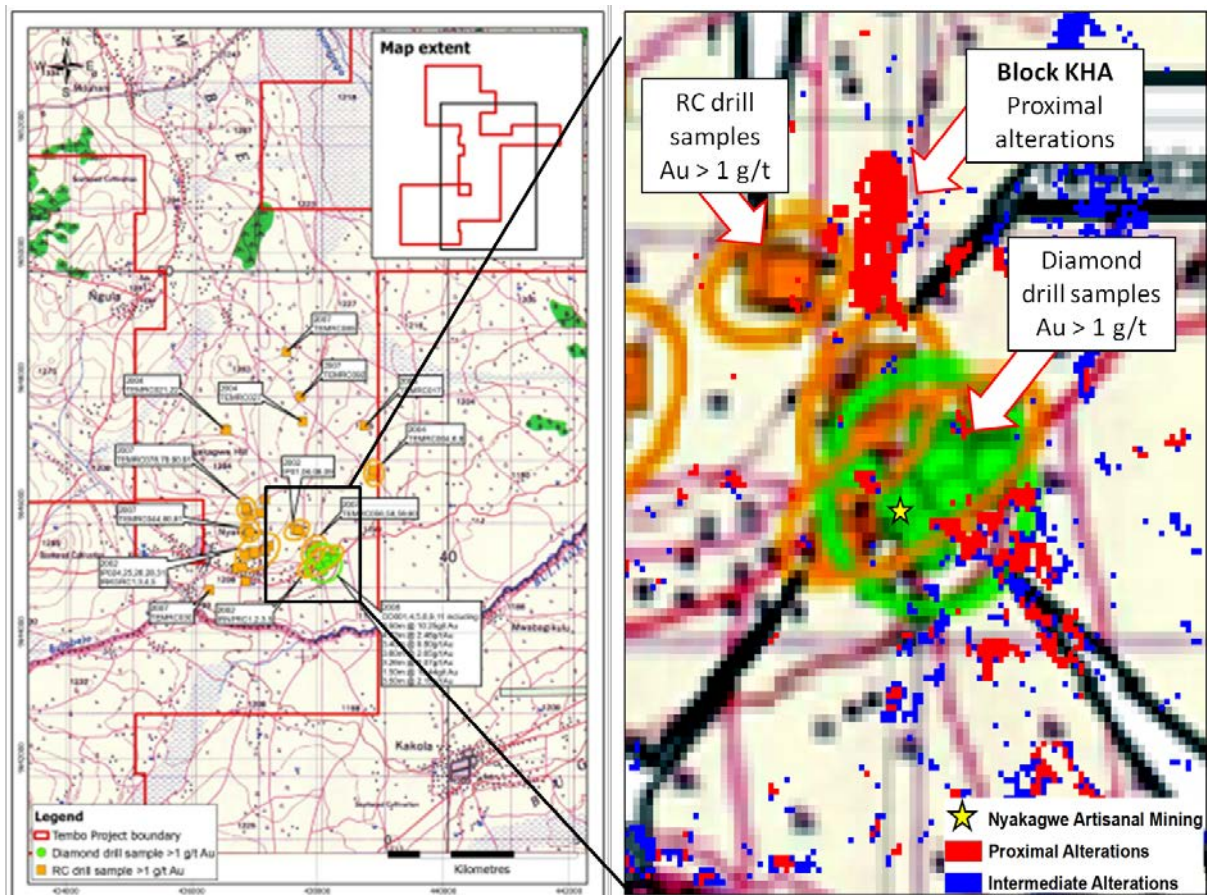
Figure 9.4 Topographic map showing exploration progress from Tembo Gold Corp. technical report, overlain with the ASTER extracted alteration zones. Block KHA proximal alterations fall within areas indicated as Au anomaly from Diamond drill and Reverse Circulation (RC) samples. See legend in left map for explanation.

10   SYNTHESIS OF RESULTS AND DISCUSSION

The three data sets, SRTM, Landsat ETM+, and ASTER, used in this study were independently analyzed. This was done to avoid any bias during analysis and interpretation since the overall objective was to develop an alteration mapping method, which-at the end-will be verified by results from other analyzed data sets. Lineaments from SRTM data have revealed the SGB to be intensively fractured and the extracted fractures agree with structural patterns of faults and shear zones in the region. The lineaments are mainly arranged in two sets, trending in a NE-SW and a NW-SE direction. The SRTM lineaments were further compared to the identified preliminary symmetrical linear alteration zones extracted from Landsat ETM+ data, which are interpreted to represent former hydrothermal fluid conduits. The linear alteration patches from Landsat ETM+ data have shown a positive correlation with some of the SRTM lineaments. Observations from the two results also indicate that the areas with intensive alteration coincide particularly with lineament triple junctions and areas with multiple and cross-cutting fractures or shear zones (Fig. 6.6).

The ability to identify individual alteration minerals as well as the relatively low cost of this method was a reason to choose ASTER data for the detailed alteration mapping in this study. The low cost of the remote sensing data used in this study is also important for the future use in African states that

are financially not as well-endowed as of many of the more industrialized countries. The use of more than one diagnostic mineral to characterize an alteration assemblage, has improved the quality of alteration mapping when compared to the conventional remote sensing methods, which mostly embraced the use of one diagnostic mineral. The method combines the extracted alterations, each alteration with a distinctive identifying value. This has managed to visualize the alteration zoning in areas affected by hydrothermal alteration around fluid upflows/focal points, and thus possibly near trap sites for economic mineralization. The mapped alteration zoning agrees with the alteration sequences reported for gold deposit models (e.g. Groves et al., 2000, Ikingura et al., 2010). Other characteristic features for hydrothermal alterations such as narrow transition zones and sharp boundaries between alteration zones have been revealed. Moreover, the size and shape of the proximal alterations agree with features outlined in gold deposits in terrains similar to Sukumaland Greenstone Belt (SGB). It has been observed that the proximal alterations coincides with areas of tectonic fracturing such as shear zones, faults and fault jogs, and triple junctions. These observations conform to the reported characteristics of Archaean lode gold deposits (e.g. Groves et al., 2000; Goldfarb et al., 2005). Therefore, from observations and the revealed alteration characteristic features, which also conform to the Archaean granite-greenstone gold deposit models, it is suggested that areas showing linear alteration zoning should be selected as future exploration targets.

Analytical follow-up by other analytical methods was performed on three selected test sites, which showed systematic alteration zoning, i.e. Block KHA, Block KHE and Block KH. The test sites were chosen to include both soil and rock covered areas. Laboratory VNIR-SWIR spectroscopy, light microscopy, SEM as well as XRD were the methods used to identify minerals from each alteration zone. This investigation focused on systematic mineralogical differences between the alteration zones and on identifying those diagnostic minerals used in the extraction of alteration zones from ASTER data. Laboratory VNIR-SWIR spectroscopy has successfully characterized and differentiated the alteration zones, and particular spectral features for some minerals, which are related to the referred alteration zone have been identified in the spectra. This can best shown by samples from Block KHA and Block KH (Fig. 7.15, Fig. 7.18). Microscopic studies of both soil and rock samples have also proved the systematic differences between the alteration zones. Thin sections from proximal alteration zones have revealed a distinct difference in mineralogy from the intermediate and distal alteration zones. Several diagnostic minerals, which characterize these alteration zones, have been identified. In Block KH, carbonates, sericite and silicified quartz were identified in proximal zones together with a high content of sulfide minerals. Locally the sulfides follow the trend of shear fabrics, which is NE-SW (e.g. Fig. 10.1).
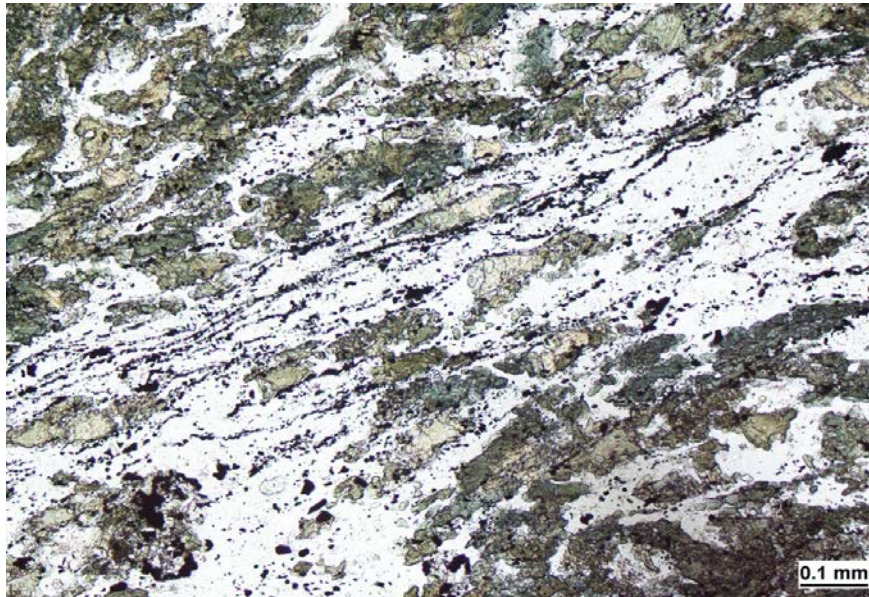
Figure 10.1 A thin section picture from sample KH 95.1 under plane polarized light. The dark green and yellowish green minerals are chlorite and epidote; the diagonal dark stringers are sulfide minerals, which follow the direction of the shear fabrics.

Both microscopic and field observations indicate that the Block KH proximal alteration area is intensively sheared (Fig. 7.20). Distal alteration zones are dominated by chlorite-epidote and some fine grained carbonate minerals. Moreover, several metals/elements, which were expected to be found in proximal alteration zones due to their association with mineralization, have been also identified. XRD analysis was an important step to prove the presence of different clay minerals and their variation in respect to the alteration zones. Although the method cannot identify all of these minerals effectively, it has identified some of the most important clay minerals. The identified clay minerals correlate with the referred alteration zones, and particularly samples from Block KHA have revealed this alteration sequence. Nacrite, kaolinite, kaolinite-dickite and kaolinite-montimorillonite were identified in the proximal alteration zone; the intermediate zone is discriminated from proximal by the presence of illite whereas the distal alteration has haloysite, kaolinite, and illite-montimorillonite/smectite which seem to be the dominant phases in the distal zone (Table 7.6).

Geochemistry was applied to investigate the characteristic behavior of some of the selected indicator elements for gold mineralization. The objective was to depict features which relate direct or indirect to both hydrothermal alteration processes and mineralization. Gold as the main target precious metal in this region and in this study revealed a local anomaly in proximal alteration zones and the same pattern is similarly shown by some of the typical pathfinder elements. Ag, As, Hg, Sb, Mo, Bi, Te, Ba, Cu, Zn, Pb, Se, S, and Tl are some of these pathfinder elements, which have shown positive correlation with Au in all three test sites. Correlation between Au and pathfinder elements is best shown on alteration maps from these areas e.g. in Block KHA, Block KHE and Block KH. Immobile elements (e.g. Ti-Al-Y) have shown features, which could be used as indicators of effects hydrothermal alteration, for example, high concentration of these elements in the proximal alterations could indicate contraction of the host rocks due to hydrothermal alteration. This has been well presented in Block KHA. LIL elements have been reported as the best indicators for the

magmatic involvement in the hydrothermal and mineralization processes (e.g. in Chamberlain, 2003). In this study some of the Large Ion Lithofile Elements (LILE) ratios have high concentration in proximal alterations and similarly, the best example can be shown in Block KHA. This observation led to a conclusion that Block KHA hydrothermal fluids had also a magmatic source. For Block KHE and Block KH, both immobile and LIL elements were not clear to lead into conclusion. Therefore, among the three test sites, Block KHA indicates to have received a relatively stronger magmatic influx.

10.1 OVERALL CONCLUSION

With reference from results of this study, satellite remote sensing data have revealed to be a useful tool in the exploration of hydrothermal mineral deposits. The data sets used, Landsat ETM+ and ASTER, both have unveiled that the SGB has been affected by hydrothermal alterations along shear zones and adjacent to intrusive bodies. SRTM lineaments and Landsat ETM+ have revealed the possibility of identifying some of the lineaments, which were possibly the channelways for hydrothermal fluids. Overlay results from SRTM lineaments and Landsat ETM+ alterations after clumping and sieving have shown to correlate with geological features and interestingly they have shown a good correlation with known gold occurrences in the region.

ASTER data have spectral characteristics that make them capable of identifying individual alteration minerals. With respect to hydrothermal mineral deposits, alteration mineral assemblages can be mapped by the approach introduced in this study, which gives a relative high degree of certainty. The method uses more than one key mineral in alteration assemblages to map an alteration zone, moreover, the technique that was used to combine the individual alteration zones made it possible to identify systematic and partly symmetrical alteration patterns/zoning around the probable fluid focal points on the surface. Alteration zoning is a potential characteristic feature for deposits formed as a result of hydrothermal processes. The Archaean granite-greenstone terrain deposits were the deposit models used in this study to test the method. For the areas which have revealed alteration zoning the alteration sequence have shown similarity to Archaean granite-greenstone gold deposit models i.e. proximal alterations made mostly by carbonates and sericite, intermediate alteration zone is made by sericite and clay (montimorillonite-illite) minerals, and distal alteration zone is made by chlorite-calcite-epidote minerals, which partly coincides with regional greenschist facies metamorphic mineral assemblages . The mineralogy of the samples from the test sites has confirmed the different alteration zones. Geochemical data of the samples collected from test sites indicate that proximal alterations are associated with gold anomalies as well as a positive correlation between gold and typical pathfinder elements. There is also positive spatial correlation between proximal alteration zones and tectonic structures interpreted from geophysical data. In the independent case study of an exploration area held by Tembo Gold Corp., areas with anomalous gold concentrations in geochemically analyzed reverse circulation and diamond drilling samples show a good correlation with proximal alteration patterns. By integrating and comparing the various data sets, which have been used to validate the method, it is concluded that the approach is relatively powerful in the analysis of both multispectral and hyperspectral remote sensing data for the purpose of identifying potential targets for the exploration of hydrothermal mineral deposits. The method increases accuracy in mapping alteration zones but also simplifies interpretation and selection of potential targets. It is time and cost effective since it can help to reduce the size of the prospecting area from large reconnaissance areas almost to the individual drill targets in the order of a deposit scale size.

10.2   References

ANGÉLICA, R.S, DA COSTA, M. L, PÖLLMANN, H, 1996, Gold, wolframite, tourmaline-bearing laterized gossans in the Amazon region, Brasil. JOURNAL OF GEOCHEMICAL EXPLORATION, 57, PP. 201-215.

BABCOCK, W. C., 1953, Intermodulation interference in radio systems. *Bell System Technical Journal*, **32**, pp. 63–73.

BARDOUX, M., 2002, Structural Controls of Gold Mineralization in the Archaean Tulawaka Greenstone sequence, NW Tanzania. *Rheos Cunsulting Inc.*

BARTH, H., 1990, Provisional geological map of Lake Victoria Gold Fields, Tanzania 1:500000 (with explanatory notes). *Geologisches Jahrbuch*, **72**, pp. 1–59.

BATH, H., 1987, Assessment of regional geology, gold and basemetal potential in the Lake Victoria Region, Tanzania. *Tanzania-German Technical Cooperation closed file report, BGR*, pp. 1–288.

BOARDMAN, J.W. AND KRUSE, F.A., 1994, Automated spectral analysis: a geologic example using AVIRIS data, North Grapevine Mountains, Nevada. *In Proceedings of the Tenth Thematic Conference on Geologic Remote Sensing, 9–12 May, San Antonio,Texas (Ann Arbor, MI: Environmental Research Institute of Michigan)*, pp.I407–I418.

BONIFACE,N., 2009, Eburnian, Kibaran and Pan-African metamorphic events in the Ubendian belt of Tanzania: Petrology, zircon and monazite geochronology. PhD thesis, Christian-Albrechts-Universität Kiel, Germany, p. 110.

BORG, G., 1991. Regional controls on the distribution of Au-occurrences in the Sukumaland Greenstone Belt, NW Tanzania. In *IGCP Project No. 255 Conference "Gold and Platinoids in Central Africa"*, 11–13 September 1991, Bujumbura, Burundi, Abstract Volume, pp. 3–4.

BORG, G., 1992, New aspects on the lithostratigraphy and evolution of the Siga Hills, an Archaean granite greenstone terrain in NW-Tanzania. *Zeitschrift für Angewandte Geologie*, **38**, pp. 89–93.

BORG, G., 1993, The Geita Gold Deposit, NW-Tanzania. Geology, Ore Petrology, Geochemistry and timing of Events. *Geologisches Jahrbuch D100*, pp. 545-595.

BORG, G., 1994, The Geita gold deposit, NW-Tanzania.- Geology, ore petrology, geochemistry and timing of events. *Geologisches Jahrbuch*, D100.

BORG, G. AND KROGH, T., 1999, Isotopic age data of single zircons from the Archaean Sukumaland Greenstone Belt, Tanzania. *Journal of African Earth Sciences,* 29/2, pp. 301–312.

BORG, G., LYATUU, D.R., RAMMLMAIR, D., 1990, Genetic aspects of the Geita and Jubilee Reef Archaean BIF-hosted gold deposits, Tanzania. *Geologische Rundschau Stuttgart*, 79/2, pp. 355–371.

BORG, G. AND MASOLLA, S.M.B., 1991, The lithotypes of the Sukumaland greenstone belt, NW-Tanzania: Geology and genetic evolution. In *IGCP Project No. 255 Conference "Gold and Platinoids in Central Africa"*, 11–13 September 1991, Bujumbura, Burundi, Extended Abstract Volume, final meeting, p. 6.

BORG, G. AND RITTENAUER, A., 2000, Syn-and Epigenetic Sulfides in Archaean BIFs of NW-Tanzania and their significance to gold mineralization. *Applied Mineralogy, Rammlmair et al. (eds) © 2000 Balkema, Rotterdam, ISBN 90 5809 163 5.*

BORG, G. AND SHACKLETON, R.M., 1997, The Tanzania and NE Zaire cratons. In *Greenstone Belts*, edited by M.J. de Wit and L.D. Ashwal (Oxford: Clarendon Press), pp. 608–619.

BROWN, A.J., CUDAY, T.J., WALTER, M.R., 2006, Hydrothermal Alteration at the Panorama Formation, North Pole Dome, Pilbara Craton, Western Australia, *Precambrian Research*, **151**, pp. 211-223.

BURNS, R., 1970, Mineralogical Applications of Crystal Field Theory, *Cambridge University Press,Cambridge*, p.224.

CAHEN, L., SNELLING, N.J., DELHAL, J., VAIL, J.R., 1984, *Geochronology and Evolution of Africa*, p. 512 (Oxford: Clarendon Press).

CAMPBELL, J. B., 1996, *Introduction to Remote Sensing*, p. 622 (New York: Guilford Press).

CARRANZA, E. J. M. AND HALE, M., 2002, Mineral imaging with Landsat Thematic Mapper data for hydrothermal alteration mapping in heavily vegetated terrain. *International Journal of Remote Sensing*, **23**, pp. 4827–4852.

CHAMBERLAIN, C.M., 2003, Geology and Genesis of the Bulyyanhulu Gold deposit, Sukumaland Greenstone belt, Tanzania, *DPhil. Thesis, university of London and for the Diploma of Imperial College of Science, Technology and Medicine*, p. 401.

CHAMBERLAIN, C.M. AND TOSDAL, R.M., 2007, U–Pb geochronology of the Lake Victoria Greenstone Terranes. Confidential report to project sponsors. Mineral Deposits Research Unit, University of British Columbia, Vancouver,Canada.

CHAVEZ, P.S. AND KWARTENG, A.Y., 1989, Extracting spectral contrast in Landsat Thematic Mapper image data using selective principal component analysis. *Photogrammetric Engineering and Remote Sensing*, **55**, pp. 339–348.

CHENG, Q., 2002, New versions of principal component analysis for image enhancement and classification. In *Geoscience and Remote Sensing Symposium, IGARSS '02. IEEE International*, 24–28 June 2002, Toronto, Ontario, Canada, **6**, pp. 3372–3374.

CHENG, Q., JING,L., AND PANAHI, A., 2006, Principal component analysis with optimum order sample correlation coefficient for image enhancement. *International Journal of Remote Sensing*, **27/16**, pp. 3387–3401.

CLARK, M.E., CARMICHAEL, D.M., HODGSON, C.J., FU.M., 1989, Wall-rock alteration, Victory Gold Mine, Kambalda, Western Australia: processes and P-T-XCO2 conditions of metasomatism. Economic Geology, 6, pp. 445-459.

CLARK, R. N., SWAYZE, G. A., GALLAGHER, A., KING, T. V. V., CALVIN, W. M., 1993, The US Gological Survey Digital Spectral Library, Version 1: 0.2 to 3.0 mm. US Geological Survey Open File Report, pp. 93–592.

CLARK, R. N., 1999, Spectroscopy of Rocks and Minerals, and Principles of Spectroscopy, in Manual of Remote Sensing, Volume 3 (Chapter 1), Remote Sensing for the Earth Sciences, (A.N. Rencz, ed.) *John Wiley and Sons, New York*, pp.3- 58.

CLIFFORD, T.N., 1970, The structural framework of Africa. In *African Magmatism and Tectonics*, edited by T.N. Clifford and I.G. Gass (Edinburgh: Oliver and Boyd), pp. 1–26.

CLOSE, D AND SCRIMGEOUR, I, R., 2013, Highlights from recent NTGS geoscience programs. Northern Territory Geological Survey, Alice Springs convention Centre, Northern Territory, *the Annual Geoscience Exploration Seminar (AGES)*, March, 2013, pp.19-20.

CLOUTIER, J., STEVENSON, R.K., BARDOUX, M., 2005, Nd isotopic, petrologic and geochemical investigation of the Tulawaka East gold deposit, Tanzania Craton. *Precambrian Research*, **109**, pp. 257–291.

CLOUTIS, E.A., 1996, Hyperspectral geological remote sensing: evaluation of analytical techniques. *International Journal of Remote Sensing*, **17**, pp. 2215–2242.

COLTELLI, M., FORNARO, G., FRANCESCHETTI, G., LANARI, R., MIGLIACCIO, M., MOREIRA, J.R., PAPATHANASSIOU, K.P., PUGLISI, G., RICCIO, D., SCHWABISCH, M., 1996, SIR-C/X-SIR multifrequency multipass interferometry: A new tool for geological interpretation. *Journal of Geophysical Research*, **101**, pp. 23127–23148.

CRIPPEN, R.E. AND BLOM, R.G., 2001, Unveiling the lithology of vegetated terrains in remotely sensed imagery. *Photogrammetric Engineering and Remote Sensing*, **67**, pp. 935–943.

CROSTA, A.P., DE SOUZA FILHO, C.R., AZEVEDO, F., BRODIE, C., 2003, Targeting key alteration minerals in epithermal deposits in Patagonia, Argentina, using ASTER imergery and principal component analysis. *International Journal of Remote Sensing*, **24**, pp. 4233–4240.

CROSTA, A. P. AND RABELO, A., 1993. Assessing Landsat TM for hydrothermal alteration mapping in central–western Brazil. In *Proceedings of the Ninth Thematic Conference on Geologic Remote Sensing*, 8–11 February 1993, Pasadena, California, USA, pp. 1053–1061.

CROSTA, A. P., SABINE, C., TARANIK, V., 1998, Hydrothermal alteration mapping at Bodie, California, Using AVIRIS Hyperspectral Data. *Remote Sensing of Environment*, **65**, pp. 309–19.

CROSTA, A.P. and MOORE, J., 1989, Enhancement of Landsat Thematic Mapper imagery for residual soil mapping in SW Minas Gerais State, Brazil: a prospecting case history in greenstone belt terrain. In *Seventh Thematic Conference on Remote Sensing for Exploration Geology,* Calgary, Alberta, Canada: Erim, pp. 1173–1187.

DANTZ, A., 1902, Die Reisen des Bergassessor Dr. DANTZ in Deutsch-Ostafrika in den Jahren 1898–1900. — Mitteilungen aus den deutschen Schutzgebieten.

DAVIS, J.C., 2002, *Statistics and Data Analysis*. (New York: John Wiley & Sons, Inc.).

DOLLAS, A., RANKIN, W.T., MCCRACKEN, D., 1998, A new algorithms for Golomb Ruler Derivation and Proof of the 19 Mark Ruler. *IEEE Transactions on Information Theory*, **44**, p. 379–382.

DUBÉ, B., AND GOSSELIN, P., 2007, GREENSTONE-HOSTED QUARTZ-CARBONATE VEIN DEPOSITS, IN GOODFELLOW, W.D., ED., Mineral Deposits of Canada: A Synthesis of Major Deposit-Types, District Metallogeny, the Evolution of Geological Provinces, and Exploration Methods: *Geological Association of Canada, Mineral Deposits Division, Special Publication No. 5*, pp. 49-73.

DUBÉ, B., MERCIER-LANGEVIN,P., HANNINGTON, M., LAFRANCE,B., GOSSELIN, G., GOSSELIN., 2007, The LaRonde Penna World-Class Au-Rich Volcanogenic Massive Sulfide Deposit, Abitibi, Québec: Mineralogy and Geochemistry of Alteration and Implications for Genesis and Exploration, Economic Geology, 102, pp.633-666.

EBERLE, D., 1988, Basic geophysical aspects of gold prospection in Nyanzian Greenstone Belts of Tanzania.. BRG internal report, Archive No. 101791, Tanzania-German Technical Cooperation, Hannover, Germany.

EILU, P. AND MIKUCKI, E.J., 1998, Alteration and primary geochemical dispersion associated with the Bulletin lode-gold deposit, Wiluna, Western Australia, *Journal of Geochemical Exploration*, **63**, pp. 73-103.

EIP, 2013, European Innovation Partinaship on Raw Materials. Annual Conference, December, 5, 2013.

ELISAIMON, E., 2008, A GIS-aided aerogeophysical, geological and geochemical investigation of the late Archaean granitoids in the Musoma-Mara Greenstone Belt, NE Tanzania. Unpublished MSc thesis, University of Dar es Salaam, Dar es Salaam, Tanzania, p. 109.

ELVIDGE, C.D. and LYON, R.J.P., 1985, Estimate of the vegetation contribution to the 1.65/2.22 μm ratio in airborne thematic-mapper imagery of the Virginia Range, Nevada. *International Journal of Remote Sensing*, **6**, pp. 75–88.

ENVI, 2009, Atmospheric correction module: QUAC and FLAASH user's guide, *ITT Visual Information Solutions* ,version 4.1.

FARMER, V.C., 1974, The Infra-Red Spectra of Minerals, (V.C. Farmer, ed.) *Mineralogical Society, London,* p.539.

FARR, T. G. AND KOBRICK, M., 2000, Shuttle Radar Topography Mission produces a wealth of data, EOS Trans. *AGU*, **81**, pp. 583–585.

FAUST, N. L., 1989, Image Enhancement. *In Supplement 5 of Encyclopedia of Computer Science and Technology, Volume 20,* edited by A. Kent and J. G. Williams (New York: Marcel Dekker, Inc.).

FRASER, S. J. AND GREEN, A. A., 1987, A software defoliant for geological analysis of band ratios. *International Journal of Remote Sensing*, **8/3**, pp. 525–532.

GARDNER, M., 1972, Mathmatical Games. *Scientific American*, **225**, pp. 108–112.

GEOLOGICAL SURVEY OF TANGANYIKA, 1952, *Geological map of East Africa, 1: 2.000.000, Coloured* (Dar es Salaam: Govt. Printer).

GHONEIM, E. and EL-BAZ, F., 2007, The application of radar topographic data to mapping of a mega-paleodrainage in the Eastern Sahara. *Journal of Arid Environments*, **69**, pp. 658–675.

GLOBAL LAND COVER FACILITY, 2012, Landsat Imagery, Overview. Landsat, link http://glcf.umd.edu/data/landsat/ (accessed 18 October 2012).

GLOBAL LAND COVER FACILITY, 2013, Earth Science Data Interface. http://glcf.umd.edu/ (accessed 01 June 2013).

GOETZ, A.F.H. AND ROWAN, L.C., 1981, Geologic remote-sensing. *Science*, **211**, pp. 781–791.

GOETZ, A.F.H., ROCK, B.N., ROWAN, L.C., 1983, Remote sensing for exploration: an overview.*Econ. Geol*. **78**, pp.573–590.

GHONEIM,E. AND ELBAZ,F., 2007, The application of Radar Topographic Data to Mapping of a Mega-paleodrainage in the Eastern Sahara. Journal of Arid Environments, **69**, pp. 658-675.

GOLDFARB, R.L., BAKER,T., DUBÉ B., GROVES, D,I., HART,C.J.R., GOSSELIN, P., 2005, Distribution, Character, and Genesis of Gold Deposits in Metamorphic Terranes. *Economic Geology*, pp. 407-450.

GOLOMB, S.W., 1972, How to number a graph. In *Graph Theory and Computing*, edited by R.C. Read (New York: Academic Press), pp. 23–37.

GOZZARD,J.R., 2006, Image Processing of ASTER Multispectral Data, *Geological Survey of Western Australia,* p. 51.

GRANTHAM, D.R., TEMPERLEY, B.N., and MCCONNELL, R.B., 1945, Explanation of the geology of degree sheet No. 17 (Kahama). *Geological Survey of Tanganyika, Bulletin*, **15**, pp. 1–32.

GRAY, I.M. AND MACDONALD, A.S., 1964, *Tanzania Quarter Degree Sheets 4NE and 5NW, Dodoma* (Tanganyika Geological Survey).

GROVES, D.I. AND FOSTER, R.P., 1993, Archean lode gold deposits. In: R.P. Foster (ed.) Gold Met allogeny and Exploration. New York, *Chapman & Hall*, pp.63-103.

GROVES, D.I, GOLDFARB, R.J,KNOX-ROBINSON, C.M, OJALA, J, GARDOLL,S, YUN, G.Y, HOLYLAND,P., 2000, Late-kinematic timing of orogenic gold deposits and significance for computer-based exploration techniques with emphasis on the Yilgarn Block, Western Australia, *Ore Geology reviews*, **17**, pp.1-38.

GUILBERT, J.M. AND PARK, C.E., 1986, The Geology of Ore Deposits, Long Grove, IL., reissued by Waveland Press, 2007.

GUPTA, R.P., 2003, *Remote Sensing Geology*, p. 655 (Heidelberg: Springer).

HALLIGAN, R., 1962, The Proterozoic rocks of western Tanganyika. *Geological Survey of Tanganyika, Bulletin*, volume **34**.

HANNINGTON, M.D., POULSEN, K.H., THOMPSON, J.F.H., AND SILLITOE, R., 1999,Volcanogenic gold in the massive sulfide environment: *Reviews in Economic Geology*, **8**, pp. 325–356.

HARPUM, J.R., 1954, Some problems of pre-Karoo geology of Tanganyika. In XIX Int. geol. Congr., 1942, Algiers, Algeria, Fasc. XX, pp. 209–239.

HARPUM J.R., 1970, Summary of the geology of Tanganyika; part V: Structural and geotectonics of the Precambrium. *Geological Survey of Tanganyika Mem.*, **1**, pp. 6–9.

HARRIS J.F., 1981, Summary of the geology of Tanganyika; part IV: Economic geology. *Geological Survey of Tanganyika Mem.* ,**1**.

HAUFF, P.L., 2005. Applied Reflectance Spectroscopy. *Spectral International INC*, version **4.1**, p. 70.

HEDENQUIST, J.W, ARRIBAS,R.A, ELISEO,G-U, 2000, Exploration for epithermal gold deposits. SEG reviews,**13**, p.245-277.

HENDERSON,G., 1960, Air-photo linearments in Mpanda area, Western Province, Tanganyika, Afrika. *American Association of Petroleum Geologists, Bulletin*, **44**, pp. 53–77.

http://glcf.umd.edu/,2013**,** Global Land Cover Facility, Earth Science Data Interface. (Website accessed on Date: 01.06.2013)

HOLMES, A. AND CAHEN, L., 1955, African geochronology. *Colon.Geol.min.Resour.*, **5/1**.

HUNT, G. R., 1979, Near-infrared (1.3–2.4 mm) spectra of alteration minerals—potential for use in remote sensing. *Geophysics*, **44**, pp. 1974–1986.

HUNT, G.R., 1977. Spectral signatures of particulate minerals in the visible and near-infrared. *Geophysics*, **42**, pp. 501–513.

IKINGURA, J.R., MUTAKYAHWA, M.K.D. , MAROBHE, I.M., MANYA, S., KAZIMOTO, E., KASANZU, C., and MSHIU, E.E., 2010, *Atlas of Gold Deposits in Tanzania.* University of Dar es Salaam and African Barrick Gold limited, p. 94.

ISHIKAWA, Y., SAWAGUCHI, T., IWAYA, S., HORIUCHI, M., 1976, Delineation of prospecting targets for Kuroko deposits based on modes of volcanism of underlying dacite and alteration halos: *Mining Geology*, **26**, pp.105–117.

JENSEN, J.R., 1996, *Introductory digital Processing*, p. 318 (New Jersey: Prentice Press).

KABETE, J., 2008, A new terrane-based tectonic subdivision of the Precambrian Shield of Tanzania and its significance to gold metallogeny. Unpublished PhD thesis, University of Dar er Salaam, Tanzania, p.353.

KABETE, J.M., GROVES, D.I., MCNAUGHTON, N.J., MRUMA, A.H., 2012, A New Tectonic and Temporal Framework for the Tanzanian Shield: Implications for Gold Metallogeny and Undiscovered Endowment. *Ore Geology Reviews,* **48**, pp.88-124.

KAZIMOTO, E., 2008, Study of integrated geochemical techniques in the exploration for gold in the North Mara Mines, Tanzania. *Unpublished MSc thesis, University of Dar es Salaam, Tanzania*, p. 188.

KINABO, B. D., HOGAN, J.P., ATEKWANA, E.A., ABDELSALAM, M.G., MODISI, M. P., 2008, Fault growth and propagation during incipient continental rifting: Insights from a combined aeromagnetic and Shuttle Radar Topography Mission digital elevation model investigation of the Okavango Rift Zone, northwest Botswana. *Tectonics*, **27**, p.1-16.

KLEIN, T.L. AND DAY, W.C., 1994, Descriptive and grade-tonnage models of Archaean low-sulfide Au-quartz veins and a revised grade-tonnage model of Homestake Au, *Open-file Report, United States Department of the Interior Geological Survey*, p.27

KREUZER,O.P., 2006, Textures, paragenesis and wall-rock alteration of lode-gold deposits in the Charters Towers district, north Queensland: implications for the conditions of ore formation, *Mineralium Deposita*, **40**, pp. 639-663.

KRÖNER, A., 1977, The Precambrian geotectonic evolution of Africa: Plate acccrection versus plate destruction. *Precambrian Research*, **4**, pp. 163–213.

KRUSE. F. A., LEFKOFF, A. B., BOARDMAN, J. B., HEIDEBRECHT, K. B., SHAPIRO, A. T., BARLOON, P. J., and GOETZ, A. F. H., 1993, The Spectral Image Processing System(SIPS) - Interactive visualization and analysis of imaging spectrometer Data. *Remote Sensing of Environment*, **44**, pp. 145–163.

KRUSE F. A., PERRY, S. L., CABALLERO, A., 2002, Integrated Multispectral and Hyperspectral Mineral Mapping, Los Menucos, Rio Negro, Argentina, Part II: EO-1 Hyperion/AVIRIS Comparisons and Landsat TM/ASTER Extensions: *In Proceedings 11th JPL Airborne Geoscience Workshop, Jet Propulsion Laboratory*, 4-8 March 2002 (This Volume).

KÜHN, S. AND GERMANN, K., 1992, Metallogenetisches Modell für die an eine archaische Eisenformation gebundene Gold-Sulfid-Vererzung von Geita, Tansania. *Z. angew. Geol*. **38**, 105-106.

KUMANAN, C.J., SARAVANAVEL, J., PALANIVEL, K., 2011, Virues of 3D GIS in Mapping Earth-Subsurfaces Geological System/Process. In *12th ESRI India User Conference,june,2011, volume **2**.*

KUSKY, T.M., RAMADAN, T.M., HASSAN, M.M., GABR ,S., 2011, Structural and tectonic evolution of El-Faiyum Depression, North Western Desert, Egypt, based on analysis of Landsata ETM+, and SRTM Data. *Journal of Earth Science*, **22/1**, pp. 75–100.

KWELWA, S., 2010, Geological characterization of the igneous intrusions and wall-rock alteration associated with gold mineralization at Golden Pride gold deposit, Nzega.Unpublished MSc thesis, University of Dar es Salaam, Tanzania.

LANG, J.R. AND BAKER, T., 2001, Intrusion-related gold systems: the present level of understanding, *Mineralium Deposita*, **36**, pp. 477–489.

LAPEARE,B.R., 2001, Re-logging of diamond drill core, chocolate reef (Buzwagi) property, Nzega greenstone belt, NW Tanzania. *A Summary report for Barrick Exploration Africa Ltd*, p.16.

LIU, L., ZHUANGA, D., ZHOUC, J. and QIUA, D., 2011, Alteration mineral mapping using masking and Crosta technique for mineral exploration in mid-vegetated areas: A case study in Areletuobie, Xinjiang (China). *International Journal of Remote Sensing*, **32(7)**, pp. 1931–1944.

LOBATO L.M. AND VIEIRA, W.REIS., 1998, Styles of Hydrothermal Alteration and Gold Mineralization associated with the Nova Lima Group of the Quadrilatero Ferrifero: Part II, The Archaean Mesothermal Gold-bearing Hydrothermal System, Revista Brasileira de Geociencias, **28**, pp. 355-366.

LOUGHLIN, W.P., 1991,Principal component analysis for alteration mapping. *Photogrammetric Engineering and Remote Sensing*, **57**, pp. 1163–1169.

LOWELL, J. D., 1991, The discovery of the La Escondida Orebody. In *Historical Perspectives of Genetic Concepts and Case Histories of Famous Discoveries*, edited by R. W. Hutchinson and R. I. Grauch (Lancaster, PA: Lancaster Press), pp. 300–313.

LOWMAN, P.D., 1991, Original shape of the Sudbury structure, Canada: A study with airborne imaging radar. *Canadian Journal of Remote Sensing*, **17/2**, pp. 152–161.

MABOKO, M.A.H. AND NAKAMURA, E., 1996, Nd and Sr isotopic mapping of the Archaean-Proterozoic boundary in southeastern Tanzania using granites as probes for crustal growth. *Precambrian Research,* **77**, pp. 105–115.

MABOKO, M.A.H., 2001, The geochemistry of Banded Iron Formations in the Sukumaland Greenstone Belt of Geita, northern Tanzania: Evidence for mixing of hydrothermal and clastic sources of the chemical elements. *Tanzania Journal of Science*, **27**, pp. 21–36.

MANYA, S. AND MABOKO, M.A.H., 2008, Geochemistry and geochronology of Neoarchaean volcanic rocks of the Iramba–Sekenke greenstone belt, central Tanzania. *Precambrian Research*, **163**, pp. 265–278.

MANYA, S. AND MABOKO, M.A.H., 2003, Dating basaltic volcanism in the Neoarchaean Sukumaland Greenstone belt of the Tanzania Craton using the Sm–Nd method: Implications for the geological evolution of the Tanzania Craton. *Precambrian Research*, **121**, pp. 34–45.

MANYA, S., MABOKO, A.H.M., and NAKAMURA, E., 2007, Geochemistry and Nd-isotopic compostion of potassic magmatism in the Neoarchaean Musoma-Mara Greenstone Belt, Northern Tanzania. *Precambrian Research*, **159**, pp. 231–240.

MANYA, S., 2004, Geochemistry and petrogenesis of volcanic rocks of the Neoarchaean Sukumaland greenstone belt, Northwestern Tanzania. *Journal of African Earth Sciences*, **40**, pp. 269–279.

MANYA, S., KOBAYASHI, K., MABOKO, M.A.H., NAKAMURA, E., 2006, Ion microprobe U–Pb zircon dating of the late Archaean metavolcanics and associated granites of the Musoma-Mara greenstone belt, northeast Tanzania: implications for the geological evolution of the Tanzania Craton. *Journal of African Earth Sciences*, **45**, pp. 355–366.

MANYA, S., 2008, Geochemistry and Nd-Isotopic composition of high silica rhyolites in the Neoarchaean Musoma-Mara Greenstone Belt, Northern Tanzania: Evidence for the presence of older continental crust. *Tanzania Journal of Science*, **34**, pp. 53–62.

MARGHANY, M. AND HASHIM, M., 2010, Lineament mapping using Multispectral Remote Sensing Data. *Research Journal of Applied Science*, **5/2**, pp. 126–130.

MARS, J.C., ROWAN, L.C., 2010. Spectral assessment of new ASTER SWIR surface reflectance data products for spectroscopic mapping of rocks and minerals. *Remote Sens. Environ*. **114**, pp. 2011–2025.

MASOUD, A.A. AND KOIKE, K., 2011, Auto-detection and integration of tectonically significant lineaments from SRTM DEM and remotely-sensed geophysical data. *International Journal of Photogrammetry and Remote Sensing*, **66**, pp. 818–832.

MATTHEW, M. W., ADLER-GOLDEN, S. M., BERK, A., RICHTSMEIER, S. C., LEVINE, R. Y., BERNSTEIN, L. S., ACHARYA, P. K., ANDERSON, G. P., FELDE, G. W., HOKE, M. P., RATKOWSKI, A., BURKE, H.-H., KAISER, R. D., MILLER, D. P., 2000, Status of atmospheric correction using a MODTRAN4-based algorithm. *SPIE Proceedings, Algorithms for Multispectral, Hyperspectral, and Ultraspectral Imagery VI*, **4049**, pp. 199–207.

MCCONNELL, R.B., 1950, Outline of geology of Ufipa and Ubende. *Geological Survey of Tanganyika, Bulletin*, **19**.

MCFALL, G. AND SINGHROY, V.H., 1989, Remote sensing applications to neotectonics studies in southern Ontario. In *SeventhThematic Conference on Remote Sensing for Exploration Geology,* Calgary, Alberta, Canada, pp. 533–546.

MESSO, C.W.A., 2004, Geochemistry of Neoarchaean volcanic rocks of the Ikoma area in the Kilimafedha greenstone belt, Northwestern Tanzania. MSc thesis, University of Dar es Salaam, Tanzania, p. 101.

MIKUCKI, E.J. AND RIDLEY, J.R. 1993. The hydrothermal fluid of Archean lode-gold deposits at different metamorphic grades: compositional constraints from ore and wallrock alteration assemblages. In: R. Kerrich (ed.) Western Australian Gold Deposits, *Mineralium Deposita*, **28**, pp.469-481

MOORE,F., RASTMANESH,F., ASADI, H., MODABBERI,S., 2008, Mapping mineralogical alteration using principal-component analysis and matched filter processing in the Tabak area, north-west Iran, from ASTER data, *International Journal of Remote Sensing*, **29**, pp. 2851-2867.

MORRIS, K., 1991. Using knowledge-base rules to map the three-dimensional nature of geologic features. *Photogrammetric Engineering and Remote Sensing*, **57(9)**, pp. 1209–1216.

MSHIU, E, E. AND MABOKO, M.A.H, 2012, Geochemistry and petrogenesis of the late Archaean high-K granites in the southern Musoma-Mara Greenstone Belt: Their influence in evolution of Archaean Tanzania Craton. *Journal of African Earth Sciences* ,**66-67**, pp.1–12.

MTIBILO, E.S., 2007, Lithological and geochemical controls for gold mineralization at Nyamulilima hill gold deposits of the Sukumaland Greenstone belt, Tanzania. Unpublished MSc thesis, University of Dar es Salaam, Tanzania.

MTORO, M., 2007, Geochemical investigation of metavolcanic rocks of the Musoma-Mara greenstone belt in the Suguti area, Northeast Tanzania. Unpublished MSc. thesis, University of Dar es Salaam, Tanzania, p. 105.

MTORO, M., MABOKO, M.A.H., MANYA, S., 2009, Geochemistry and geochronology of the bimodal volcanic rocks of the Suguti area in the southern part of the Musoma-Mara Greenstone Belt, Northern Tanzania. *Precambrian Research*, **174**, pp. 241–257.

MORRIS, R.V., GOLDEN, D.C., MING, D.W., SHELFER, T.D., JORGENSEN, L.C., BELL, J.F., GRAFF T.G., MERTZMAN, S.A., 2001. Phyllosilicate-poor palagonitic dust from Mauna Kea volcano (Hawaii): A mineralogical analogue for magnetic martian dust? *Journal of geophysical research,* **106***, pp.5057-5083.

MUELLER. AG. AND GROVES. O.J., 1991. The classification of Western Australian greenstone-hosted gold deposits according to wallrock-alteration assemblages: Ore Geology Revicws, **6**, p. 291-332.

MUHONGO, S., HAUZENBERGER, C., AND SOMMER, H., 2003, Vestiges of Mesoproterozoic events in the Neoproterozoic Mozambique Belt: the East Africa perspective in the Rodinia puzzle. *Gondwana Research*, **6**, pp. 409–416.

NAYLOR, W.I., 1961, Geology of the Geita district, Quarter degree sheet 20 and 32. Rec. *Geological Survey of Tanganyika*, **9**, 13–18.

NEUMANN, M., FERRO, L., AND REIGBER, A., 2010, Estimation of forest structure, ground, and canopy layer characteristics from Multibaseline Polarimetric Interferometric SAR Data. *IEEE Transactions on Geoscience AND Remote Sensing*, **48/3**.

PALACHE, C, H. BERMAN, AND C. FRONDEL, 1951, Dana's system of mineralogy, (7th edition), **2**, pp. 482–486.

PAUL, N.D. AND GOLDSMITH, A.C., 2012, Technical Report on the gold project, Geita Region, Tanzania. Prepared on behalf of Tembo Gold Corp, The Mineral Corporation, p. 77.

PEARSON, R. L. AND MILLER, L. D., 1972, Remote sensing of standing crop biomass for estimation of the productivity of the shortgrass prairie, Pawnee national grasslands, Colorado. In *The 8th International Symposium on Remote Sensing of th Environment*, pp. 1355–1379.

PETERS, S. G., 1987, Geology, fluid characteristics, lode controls and oreshoot growth in mesothermal gold-quartz veins, northeastern Queensland. *PhD thesis, James Cook University, Townsville*

PETERS, S. G. AND GOLDING, S. D. (1989) Geologic, fluid inclusion and stable isotope studies of granitoid-hosted goldbearing quartz veins, Charters Towers, northeastern Australia. in The Geology of Gold Deposits: The Perspective in 1988 (Keays, R. R. et al., eds.). *Econ. Geol. Monogr*, **6**, pp. 260–273.

PHILLIPS,G.N. AND GROVES, D.I., 1984, Fluid access and fluid-wallrock interaction in the genesis of the Archaean gold-quartz vein deposit at Hunt mine, Kambalda, Western Australia. *In: R.P. Foster (Editor), Gold '82: the Geology, Geochemistry and Genesis of Gold Deposits. Balkema, Rotterdam*, pp. 389-416.

PINNA, P., MUHONGO, S., MCHARO, B.A., LE GOFF, E., DESCHAMPS, Y., RALAY, F., MILESI, J.P., 2004, Geology and Mineral Map of Tanzania 1:2000000 (Dépôt légal 2ᵉ trimester).

PIRAJNO, F., 2009, *Hydrothermal Processes and Mineral Systems*, p. 1250 (Springer Science and Business Media).

POULSEN, K.H., ROBERT, F., DUBÉ, B., 2000, Geological Classification of Canadian gold deposits: *Geological Survey of Canada Bulletin **540***, p.106.

QUENNELL, A.M., MC KINLAY, A.C.M.L, AITKEN, W.G., 1956, *Summary of the Geology of Tanganyika: Part I; Introduction and Stratigraphy*, p. 264 (Dar es Salaam: Geological Survey of Tanganyika, Memoir 1).

RAMMLMAIR, D., HDHNDORF, A., BORG, G., HIZA, G.N., 1990, Nouvelles datations isotopiques des granites et des gabros de la region 'Greenstone'-Granitique du Sukumaland, N.W.-Tanzanie. In *15th Colloquium of African Geology*, Nancy, France, **Abstract Volume**,p. 43.

RAMMLMAIR, D.,1991, A preliminary report on the geology of the Siga Hills, NW Tanzania. Part III:Characteristics of granitoids from the Siga Hills project area. — *Tanzanian-German Technical Cooperation open file report*, 11505/91,p .71.

RANJBAR, H. AND HONARMAND, M., 2007, Exploration for base metal mineralization in the Southern part of the Central Iranian Volcanic Belt by using ASTER and ETM+ Data. *Journal of Engineering Science*, **3**, pp. 23–34.

RANJBAR, H., MASOUMI, F., CARRANZA, E. I. M., 2011, Evaluation of geophysics and Spaceborne Multispectral Data for alteration mapping in the Sar Cheshmeh Mining Area, Iran. *International Journal of Remote Sensing*, **32**, pp. 3309–3327.

ROBERT, F., BROMMECKER, R., BOURNE, B.T., DOBAK, P.J., MCEWAN, C.J., ROWE, R.R., ZHOU, X., 2007, Models and Exploration methods for Major Gold Deposit Types, In Proceedings of Exploration 07: Fifth Decennial International Conference on Mineral Exploration, *Ore Deposits and Exploration Technology*, paper 48, pp. 691-711.

ROCCA, F AND REID,D.G., 2004, Tulawaka Mine Technical Report, *Pangea Minerals Limited*.

RODRIGUEZ, E., MORRIS, C.S., and BELZ, J.E., 2006, A global assessment of the SRTM Perfomance. *Photogravimetric Engineering and Remote Sensing*, **72**, pp. 249–260.

ROUSE, J. W., HAAS, R. W., SCHELL, J. A., DEERING, D. W., and HARLAN, J. C., 1974, Monitoring the vernal advancement and retrogradation (greenware effect) of natural vegetation., NASA/GSFCT, Type 3, Final Report. Greenbelt, MD, USA.

ROWAN, L.C. AND MARS, J.C, 2003, Lithological Mapping in the Mountain Pass, California area using Advanced Spaceborne Thermal Emission and Reflection Radiometer (ASTER) data, Remote Sensing of Environment, 84, pp. 350-366.

RYAN,L AND SPEERS, R., 2002, The Geology and Structural Controls on mineralization at Nyankanga Deposit, Geita, Tanzania. *Geita Gold mine Ltd*, p .42.

SABINS, F.F., 1996, Remote Sensing: Principles and Interpretation, (New York: Worth publishers), p.494.

SABINS, F.F., 1999, Remote sensing for mineral exploration. Ore Geology Reviews 14, 157–183.N.W.-Tanzanie. In *15th Colloquium of African Geology*, Nancy, France, Abstract Volume, p. 43.

SAHA, K.K., DAVE, H.D., MITRA, D.S., 2006, Study of tectonic elements of Punjab Plains from satellite imagery, drainage network and gravity anomalies. In *6th International Conference and Exposition on Petroleum Geophysics, Kolkata, India*,pp.43-48.

SANFO, Z.A.K., 2002, Tulawaka Soil Orientation Survey Report, *Barrick Exploration Africa Limited*.

SANTORO, N., ATKINSON, M.D., URRUTIA, J., 1986, Integer sets with distinct sums and differences and carrier frequency assignments for nonlinear repeaters. *IEEE Transactions on Communications*, **34**, pp. 614–617.

SEGAL, D. B., 1983, Use of Landsat Multispectral Scanner Data for the definition of limonitic exposures in heavily vegetated areas. *Economic Geology*, **78**, pp. 711–722.

SEMKIWA P.M, 2005, Opportunities for Mineral Resource Development in Tanzania. Ministry of Energy and Minerals, Republic of Tanzania (4th Edition), p. 130.

SHEARER, J.B., 1990, Some new optimum Golomb Rulers. *IEEE Transactions on Information Theory*, **It-36**, p. 379–382.

SILLITOE R.H, (1991), Intrusion-related gold deposits. In: Foster RP (ed) Gold metallogeny and exploration. *Blackie, Glasgow*, pp 165-209

SILLITOE, R.H. AND THOMPSON, J.F.H, 1998, Intrusion-Related Vein Gold Deposits: Types, Tectono-Magmatic Settings and Difficulties of Distinction from Orogenic Gold Deposits, *Resource Geology*, **48**, pp.238-250.

SINGH, A. AND HARRISON, A., 1985, Standardized principal components. *International Journal of Remote Sensing*, **6**, p. 883.

SLATER, J. A., GARVEY, G., JOHNSTON, C., HAASE, J., HEADY, B., KROENUNG, G. AND LITTLE, J., 2006,
The SRTM data "finishing" process and products. Photogrammetric Engineering & Remote Sensing, 72, pp. 237-247.

SPATZ, D. M., 1997, Remote sensing characteristics of the sediment- and volcanic-hosted precious metal system: Imagery selection for exploration and development. *International Journal of Remote Sensing*, **18**, pp. 1413–1438.

SPURR, A.M.M., 1952, Mbeya District. *Annu.Rep.geol.Surv.Tanganyika*, **1950**, pp. 40–42.

STOCKLEY, 1936, Geology of the south and southeastern regions of the Musoma District. *Geological Survey of Tanganyika,Short paper*, **13**, pp. 1–48.

STOCKLEY., 1948, The geology and mineral resource of Tanganyika territory.*Geogical Survey of Tanganyika, Bulletin,* **20**, pp. 1–37.

STOCKLY, G.M., 1943, The pre-Karoo stratigraphy of Tanganyika. *Geological Magazine*, **53**, pp. 161–170.

SURVEY AND MAPPING DIVISION, MINISTRY OF NATURAL RESOURCES AND TOURISM, THE UNITED REPUBLIC OF TANZANIA, 1996, Forest Resources Management Project. *Printed in UK on behalf of Surveys and Mapping Division, Ministry of Lands, Tanzania*.

TANGESTANI, M. H., MAZHARI, N., AGAR, B., MOORE, F., 2008, Evaluating Advanced Spaceborne Thermal Emission and Reflection Radiometer (ASTER), data for alteration zone enhancement in a semi-arid area, Northern Shahr-e-Babak, SE Iran. *International Journal of Remote Sensing*, **29**, pp. 2833–2850.

TAYLOR, P., 1977, *Quantitative Methods in Geography : An Introduction to Spatial Analysis*. (Boston, Massachusetts: Houghton Mifflin Company).

TESHA, A.L., 2003, Removal of barriers to introduction of cleaner artisanal gold mining and extraction technologies. Global Mercury Project-Tanzania. Dar es salaam.

THIBOUTOT, H., 1991, Bulyanhulu Gold Project, Kahama District – Technical Report by *Placer Dome (Kahama) Ltd*, p. 24.

THOMPSON, A.J.B. AND THOMPSON, J.F.H., 1996. Atlas of alteration: a field and petrographic guide to hydrothermal alteration minerals. *Geological Association of Canada, Mineral Deposits Division*.

THOMPSON, A.J.B., HAUFF, P.L., ROBITAILLE A.J., 1999, Alteration mapping in exploration: Application of short-wave infrared (SWIR) spectroscopy: SEG Newsletter, **39**, p. 1, pp.16–27.

THOMPSON, P, H., 2002, Second Report on the Petrography of Tulawaka Samples: Implications for Metamorphic Conditions, Stratigraphy, Deformation and Mineralization, *Peter H. Thompson Geological Consulting Ltd*.

TREADGOLD, T, 2012, Prospecting From Space. *Mining Journal of 23 November, 2012*, p. 10.

TRIPATHI, N., GOKHALE, K., SIDDIQU, M., 2000. Directional morphological image transforms for lineament extraction from remotely sensed images. *International Journal of Remote Sensing*, **21/17**, pp. 3281–3292.

VAN DER MEER, F.D., VAN DER WERFF, H.M.A., VAN RUITENBEEK, F.J.A., HECKER, C.A., BAKKER, W.H., NOOMEN, M.F., VAN DER MEIJDE, M., CARRANZA, E.J.M., 2012, Multi-and hyperspectral geologic remote sensing: A review. *International Journal of Applied Earth Observation and Geoinformation*, **14**, pp. 112–128.

VIEWSPEC PRO., 2000, Software applications, *ASD Inc. Boulder, Colorado*

VOS, I. M. A., BIERLEIN. F. P., STANDING, J. G., Davidson, G.J., 2009, The geology and mineralization at the Golden Pride gold deposit, Nzega Greenstone Belt, Tanzania. *Mineralium Deposita*, **44/7**, pp. 751–764.

WADE, F.B. AND OATES, F., 1938, An explanation of degree sheet No.52 (Dodoma). Geological SurveyTanganyika Short Paper 17, Dar Es Salaam, Tanzania.

WEISER, T., 1986, Microscopic Analysis of Sulfide Associated Ores in selected Rock Samples from Gold Occurrences in the Lake Victoria Region, Tanzania: Tanzania-Germany Technical cooperation, *open file report, BGR* , Hannover, pp. 1-12..

WALTON, G. AND JAMBOR, J, 1998, *Pathways' 98, Extended Abstracts Volume*, Vancouver, Canada. British Columbia & Yukon Chamber of Mines/Society of Economic Geologists, p. 248.

WESSELS, K. J., PRINCE, S. D., FROST, P. E., ZYL, D. V.,2004, Assessing the effects of human-induced land degradation in the former homelands of northern South Africa. *Remote Sensing of Environment*, **91**, pp. 47–67.

WILFORD, J. AND CREASEY, J., 2002, Landsat Thermatic Mapper. In *Geophysical and Remote Sensing Methods for Regolith Exploration*, edited by E. Rapp (Open File report), pp. 6–12.

WIRTH, K.R., VERVOOT, J.D., WEISBERGER, B., 2004, Origin and evolution of the Kilimafedha greenstone belt, eastern Tanzania Craton: Evidence from Pb isotopes. *Geological Society of America Abstracts with Programs*, **36**, p. 244.

WWW.EC.EUROPA.EU, 2013, European Innovation Partinaship, 2013, HTTP://EC.EUROPA.EU/ENTERPRISE/POLICIES/RAWMATERIALS/INNOVATIONPARTNERSHIP/INDEX_EN.HTM , IN THE DATE OF 13.11.2013.

YEATS, C.J. AND VANDERHOR, F., 1998, Archaean lode-gold deposits, *AGSO Journal of Australian geology and Geophysics*, **17**, pp. 253-258.

YOUSSEF,A.M., 2009, Mapping the mega paleodrainage basin using Shuttle Radar Topography Mission in Eastern Sahara and its impact on the New Development Projects in Southern Egypt. *Geospatial Information Science*, **12/3**, pp. 182–190.

YU, L., PORWAL, A., HOLDEN, E., DENTITH, M.C., 2011, Suppression of vegetation in multispectral remote sensing images. *International Journal of Remote Sensing*, **32**, pp. 7343–7357.
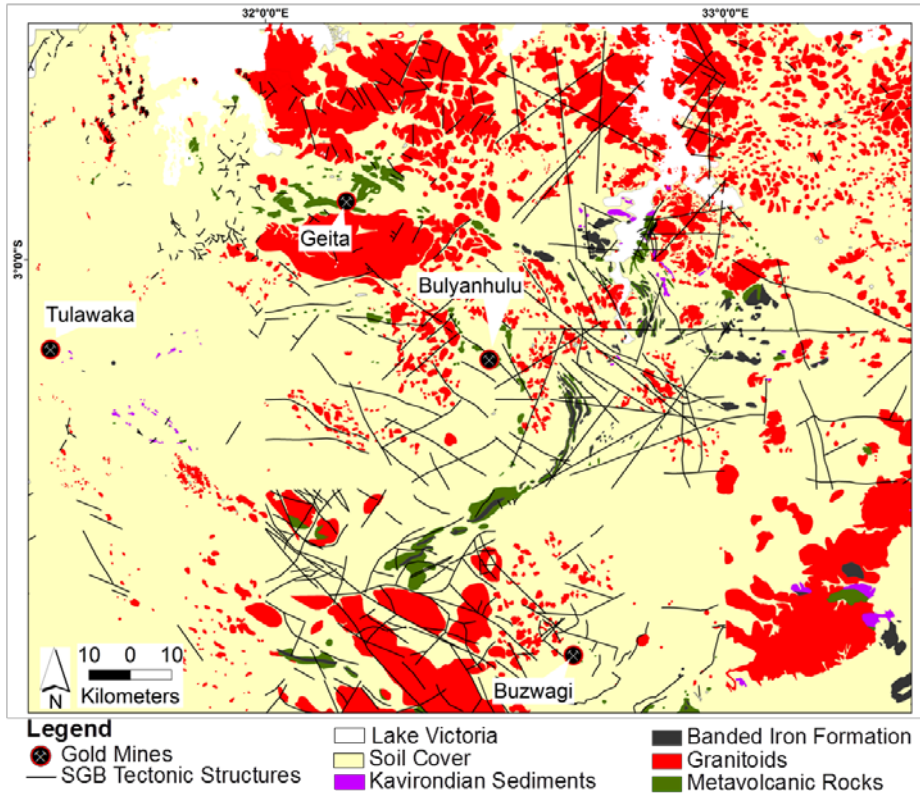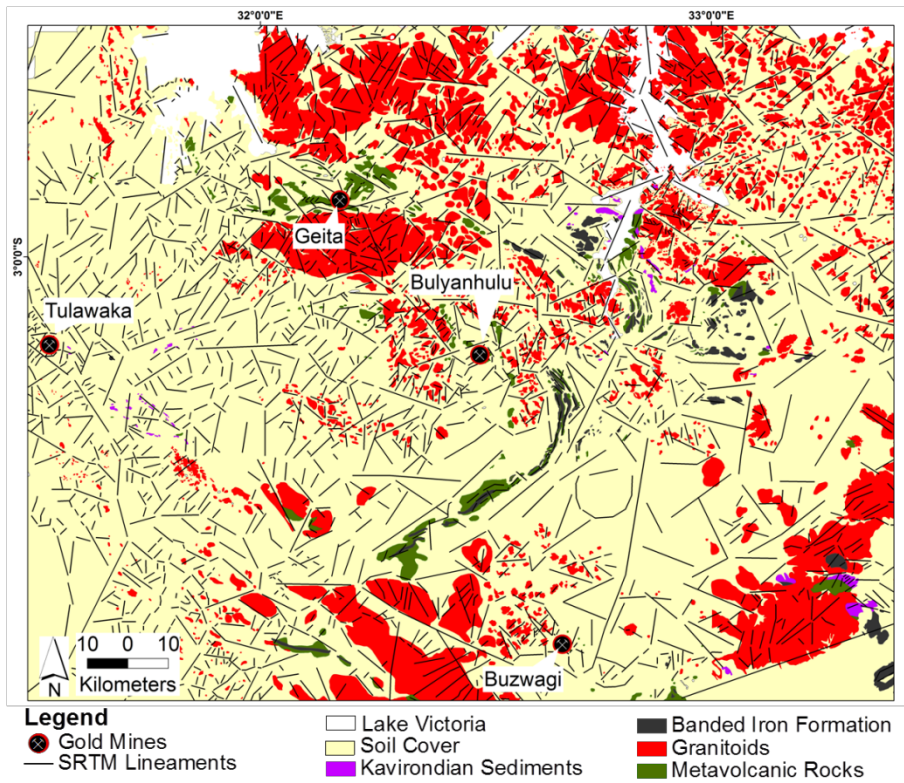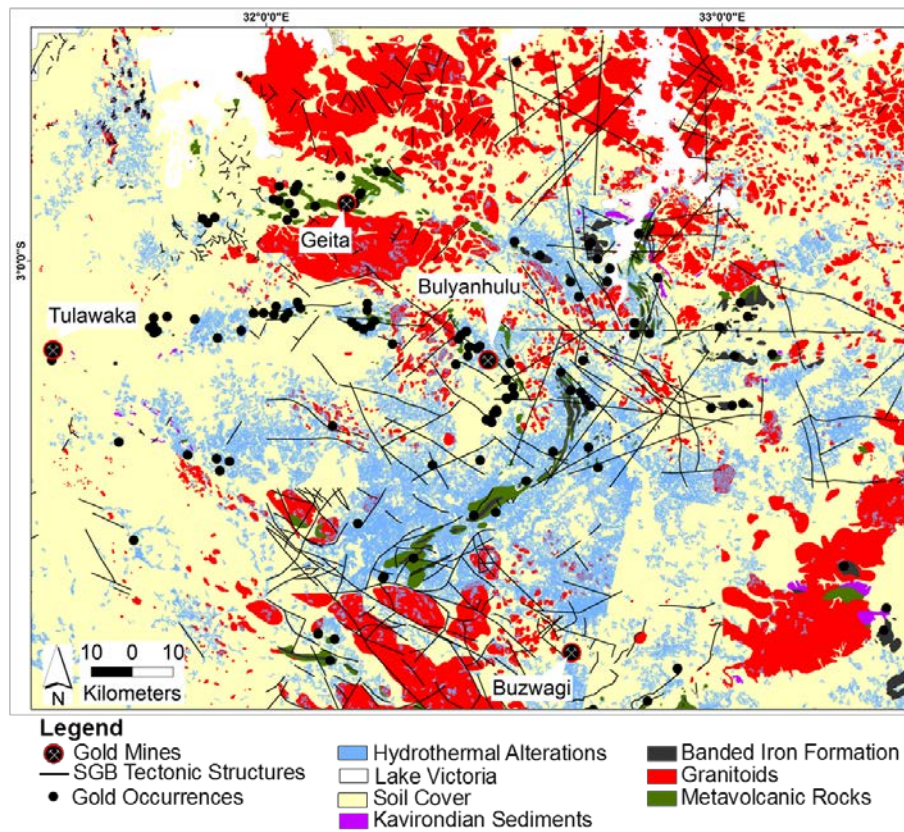
Appendix 1 The SGB geological map overlain with the documented tectonic lineaments
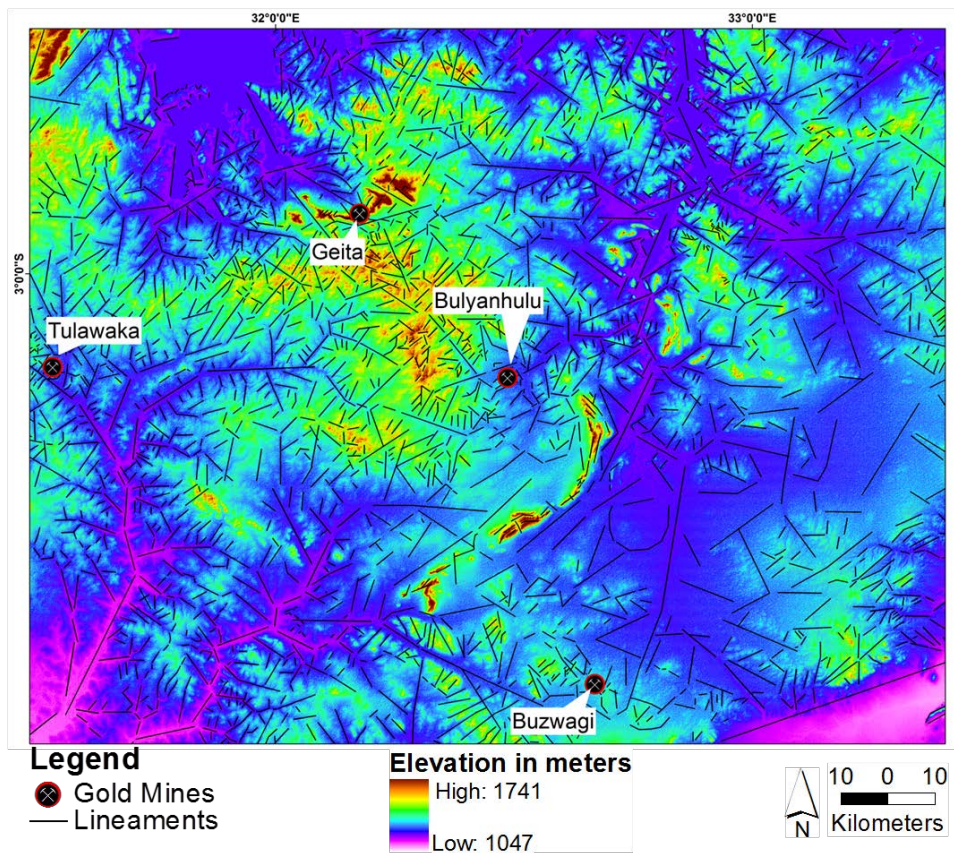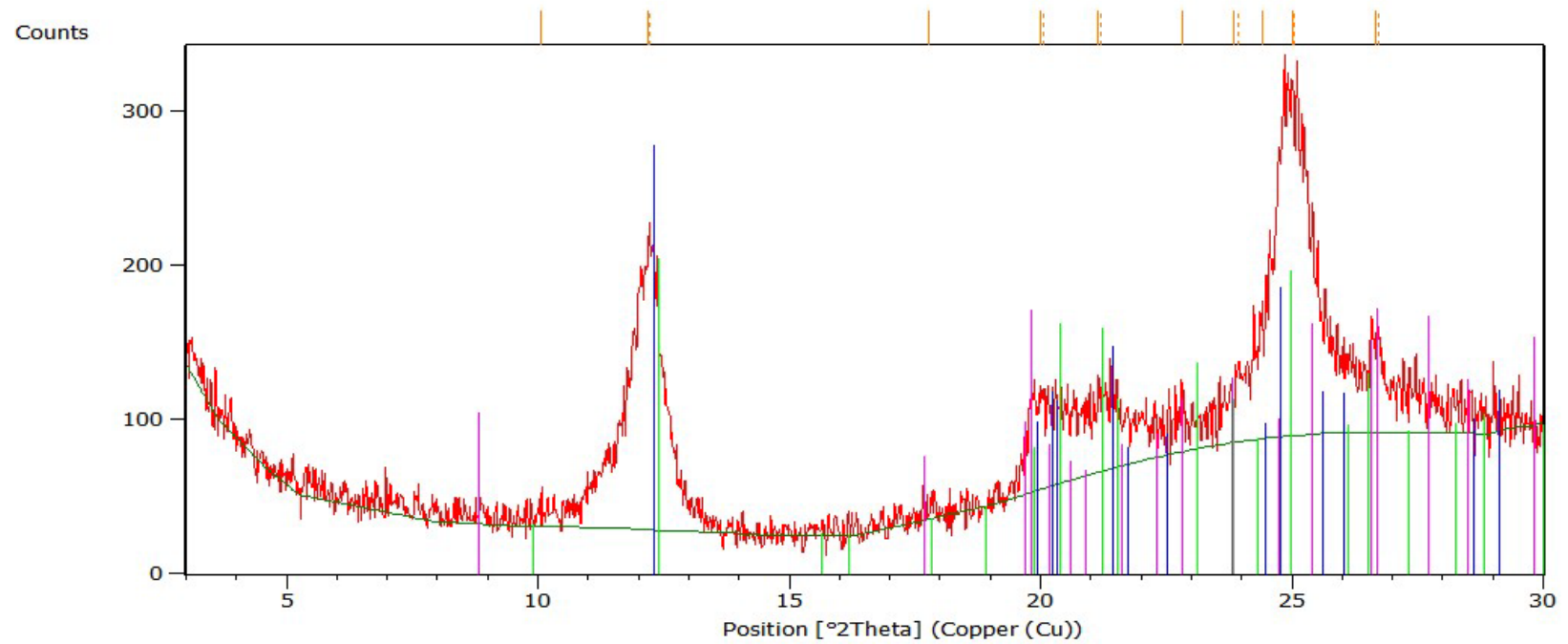

Appendix 2 The SGB SRTM image overlain with the extracted SRTM lineaments

Appendix 3 The SGB geological map overlain with the extracted SRTM lineaments
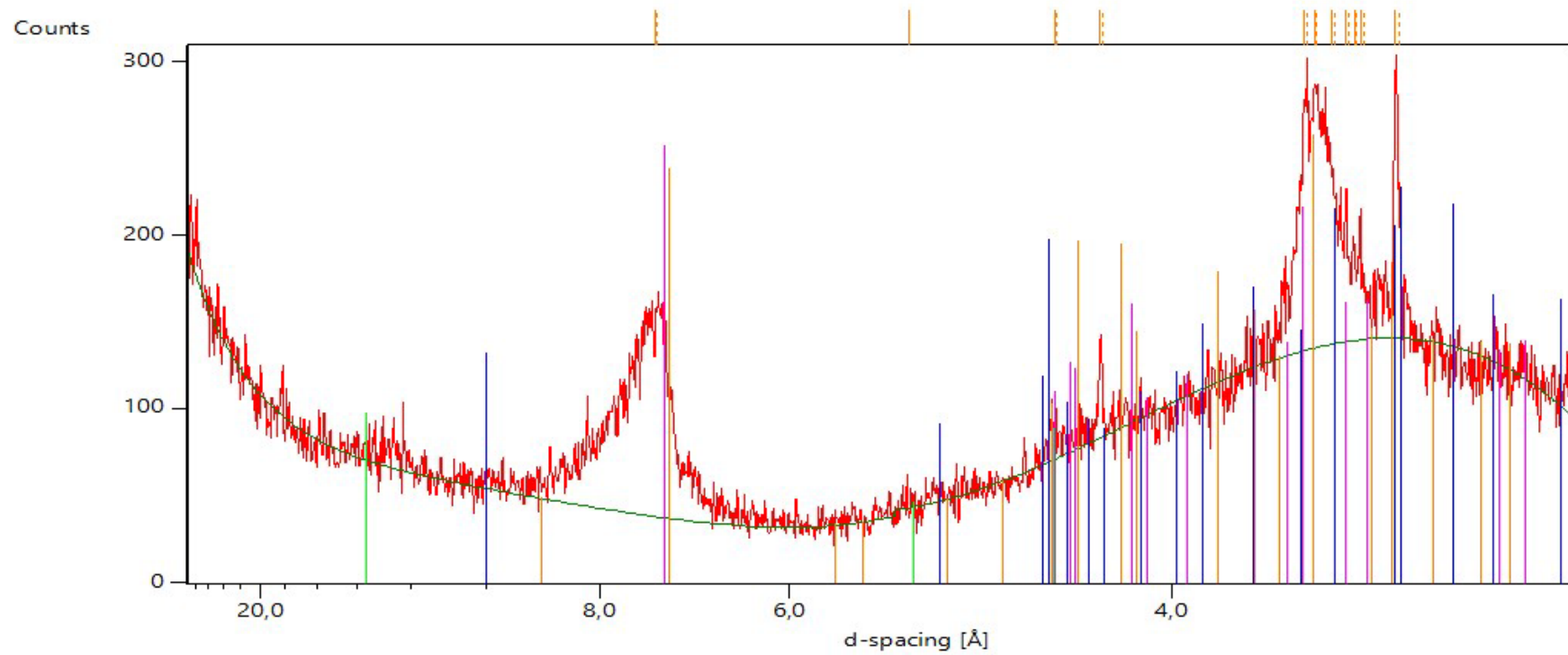

Appendix 4 The SGB geological map overlain with the previous documented tectonic lineaments and hydrothermal alteration from Landsat ETM+ data
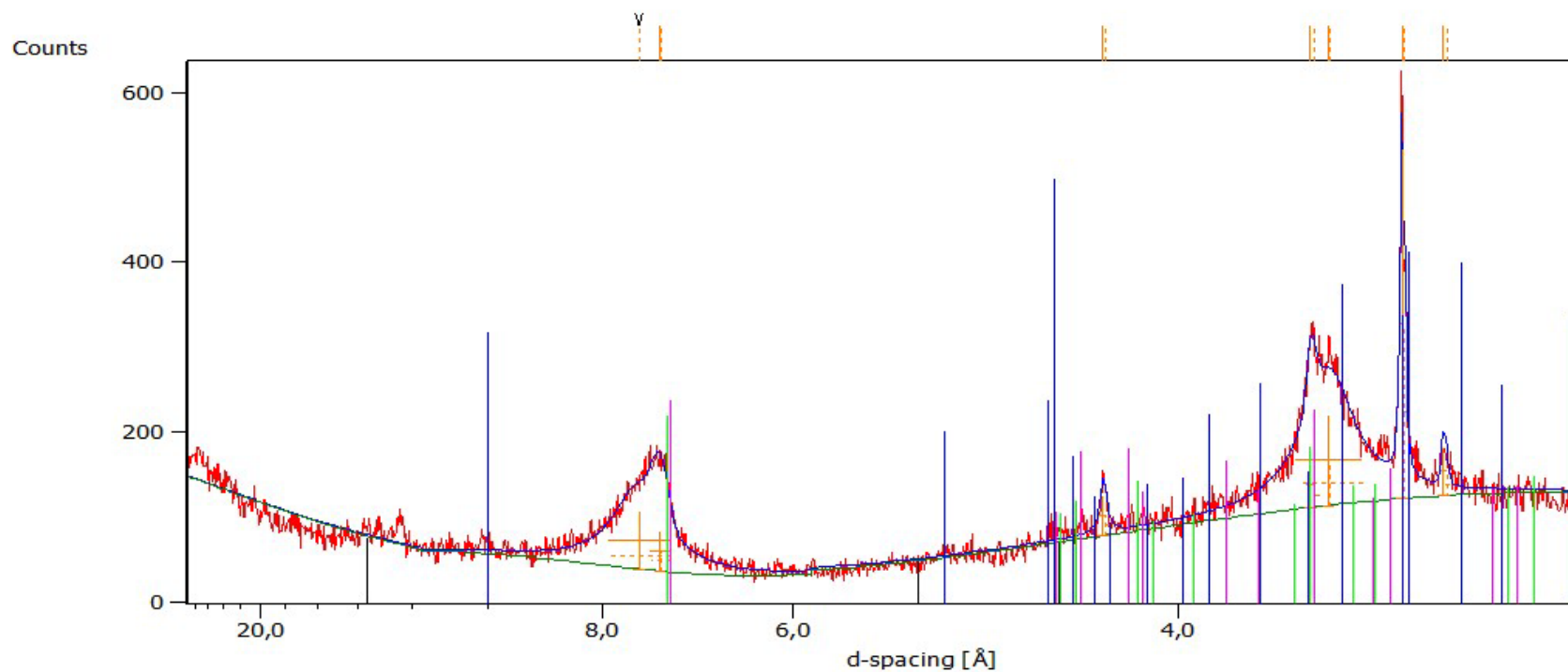
Appendix 5 Diffractogram of clay minerals in KHA 24 sample

Appendix 6 Diffractogram of clay minerals in KHA 27 sample

Peak List

01-070-3754; Illite; K (Al4 Si2 O9 (O H)3)	
00-029-1498; Montmorillonite-15A; Na0.3 (Al , Mg)2 Si4 O10 (O H)2 !4 H2 O	
01-076-0631; Nacrite; Al2 Si2 O5 (O H)4	
01-078-2110; Kaolinite; Al4 (O H)8 (Si4 O10)	

Appendix 7 Diffractogram of clay minerals in KHA 28 sample
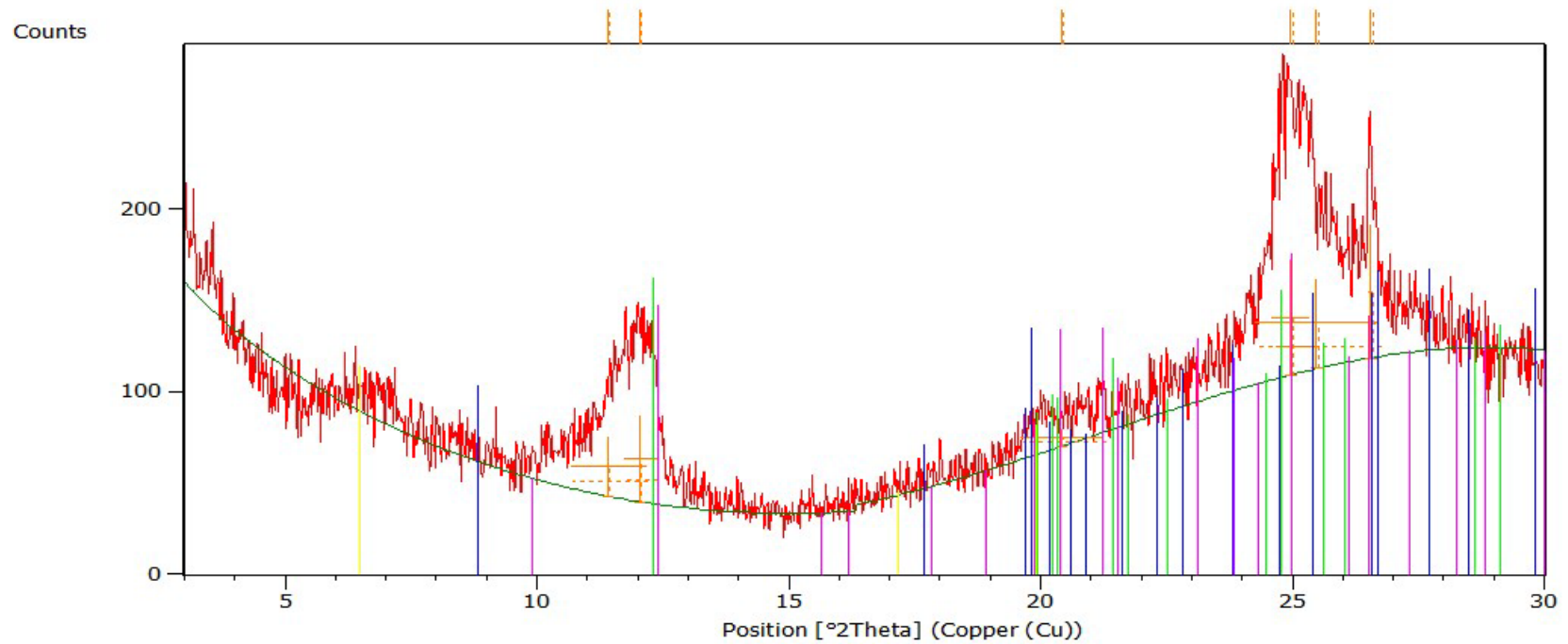
Peak List

01-070-3754; Illite; K (Al4 Si2 O9 (O H)3)

01-076-0631; Nacrite; Al2 Si2 O5 (O H)4

01-089-6538; Kaolinite; Al2 (Si2 O5) (O H)4

00-029-1498; Montmorillonite-15A; Na0.3 (Al , Mg)2 Si4 O10 (O H)2 !4 H2 O

Peak List

01-070-3754; Illite; K (Al4 Si2 O9 (O H)3)

01-076-0631; Nacrite; Al2 Si2 O5 (O H)4

01-078-2110; Kaolinite; Al4 (O H)8 (Si4 O10)

00-029-1498; Montmorillonite-15A; Na0.3 (Al , Mg)2 Si4 O10 (O H)2 !4 H2 O

Appendix 8 Diffractogram of clay minerals in KHA 29 sample

Appendix 9 Diffractogram of clay minerals in KHA 30 sample

Appendix 10 Diffractogram of clay minerals in KHA 32 sample
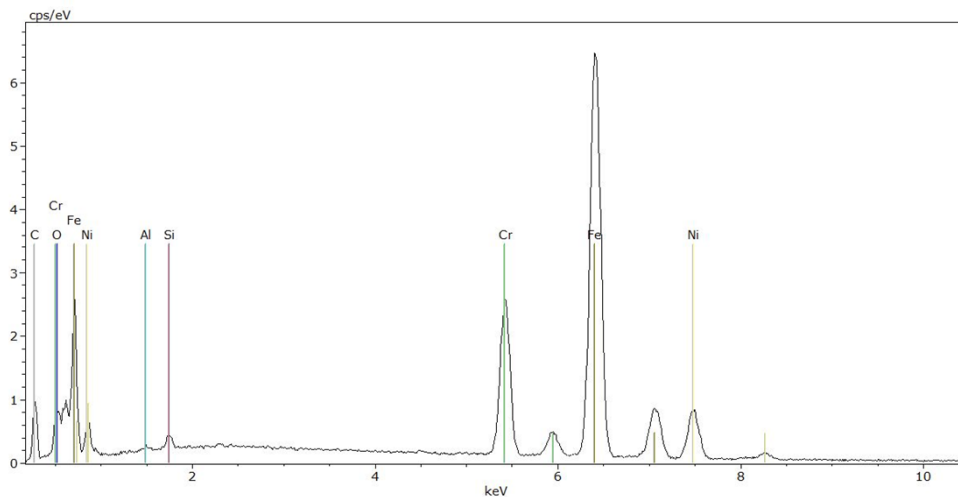
Element	Atomic Concentrations (%)	Sigma(%)
C	0,0	0,0
O	6,6	1,1
Al	0,5	0,1
Si	1,0	0,2
Cr	14,6	1,2
Fe	64,7	5,3
Ni	12,7	1,2
SUM	100,0	

Appendix 11 KHA 23, SEM results indicating Chromite and possible Fe-Oxides
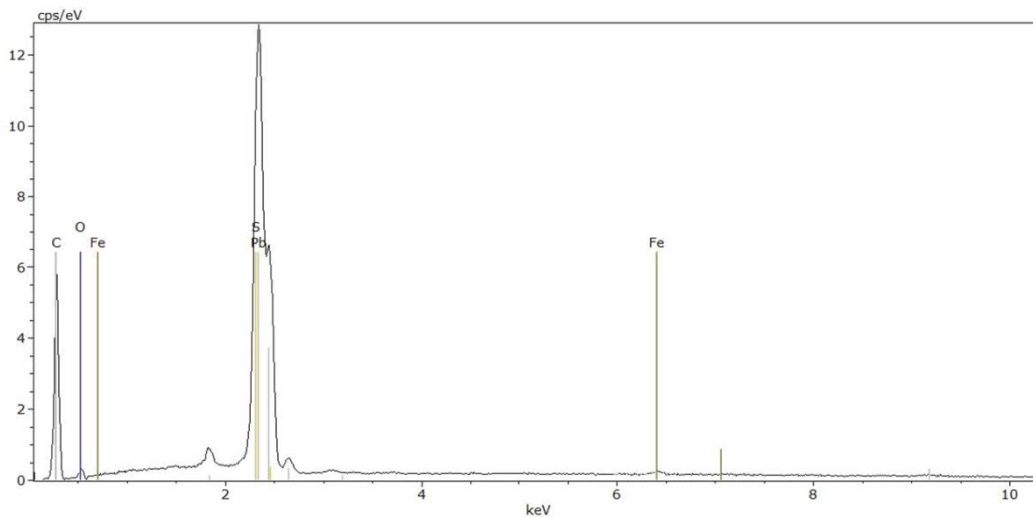
Element	Atomic Concentrations (%)	Sigma(%)
C	0,0	0,0
O	14,9	1,4
S	43,6	1,4
Fe	2,0	0,2
Pb	39,4	6,7
SUM	100,0	

Appendix 12 KHA 23, SEM results, Galena
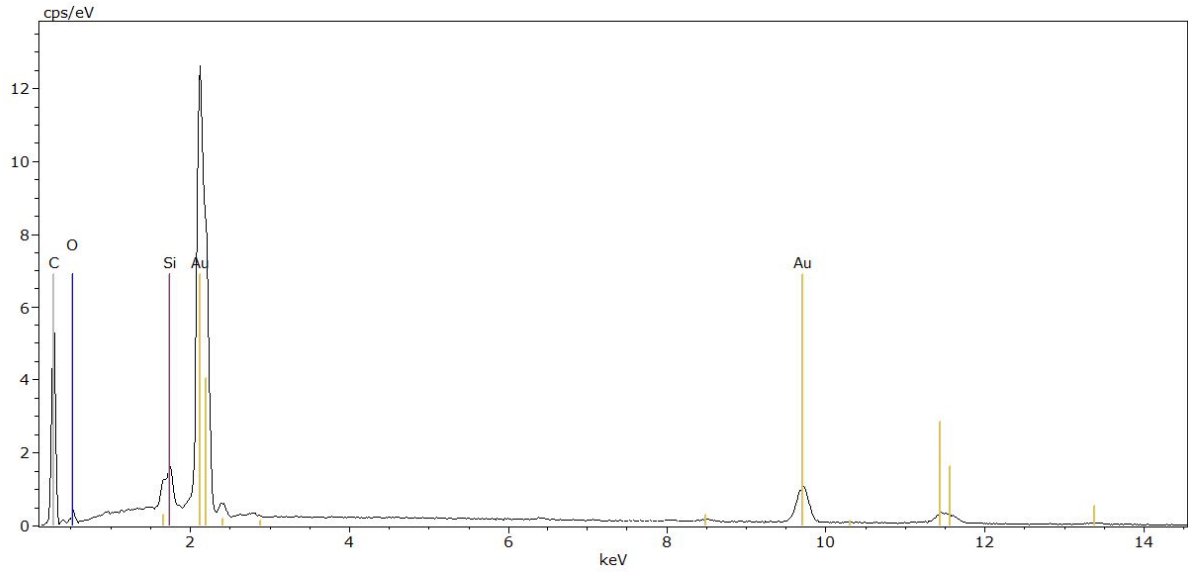
Appendix 13 KHA 23, SEM results, Gold

Element	Atomic Concentrations (%)	Sigma (%)
C	0,0	0,0
O	11,6	1,2
F	12,5	1,4
Al	8,6	0,5
Si	7,6	0,4
S	1,1	0,1
Ca	1,2	0,1
La	19,7	2,5
Ce	32,4	4,0
Pr	2,8	0,5
Nd	2,4	0,4
SUM	100,0	
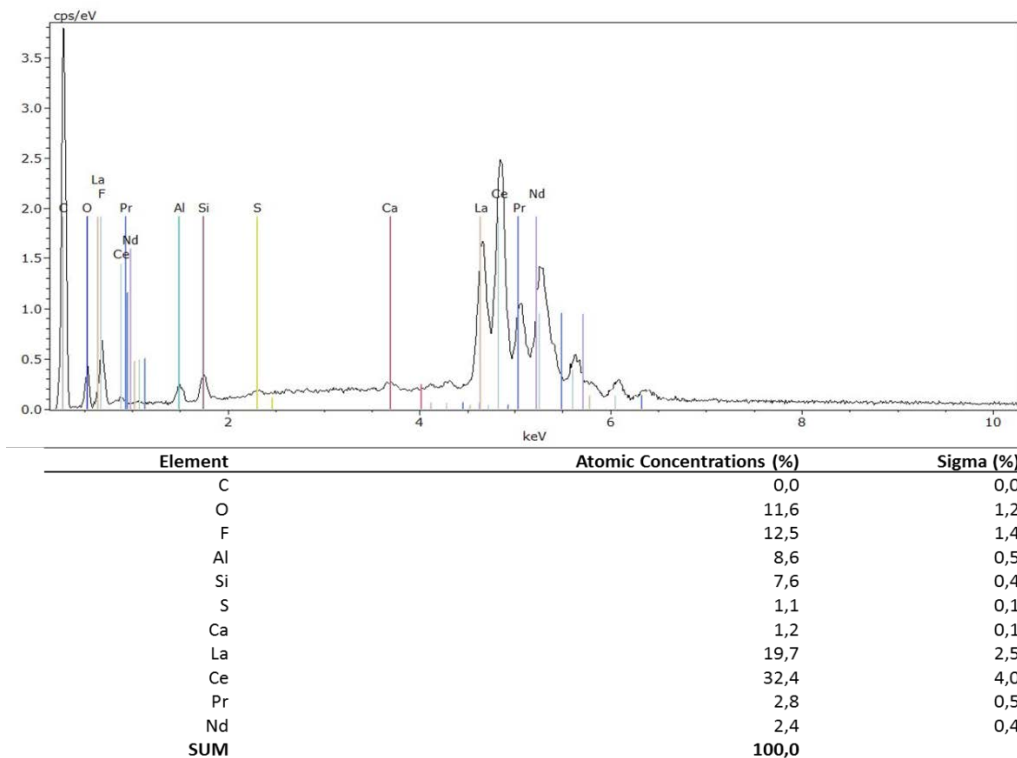
Appendix 14 KHA 23, SEM results showing REE-Fluorocarbonate
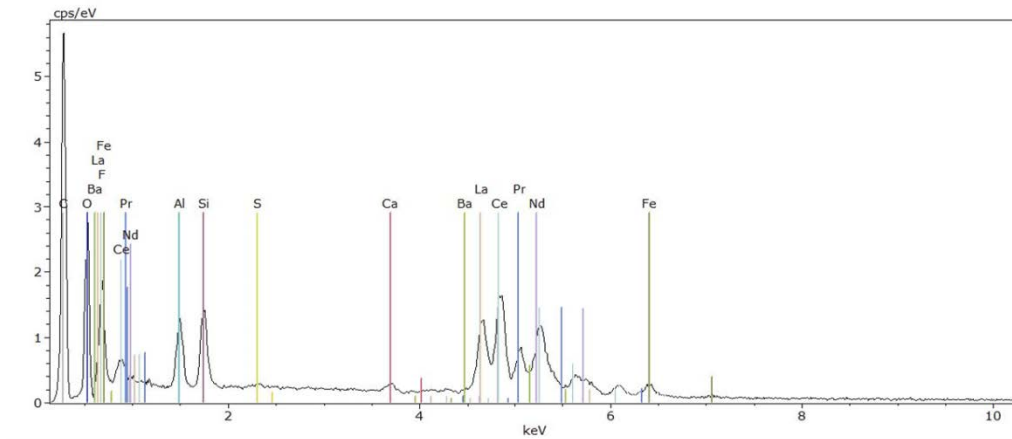
Element	Atomic Concentrations (%)	Sigma (%)
C	0,0	0,0
O	43,9	5,8
F	15,9	2,9
Al	8,1	0,7
Si	6,4	0,6
S	0,3	0,1
Ca	0,8	0,2
Fe	2,1	0,3
Ba	0,4	0,2
La	7,4	1,9
Ce	10,8	2,6
Pr	1,1	0,4
Nd	2,8	0,8
SUM	100,0	

Appendix 15 KHA 23, SEM results showing REE-Fluorocarbonate
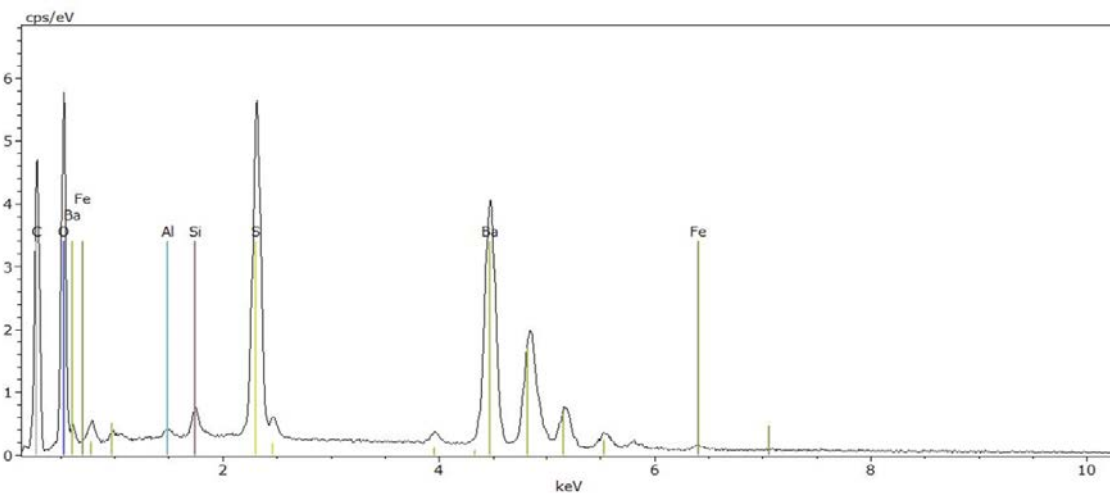
Element	Atomic Concentrations (%)	Sigma (%)
C	0,0	0,0
O	63,7	8,9
Al	0,5	0,1
Si	1,5	0,2
S	17,2	1,5
Fe	0,5	0,2
Ba	16,6	4,5
SUM	100,0	

Appendix 16 KHA 23, SEM results, Barite
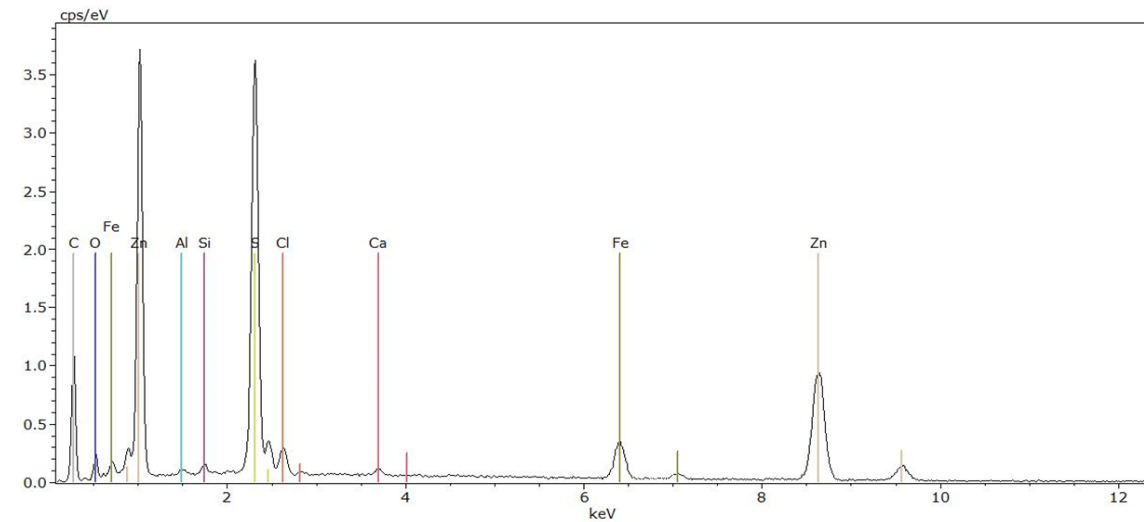
Element	Atomic Concentrations (%)	Sigma (%)
C	0,0	0,0
O	12,4	2,8
Al	0,9	0,2
Si	1,0	0,2
S	38,1	2,8
Cl	3,4	0,4
Ca	0,7	0,2
Fe	6,3	0,8
Zn	37,3	4,4
SUM	100,0	

Appendix 17 KHA 24, SEM results, Sphalerite
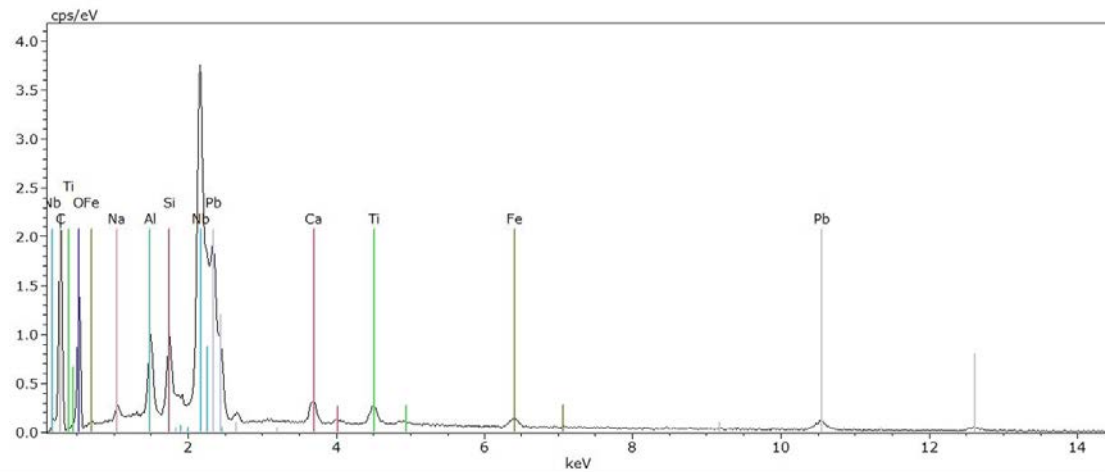
Element	Atomic Concentrations (%)	Sigma (%)
C	0,0	0,0
O	64,8	10,6
Na	1,6	0,3
Al	4,9	0,5
Si	3,6	0,4
Ca	2,4	0,3
Ti	2,0	0,3
Fe	1,3	0,3
Nb	15,5	3,8
Pb	4,0	2,2
SUM	100,0	

Appendix 18 KHA 26, SEM results, niobium oxide (pyrochlore)
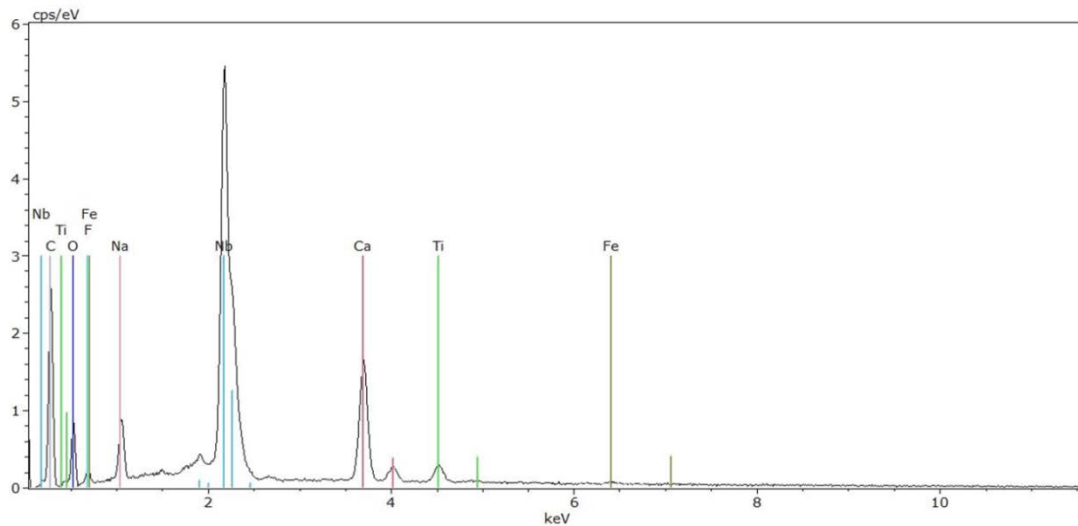
Element	Atomic Concentrations (%)	Sigma (%)
C	0,0	0,0
O	48,1	9,0
F	8,1	2,5
Na	8,7	1,1
Ca	12,7	1,2
Ti	2,2	0,3
Fe	0,4	0,2
Nb	19,7	5,0
SUM	100,0	

Appendix 19 KHA 26, SEM results showing pyrochlore
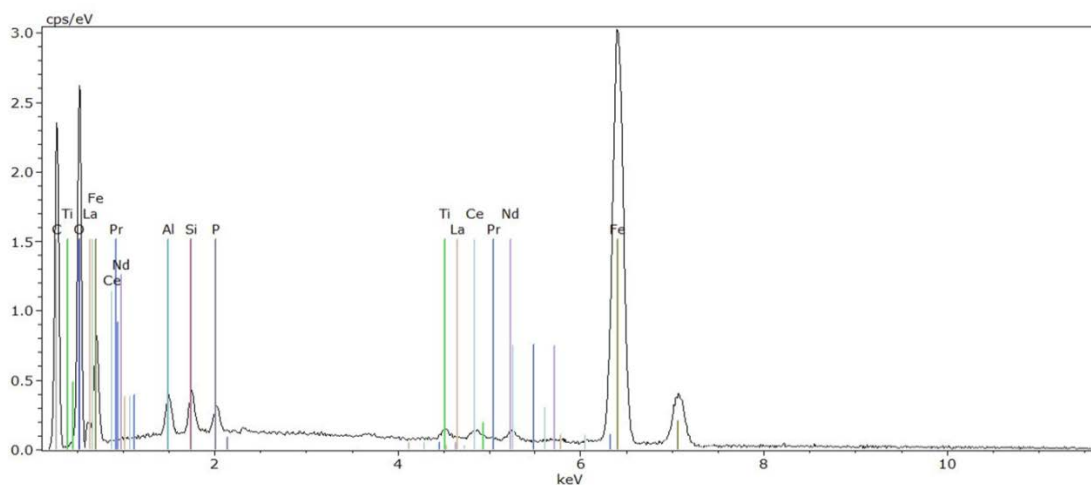
Element	Atomic concentrations (%)	Sigma(%)
C	0,0	0,0
O	50,5	8,7
Al	2,3	0,4
Si	1,7	0,3
P	1,1	0,2
Ti	0,7	0,2
Fe	42,4	5,1
La	0,2	0,2
Ce	0,6	0,3
Pr	0,1	0,2
Nd	0,4	0,3
SUM	100,0	

Appendix 20 KHE 3, SEM results, Fe-oxide (hematite?) with REE
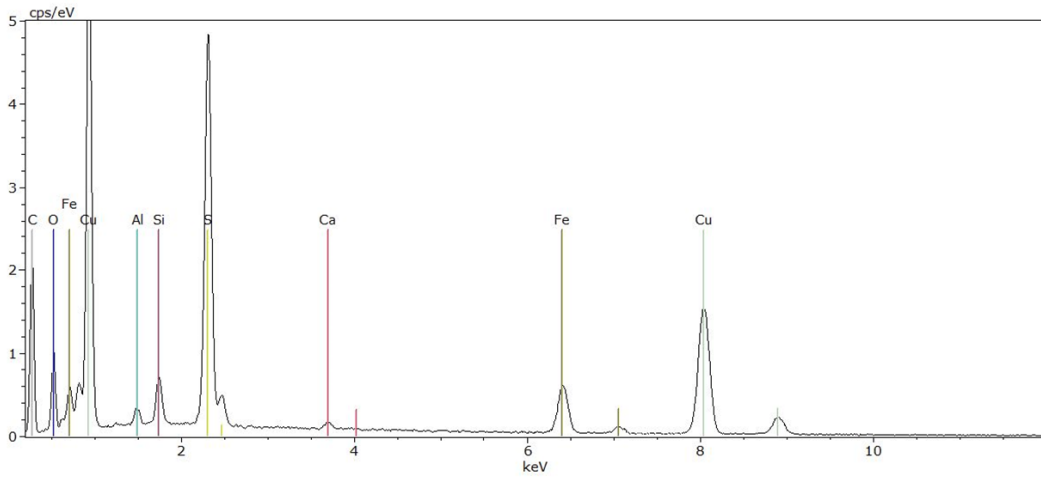
Element	[Atomic Concentrations(%)	Sigma (%)
C	0,0	0,0
O	27,1	4,9
Al	1,2	0,2
Si	2,8	0,3
S	25,5	2,2
Ca	0,7	0,2
Fe	7,5	0,9
Cu	35,1	4,4
SUM	100,0	

Appendix 21 KHE 9, SEM results, Chalcopyrite
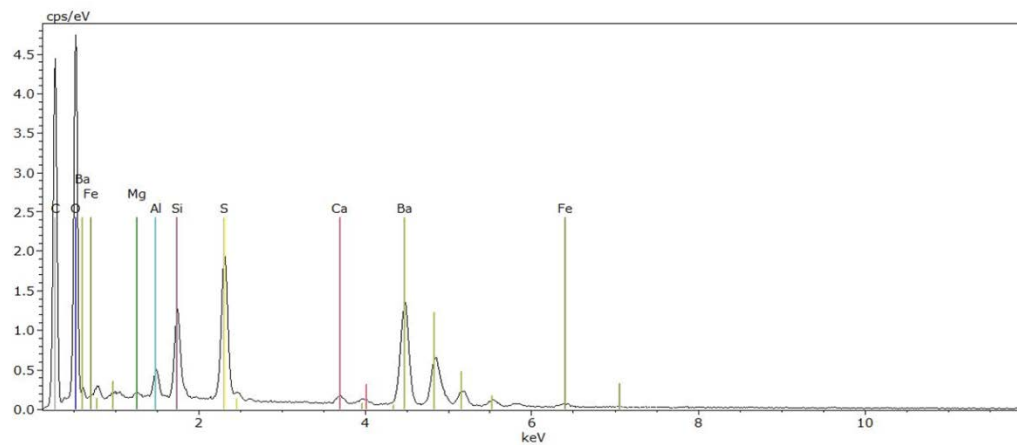
Element	Atomic Concentrations (%)	Sigma(%)
C	0,0	0,0
O	76,2	15,3
Mg	0,3	0,1
Al	1,4	0,3
Si	3,7	0,5
Si	8,5	1,1
Ca	0,6	0,2
Fe	0,7	0,3
Ba	8,6	3,4
SUM	100,0	

Appendix 22 KHE 9 SEM results showing Barite

Element	Atomic Concentrations (%)	Sigma(%)
C	0,0	0,0
O	73,1	10,5
Al	2,6	0,3
Si	6,7	0,6
Ca	0,9	0,2
Fe	1,8	0,3
Hg	14,9	6,0
SUM	100,0	
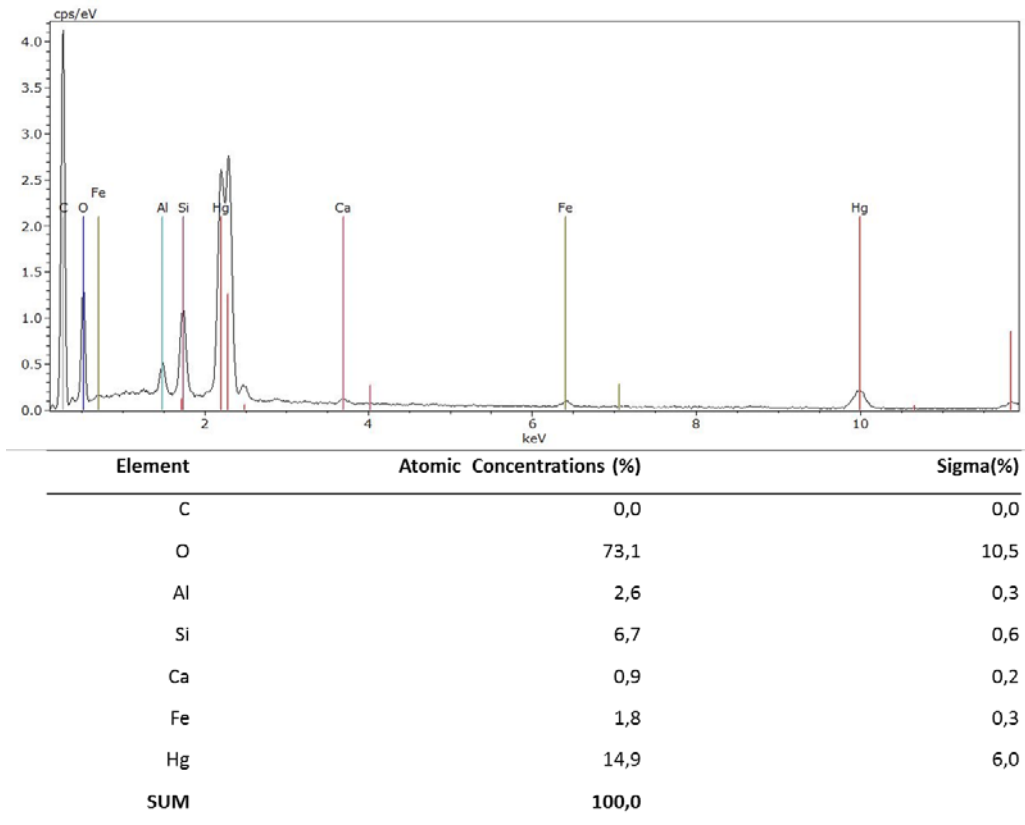
Appendix 23 KHE 9 SEM results showing the possible presence of edgarbaileyite, $Hg_6Si_2O_7$

Element	Atomin Concentrations (%)	Sigma (%)
C	0,0	0,0
O	1,1	0,7
Si	6,0	0,9
S	53,0	4,1
Ca	1,9	0,3
Fe	38,0	3,6
SUM	100,0	
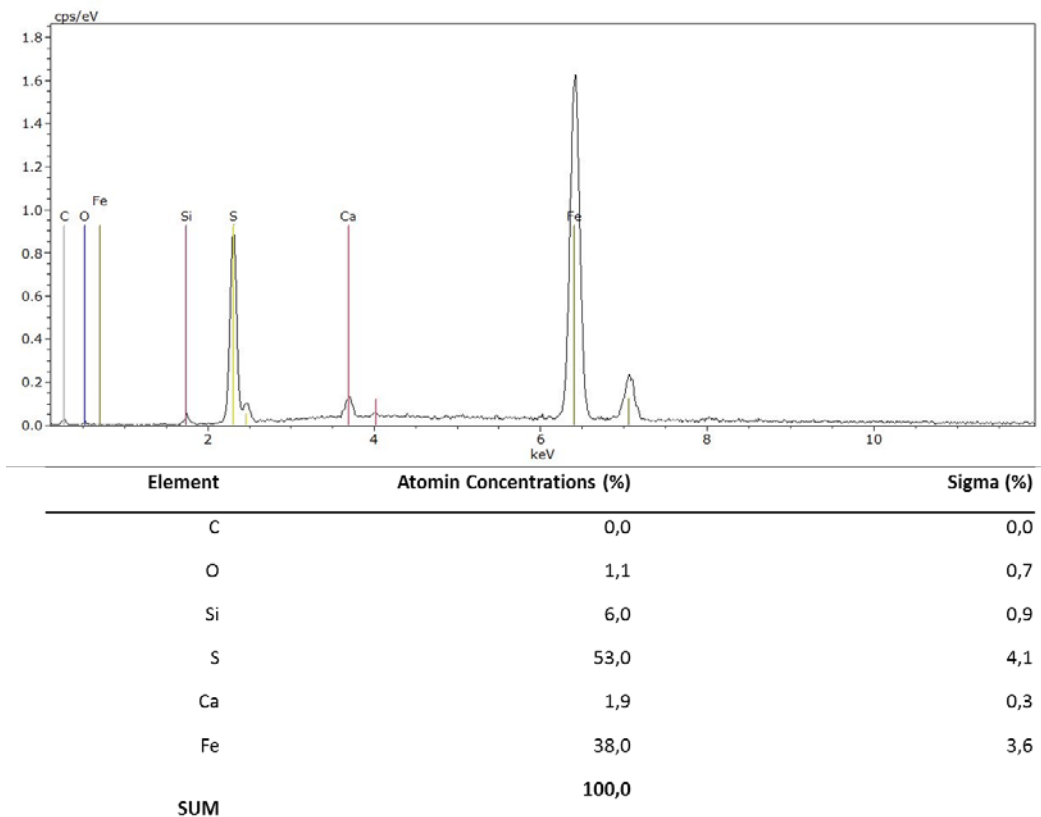
Appendix 24 KHE 9, SEM results, Pyrite

Element	Atomic Concentrations (%)	Sigma(%)
C	0,0	0,0
O	46,6	7,3
F	27,9	5,5
Al	1,8	0,3
Si	3,2	0,4
Ca	1,2	0,2
La	6,5	1,9
Ce	8,8	2,5
Pr	1,3	0,5
Nd	2,5	0,9
Sm	0,1	0,1
SUM	100,0	
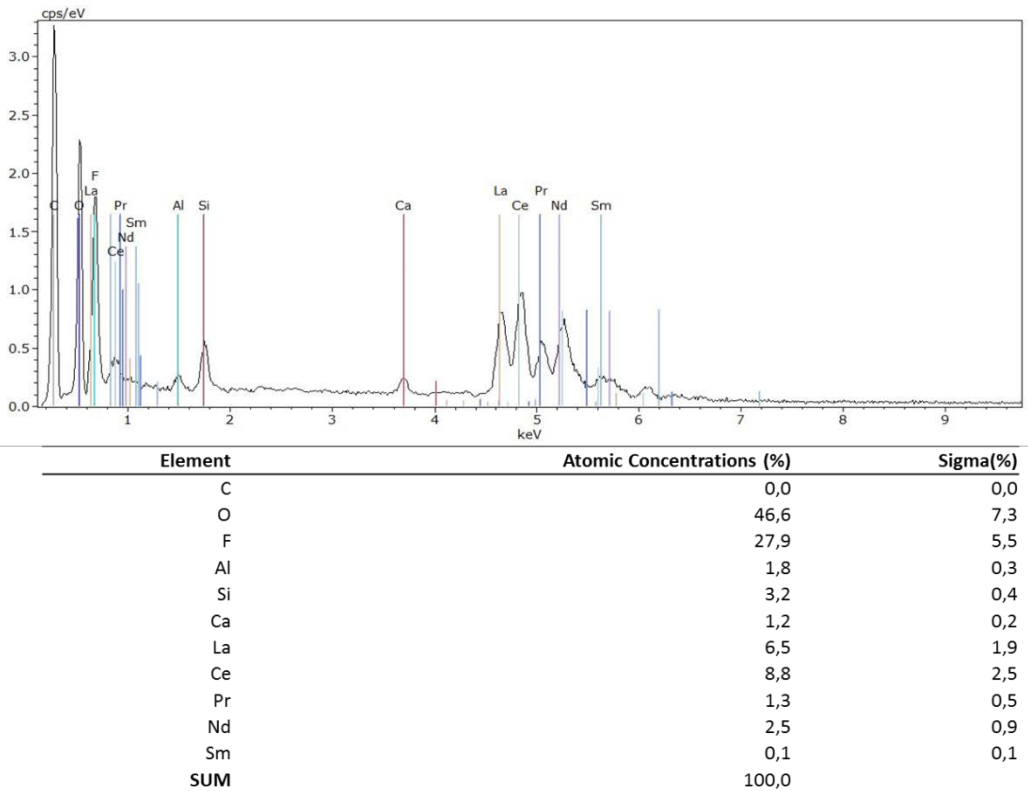
Appendix 25 KHE 9, SEM results, REE- fluorocarbonate

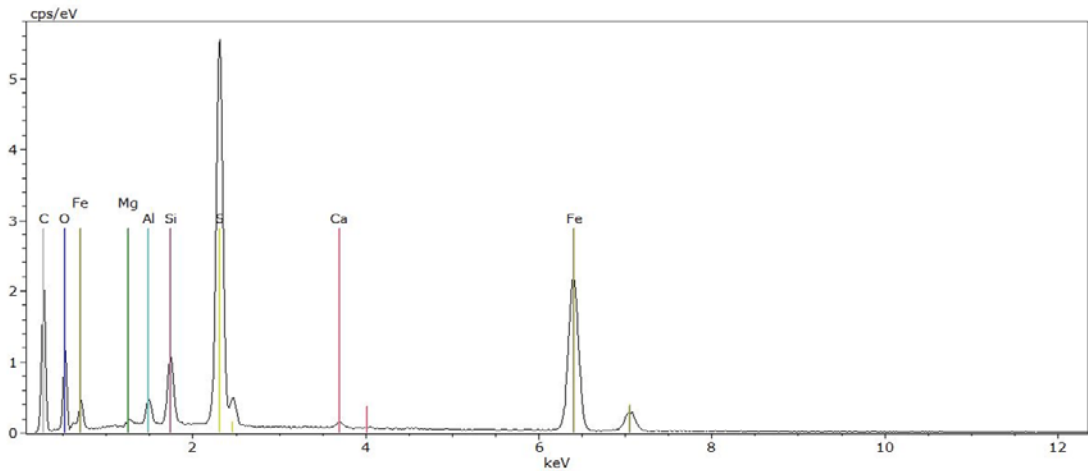| Element	Atomic Concentrations(%)	Sigma (%)
C	0,0	0,0
O	43,2	6,8
Al	2,8	0,4
Si	3,8	0,4
S	3,5	0,4
Fe	6,9	0,8
Co	2,4	0,4
Ni	11,4	1,4
Cu	15,7	2,0
Zn	1,8	0,4
Sn	8,5	2,1
SUM	100,0	
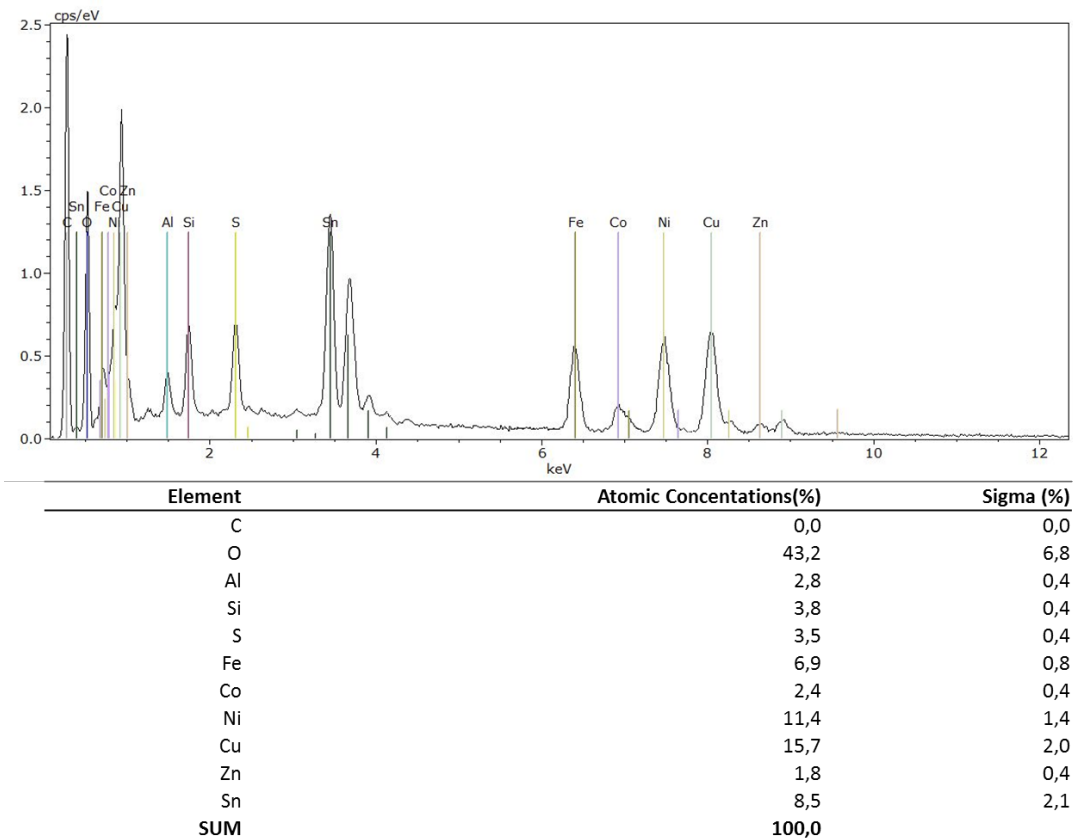
Appendix 26 KHE 9 SEM results, more than one mineral, sulfide, oxide sulphates, cassiterite
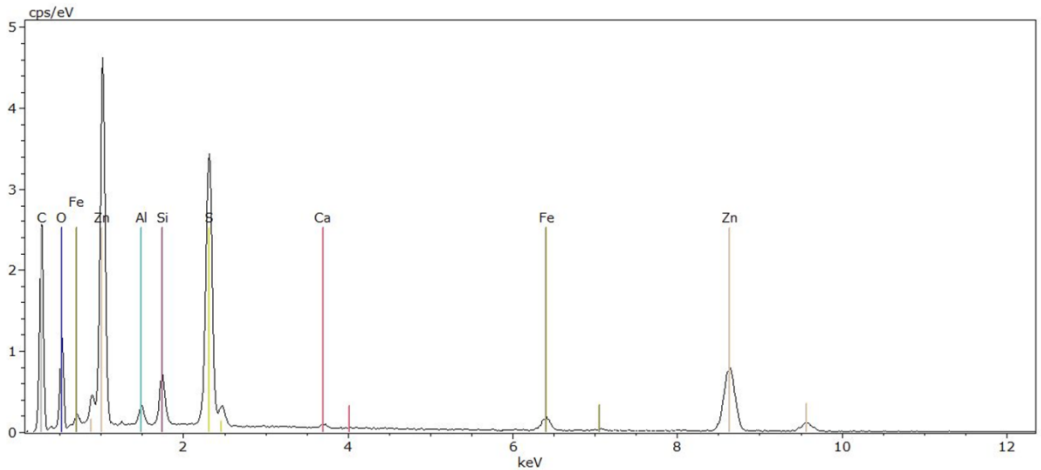
Element	Atomic Concentrations(%)	Sigma (%)
C	0,0	0,0
O	43,3	8,5
Al	1,8	0,3
Si	4,0	0,5
S	22,8	2,2
Ca	0,4	0,1
Fe	2,9	0,5
Zn	24,8	3,8
SUM	100,0	

Appendix 27 KHE 9, SEM results, Sphalerite

Element	Atominc Concentrations (%)	Sigma (%)
C	0,0	0,0
O	35,0	7,5
Mg	0,6	0,2
Al	2,1	0,3
Si	4,4	0,6
S	26,4	2,7
Ca	0,6	0,2
Fe	30,9	4,1
SUM	100,0	

Appendix 28 KHE 9, SEM results, Pyrite
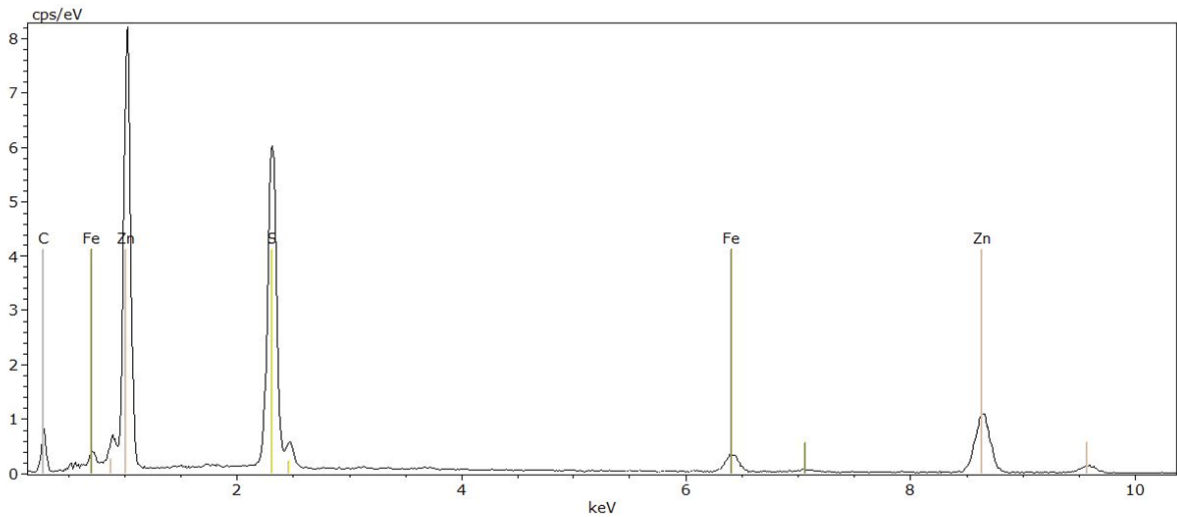
Element	Atomic Concentrations (%)	Sigma(%)
C	0,0	0,0
S	49,8	3,6
Fe	6,4	0,7
Zn	43,8	4,9
SUM	100,0	

Appendix 29 KH 95.1, SEM results, Sphalerite
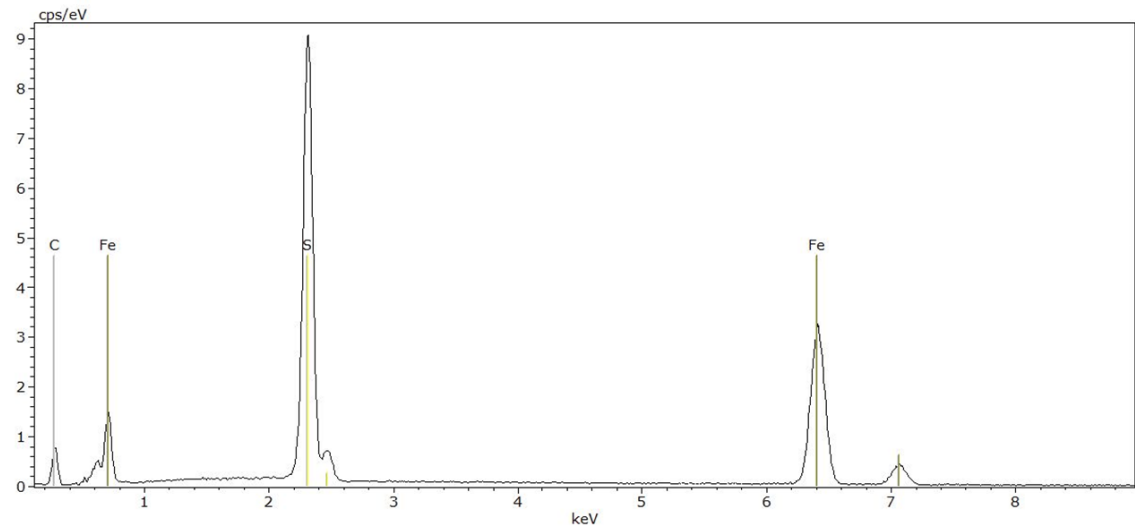
Element	Atomic Concentrations (%)	Sigma (%)
C	0,0	0,0
S	55,5	4,4
Fe	44,5	4,6
SUM	100,0	

Appendix 30 KH 95.1, SEM results, Pyrrhotite
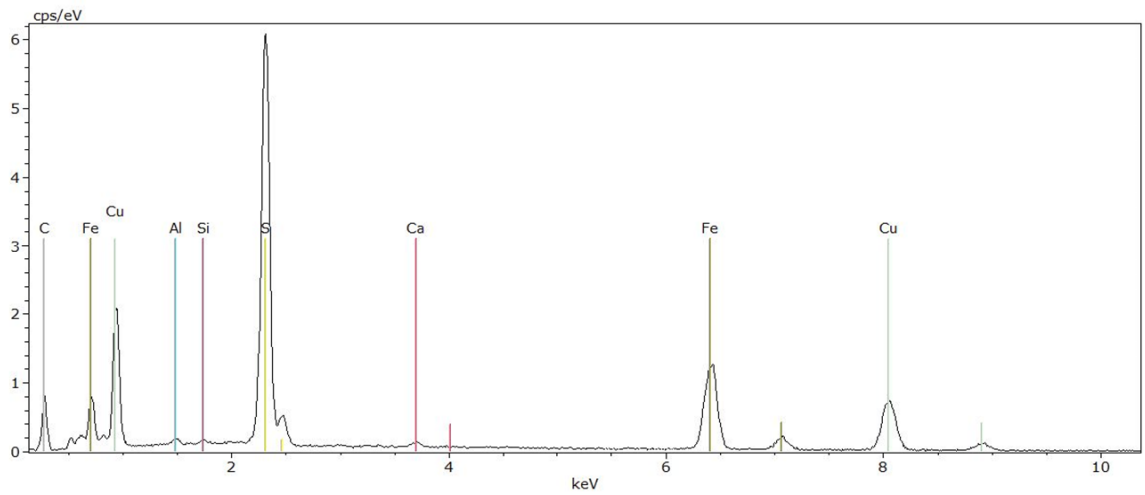
Element	Atomic Concentrations (%)	Sigma (%)
C	0,0	0,0
Al	1,2	0,2
Si	0,6	0,1
S	48,7	3,6
Ca	1,0	0,2
Fe	25,4	2,6
Cu	23,0	2,7
SUM	**100,0**	

Appendix 31 95.1 SEM results, Chalcopyrite

<div align="center">

C U R R I C U L U M   V I T A E

</div>

1. PERSONAL INFORMATIONS

Full name: Elisante Elisaimon Mshiu

Nationality: Tanzanian

Place of birth: Hai ,Kilimanjaro

Date of birth: 25th/09/1978

Marital status: Married

Department/College: Geology/College of Natural and Applied Science

Address: P.O.Box 35052, Dar Es Salaam, Tanzania

2. TERTARY EDUCATION:

M.Sc. (Geology)   Oct, 2005 - March, 2008   University of Dar es Salaam
B.Sc with Geology   Oct, 2001- June,   2005   University of Dar es Salaam

3. ACADEMIC POSTS HELD AT THE UNIVERSITY OF DAR ES SALAAM

- Assistant Lecturer   December, 2008–October, 2010-the start of PhD study leave
- Tutorial Assistant   February, 2007 - December, 2008

4. PROFESSIONAL AFFILIATION

Geological Remote Sensing and GIS, Geochemistry, Mineral Exploration

5. AWARDS

- Certificate of attending the short course in Economic Geology **"The Role of the Geologist in the Mineral Business"**, Freiberg-Germany, December, 2011.
- Certificate of attending the short course in the Geochemistry of PGE elements **"The PGE: an overview on their geochemistry"** by Prof. Marian Tredoux from University of Free State, Bloemfontein, South Africa. At Martin Luther University, Halle (Saale) -Germany, July, 2011.
- PhD Scholarship, **DAAD-MoEVT, October 2010.**
- Certificate of Regional Workshop on Gemstones: Their Geology and Gemology, **University of Dar es Salaam, October 2009.**
- Certificate of Geodata Management training, **Royal Museum for Central Africa, Belgium, December 2008.**
- Certificate of Introduction to ArcGIS II, **Environmental Research Institute, Dar es Salaam Tanzania, December 2007.**

6. RESEARCH PROJECTS

- Gold Atlas of Tanzania, cooperation between University of Dar es salaam (*UDSM) and African Barrick Gold (ABG), 2008-2010.*

- Rock phosphate and lime for small-scale farming in Tanzania, cooperation between University of Dar es salaam, Geology Department *and University of Copenhagen, 2009.*

- Environmental monitoring of volcanism hazards in Rungwe and Oldoinyo Lengai mountains,*2008-2009.*

- A GIS-aided aerogeophysical, geological and geochemical investigation of the late Archaean granitoids in Musoma-Mara Greenstone Belt, northeast Tanzania, *M.Sc Project, September, 2005-December, 2007.*

7. TEACHING ASSISTANTISHIP AND SUPERVISION

GY 258: Remote Sensing and GIS I   (1st semester 2009/2010)

GY 368: Remote Sensing and GIS II   (2nd semester 2008/2009)

GY 258: Remote Sensing and GIS I   (1st semester 2008/2009)

8. PUBLICATION IN REFFERED JOURNALS

- Kalvig, P, Fold, N, Jonsson, J.B, **Mshiu, E. E,** 2012. Rock phosphate and lime for small-scale farming in Tanzania, East Africa, *Geological Survey of Denmark and Greenland Bulletin* 26, pp.85–88.
- **Mshiu, E. E** and Maboko, M.A.H, I 2012. Geochemistry and Petrogenesis of the Late Archaean high-K Granites in the Southern Musoma-Mara Greenstone Belt: Their Influence in Evolution of Archaean Tanzania Craton. Journal of African Earth Sciences 66-67, pp. 1–12
- **Mshiu, E. E,** 2011. Landsat Remote Sensing Data an Alternative Approach for Geological Mapping in Tanzania: A case study in Rungwe Volcanic Province, South-Western Tanzania. *Tanzania Journal of Science,* volume 37, pp. 26-36.

9. BOOK CHAPTERS / BOOKS

- Ikingura, J.R., Mutakyahwa, M.K.D., Marobhe, I., Shukrani, M., Charles, K., Kazomoto, E, **Mshiu, E.E,** 2010. Gold Atlas of Tanzania. *Jamana Printers, 2010,Dar es Salaam,*p.87

Signature   **Date**: 14 July, 2014

Eidesstattliche Erklärung / _Declaration under Oath_

Ich erkläre an Eides statt, dass ich die Arbeit selbstständig und ohne fremde Hilfe verfasst, keine anderen als die von mir angegebenen Quellen und Hilfsmittel benutzt und die den benutzten Werken wörtlich oder inhaltlich entnommenen Stellen als solche kenntlich gemacht habe.

I declare under penalty of perjury that this thesis is my own work entirely and has been written without any help from other people. I used only the sources mentioned and included all the citations correctly both in word or content.

15·07·2014
_____
Datum / Date

_____
Unterschrift des Antragstellers / _Signature of the applicant_